MIHAELA BUCIUMEANU

PREDICTION OF FRETTING FATIGUE LIFE

PREVISÃO DA VIDA DE FADIGA COM FRETTING

Minho University

2009

Publicação subsidiada pela Fundação para a Ciência e a Tecnologia

Acknowledgements

I wish to express my profound gratitude to Prof. Filipe Samuel Silva and Prof. António Augusto Sousa Miranda in the Mechanical Engineering Department at University of Minho, Guimaraes, Portugal, for their able guidance, constant encouragement and persistent interest given throughout the duration of this research. The knowledge and experience that I have gained under their supervision will forever be valuable and appreciated.

Special thanks are due for the assistance provided by the staff members of Material testing laboratory, Tribology laboratory and Metrology laboratory, particularly, Mr. Fernando Araújo, Mr. Sérgio Carvalho, Mr. Victor Neto and Mr. Carlos Alberto. I would like to thank to Mrs. Sandra and Mrs. Maria Luisa. I would like also to thanks to my colleagues Nuno, Joao, Bruno, Oscar, Helder and Alexandra.

I would like to thank my colleagues in Machine Design Department, Mechanical Engineering Faculty, at “Dunarea de Jos” University of Galati, Romania for moral support and motivating suggestions. I would like to thank Prof Liviu Palaghian for guidance and valuable advices.

I would like to thank to the Portuguese foundation “Foundation for Science and Technology” (Portugal) for their financial support through the PhD grant with the reference SFRH / BD / 19555 / 2004.

I would like to thank my best friend Dr. Senthivel Ramakrishnan for encouragement and friendship along this work.

I wish to express my heartfelt appreciation and very special thanks to my family for their patience, support and inspiration through the entire duration of this research.

Mihaela Buciumeanu

Abstract

Fretting fatigue occurs at the interface between two contacting bodies that are pressed against each other in the presence of cyclic loads that gives rise to a small relative displacement. Fretting fatigue occurs in many machines and engineering structures where vibrating elements are in contact with each other. There are over 50 parameters that influence the fretting fatigue phenomenon out of which the most important are: relative displacement amplitude, normal contact load and tangential contact load. Despite of wide research on variables that affect fretting phenomena, there are still ambiguities and contradictions regarding the contact degradation process, mainly in the fretting fatigue case (partial slip regime) where the contact zone is more complex compared to the gross slip regime. When the materials are subjected to fretting fatigue, the effect of the intrinsic materials properties is more pronounced than under plane fatigue conditions, because there is the effect of fatigue (cracking) plus the effect of fretting (wear).

In order to understand the influence of the intrinsic material properties on fretting fatigue phenomena three materials (Al7175, Ck45, and Ti6Al4V) with very different cyclic properties as well as different wear properties, have been tested. All three materials were in contact with conventional 34CrNiMo6 steel.

A novel device, capable of reproducing this phenomenon, was specially designed. The results from the fretting fatigue tests highlighted that the damage induced by fretting increased the fatigue damage, resulting in a shorter life of the component (specimen).

It was observed that Al7175 and Ti6Al4V alloys are more sensitive to fretting fatigue than Ck45 steel. The reason was mainly attributed to the well known poor tribological characteristics of the aluminum and titanium alloys.

It was also confirmed the presence of an asymmetrical fretting scar in fretting fatigue situations (rarely highlighted in technical literature). In this work, and for the first time, an explanation for such behaviour was proposed. The explanation is based on the stress state of the specimen. In fretting fatigue case the specimen stress state, besides the stress due to contact of the pad, changes with the machine load cycle, and it is reasonable to expect that the wear behaviour of materials might be affected by the specimen stress state. The different wear behaviour (due to different stress state) during a fatigue cycle is proposed to be the cause for the asymmetrical fretting fatigue scar. In order to validate this assumption several reciprocating wear tests under an additional elastic stress state were carried out. The results from the reciprocating wear

tests were then extrapolated to the fretting fatigue case. It was observed that the additional elastic bulk stress has a substantial influence on the wear behaviour of the materials used in the study. It was concluded, therefore, that it is pertinent to take it into consideration in wear assessment, and consequently in fretting fatigue predictions. In order to take into account the elastic bulk stresses imposed by external loading, a physical model that is a modification of the Archard´s model for the prediction of wear volume was proposed. To study the influence of the additional elastic stress state on the wear behaviour of the materials, a new wear device was designed, built and assembled in a pin-on-plate reciprocating wear machine.

In order to develop a method that could be useful to estimate the fretting fatigue life, two strain based fatigue models have been chosen. The first approach is the Smith-Watson-Topper´s model and the second approach is the Morrow´s model. These models were chosen because they are the models that include more intrinsic material properties being then more appropriate to understand either the influence of the material properties as well as to establish a comparison among different materials. The former model was already used in fretting fatigue while the later was tested for the first time in this work. Mean stress effects, due to R ratio and to contact load, were included in both models. The Morrow´s model was modified in order to introduce the local stresses involved in the fretting fatigue process (normal, tangential and axial loads).

Furthermore, and in order to obtain good predictions of the fretting fatigue life, as obtained in experimental tests, two modifications to the previous models, were proposed in this work. Both modifications are related to the effect of the contact damaged area in fatigue life. The first modification, herein called the “fretting scar effect”, takes the form of a stress concentration factor, K_t, and is related to the global shape of the scar geometry. The second modification is a surface finishing factor, K_s. This modification is based on the fact that fretting fatigue cracks initiate predominantly at the surface between the two contact zones (slip and stick). In this region, the surface roughness condition seems to be sufficiently important (substantially high roughness values) in order to be considered relevant in fatigue life predictions.

The previous two modifications affect only the elastic term component of the models.

It was also verified that better predictions could be obtained with a new parameter, which affects the plastic component of the models. This parameter is the so-called ‘Bauschinger effect’, which reflects a material deviation from the ideal elastic-plastic

behavior. This effect, never used for fatigue life (initiation) predictions nor incorporated in existing models (SWT and Morrow), was added to the previous models.

The predictions, by using the two previous modified models, seemed to be adequate for fretting fatigue life quantifications, depending on the model and material tested. It was concluded that the added parameters, on the elastic and plastic terms, are relevant ones in order to obtain improved fretting fatigue predictions as well as to allow the models to become more universal equations.

Resumo

A fadiga com fretting ocorre na interface entre dois corpos em contacto que se encontram pressionados um contra o outro na presença de cargas cíclicas e de pequenos deslocamentos relativos. A fadiga com fretting ocorre em muitas máquinas e estruturas de engenharia onde elementos, em contacto uns com os outros, estão sujeitos a vibração. Há mais de 50 (cinquenta) parâmetros que influenciam o fenómeno da fadiga com fretting dos quais os mais importantes são: a amplitude de deslocamento relativo, as cargas normais e as cargas tangenciais. Apesar da ampla investigação sobre as variáveis que influenciam o fenómeno de fretting, ainda há dúvidas e contradições quanto ao processo de degradação dos materiais, principalmente, no caso da fadiga com fretting, e no regime de deslocamento parcial, onde a zona de contacto é mais complexa em comparação com o regime de deslocamento total. Quando os materiais são submetidos a fadiga com fretting o efeito nas propriedades intrínsecas dos materiais é mais evidente do que quando sujeitos apenas a fadiga sem fretting, porque há o efeito da fadiga (fissura) somado ao efeito do fretting (desgaste).

A fim de compreender a influência das propriedades intrínsecas das materiais no fenómeno da fadiga com fretting foram testados três materiais (Al7175, Ck45, e Ti6Al4V) com muito diferentes propriedades de fadiga cíclica assim como diferentes propriedades de desgaste.

Um novo dispositivo, capaz de reproduzir esse fenómeno, foi especialmente projectado. Os resultados dos ensaios da fadiga com fretting mostraram que o dano induzido por fretting aumenta o dano por fadiga, reduzindo a durabilidade (vida útil) do componente (provete).

Observou-se que as ligas Al7175 e Ti6Al4V são mais sensíveis à fadiga com fretting do que o aço Ck45. Tal fato pode ser justificado pelas conhecidas características tribological do alumínio e titânio que são inferiores em relação às mesmas características do aço Ck45.

Confirmou-se, também, que a zona danificada pelo fretting, tem uma forma assimétrica (aspecto raramente destacado na literatura técnica). Neste trabalho, e pela primeira vez, uma explicação para tal fenómeno foi proposta. A explicação é baseada no estado de tensão do provete. No caso da fadiga com fretting, o estado de tensão, para além das tensões de contacto, mudam com o ciclo de carga da máquina de fadiga. É razoável esperar que o comportamento de desgaste dos materiais seja afectado pelo estado de tensão do provete, introduzido pela máquina. O diferente

comportamento ao desgaste (devido ao diferente estado de tensão do provete) durante o ciclo da fadiga é proposto como sendo a causa da pista com forma assimétrica, na fadiga com fretting. A fim de validar tal hipótese, vários ensaios de desgaste alternativos sob um estado de tensão adicional do provete, no regime elástico, foram realizados. Observou-se que este estado de tensão adicional, tem uma influência significativa no comportamento de desgaste dos materiais utilizados no estudo. Desta forma, torna-se importante considerar este estado de tensão adicional na avaliação de desgaste e, consequentemente, na previsão da durabilidade à fadiga com fretting. Para casos de desgaste, e a fim de considerar-se o estado de tensão, no regime elástico, imposto por uma carga externa, ou seja, a máquina de fadiga, propõe-se neste trabalho, um modelo físico que é uma modificação do modelo de Archard para a previsão do volume de desgaste. Para estudar-se este fenómeno, influência de um estado de tensão adicional, no regime elástico, no comportamento de desgaste dos materiais, um novo dispositivo pino-sobre-placa foi desenvolvido e associado a uma máquina de desgaste alternativo.

A fim de se desenvolver um método que possa ser útil na previsão de vida de fadiga com fretting, foram escolhidos dois modelos de previsão baseados em deformação (strain-life-approach)**.** O primeiro é o modelo de Smith-Watson-Topper e, o segundo é o modelo de Morrow. Estes modelos foram escolhidos por incorporarem muitas propriedades intrínsecas dos materiais, quer propriedades plásticas quer elásticas. Sendo assim seriam os modelos mais apropriados para se compreender tanto a influência das propriedades do material, bem como se modificarem ou ainda para se estabelecerem comparações entre materiais com diferentes propriedades. O primeiro modelo (SWT) já é utilizado no caso da fadiga com fretting, enquanto o segundo (Morrow), foi testado pela primeira vez neste trabalho, na situação de fadiga com fretting. Os efeitos da tensão média, quer devidos à razão de tensões quer devidos ao contacto, foram incluídos nos dois modelos sendo que o foram pela primeira vez no segundo modelo (Morrow).

A fim de obter uma estimativa adequada da vida de fadiga com fretting, de acordo com os resultados experimentais, duas modificações aos modelos anteriores, foram propostas neste trabalho. As duas modificações estão relacionadas com o efeito da área danificada na área de contacto, na vida de fadiga. A primeira modificação, aqui chamada de " efeito da pista de fretting", assume a forma de um factor de concentração de tensão, K_t, e está relacionada com a geometria da zona de contacto. A segunda modificação assume a forma de um factor de acabamento superficial K_s. Esta alteração

é baseada no facto de que as fendas de fadiga, no caso de fadiga com fretting, iniciarem-se predominantemente na superfície entre as duas zonas de contacto (zona de deslizamento relativo e zona de deformação). Nesta região, as condições da rugosidade da superfície são substanciais e deverão ser consideradas nos modelos de previsão da vida de fadiga com fretting.

Estas duas alterações afectam essencialmente a componente de deformação elástica dos modelos.

Verificou-se também que melhores previsões podem ser obtidas se se adicionar um novo parâmetro, que afecta a componente plástico dos modelos. Este parâmetro é conhecido como "efeito de Bauschinger", e reflecte um desvio em relação ao comportamento elasto-plástico ideal do material. Este efeito não é tido em consideração nos modelos testados (SWT e Morrow) nem em qualquer outro modelo de previsão de vida dos materiais, tendo sido proposto como relevante, pela primeira vez neste trabalho.

As previsões, usando os dois modelos anteriores, quando modificados, mostraram ser adequadas para a quantificação da vida de fadiga com fretting, dependendo todavia bastante do material testado. Assim, conclui-se que os parâmetros adicionados, quer na componente elástica quer na componente plástica, das equações, são relevantes para se obterem previsões de vida de fadiga com mais rigor assim como para tornar os modelos usados (SWT e Morrow) mais universais.

Keywords

FRETTING FATIGUE
RECIPROCATING WEAR
CYCLIC PROPERTIES
SMITH-WATSON-TOPPER (SWT) PARAMETER
MORROW PARAMETER
STRESS CONCENTRATION FACTOR
SURFACE FINISH FACTOR
BAUSCHINGER EFFECT
FATIGUE LIFE

Table of contents

List of figures

Chapter 1

Chapter 2

Chapter 3

Chapter 4

Chapter 5

Annex A

Annex B

List of tables

Chapter 3

Chapter 4

Chapter 5

Annex A

Annex B

Nomenclature

Symbols

$_D$	Degradation degree
$F_{(L_a)}$	Influence of fatigue on life (axial load)
$FF_{(F_n,F_t)}$	Influence of fretting on life, due to loads (normal and tangential) involved into the process (contact)
W	Wear influence
$S_{FF,W}$	Synergetic factor between fatigue, fretting and wear
μ_s	Coefficient of static friction
μ_d	Coefficient of dynamic friction
μ	Coefficient of friction in the slip condition
F_n	Normal contact load
F_t	Tangential load
F_{tp}	Pad pre-tangential load
L_a	Machine axial load
F_n	Maximum normal contact load
$F_{t,max}$	Maximum tangential load
$F_{t,min}$	Minimum tangential load
δ	Relative displacement
c	Half of the stick zone width
a	Half of the contact width
z	Probability of removing an atom from the surface when it encounters an atom of the opposing member
V	Volumetric material loss
K	Wear coefficient
H	Hardness
HB	Brineell hardness
HV	Vickers Hardness
S	Sliding distance
τ	Local value of shear stress within the contact region
$\varepsilon_{a,FF}$	Total fatigue strain amplitude
$\frac{\Delta\varepsilon_e}{2}$	Elastic strain amplitude
σ_f'	Fatigue strength coefficient
$\frac{\Delta\varepsilon_p}{2}$	Plastic strain amplitude
E	Young's modulus
N_f	Number of cycles to crack initiation
b	Fatigue strength exponent
ε_f'	Fatigue ductility coefficient
c	Fatigue ductility exponent
n'	Cyclic strain hardening exponent
K'	Cyclic strength coefficient

σ_{max}	Maximum machine axial stress,
$\sigma_{max,FF}$	Maximum fretting fatigue stress
p_0	Maximum Hertzian pressure
σ_a	Machine axial stress amplitude
σ_{a,F_t}	Tangential stress amplitude
υ	Poisson's ratio,
σ_y	0.2% Yield strength
σ_r	Tensile strength
ρ	Distance on the surface from a given point to the centre of the contact
$\Delta\tau$	Shear stress amplitude
τ_{max}	Maximum shear stress on the critical plane
$R\tau$	Shear stress ratio
m	Fitting parameter
A, B, C, D	Constants obtained experimentally
k	Fitting fatigue life data
$(\Delta\gamma/2)$	Maximum cyclic shear strain amplitude on a particular plane
$(\sigma_{n,max})$	Maximum normal stress to a particular plane at any time during the cycle
τ_f'	Shear fatigue strength coefficient
γ_f'	Shear fatigue ductility coefficient
b_0	Shear fatigue strength exponent
c_0	Fatigue ductility exponent
G	Shear modulus
$2N_i$	Number of reversals to the formation of a surface crack of a certain length
$\left(\sqrt{J_2(t)}\right)$	Second invariant of the stress deviator
$(P_{h\,max})$	Maximum value of the hydrostatic pressure.
S	Deviatoric part of Σ
σ_d	Alternating bending fatigue limit
τ_d	Alternating shear fatigue limit
d_c	Scalar variable to quantify the cracking risk
A	Real area of the contact
p_0	Yield pressure of the material
λ	Order of the singularity
τ	Relevant stress component
F	Geometric factor
τ_∞	Remote shear stress
σ_m	Machine load mean stress
$\sigma_{m,global}$	Global mean stress
$F_{t,m}$	Mean value of the tangential load
$F_{n,m}$	Mean value of the normal load
K_t	Stress concentration factor
K_s	Surface finish factor
p_t	Depth of the fretting scar
l	Length of the specimen

L	Width of the specimen
w	Height of the specimen
d	Grain size
R_a	Average roughness
L	Length of assessment
σ_{add}	Additional elastic stress
β_σ	Bauschinger stress parameter
β_ε	Bauschinger strain parameter
β_E	Bauschinger energy parameter
E_s	Returned energy (elastic strain energy)
E_p	Plastic prestrain energy
β	Strain shift
ΔW_p	Absorbed plastic strain energy density
ΔW_e	Elastic strain energy
β_{BAU}	Proposed Bauschinger stress parameter
ε_{BAU}	Bauschinger effect coefficient
$\varepsilon'_{f,BAU}$	Fatigue ductility coefficient with BAU correction
N_t	Transition fatigue life point

Abbreviations

COF	Coefficient of friction
SWT	Smith-Watson-Topper parameter
MSSR	Modified shear stress range parameter
F	Findley parameter
FSK	Fatemi-Socie-Kurath
BAU	Bauschinger effect
RCFM	Running conditions fretting maps
MRFM	Material response fretting maps
PSR	Partial slip regime
GSR	Gross slip regime

Chapter 1
Introduction

Chapter 1 gives a briefly historical perspective about fretting phenomena and also the motivation of this research. The objectives and the structure of the thesis are also presented in this chapter.

1.1 Brief historical perspective and the motivation of the study

When the synergetic effect (fatigue plus fretting) exists, there occurs one of the most damaging phenomena, known as *fretting fatigue*. This synergetic effect can be written as

$$D = F_{(L_a)} + FF_{(F_n,F_t)} + W + S_{F,FF,W} \quad (1.1)$$

where: D - degradation degree; $F_{(L_a)}$ - influence of fatigue on life (axial load); $FF_{(F_n,F_t)}$ – influence of fretting on life, due to loads (normal and tangential) involved into the process (contact), W - wear influence; $S_{F,FF,W}$ - synergetic factor between fatigue, fretting and wear.

Fretting is a deteriorating process that has been recognized as a failure mode of major importance [1]. Fretting fatigue is a common occurrence since the most mechanical systems and engineering structures (for example: aircrafts, spacecrafts, automobile, electrical equipment, manufacturing equipment, human body implants, etc.) are subjected to vibration on the components connections. Although the surfaces may appear to be stationary with respect to one another, vibrations (or forces) will give rise to a small reciprocating displacement (microslip) [2].

As reported in ref. [3] fretting was first described by Eden, Rose and Cunningham (1911), who found that brown oxide debris, was formed in the steel grips of their fatigue machine in contact with a steel specimen. Further technological advancements and more complex geometries on machinery led to significant fretting fatigue problems [reported in ref. 4].

In 1927, Tomlinson [cited in ref. 5] was the first to actually study this process. He designed a fretting fatigue machine consisting of contacting annuli in small amplitude rotational oscillation. The movement was controlled by a long level system. Because the resultant debris of steel specimens was the red iron oxide α-Fe_2O_3, which had risen from a chemical reaction with oxygen in the air, Tomlinson created the expression *fretting corrosion*. The investigation also established that the damage could have been caused by movements with amplitude as small as a few millionths of inches and the important fact that relative movement, which was termed “slip”, had to occur [reported in ref. 3].

In the 1930s [cited in ref. 4], premature failures of railway care axles forced the railroad companies to investigate the causes. Investigations were initiated to determine the reasons behind fretting failure. Discontinuities, inhomogeneities and stress

concentrations from manufacturing and design were given most of the credit. Fretting fatigue was not the term used to discuss these failures. Most of the materials in use at that time were steels, and it was noticed that most of the components where failures were occurring were pitted and covered with a rust-like deposit, strong indicators that fretting was a possibility.

In 1939 Tomlinson, with the help of Thorpe and Gough [cited in ref. 4], performed another early investigation into the effects of fretting corrosion. What they observed in the experimentation and in-field experience convinced them that the corrosion products were mechanical rather than chemical in nature. It was later recognized that fretting fatigue, although referred to as fretting corrosion at the time, was mechanical and environmental in nature.

The next important step in the development of fretting studies was made in 1941 (Warlow-Davies) [reported in refs. 3, 4] when fretting damage was produced on the gage length of steel fatigue specimens and subsequent reduction on fatigue strength was found do to the pitting of the surface between 13% and 17%. The fretting and fatigue portions of the fretting tests were kept separate to investigate the effect of fretting on fatigue life. Pure fatigue tests were conducted without pre-fretting to examine the change in fatigue life when compared to the pre-fretted tests. This result was to be expected, but later investigations showed that the conjoint action of fretting and fatigue, which is the usual case in practice, was much more dangerous, producing strength-reduction factors of 2 and 5 and even greater (around 20%). At this time, the effect of fretting fatigue was attributed to the relative motion between the surfaces in contact.

Later work by McDowell in 1953 [cited in ref. 6] studied the simultaneous action of fretting and fatigue. Subsequent pioneering work was conduced by Fenner and Field (1958) and by Waterhouse. Waterhouse´s extensive work was summarized in his books of 1972 and 1981. In the development of our understanding of the similar mechanics, the first major achievement, which is still commonly used, was the analysis of the general Hertzian contact under conditions of partial slip, by Midlin in 1949.

Bramhall in 1973 [reported in ref. 7] noticed an apparent size effect in fretting, and also pioneered the use of Hertzian contacts to introduce fretting damage.

In 1985 [reported in ref. 3], studies demonstrated that fretting accelerated the crack initiation process greatly. In normal fatigue, crack initiation may account for 90% of fatigue life, whereas in fretting fatigue, initiation could occur in 55% of the fatigue life. But the initiation life on fretting fatigue case even nowadays is a contradictory subject (see 2.3.1 Introduction).

Another interesting step in fretting fatigue understanding was made in 1988 by Vingsbo and Soderberg [8]. It was introduced the concept of fretting maps. It was found one of the most interesting relation between the relative displacement amplitude and fretting fatigue life (see 2.1.2.3 Relative displacement amplitude). On the same year (1988), Hills al at. [9] by carrying out a series of experiments (aluminum alloy, HE15-TF) under closely controlled conditions indicated that the size of the contact has marked effect on fretting fatigue life.

In the last years several models have been used in order to predict the fretting fatigue initiation life, as the critical point approach (Ruiz parameter) [6,10] and the critical plane approach (Smith-Watson-Topper parameter, Findley parameter etc.) [11-13]. Regarding the use of a critical point approach, it offers the advantages of being simple scalar parameter that captures two of the main drivers for crack formation in fretting. These two main drivers are the maximum tangential stress along the interface and the energy dissipated: Still, this parameter has some weakness. The frictional work term is found rather arbitrarily. Also, although it can be used to capture the location of crack nucleation, it is unable to determine its orientation. Many conventional fretting fatigue researchers recommend using the critical plane based predictive parameters and criteria, because crack nucleation and initiation in fretting fatigue occurs in a contact region between two bodies which is governed by a state of stress that is multiaxial in nature. It was the recent option of Namjoshi [14]. However, because the stress required for these parameters cannot accurately be measured using test equipment, they need to be determinate through simulations of tests. These simulations can be based on the analytical solutions as well as numerical methods, such as finite element analysis.

From an engineering perspective, much effort has been devoted to find out in a systematic and scientific manner explanation for this phenomenon (research, studies and conferences).

It is evident that fretting research has been conducted to determine the variables that influence this phenomenon (e.g. the normal, tangential and axial loads, relative displacement amplitude, frequency, environment, and many other variables) and the influence of these on life. Due to the influence of many variables on the fretting process, many researchers have attempted to characterize each by focusing on variations of one variable, while holding others constant.

Life prediction of engineering components subjected to fretting fatigue appears to have advanced, but certain aspects of the mechanism of fretting are still not thoroughly understood. Hoeppner [15] in a study about different practical cases where fretting

fatigue arise (e.g. propeller hub/drive shaft flange assembly of aircraft engine, gas turbine disc/shaft connection, etc.) stated that even much progress has been done in the last years in both understanding and design for fretting fatigue, prevention and control, “*much remains to be done*”.

1.2 Scope and aims of the thesis

In this thesis, a theoretical and experimental investigation in the field of fretting fatigue is described.

The main objective of this work is, besides the understanding of the fretting fatigue mechanisms, to use the stress and strain state (considering its modification with cycles-cyclic hardening/softening; Bauschinger effect) and wear of the fretting contact and apply it to conventional fatigue theories in order to develop a method that could be used as a tool that the practising engineer could use in the screening (selection) of material systems.

The main objectives of this work are:

- Development of a routine and characterization technology necessary to study the fretting fatigue behaviour;
- Understanding the mechanisms involved in fretting fatigue crack initiation, namely stresses, strains, displacements, and wear ;
- Development of a physical mechanism for the process;
- Study of the influence of external features as well as intrinsic material properties such as fatigue cyclic plastic properties of materials, over the stress and strain state of the fretting contact and mechanisms of crack nucleation;

It is expected that the thesis is of interest, as the knowledge of fretting fatigue is therefore essential for any engineer or technologist concerned with design/maintenance of the mechanical equipments, which almost always contains a large number of small amplitude sliding contacts.

1.3 Thesis structure

The flow chart presented in figure 1.1 shows the general line (evolution) of the thesis and also the steps forward in order to better understand the fretting fatigue phenomenon and subsequently to obtain a better tool to predict the fretting fatigue life.

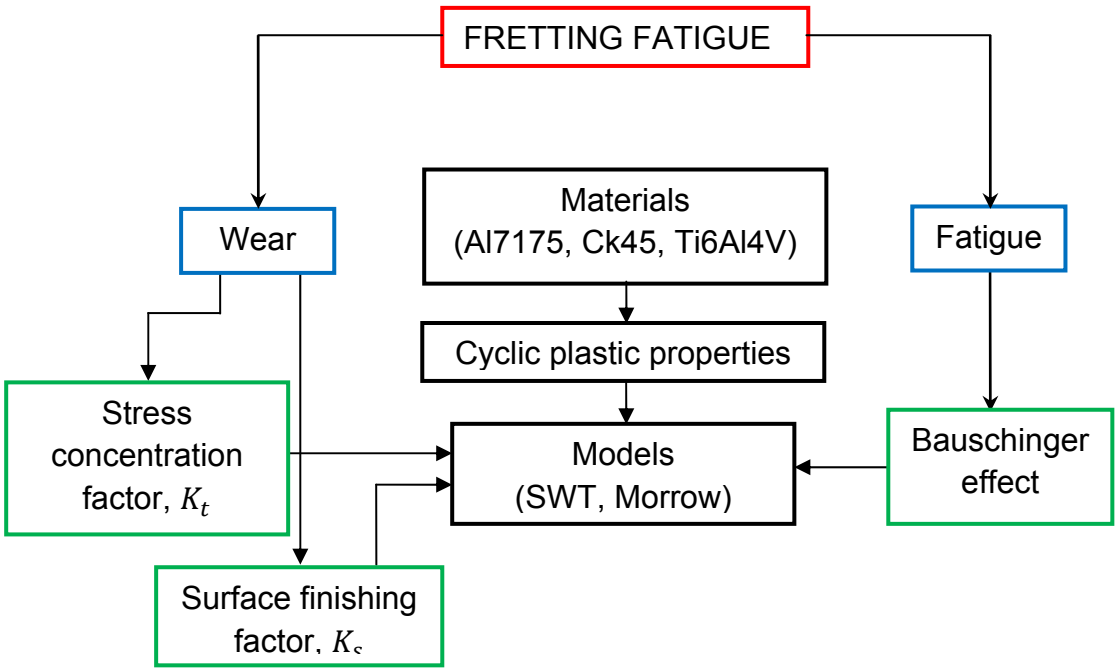

Figure 1.1 Flowchart of the evolution of the thesis

This thesis consists of six chapters and two complementary sections (annexes and references).

Chapter 1 gives a brief historical perspective about fretting phenomena and also the motivation of this research. The objectives and the structure of the thesis are also presented in this chapter.

A state of the art in fretting fatigue is presented in *Chapter 2*. This chapter is divided into three sections. The first section is attributed to the fretting fatigue fundamentals. It is provided a detailed description of the most important parameters (e.g. normal load, tangential load and the relative displacement amplitude) that influence fretting fatigue phenomena. A physical justification is given for the fretting scar evolution. The most used fretting fatigue apparatus are also presented. The second section of this chapter is dedicated to the influence of the additional elastic stress state on the wear behaviour of the materials and consequently its influence on fretting fatigue

behaviour. From the third section can be depicted the theoretical background about life prediction models. The most used models to predict fretting fatigue initiation life are presented in detail. At the end of this section can be depicted the theoretical base of the Bauschinger effect.

Chapter 3 presents the techniques and procedures used in the present study. The properties of the materials, the geometry of the specimens and of the pad/pin are presented. Particular consideration is given to the novel device, capable of reproducing the fretting fatigue phenomenon. Also in this chapter is presented the new reciprocating wear device. The tests conditions for the fretting fatigue and reciprocating wear tests are presented. Also at the end of this chapter are presented some conclusions regarding the experimental techniques.

In *Chapter 4* are presented the experimental results and discussions of fretting fatigue and reciprocating wear tests. Morphological characterisation of the contact surfaces (from fretting fatigue and also reciprocating wear tests) by different techniques is also treated in this chapter. Conclusions drawn from the experimental work are also presented.

Chapter 5 is dedicated to the prediction models for fretting fatigue life**.** It is presented the theoretical base of the present approach, considering the modifications with the stress concentration factor effect, the surface finish factor (roughness) and the Bauschinger effect.

Chapter 6 gives the major concluding remarks and findings of this research program together with possible future lines of work related with the present research.
Finally three complementary sections, the references and two annexes are presented. In annex A are provided the results of a sensitivity analysis in order to verify the sensitivity of models and of the materials used in this work at the elastic and the plastic domain. In annex B are provided the results of plain fatigue tests and the analytical life prediction using the SWT and Morrow models. Bauschinger effect was incorporated in both models and better predictions were obtained.

Chapter 2
Theoretical background & literature survey

In this chapter, an extended state of the art in fretting fatigue is presented. A physical justification is given for the fretting scar evolution, based on the evolution of the most important fretting fatigue parameters and on wear sensitivity to the stress state of the specimen. The most used fretting fatigue apparatus are also part of chapter 2. A detailed theoretical background about life prediction models is presented.

2.1 Fretting fatigue fundamentals

2.1.1 Introduction

Fretting fatigue has been studied for a long time as a “separate” area of fatigue where the mechanical damage over the surface was considered to have a dominant role in decreasing the fatigue performance of materials. It is well known that fatigue, which is the most frequent mechanics that deal with failure analysis, arise due to repeated loading and involves the gradual development and growth of a crack [1,16]. The definition of fretting is not as well accepted as the fatigue definition. Generally, *fretting* is defined as a special process that occurs in the contact area between two components under load giving rise to a slight relative displacement due to vibration or some other forces [17].

Fretting failure of mechanical components has gradually come to be recognized as a failure mode of major importance. At the interface (contact) there is an interaction among wear, corrosion and fatigue. Thus, this phenomenon involves many aspects of contact mechanics, multiaxial fatigue, tribology and materials science.

Directly or indirectly the damage in fretting fatigue is caused by several factors/variables. Some researchers stated that almost fifty parameters may influence fretting damage [18-21]. Figure 2.1 presents some of the most important variables/factors that influence fretting fatigue phenomena [22,23]. All these factors are interrelated [24]. For instance, Madge et al. [25] stated that the COF affects the slip distribution, whilst COF depends on normal load; furthermore, COF changes with the number of fatigue cycles.

Vingsbo and Soderberg [8] specified three types of surface degradation on fretting situation: fretting corrosion, fretting wear and fretting fatigue. From figure 2.2 can be seen that fretting can be generally summarized as: *fretting fatigue* (partial slip) and *fretting wear* (gross slip) [26, 27]. It should be noted that these forms of damage often coexist in the same contact [28]. Fretting fatigue is associated with the stick-slip (partial slip) contact conditions and is characterized by early crack nucleation and growth leading to failure. Fretting fatigue is fretting in the presence of a bulk fatigue load. In this case the fatigue cracks can develop and will propagate if the bulk load is sufficiently large. Fretting wear is associated with the gross slip contact conditions and is characterized by permanent material loss. Fretting wear involves small cyclic displacements as a result of contact alone. Fretting wear is an accumulation of damage

that occurs at component interfaces that are subjected to high contact stresses coupled with low-amplitude oscillation [29]. Corrosion (for oxidation metals - one of the immediate consequences of the process in normal atmospheric conditions is the production of oxide debris) has been accepted to the whole field of fretting phenomena and incorporates the two manifestations (symptoms) of fretting fatigue and fretting wear [3].

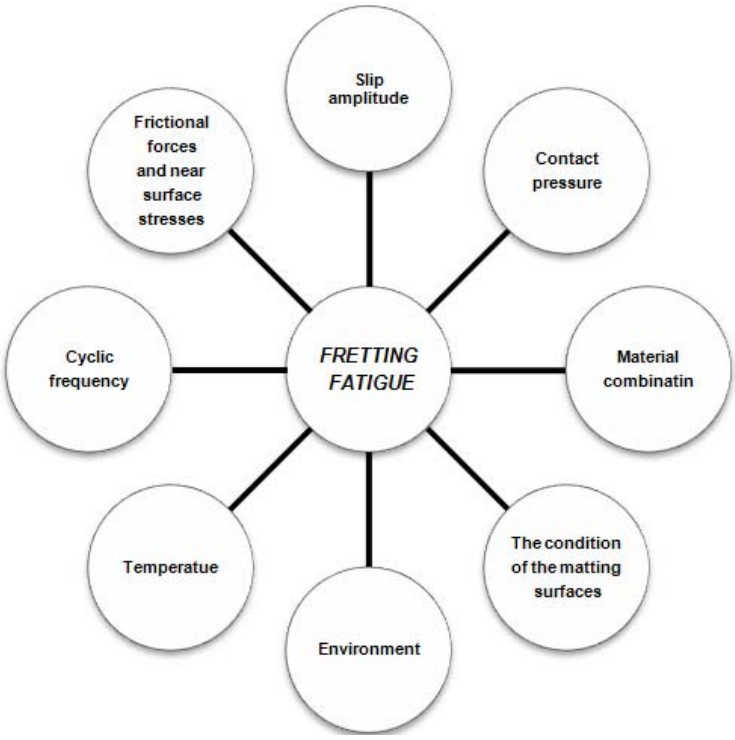

Figure 2.1 Some of the interrelated factors that influence fretting fatigue phenomena

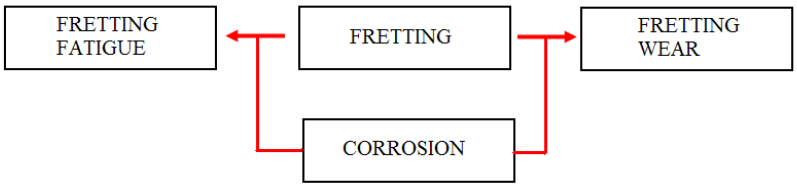

Figure 2.2 Types of surface degradation on a fretting situation [30]

Fretting fatigue is the most damaging aspect of fretting that leads to early cracking and shorter life relative to the plain fatigue situation. Under fretting fatigue conditions, fatigue strength or endurance limits can be reduced by as much as 50 to 70% during fatigue testing (see 2.3.1 Introduction). During fretting fatigue, cracks can initiate at very low stresses, well below the fatigue limit of non-fretted specimens. Cracks due to

fretting are usually hidden by the contacting components and are not easily detected. If conditions are favorable for continued propagation of cracks initiated by fretting, catastrophic failure can occur.

There are many application fields were this phenomena arise such as the aerospace industry, human body implants, the automobile industry, etc [1,5,15,27,31-37]. Much attention has been given to fretting fatigue of aerospace materials in recent years because of the impact that unfortunate catastrophic air disasters have on individuals and families [1,13,35,38-40]. For example, on January 24, 1998, a Lake LA-4-200, N2994P, registered to Sylvan Educational Endeavors, was substantially damaged during take-off from Lake Evers, near Sarasota, Florida. Metallurgical examination of the failed fitting/beam attach for the left horizontal stabilizer that revealed it failed due to fatigue caused by fretting wear. Additionally, a crack associated with fretting wear was detected on the right side fitting/beam attach part. Fretting wear was also detected on both the left and right angle/top beams [reported in 41]. Figure 2.3 [30] shows that fretting fatigue phenomenon occurred in a formed automotive suspension component that is attached to another component by means of a screw (zone A). Besides the load transmission there is a relative motion between the screw head and the component. Figure 2.3a presents the formed suspension component and figure 2.3b shows a detail of the fretting fatigue damage location (the crack due to fretting).

(a) (b)

Figure 2.3 Case study - formed automotive/vehicle suspension component: a. a formed component; b. detail of the fretting fatigue damaged location [30]

2.1.2. Factors influencing fretting fatigue

Several researchers stated [4,42] that there are around 50 factors that might cause considerable variation in the fretting fatigue behaviour/life. Few notable among them

are: normal load, tangential load, relative displacement amplitude, applied bulk load, contact geometry, temperature, frequency, hardness, coefficient of friction, surface conditions etc. Although these factors will be presented separately, it will be seen that there are strong synergy links between many of those variables.

At present, it is generally accepted that some (unknown) convergence of some local parameters is responsible for a reduction in fatigue life. However, the exact characteristics of all influencing parameters and their individual relative effects on fatigue life are not known. Technical literature reports vary, sometimes significantly, in the assessment of the influence of these variables. The difference can be explained by the use of testing procedures of the fretting process that have not been standardized yet, different materials, geometries (2.1.2.4 Brief presentation of other factors on fretting fatigue life), different types of loads and equipments (see 2.1.4 Types of fretting fatigue tests and apparatus). This causes a large scatter on the results, making it sometimes difficult to draw quantitative conclusions regarding the changes and influence of the various factors involved. All these facts create extreme difficulties in obtaining experimental data on the influence of a single variable on the fretting process.

2.1.2.1 Normal contact load

Normal contact load is a significant variable on fretting fatigue, being important to look at its effect on fretting fatigue life. In general, if normal contact load increases the fretting fatigue life should decrease because of the monotonous increase in frictional stress amplitude with contact pressure. The reports in the technical literature regarding its influence on fretting fatigue life lead to contradictory conclusions [43]. Some researches state that normal contact load have a significant influence on fretting fatigue life [44,45] while others consider that its influence is insignificant [46-48]. In order to asses the effect of normal load on fretting fatigue life it is important to look at its variation with the number of cycles, and also at its interaction with different factors/variables.

I. Evolution of the normal load during fretting fatigue tests

Jin and Mall [31] showed that the normal load decreases during a test to about half the value of the initial load. They attributed this decrease to the material removal which did not cause specimen rupture. The same authors in another test kept the normal load approximately constant by increasing it after each drop of 10% (for gross slip regime).

The fretting fatigue life of the specimen when the normal force was maintained approximately constant was shorter than when the normal load decreased during the test. In order to overcome the previous phenomena several authors used different arrangements in their devices. Most of them applied the normal load using a set of springs in order to maintain it roughly constant during the whole test [46,49-53]. Szolwinski and Farris [54], in order to apply a constant normal load to the pad, used a set of drawbars passed through the chassis. Matlik and co-authors [55] also maintain the normal load almost constant by tightening through rod nuts on the normal load transfer through rod. Using these devices the normal load was roughly constant during the duration of the tests.

II. Interference between normal load and different factors/variables, and the influence on life

Regarding the influence on the normal load on fretting fatigue life the technical literature presents contradictory results as mentioned before. This can be attributed to the different conditions and apparatus used to study the fretting fatigue phenomena.

Nakazawa and co-authors [44] reported that fretting fatigue life (crack "initiation") decreases linearly with the increase of normal force. For an austenitic stainless steel, it was found a critical contact pressure above which no further degradation occurred. It was observed that the fretting fatigue life was almost unchanged at contact pressures of 15–45 MPa. However, it decreases drastically at contact pressures beyond 60 MPa. It was also mentioned that the contact pressure dependence on life is depended on the materials used. Also it was observed the increase of the fretting scar depth with the increase of contact pressure. A similar behaviour has been observed by others researchers [45,56].

Ramalho el at. [46] evaluated the effect of the normal load on fretting fatigue life of EN H320 M steel. They reported that within the range investigated the normal load do not significantly affect fretting fatigue life. They observed only a small variation for a high contact pressure. Fouvry et al. [47] carried out some experiments under partial slip conditions. The results showed that the normal load had a very low effect on the nucleation conditions. The same behaviour was obtained by Proudhon an co-workers [48].

Ramakrishna et al. [18] observed that with an increase in contact pressure, the fretting fatigue life exhibited a variable behaviour. It has been shown that by increasing the contact pressure, fretting fatigue life reached a minimum at 100 MPa contact

pressure, and reached a maximum at a contact pressure of 150 MPa decreasing thereafter. This behaviour was attributed to changes on frictional stress, critical relative slip, crack growth retardation effect due to crack closure at high contact pressure and stress concentration effect.

Several researchers reported that the effect of *normal load* on fretting fatigue life depends on the load application *frequency*. Iyer and Mall [57] observed that at 1 Hz, normal load affects fretting fatigue life, while at 200 Hz no effect on the fretting fatigue life was observed. Jin and Mall [22] reported a different result. At 2 Hz fretting fatigue life was not affected by the increase on the normal load. They considered that there are other factors, whose effect is greater than of normal load.

Some researchers observed that the *normal load* has a very close relation with the tribological condition in the contact – *wear*. Experimental research of Magaziner et al. [58] demonstrated that the wear volume is related with the magnitude of the normal load. It was concluded that there is a linear relation between normal load and wear volume. Sarkar el at. [59] also examined the effect of normal load on the wear mechanism, under fretting wear tests. It was noted a transition in the wear mechanism by increasing the normal load from 8 to 10 N. Although the tribochemical wear remained active, the plastic deformation induced damage significantly contributed to increase the wear rate of Ti3SiC2. There are also contradictory results regarding the relation between normal load anw wear. For instance, according to Bryggman [60] the overall wear scar is little affected by the variation of the normal load.

The relation between *normal load* and *relative displacement amplitude* was also studied. It has been stated [31,61,62] that the slip zone size is dependent upon the magnitude of the normal load. Jin and Mall [31,61] examined the effect of normal load on the slip zone, having observed that by increasing the normal load from 1334 N to 4000 N the slip zone decreased.

2.1.2.2 Tangential contact load

The tangential load is a consequence of the contact friction between pads and specimen and it is another parameter that affects the fretting fatigue life of a component/specimen. In a fretting fatigue situation the tangential load is typically cycled with the bulk load cycles.

n order to see the influence of this parameter in the fretting fatigue behavior, firstly it will be presented its variation of it with the number of cycles (for different fretting fatigue equipments) and then its interference parameter with different factors/variables.

I. Evolution of the tangential load during fretting fatigue tests

It has been observed that there are contradictory results in relation to tangential load evolution during a test. The explanations for the obtained results are also not coincident.

Jin and Mall [22] showed that the maximum tangential load in some situations continuously increased, or increased and suddenly dropped. The sudden drop in tangential load was explained by the decrease in the applied normal contact load, resulting from material removal of both specimen and pad. Jin [31] in another investigation, showed the typical evolution of tangential load under both partial slip and gross slip fretting conditions: in partial slip the tangential load quickly stabilized and remained constant throughout the test; in gross slip conditions the tangential load monotonically increased and then decreased at some points during fretting cycles. Wittkowsky [49] observed with his particular apparatus that the maximum tangential load decreased in the beginning (few hundred of cycles) then stabilized with the increasing number of cycles.

Regarding the variation of the maximum and minimum tangential force ($F_{t,max}$ and $F_{t,min}$) with the number of cycles, it increased/decreased, respectively, during the early stage of fatigue and then stabilized to certain values. Under the partial slip fretting regime the maximum tangential load was maintained to a low value and for the gross slip fretting regime it increased up to a certain point and then decreased. The drop of the maximum tangential force was due to the removal of material at the contact surface [63]. Regarding the evolution of the amplitude of tangential load during a fretting test, some research works [8,30] state that it initially increases and then stabilizes after about 100 cycles. Huang [64] carried out fretting tests under different conditions. He observed, for all fretting regimes, an initial drop in the tangential load amplitude reaching a minimum in less than 200 cycles. For the partial slip situation, the tangential load amplitude remains stable. For the mixed and gross slip regimes the tangential load amplitude rapidly increases over the next 2000 cycles until the response becomes quasi-stable. The drop of the tangential load amplitude in the beginning of the test is attributed to the formation of a tribologically transformed structure in the surface layer.

II. Interference between tangential load and other factors/variables

As the *tangential load* is in synchronism with the axial load of the machine, the magnitude of the tangential force is larger at a higher bulk stress than at a lower applied bulk stress [65].

Any small change in the tangential load leads to a big change in the relative displacement amplitude. Zhou [66] in another investigation observed that as the tangential load increases the slip region also increases and the stick zone decreases, until full slip occurs within the contact.

2.1.2.3 Relative displacement amplitude

Relative displacement amplitude has been recognized as one of the most important parameters in fretting fatigue behaviour which control crack initiation and propagation processes [7,8,22,46,67,68].

The influence of relative displacement amplitude has been known for many years. One of the first comprehensive investigations of the effects of slip was carried out by Nishioka and Hirakawa (1969). Their investigations were concentrated mainly on the partial slip regime but other works extended the study to the regime of fully-sliding contact (Spink, 1990) [7].

In order to highlight the effects of the relative displacement amplitude in fretting fatigue life first we will see how it changed with the number of cycles (for different equipment and test conditions), and also which are the interactions of this with different factors/variables.

I. Evolution of the relative displacement amplitude during fretting fatigue tests

Much attention has been given to the average and the maximum value of the relative displacement amplitude for total fatigue life, but very little attention has been given to its evolution during a test. Vingsbo and Soderberg [8] showed that there is a critical value of the relative displacement amplitude below which fretting fatigue life decreases with amplitude, and above which fretting fatigue life increases with amplitude. Favrow and Anton [as reported in 22] observed that relative displacement amplitude has a much bigger effect on the fretting fatigue life on the Ti-6Al-4V alloy that the normal contact load. A study of the effect of the relative displacement amplitude on

the fretting fatigue life of an automotive formed suspension component [30], showed an increase in fatigue life by increasing the relative displacement amplitude (above 30 μm).

II. Interference between relative displacement amplitude and other factors/variables

The effect of the relative displacement amplitude on fretting fatigue life (figure 2.4) has been reported by Vingsbo and Soderberg [8]. It has been summarized the effect of slip amplitude on wear rate and fretting fatigue life. At low slip amplitude fretting is mild and long fatigue lives were recorded. The wear rate is correspondingly low. As the slip amplitude is increased, the fatigue life falls and the wear rate increases as a result of the increased fretting. A minimum in fatigue life is eventually reached, often around the transition from partial slip to full sliding. The wear rate continues to increase if slip amplitude is increased beyond this value, but the fretting fatigue life increases again. This phenomena of increased life is often interpreted as being the result of the rapid increase on in wear rate. Although fretting is quite severe and cracks are readily initiated, the enhanced wear rate means that embryo cracks are worn away before they have chance to grow, and hence wear becomes the dominant manifestation of fretting [7]. This relation between the relative displacement amplitude, wear and fretting fatigue life has been confirmed by others researchers [58,60,62].

Based on the experimental fretting data, different numerical values of the upper transition of the relative displacement amplitude have been proposed in the literature, mostly in the range 150 – 300 μm. A lower transition of the relative displacement amplitude bellow which no surface damage occurs may also exist, but it has been shown that fretting damage can occur for displacement amplitudes down to, and even below, 1 μm [8]. For example, Tomlinson [cited in ref. 3] showed that extremely small movements of the order of a few nanometers were capable of causing damage in the case of a steel specimen.

Huang et al. [69] observed the effect of relative displacement amplitude on coefficient of friction (COF). The results showed a significant difference between the two alloys: AZ91D and AM60B alloys. In the range of low amplitudes, the increase of COF with the relative displacement amplitude was much higher in the case of AZ91D alloy than AM60B alloy.

Madge and co-authors [70] observed that the propagation period is less sensitive to relative displacement amplitude than the initiation period.

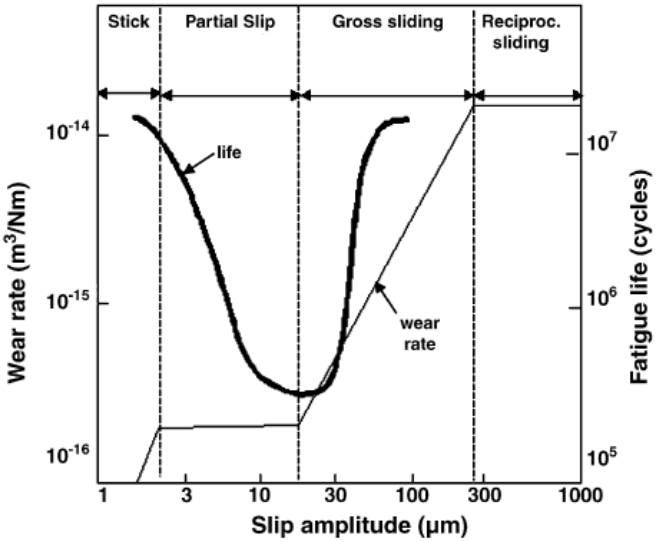

Figure 2.4 Fretting fatigue life vs. relative displacement amplitude [8]

Pape and Neu [71] investigated the fretting fatigue behavior of 4340 steel and they observed that by increasing the relative displacement amplitude between the two contacting bodies there is a slight increase in the surface roughness.

2.1.2.4 Brief presentation of other factors on fretting fatigue life

Besides normal load, tangential load and relative displacement amplitude there are other factors (for example, materials, surface roughness, coefficient of friction, contact geometry, frequency, environmental conditions, temperature etc.) that have influence on fretting fatigue life/behaviour. As these factors are not part of the present research a brief presentation will be provided in this section.

Materials

Extensive fretting research has been carried out on a wide range of materials, including combinations of similar [22,39,72-75] and dissimilar materials [30,45,76]. It is reasonable to study the fretting fatigue behaviour of dissimilar materials because there are many applications where contact occurs between dissimilar materials. For example, the contact between screw/washer and a formed suspension automotive component [30]; disk/blade attachments in the higher stages of compressor or turbine part of the aircraft jet engines [45].

In the last years much attention has been given to materials used in the aerospace industry, that combine high mechanical properties with low density. Titanium and aluminum [77.78] alloys (for example: Ti-6Al-4V alloy and Al7175 alloy) are widely used

in aeronautical applications. The fretting fatigue behaviour of titanium alloys (particularly Ti-6Al-4V alloy, that is the most widely used since the mid-1980s) had been studied by many researches [22,39,73-75,79]. Ti6Al4V has several microstructural features that lead to highly heterogeneous deformation fields in the fretting damage zone, including two crystallographically distinct phases, slip strength anisotropy, and texture. It is imperative to account for these aspects when evaluating the performance of this material under fretting fatigue conditions [80].

There are also researchers that have been chosen to investigate the fretting fatigue behaviour between dissimilar materials. For example, Ti–6Al–4V/Al2024 [81], Ti–6Al–4V/ Inconel 718 [81,82], 30NiCrMo8/52100 [83], etc.

As expected all these materials have a different behaviour under fretting fatigue conditions because of their different mechanical and cyclic properties. For example, Gaspar and co-authors [84] investigated the effect of alumina and steel on the fretting behaviour. The material used for the specimen was a stainless steel 310 (AISI) and for the pad they used two different materials, namely AISI 52100 steel and corundum (99.7% Al_2O_3-alumina). Different wear mechanisms for the two types of pad materials tested were observed. The steel pad promoted the formation of iron oxides in the sliding areas of the fretting contacts. These oxide layers formed had a protective effect against fretting wear. As a result, the wear volumes for steel were lower than those for the alumina pad. Ivabuchi [85] carried out fretting fatigue tests with two materials: Co-29Cr-Mo alloy and Ti-6Al-4V alloy against Al_2O_3 in a quasi-body fluid (Hanks ´solution). Titanium alloy showed a better fretting resistance compared with Co-alloy.

Surface roughness

Surface roughness affects the mechanism of fretting fatigue, as this phenomena arises as result of surface interaction between contacting bodies. Some efforts have been made to understand the effect of surface roughness on fretting resistance, and different results were obtained.

Contrarily, to the fatigue situation, where a rough surface is very dangerous because it contains potential stress raisers (asperities concentrate the load in small areas of contact producing correspondingly high level of stress), in a fretting fatigue situation it has been reported that a high degree of surface finish accentuates fretting damage [3,27,86,87]. Waterhouse and Trowsdale [87] stated that increasing roughness is progressively less damage in fretting fatigue because the incipient cracks are prevented from propagation by the compressive stress imposed by fretting pad.

Increased roughness results in smaller discreet areas of real contact so that the critical volume of material per contact to initiate a crack, as proposed by Bramhall, is not achieved. A rough surface has a higher plasticity index than a smooth surface, so some plastic deformation will occur at the tips of the asperities.

There are also studies that reported that the increase in surface roughness leads to an increase of others parameters that will increase damage. For instance, the increase in surface roughness results in an increase in the coefficient of friction, which is not beneficial for fretting fatigue resistance [27,61,86].

The main difficulty in fretting fatigue situation is that the roughness is different in the stick and in the slip zones, and this changes during the life time [72]. It is well known [11,88] that the surface roughness of the slip is much higher compared to the roughness of the stick zone. As a result, the increase of the surface roughness of the contacting bodies is attributed to the occurrence of slip [39,61]. Sometimes was also observed a slight increase of roughness in the stick region, which has been attributed to asperity yielding and microwelding [8]. In some situations [73], conditions and relative displacements of the order of tens of microns, of the type produced with some test apparatus no correlation could be drawn between surface roughness and fretting damage for the mixed stick-slip zone. Regarding the variation of roughness with the number of cycles it has been reported that the roughness increases with the number of cycles [39].

Although in many studies [89,90] it has been suggested that the initial surface roughness of the contacting bodies is a factor that could markedly alter the total fatigue lives (the fretting fatigue behaviour), the effect of roughness is still neglected in the analysis to estimate fretting fatigue life.

Coefficient of friction

In the fretting fatigue case it is important to draw a clear difference between the static coefficient of friction and the dynamic coefficient of friction (or kinetic COF, or normalized frictional force). The *static coefficient of friction* is defined as the "friction coefficient corresponding to the maximum force that must be overcome to initiate macroscopic relative motion between two bodies. The *dynamic coefficient of friction* is calculated as the ratio of the tangential to the normal load and it is defined as the "coefficient of friction under conditions of macroscopic relative motion between two bodies". The stick-slip situation occurs when the dynamic coefficient of friction is higher than the static coefficient of friction [23].

The coefficient of friction depends on the fretting regime. If the two bodies are subjected to fretting in partial slip (as in the case of the present study), there will be surface modification due to relative motion in the slip zones. Figure 2.5 shows the evolution of the friction coefficient during fretting contact in the partial slip regime (Hertzian case). It can be seen in Figure 2.5 (a) that initially the COF is constant in both zones of contact (slip and stick). From figure 2.5 (b) it can be observed that after n cycles, when the central zone will develop (stick zone) the COF increases in the slip zone. This increase was attributed to surface modification [91].

As reported in [27] the increase of COF modifies the stress level and changes the location of the maximum loading. Less COF should lead o a smaller slip region, and consequently low damaged area. In practice, much effort has been made to reduce the COF. The decrease in COF can also improve the fretting fatigue strength because of the decrease in the alternating tensile tangential stresses. It is these high alternating stresses that result in local high strain fatigue and the rapid initiation of fatigue cracks.

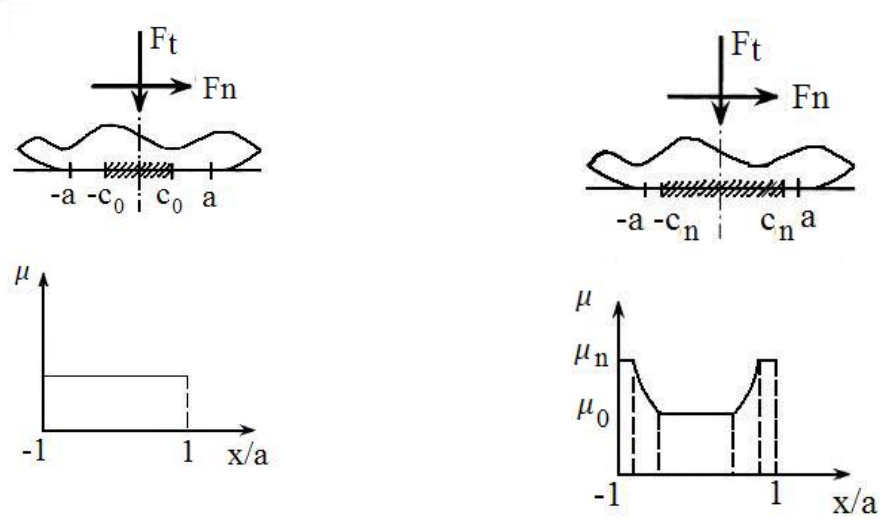

Figure 2.5 Evolution of friction coefficient during fretting contact (Hertzian case): a. initial conditions and b. after n cycles [91]

As it is already known the COF decreases with an increase on the normal load [92,93]. Fouvry et. al. [92] showed that for 300 N normal load, the friction coefficient was equal to 0.97 whereas it decreased to 0.85 when the applied normal load was 500 N.

Regarding the evolution of the COF with the number of cycles, several researchers reported [40,94,95] that COF increases during the early part of a fretting fatigue test and then reaches a constant value in about a couple of a hundred to thousands cycles. Lee and Mall [95] attributed the increase of static COF in the beginning of the tests to the increase of roughness of the contact surface due to the fretting action. It was also stated

that increasing the applied bulk stress, applied relative slip and the hardness of the pad material, results in an increase of the dynamic COF. A opposite behaviour (decrease of dynamic COF) is observed if the normal load, temperature or frequency are increased.

The main difficulty is which value of the COF should be used in the fretting fatigue damage analysis. The COF value typically assumed in these analyses represents an average value under steady-state conditions in a gross sliding test. Swalla et al. [96] studied the COF on the local elastic/plastic state stress. The COF in Swalla´s experiments was measured during the first 200 fretting cycles when gross sliding occurs, and increased from 0.36 (at cycle 60) to about 0.75. It was found that using a higher COF in elastic/plastic analysis (FEA) of fretting fatigue the results are closely approximate to the experimental observations.

Contact geometry

In a practical application, by designing the appropriate contact geometry, stress concentration and consequently the fatigue cracks can be avoided. For example, in a study [30] about an automotive-formed suspension component it was showed that a significant improvement in fatigue life could be achieved with a small change on the contact geometry (introducing a curvature radius on the head of the original screw). This small change on the geometry reduced locally the stress level and increased the relative displacement amplitude and consequently fatigue life.

Hills and Nowell [7] classified the most used contacts in fretting situations, as follows:

(a) incomplete and non-conformal
(b) complete
(c) incomplete but with singularity
(d) incomplete and conformal
(e) receding.

The geometry of the most used contacts is presented in figure 2.6.

Several studies showed that there is a great influence of the contact geometry on life, being identified a critical contact width [72,79,97] at which a drastically change in fretting fatigue life was observed. Magaziner [72] showed that the critical contact width is a demarcation of value condition between partial slip and gross slip. The tests with a contact width greater than the critical value had relatively shorter lives. Fatigue occurred

in less than 75000 cycles. On the other hand, tests with contact width less than the critical value had almost infinite life, e.g. greater than 1 million cycles. Changes in relative displacement amplitude with the contact width have also been observed.

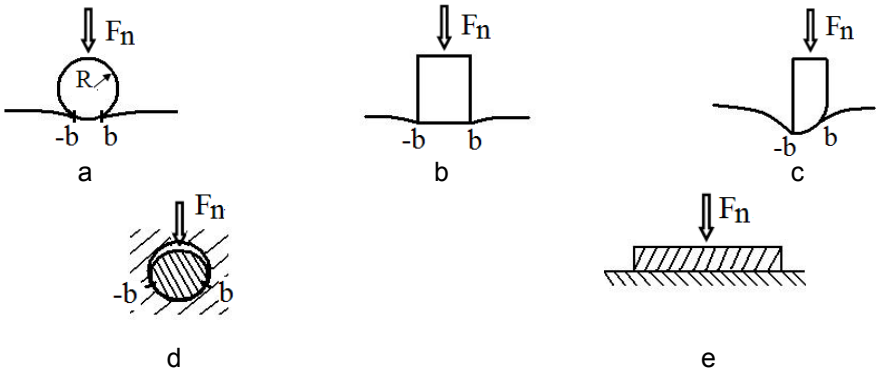

Figure 2.6 Geometry of contacts [7]

Regarding the influence of contact geometry in other variables, Navarro [98] used different geometries for the pad (cylindrical and spherical) observing that throughout the tests that were analyzed, the stress level are higher in spherical contacts than in cylindrical contacts. It was also stated that the initiation phase is more important in cylindrical contacts than in spherical contacts. Lykins and co-authors [51] by changing the contact conditions (the pad geometry) obtained a considerable variation in the slip amplitude at the contact surface.

Load frequency

Load frequency interacts with several parameters (e.g. normal load, temperature etc) and influences the fretting fatigue behaviour.

Regarding the relation between frequency and normal contact load, it was observed [57], for low frequency (0.1 Hz -1 Hz) and high normal load, a considerable reduction on fretting fatigue life. Increasing the frequency (to around 200 Hz) the previous effect was not discerned. The reduction of life at low frequency was attributed to the increase of wear volume [reported in 3].

Bryggman et al. [60] observed that increasing load frequency leads to a higher temperature rise in the narrow fretting zone, this leading to more damage.

In the partial slip situation, although there was little effect on measurable wear, the increase in the interfacial strain rate at high frequencies led to increased fatigue damage and increased corrosion due to the rise in temperature. However in the gross slip situation there was little effect over the frequency range 100 to 20×10^4 Hz [3].

Environmental effects

Obviously, most investigations reported cases of fretting in normal atmospheres, but there are also situations in which fretting occurs under different conditions. The effect of environment on fretting fatigue depends on the material and its corrodibility, and should be taken into account in the fretting fatigue studies.

Some researchers stated that the environmental effects are secondary, but for example the fretting fatigue lives for 7075-T5 aluminum alloy specimens tested in a vacuum were found to be between 10 and 20 times longer than lives for specimens tested in air. Elliot [99] concluded that the fretting fatigue life in air compared to a vacuum is material dependent.

Temperature

The contact temperature is a dependent variable, being a function of size and shape of the real contact area, as well as of the thermal properties of the contacting bodies, coefficient of friction, normal load and sliding velocity. Temperature may affect the process of fretting in two ways: firstly, the corrosion and oxidation rates usually increase with temperature; secondly, the mechanical properties of materials change with temperature. There are not many studies giving attention to this subject and the published results vary significantly.

Regarding the temperature produced in the fretting contact zone, it has been reported in the technical literature that it is bellow 10˚C [100].

Generally speaking most of the researchers observed that the fretting fatigue life of the components working at high temperatures is much shorter. Lee and co-authors [75] in his study about fretting fatigue behaviour of shot-peened Ti–6Al–4V alloy at elevated temperatures found that the conventional fatigue strength of shoot-peened specimens decreased with the increase of the temperature, and attributed this to increased roughness.

Jin and co-authors [65] studied the fretting fatigue crack initiation in titanium alloy, Ti6Al4V, at elevated temperature. The results of these experiments are as follows: first of all, experiments indicate that the 260°C of temperature did not change the fretting properties of this material. It was observed that the life reduction due to the fretting fatigue elevated temperature is the same as at room temperature fretting fatigue. Low temperature, on the contrary cause an increase on fretting damage which generally increases with the number of cycles [101,102].

2.1.3 Fretting regimes. Fretting maps

The technical literature presents associations between several variables, such as normal load, tangential load, relative displacement amplitude and maximum cyclic stress. These relations are presented as fretting maps [13,66,92,103-111] which are used to describe the fretting process. Most of them were established for fretting wear conditions, very few referring to fretting fatigue conditions (including fatigue cyclic stresses). Fretting maps were established not only for materials such us aluminium alloy, iron-based alloy and titanium alloy, but also for various surface modification coatings, including shot-peening plus ion-sulfurization, ion plated TiN and radio-frequency (RF) sputtered MoS_2 coatings.

Vingsbo and Soderberg [8] were the first to introduce the concept of fretting map (Figure 2.4, Section 2.1.2.3 Relative displacement amplitude).

Two categories of fretting maps can be found in the technical literature [13,27,31,87,106,112]:

(i) *running condition fretting map* (RCFM) involving contact conditions or fretting regimes (stick, partial and gross slip);

(ii) *material response fretting map* (MRFM) involving non-degradation, cracking and wear (or debris formation) as a function of normal force and relative displacement for a given experimental condition.

Fretting maps present the interference between different parameters, as follows:

- *tangential load (or/and wear rate) - relative displacement amplitude* ([8,113]. With this type of fretting maps it can be found the critical relative displacement amplitude and tangential load values for the transition from one fretting regime to another. So, it is possible to identify the fretting regimes.
- *normal load - relative displacement amplitude* [8,27]. The normal load increases linearly with the relative displacement amplitude and from this fretting map the fretting fatigue regimes can be identified.
- *contact pressure - relative displacement amplitude*. The contour of fretting fatigue life instead of crack nucleation and propagation was clearly observed. With this map was not possible to identify the fretting regimes and wear conditions [113].

- *normal load and tangential force* These maps show the interdependence between normal and tangential load variations in controlling the contact conditions. Vingsbo [8] stated that by increasing the normal load the wear rate will be reduced.
- *frequency - relative displacement amplitude* Vingsbo et al. [8] stated that frequency is a more powerful instrument than forces and displacements for controlling the fretting characteristics, as frequency variations will influence the mechanical properties of the material both through temperature effects and strain rates hardening effects.
- *normal load* and *maximum cyclic stress*. Petiot [87] stated that fretting-fatigue regimes (accommodation of displacements) and damage mechanisms can be identified with operating parameters (F_n – normal load, σ_{max} – maximum stress) by varying the clamping force for each σ_{max} value investigated (unprotected 3Cr-1MoV steel). This type of fretting maps is give information on the susceptibility of the alloy to fretting crack nucleation.

Normal load, tangential load and relative displacement amplitude seem to be the most important parameters that control fretting, as the majority of the fretting maps are based on them.

Three regimes have been identified increasing the applied displacement amplitude [114]:

1. Partial slip regime (PSR) (stable partial slip)
2. Mixed fretting regime (MFR) (unstable combination of partial-gross slip conditions)
3. Gross slip regime (GSR) (stable gross slip conditions)

Figure 2.7 shows the illustration of the partial and gross slip regimes. It can be seen that the partial slip is characterized by a closed elliptical fretting loop, associated with a composite contact displaying sliding and sticking zone. The gross slip condition which is indentified by a quadratic dissipative fretting loop is related to full sliding occurring over the entire interface.

As it was mentioned in the beginning of this chapter (2.1.1 Introduction**)** there are different modes of fretting, tangential and radial fretting. Up to now, to the author's knowledge all maps are limited to tangential fretting.

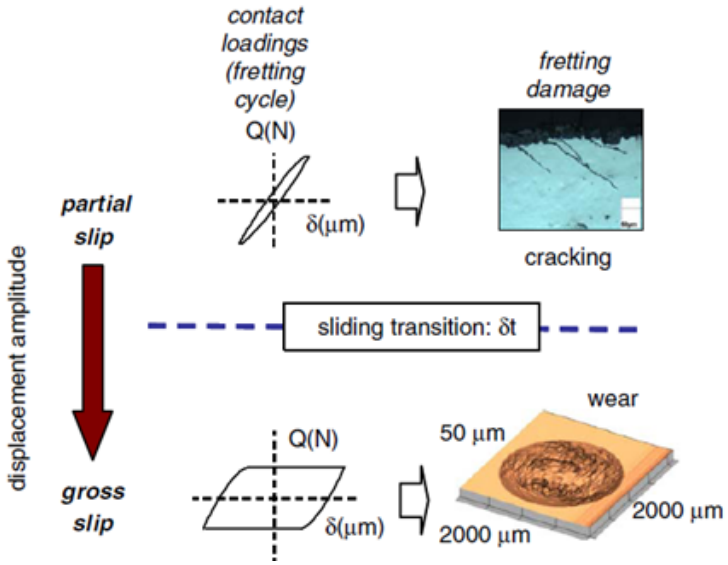

Figure 2.7 Illustration of the fretting regimes: partial slip and gross slip [114]

2.1.4 Types of fretting tests and apparatus

D. A. Hills and D. Nowell [7] have presented three general categories of fretting fatigue tests:

(i). *Simulation of a real engineering fretting problem.*

In this kind of tests the intention is to reduce as carefully as possible, either full size or possibly on a reduced scale, the contact problem arising in the prototype. This clearly has a big advantage over other kind of tests in so far as there is a real attempt to simulate the conditions of the fretting contact itself as accurately as possible. Results obtained with this test apparatus could be carried over without modification to the real engineering problem.

(ii). *Material ranking tests*

The intention of these tests is to assess a material´s resistance to fretting fatigue in some general way. A simplified geometry is chosen so that accelerated tests may be conducted, but little attention is paid to the details of the contact conditions. Instead, it is assumed that the same contact geometry is repeated for every test. It is also tacitly assumed that the material ranking may be carried over to other kinds of fretting contact. The advantage of this kind of experiment is that the tests may be run very rapidly.

(iii). *Idealized fretting fatigue tests*

This basic philosophy here is to carry out a series of tests under very well defined, simple contact geometries. These are chosen so that it is possible to deduce in closed form as many of the pertinent variables as possible (for example: stress, relative displacement). The objective is to understand much as is possible the mechanism of fretting fatigue process. Tests of this type are therefore quite different from others mentioned above, as the results are intended to be applicable to a wide range of geometries quite different from those used in the tests themselves.

Each category of tests has its merits, and serves a different purpose. Furhermore, in order to study and gain a better understanding of fretting, it is essential to recognize the two types of fretting: fretting wear and fretting fatigue. Figure 2.8 shows the fretting test conditions and damage evolution. They are interconnected but they also exhibit some specific characteristics. As a result, two different tests have been developed:

1. The *fretting wear test* where a contact load is generated by a relative motion between two surfaces. This corresponds to very small displacement amplitudes of a classical tribological wear test called “reciprocating test”.

2. The *fretting fatigue test* corresponds to the adaption of a fatigue test where two pads are pressed on the fatigue specimen. Submitted to external bulk loading the strain generated through the fatigue specimen induced a relative displacement between the two contacting surfaces and consequently a cyclic tangential contact loading. This configuration is used to analyze cracking because after crack nucleation the external bulk loading favors the propagation and then the breaking of the specimen [24].

While experimental research into fretting has been conducted for decades, it is still difficult to invent an apparatus to capture the complex mechanical and environmental conditions driving fretting damage present in even apparently basic mechanical systems. The factors/variables that influence directly or indirectly the fretting phenomena (previously presented in Section 2.1.2 Factors influencing fretting fatigue) have a strong dependence on the test method. Each researcher uses his own type of test method. A standard method has not been established yet, since situations are different among researchers and depend on what they wish to study. Kondo [115] stated that the significant dependence on test methods introduces complexity in the understanding of fretting (fatigue).

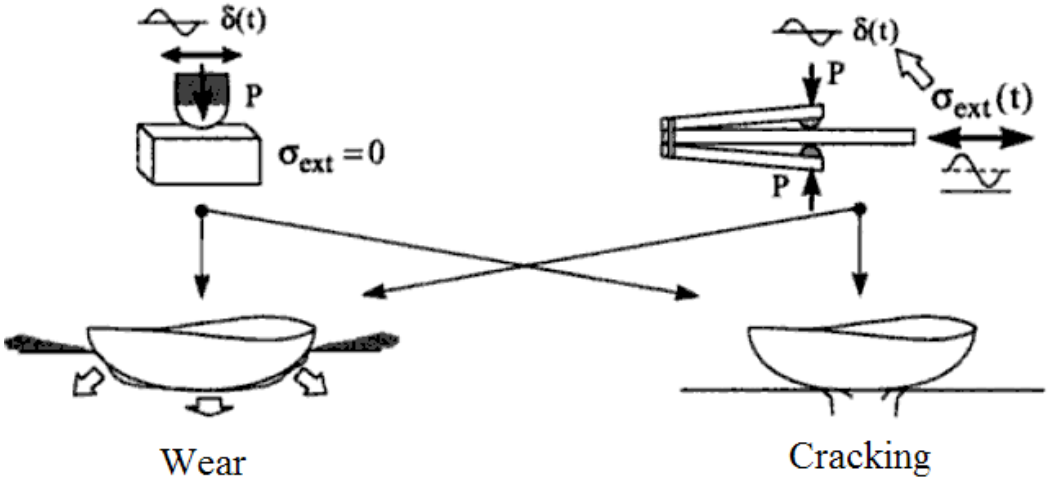

A b

Figure 2.8 Fretting test conditions and damage evolution: a. fretting wear test; b. fretting fatigue test [24]

In the technical literature fretting fatigue testing equipments can be found ranging from very simple devices to more complex systems. Almost all the devices for fretting fatigue use a servo hydraulic testing machine [45,49,75,116].

However, most fretting fatigue features involve the application a cyclic tangential load to the pads and a normal load that presses the pads into contact against the specimen. In many configurations, an additional cyclic bulk stress is induced in the specimen under the influence of oscillatory torsional, bending or axial loading [11].

The geometry of the pads can be spherical, cylindrical or flat For most fretting fatigue testing, fretting pads are positioned on opposite faces of the sample and can be either single or double tracks.

Figure 2.9 shows the most commonly used type of fretting fatigue apparatus. It uses two fretting pads that are pressed against the specimen surface, a constant normal load being applied via the lateral springs. While the force applied to these springs is kept constant, it is possible to apply a cyclic axial stress on the specimen (the pads are kept fixed in the vertical axis with the help of two springs). With this type of apparatus it is only possible to measure the axial load by a load cell that is part of the servo hydraulic test system. The contact force is measured on each side of the fretting specimen by pressure gages, being assumed that it remains constant during the whole fretting fatigue test [44,50,75].

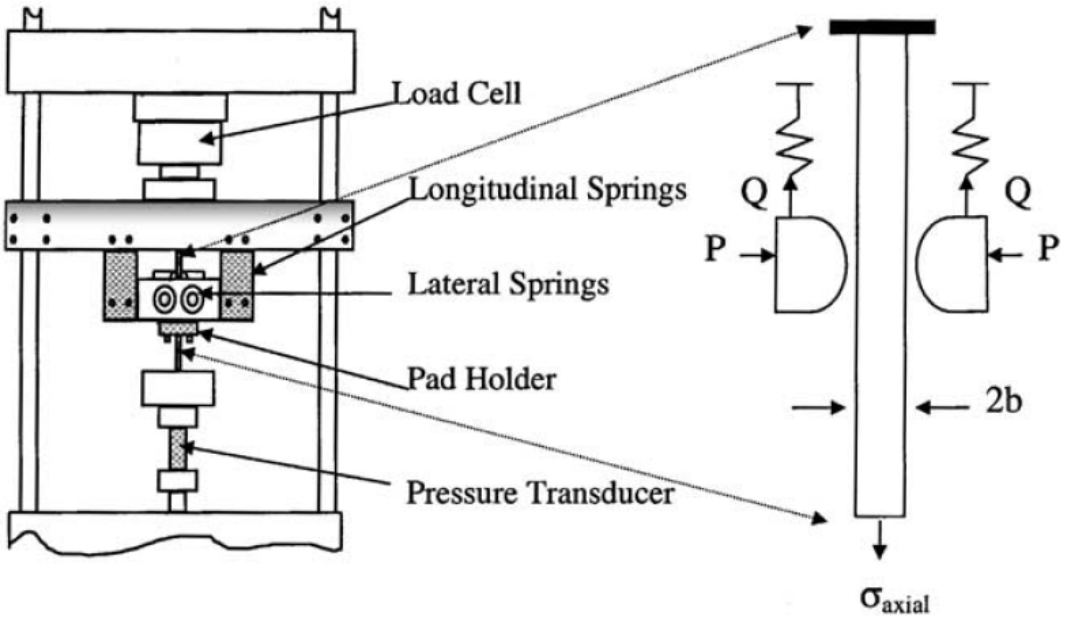

Figure 2.9 The most commonly used fretting fatigue test apparatus [45,50,75]

Another type of fretting fatigue apparatus can be seen in figure 2.10. The device is assembled on a servo hydraulic machine. Throughout each test this system is capable of monitoring data including the normal force and the relative displacement between pads and specimen (clip gage displacement). The main advantage of this apparatus when compared to the one shown in figure 2.9, is its ability to measure the relative displacement of the fretting pads by means of a clip gage (see figure 2.10) [116].

One of the most complete apparatus for performing fretting fatigue experiments is shown in figure 2.11 [49]. This apparatus, like those presented previously, was designed to be used in conjunction with a servo hydraulic test system. It is claimed that this device can allow accurate measurements of the normal force, the tangential contact force and the relative displacement between contacting surfaces. This equipment uses two load cells to measure the normal force and four load cells to measure the tangential force exerted on the fretting pads by the specimen. The friction coefficient is determined as the quotient of the tangential by the normal force values.

All the apparatus described in the technical literature to perform fretting fatigue tests are able to use contact pads of variable geometry, but the system shown in figure 2.11 allows more precise control and measurement of the fretting parameters than the others.

There are also brige –type tests that were first used by Pape and Neu [71] which use a specimen with two physically quite separate contacts connected in the form of a bridge. Almost invariable the bridges have contacting pads which have flat faces, and

therefore form complete contacts. The scheme of the bridge apparatus is presented in figure 2.12.

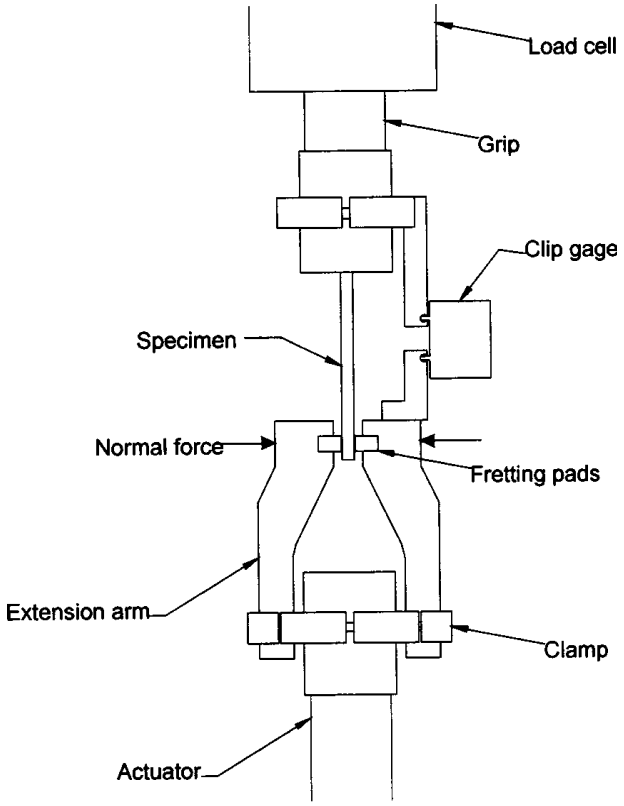

Figure 2.10 Schematic of a type of fretting fatigue apparatus [116]

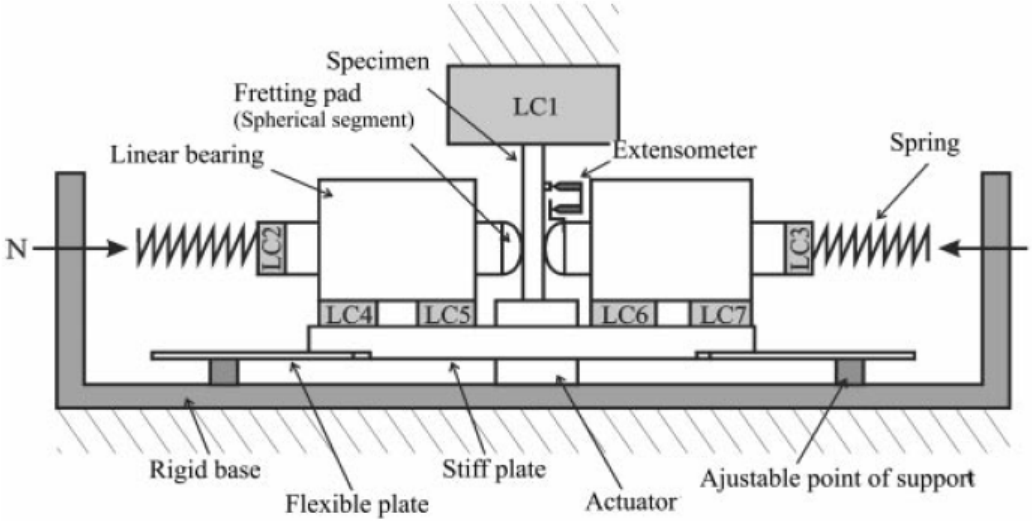

Figure 2.11 Schematic of a type of fretting fatigue apparatus [49]

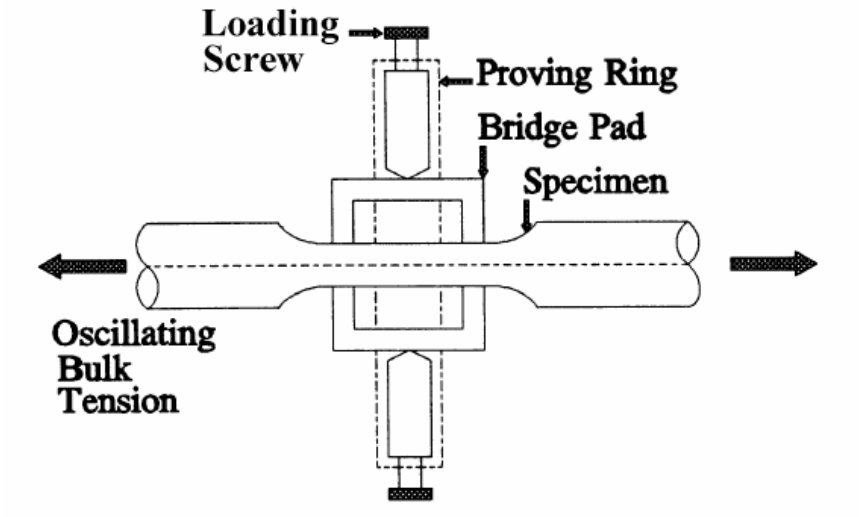

Figure 2.12 Scheme of the bridge apparatus [7]

2.2 Effect of wear on the fretting fatigue process

2.2.1 Introduction

As it has been explained before fretting occurs when two contacting surfaces are subjected to reciprocating motion of small amplitude, of the order of micrometers, whereas the conventional reciprocating motion producing wear involves a much larger amplitude. Fretting is a very complex phenomena, and its wear mechanism involves various types of wear such as adhesive, abrasive, oxidation and fatigue wear. In general, at least two or more mechanisms can occur simultaneously, depending on the operation parameter. The wear mechanism of the reciprocating sliding is comparatively simpler. Because over the years a large number of studies have been carried out many characteristics of reciprocating sliding were understood.

However the effect of the amplitude of reciprocating sliding seems to be ambiguous in the literature, because of the complexity of fretting and the combined effect of contact conditions and materials. Therefore, in literature different transition values for different materials have been presented. Vigo and Soderberg [8] as well as Ohmac and Tsukizoc [as cited in ref.117] suggested that the transition from fretting to reciprocating sliding wear lies at 300 μm, Toth [as cited in ref.117] suggests 50 μm, while Lewis and Didsbury [as cited in ref.117] concluded that the transition occurs at 70 μm.

The kinematic description of the fretting fatigue process is given in figure 2.13. It can be seen that there is compression strain on one side and tensile strain on the other side of the contact zone. For each fatigue cycle the strain on each side will change from tensile to compression strain [118].

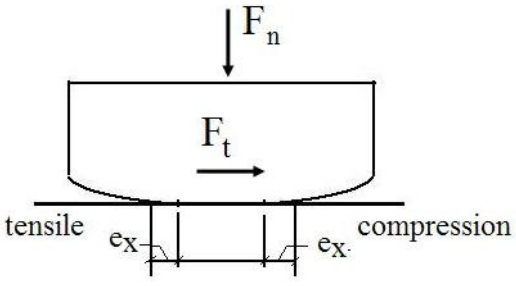

Figure 2.13 Kinematics of the fretting fatigue process (for one cycle) [118]

The fretting fatigue process is strongly influenced by the connection between the stress state (fatigue – axial load and fretting – normal and tangential load) and the wear in the contact region. Thus, it is reasonable to expect that wear, and consequently the

fretting fatigue behaviour/performance of the materials, might be differently affected if the material (specimen) is in tension or compression.

In the technical literature there are many studies presenting models/parameters to predict the fretting fatigue life. Most of them are based on stress and do not take into consideration the influence of wear. Madge and co-workers [118] have shown that wear is a critical aspect for the prediction of fretting fatigue and can have a major effect on the evolution of stresses and damage parameters (e.g. Smith – Watson - Topper), and hence on the predicted fatigue life and crack initiation location. They stated that the fundamental and important effect of wear on fretting fatigue cannot be predicted by models which do not include the effect of material removal due to wear. In particular, fretting studies should not be concerned only with the deformation and stresses at the bodies surfaces, but also with the depth of the surface layers.

In practical applications, when two components are in contact, besides the local contact stresses, one of the components may be under an additional stress state, either in tension or in compression. Perhaps the most common way in which additional stress states exist in a component is when residual stresses are introduced in the component surface. These residual stresses may be introduced due to plastic deformation of the surface of the component. It is also possible to have an additional stress state in a component when there is thermal deformation on the component. This is the case, for example, of disc brakes. An additional stress state may also exist if an external load is applied on the component, thus introducing elastic tensile or compressive stresses. Independently of the way the additional stress state is introduced in the material, it is reasonable to expect that this additional stress state in the disk may affect its wear behaviour.

While technical literature presents different studies relating wear with additional stresses as introduced with plastic deformation (residual stresses) [119,120], only one study was found [121] where the wear behaviour is directly related with the additional stress states in the elastic domain.

2.2.2 Relations between wear and some parameters that control the wear mechanism

As wear is sometimes related directly to hardness or, in other cases, related to residual stresses, or even indirectly assessed, a brief state-of-the-art of those relationships will be subsequently made. Traditionally the wear resistance is correlated to the surface hardness of the materials [122,123]. However, as schematically

presented in figure 2.14, some studies relate directly wear to residual stresses [119,120]. It is also possible to establish indirect relationships between wear and the residual stresses. It is common that residual stresses are related to hardness and therefore wear relations based on hardness are used.

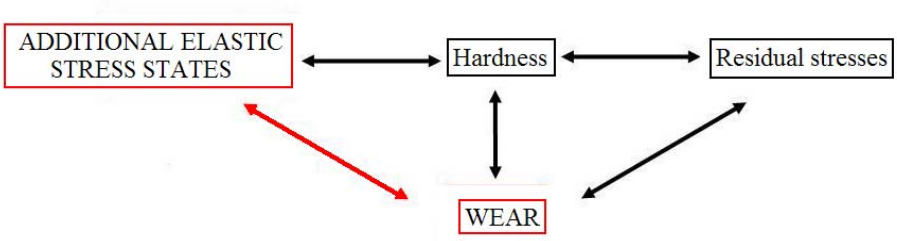

Figure 2.14 Relations between wear and some parameters that control the wear mechanism [124]

Wear/Hardness

Most of the researchers consider important to express the material response in wear as a function of a basic material parameter as hardness [122]. Hardness is considered the main material parameter governing its wear behaviour. For example, Xu and co-authors [123] investigated the effect of hardness in the wear resistance. Their results showed that the relative wear resistance increases with increasing hardness.

The first attempt to relate wear to the mechanical properties of materials was made by Tonn in 1937 [as reported in ref. 125], who proposed an empirical formula for abrasive wear. Later, in 1940, Holm [as reported in ref. 125] using the atomic mechanism of wear as the starting point, calculated the volume of substance worn over a unit sliding path,

$$W = z\frac{F_n}{HB} \tag{2.1}$$

where z is the probability of removing an atom from the surface when it encounters an atom of the opposing member, F_n is the normal load; HB – the Brineell hardness [123].

In particular, Archard proposed in 1953 [as reported in ref. 126] one of the first laws of wear which was considered as a major scientific contribution. It states that dW/dt, the mass of detached matter from the solids in contact per unit time, is directly proportional to the applied pressure P multiplied by the sliding speed V. Equality is observed by the wear coefficient K:

$$\frac{dW}{dt} = KPV \tag{2.2}$$

According to the case, scientists have tried to apply Archard´s law to their own experiences changing the coefficient by several orders of magnitude, and have attempted to complete the law by adding new parameters.

The basic model that is usually used to describe the wear mechanism is the well known Archard´s linear wear equation, given by:

$$V = K\frac{F_n}{H}S \tag{2.3}$$

where $\boldsymbol{V}$ is the volumetric material loss of the body, $\boldsymbol{K}$ - the wear coefficient (it is dimensionless and always less than unity), $\boldsymbol{H}$ is the hardness of the softer body in contact, $\boldsymbol{F_n}$ is the applied normal load and $\boldsymbol{S}$ the sliding distance [126].

Wear/Residual stresses

In the attempt to increase the wear resistance of a material many studies were carried out in the last years using mechanical surface treatments. These treatments commonly introduce residual stresses in the material and its effect on the wear behaviour of the material can be considerable. The residual stresses can be either compressive or tensile.

Cold and hot rolling, shot peening, and more recently laser shock processing and ultrasonic peening, are technological processes that change the material properties in a micro-structural layer under the surface to some millimeters into the material in order to increase the wear resistance. Sanchez-Santana and co-authors [119] investigated the effect of laser shock processing surface treatment on the wear of 6061-T6 aluminium alloy. It was observed that this technical process reduces the wear rate due to the compressive residual stress field induced [119]. In another study on laser peening [120], it was found that the wear rate improves with compressive residual stresses, but only at low contact pressures (pin-disc). Above a critical point, at about 100 MPa of contact pressure, the wear rate reduces with compressive residual stresses.

Wear/Residual stresses or additional elastic stress state

Hardness testing is a well known experimental method used to determine the constitutive property of materials. Then, hardness is correlated with wear by using traditional equations as equation 2.1.

There are two ways of introducing stresses on the material without changing its chemical composition: (i) introducing residual stresses by plastic deformation of the

material surface by using shot peening, laser peening, etc; (ii) introducing an additional stress state by externally loading the component. In this case the component is under an elastic additional stress state.

In what concerns the residual stresses there are some studies correlating hardness and compressive residual stresses. An example is Laser Peening (LP). During this process, shock waves are applied to the sample surface in order to improve the mechanical properties. LP has been shown to improve hardness in a number of metallic materials [120]. This type of surface treatment is known to generate compressive residual stresses and high density arrays of dislocations. It was concluded that LP treatments generate compressive residual stresses (approx., 400MPa) accompanied by a hardening (+10% on hardness) on the sample surface.

Research works concerning the relation between hardness and the stress state of the material, when the stress state is in the elastic domain as introduced, for example, by imposing an external load to a component, are scarce. Carlsson and Larsson [127] in a research paper highlighted two studies: one performed by Kokubo and another carried out by Sines and Carlson. In these works several materials were subjected to applied elastic tensile and compressive uniaxial stresses. It was found that Vickers hardness has only a very small influence on sign and size of the applied stress. They concluded that the effect of the additional stress on hardness was small. No other definite conclusion could be drawn from their investigations, except that there is a small influence of additional elastic stress states on hardness.

Wear/ Additional elastic stress state

Studies on the effect of an additional elastic stress state (stress introduced by an imposed external load) on the wear behaviour of a component are very limited. As a fact only a study was found where Mitchell and Shrotriya [121] investigated the wear response of a cobalt-chromium alloy as a function of a contact load at a nano-level and an additional elastic stress state, as introduced by a bending moment on the specimen, both under compression and tension. This study revealed that for a constant contact pressure the wear rate is accelerated by compressive stresses while the tensile stresses tended to decrease it. The obtained behaviour attributed the change in depth of the wear scar to a surface oxide layer damage and repassivation process.

2.3 Fretting fatigue modelling

2.3.1 Introduction

Generally, fretting fatigue life can be divided into two segments: firstly the initiation or nucleation, and secondly the propagation of a crack. Physically, the former is the period of time required for damage in the fretting contact to develop into a crack of some arbitrary small size. The exact definition of the transition from crack initiation to crack propagation is usually dependent on different theories, namely crack closure, crack growth orientation, capability of the crack evaluation techniques, etc. Based on the different theories, some authors assume crack initiation till a crack length of 0,4 mm, or 0,5 mm, or even 1mm. Other authors assume that crack initiation corresponds only to the first 10 μm. It is not a purpose of this work to define which theory is right or wrong. It is assumed in this work that crack initiation corresponds to about 80-90% of life, as stated by many recent authors. The assumption that initiation life corresponds to almost the whole life of the specimen is also based on results of relative displacement amplitude, made on the same fretting fatigue tests [128].

Some of the research papers assuming that the fretting fatigue initiation life corresponds to almost the total life (80 - 90% of total life), are for example: [51,52,129]. In the last 2 papers is stated that about 90% of total life is spent on crack initiation.

Several authors [89,130] consider that crack propagation corresponds to almost the whole fatigue life. It is worth to note that on the last paper, propagation life started with a crack length of $10\mu m$.

Life prediction models can be included in one of the following general approaches.

The critical point approach theorizes that fretting fatigue damage initiates at a specific point. A scalar is used to describe this point were crack initiation occurs due to a maximum stress or strain.

A well known example of this approach was derived by Ruiz [reported in 131,132]. By analyzing the contacting surfaces of a dovetail joint between the blade and the discs in a gas turbine, they concluded that the surface damage due to fretting depends on work done by the frictional force between the contacting bodies. Thus, they proposed a fretting fatigue parameter which combines the effect of stress and fretting damage given as

$$K_1 = \tau \cdot \delta \tag{2.4}$$

where τ is the local value of shear stress within the contact region and δ is the relative displacement amplitude between the bodies.

The critical plane approach relies on the idea that the critical damage accumulation depends on both the nominal and shear strain along a specific plane. Critical plane parameters are averaged over the fretting fatigue process zone.

Generally speaking, the critical plane approach is done by finding the maximum shear strain amplitude and the plane on which it acts, and then using the maximum normal stress acting upon this plane to obtain the effect of the mean stress [129].

The critical plane based fatigue parameters (described in detail subsequently in this chapter) are:

- Smith-Watson-Topper (SWT) parameter
- Modified shear stress range (MSSR) parameter
- Findley (F) parameter
- Fatemi- Socie-Kurath parameter
- Crossland's multiaxial fatigue criterion

Many fretting fatigue researchers recommend the use of the critical plane based predictive parameters and criteria, because crack nucleation and initiation in fretting fatigue occurs in a contact region between two bodies which is governed by a state of stress that is multiaxial in nature. This has been recently proposed by Namjoshi [14]. However, because the stress required for these parameters cannot be measured accurately using test equipment, they need to be determinate through simulations of tests. These simulations can be based on analytical solutions as well as numerical methods, such as finite element analysis.

SWT [13,51,52,70,133] is the most commonly used model in fretting fatigue for predicting the initiation life. For instance, Lykins [52] investigated the fretting fatigue crack initiation behavior of titanium alloy, Ti6Al4V, using the SWT parameter. The predictions were in good agreement with the experimental observations. Fridrici [133], successfully used the SWT parameter in the case of shot peening specimens. In order to incorporate the compressive residual stresses effect induced by the shot peening on the crack nucleation in fretting wear contact a new residual stress parameter was added to the model.

Araujo [2] has demonstrated that the use of the SWT and the FS (Fatemi- Socie) approaches to estimate the fretting fatigue initiation life of Al4%Cu and Ti-6Al-4V, are not adequate if the calculations are based exclusively on surface stress-strain behavior at highly stressed points. This suggested that these methods would not be adequate for

evaluating fretting fatigue initiation life in tests with different geometries, and that the reason for the poor performance of the predictive methodology is the presence of high stress gradient effects. They considered that these methods should be modified to account for the stress gradient effect and proposed two averaging methods which combined with a multiaxial fatigue criterion would give a less conservative prediction of fretting fatigue initiation life. The first method is an average of the SWT and the FS parameters over a characteristic depth on the critical plane. The second method is an average of the stresses over a characteristic elementary volume. Both averaging methods produced similar results.

Giannakopoulos et al. [134] stated that the fretting problem can be approached as a plain fatigue problem subjected to a localized stress concentration. They developed an analytical model for fretting fatigue at a rounded corner punch contacting a substrate and an analogy was made with fatigue crack initiation at a notch tip. They examined the similarities and differences between stress concentration factors at the edge of the sharply rounded punch-on-flat contact and the tip of a blunt crack. The notch analogue methodology provided a direct connection between the round cornered flat punch fretting fatigue crack initiation life and the plain fatigue crack initiation life of a smooth specimen of the same material. The predictions of the model were compared with fretting fatigue experiments on Ti-6Al-4V showing good agreement.

Madge and co-workers [25] showed that wear is a critical aspect for the prediction of fretting fatigue, and can have a major effect on the predicted evolution of stresses and damage parameters (e.g. SWT), and hence on predicted fatigue life and failure position. They stated that this fundamental and important effect of wear on fretting fatigue cannot be predicted by models which do not include the effect of material removal due to wear. They performed a finite element simulation (removed – element simulation) that combine simultaneously a fretting wear model (on a modified version of Archard wear equation which is used to predict the effect of the material removal due to wear) and the fretting fatigue Smith-Watson-Topper parameter, which includes the effect of peak stress.

The singularity parameter has been used by several authors [6,130,135-137] in order to predict the crack initiation. The ingularity parameter uses a similar approach as the critical plane parameters, but uses a much simpler scalar term for the driving force parameter. In 1988, Hattori [reported in 130,136,137] used for the first time this approach.

The main disadvantage of this model is that it is not able to capture microslip. The model essentially assumed that the contact is in the stick regime. The model is not applicable to gross slip fretting conditions, although those conditions would likely lead to a wear situation anyway. Also, the amount of plastic deformation present at the edge of the contact must be small compared to the size of the singular stress field.

Finally, there is ***the crack growth approach***. In this case, the models assume that a crack is present and then predicts the life based on the growth of the crack [6,12,21,102,125,126,138,139]. There will not be further mention of these methods (growth process), as they are not the object of this study.

2.3.2 The basic strain-life equation

Figure 2.15 shows schematically the strain-life fatigue curves. The total fatigue strain amplitude in figure 2.15 has been resolved into elastic and plastic strain components. As it is already known at a given life, the total fatigue strain amplitude is the sum of the elastic and plastic strains. The empirical relationship used to define the total number of cycles to fatigue failure of metallic materials can be expressed in the following form:

$$\varepsilon_a = \frac{\Delta\varepsilon_e}{2} + \frac{\Delta\varepsilon_p}{2} = \frac{\sigma_f'}{E}\left(2N_f\right)^b + \varepsilon_f'\left(2N_f\right)^c \tag{2.5}$$

where ε_a - total fatigue strain amplitude;

$\frac{\Delta\varepsilon_e}{2}$ - elastic strain amplitude;

$\frac{\Delta\varepsilon_p}{2}$ - plastic strain amplitude;

σ_f' - is the fatigue strength coefficient;

E - is the Young's modulus;

N_f - is the number of cycles to crack initiation;

b- is fatigue strength exponent;

ε_f' - is the fatigue ductility coefficient;

c- is the fatigue ductility exponent.

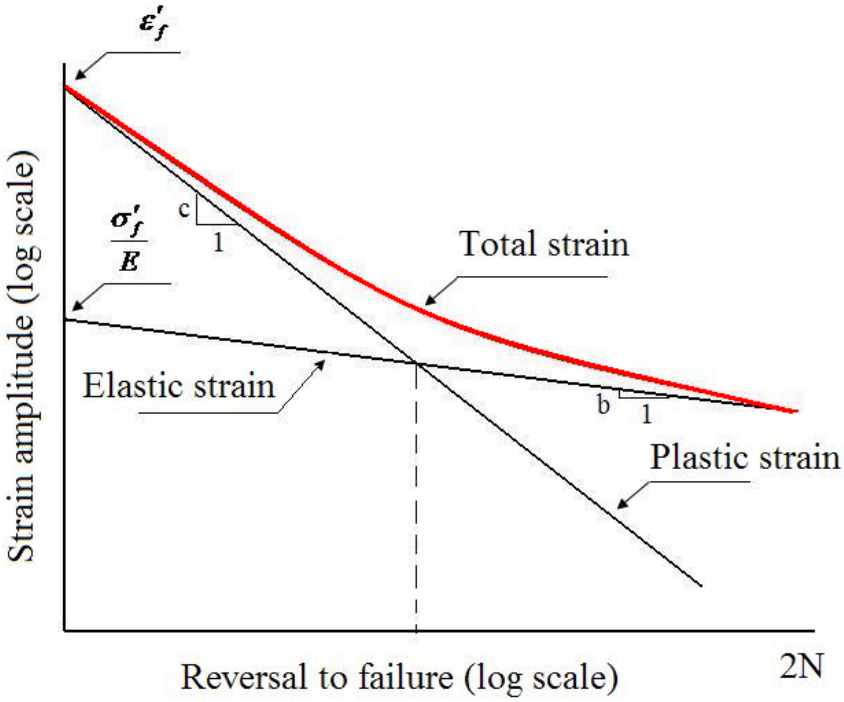

Figure 2.15 Strain life curves showing total elastic and plastic strain components [124]

Dividing the Basquin's equation [140] by the modulus of elasticity gives the equation for the elastic strain amplitude-life curve:

$$\frac{\Delta\varepsilon_e}{2} = \frac{\Delta\sigma}{2E} = \frac{\sigma_a}{E} = \frac{\sigma_f'}{E}(2N_f)^b \tag{2.6}$$

The relation between plastic strain and life (the Coffin-Manson's equation) is represented by

$$\frac{\Delta\varepsilon_p}{2} = \varepsilon_f'(2N_f)^c \tag{2.7}$$

Equation (2.5) does not consider eventual mean stresses during cyclic loading [140]. It should be mentioned that the predicted analytical life is the initiation life.

2.3.3 Smith-Watson-Topper (SWT) model

a) SWT for the plain fatigue case

Smith et al. [12] proposed a suitable relation that includes both the cyclic strain range and the maximum stress. This model, commonly referred to as the SWT parameter, was originally developed and continues to be used as a correction for the machine load mean stresses in uniaxial loading conditions [12]. The SWT parameter for multiaxial loading is based on the total fatigue strain amplitude, ε_a and the maximum

tensile stress, σ_{max} normal to the crack plane during a loading cycle it is expressed in the following mathematical form

$$SWT = \sigma_{max} \cdot \varepsilon_a \tag{2.8}$$

The maximum tensile stress value is for plane alternating fatigue test is given by

$$\sigma_{max} = \frac{\Delta\sigma}{2} = \sigma_f'(2N_f)^b \tag{2.9}$$

and by multiplying the strain-life equation (2.5), the SWT mean stress correction formula is expressed as follows:

$$\sigma_{max} \cdot \varepsilon_a = \frac{(\sigma_f')^2}{E}(2N_f)^{2b} + \sigma_f'\varepsilon_f'(2N_f)^{b+c} \tag{2.10}$$

b) SWT for the fretting fatigue case

Prior to the application of the SWT parameter to the fretting fatigue case some corrections were introduced in order to take into consideration all the stresses involved in the contact. As it is already known the crack initiation occurs on the plane (critical plane) where the product between the maximum stress and the total strain amplitude is maximum. So, the maximum fretting fatigue stress ($\sigma_{max,FF}$) normal to the trailing edge of the contact can be estimated as a superposition of the fretting contact stresses and the machine applied axial stress, being defined as

$$\sigma_{max,FF} = \sigma_{max} + 2p_0\sqrt{\mu F_{t,max}/F_{n,max}} \tag{2.11}$$

where σ_{max} - is the maximum machine axial stress, p_0 - is the maximum Hertzian pressure, μ - is the coefficient of friction in the slip condition, $F_{n,max}$ - is the maximum normal contact load, $F_{t,max}$ - is the maximum tangential load, [11].

Furthermore, the total fretting fatigue strain amplitude is given by [13].

$$\varepsilon_{a,FF} = \frac{1 - 2\upsilon^2 - \upsilon^3}{E}(\sigma_a + \sigma_{a,F_t}) \tag{2.12}$$

where υ - is the Poisson's ratio, E - is the Young's modulus, σ_a - is the machine axial stress amplitude; σ_{a,F_t} - is the tangential stress amplitude.

Figure 2.16 shows a sketch of the contact zone. The tangential stresses on the surface are given by:

i) in the slip zone

$$\sigma_{F_t,slip} = \frac{3\mu F_n}{2\pi a^2}\left(1 - \frac{\rho^2}{a^2}\right)^{1/2} \qquad c \le \rho \le a \tag{2.13}$$

ii) the stick zone is given by

$$\sigma_{F_t,stick} = \frac{3\mu F_n}{2\pi a^2}\left[\left(1-\frac{\rho^2}{a^2}\right)^{1/2} - \frac{c}{a}\left(1-\frac{\rho^2}{c^2}\right)^{1/2}\right] \quad 0 \le \rho \le c \tag{2.14}$$

where a - is half-width of contact, ρ - is the distance on the surface from a given point to the centre of the contact, c - is the half-width of the stick zone [141,142].

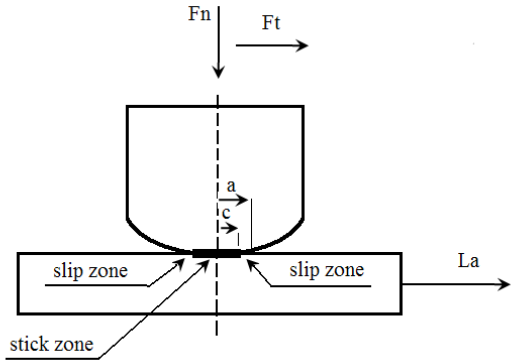

Figure 2.16 Sketch of the contact zone [124]

Making the substitutions of maximum stress, $\sigma_{max,FF}$ (eq. 2.11) and the total strain amplitude $\varepsilon_{a,FF}$ (eq. 2.12) in eq. (2.10), the SWT parameter that can be applied to the fretting fatigue situation takes the following form:

$$\left(\sigma_{max} + 2p_0\sqrt{\mu F_{t,max}/F_{n,max}}\right)\cdot\left(\frac{1-2v^2-v^3}{E}\right)\left(\sigma_a + \sigma_{a,F_t}\right) = \frac{\left(\sigma_f'\right)^2}{E}\left(2N_f\right)^{2b} + \sigma_f'\varepsilon_f'\left(2N_f\right)^{b+c} \tag{2.15}$$

2.3.4 Modified shear stress range (MSSR) parameter

The shear stress range,

$$\Delta\tau = \tau_{max} - \tau_{min} \tag{2.16}$$

was calculated using a program written by Namjoshi [14].

In order to include the effect of the mean axial/shear stress on the fretting fatigue this parameter was slightly modified using the amendment proposed by Walker [reported on 143]:

$$\Delta\tau_{crit,effective} = \tau_{max}(1-R\tau)^n \tag{2.17}$$

where τ_{max} means the maximum shear stress on the critical plane, $R\tau$ refers to the shear stress ratio, τ_{min}/τ_{max} on the critical plane, and m is a fitting parameter [139].

The MSSR parameter hypothesis that fretting fatigue crack nucleation is related to the maximum shear stress range. The parameter considers all possible planes averaged over a finite volume. To find the MSSR parameter, first an analytical or finite element analysis is performed to calculate the maximum shear stress on all points in the contact region. Next, the plane where the magnitude of the shear stress range is at a maximum is determined at all the points. Then, the critical location and the corresponding critical plane are determined where the shear stress range is a maximum [6].

This is considered to be the premier fretting fatigue predictive parameter. It is a modified version of the shear stress range critical plane parameter, MSSR [14], which combined the better features of the other critical plane parameters. It is thought that this parameter is the best for determining the effects of fretting fatigue for several reasons. It is based on the both normal and shear stresses, so therefore it eliminates the effect of pad geometry. Also, it includes aspects of the shear stress range parameter, which was the only parameter mentioned by Namjoshi [14] to be satisfactory for determination of both crack location and orientation. This modified version of the shear stress range parameter is expressed as follows:

$$MSSR = A\Delta\tau_{crit}^{B} + C\sigma_{max}^{D} \tag{2.18}$$

where: A, B, C and D are constants obtained experimentally which were found to be $A = 0.75$, $B = 0.5$, $C = 0.75$ and $D = 0.5$. In this approach the critical plane is determined by the maximum value of the shear stress range, not by the maximum value of the MSSR parameter [6,144].

2.3.5 The Findley Parameter

The Findley parameter [14,145], created in 1960 for plain fatigue analysis states that fretting fatigue crack nucleation is related to both the shear stress amplitude and the maximum normal stress, on the maximum shear plane. The Findley parameter relates the shear stress amplitude, $\Delta\tau$, and the maximum stress normal on the maximum shear plane, σ_n^{max}, as shown in the following equation

$$F = \Delta\tau + k\sigma_n^{max} \tag{2.19}$$

The value for the multiplying factor k is determined by fitting fatigue life data empirically. This parameter is also calculated at all points along the planes where the maximum values occur, yielding the location and the critical plane [6,139].

2.3.6 Fatemi-Socie-Kurath parameter

The FSK model essentially assumed that the fatigue life is depended on the maximum cyclic shear strain amplitude on a particular plane $(\Delta\gamma/2)$ modified by the maximum normal stress to this plane at any time during the cycle $(\sigma_{n,max})$. The FSF parameter can be correlated with to nucleation life through the relation

$$\frac{\Delta\gamma}{2}\left(a + k\frac{\sigma_{n,max}}{\sigma_y}\right) = \frac{\tau_f'}{G}(2N_i)^{b_0} + \gamma_f'(2N_i)^{c_0} \tag{2.20}$$

with the left hand side being the FSK parameter containing a normalized factor (σ_y/k), where σ_y is the cyclic yield strength and the factor k, which is usually close to the unity. The strain-life curve generated from fully reversed torsional fatigue tests is represented by the right hand side, where τ_f' is the shear fatigue strength coefficient, γ_f' the shear fatigue ductility coefficient, b_0 is the shear fatigue strength exponent, c_0 the fatigue ductility exponent, G is the shear modulus, and $2N_i$ the number of reversals to the formation of a surface crack of a certain length (often 0.5-1 mm long). Under torsional fatigue, the $\sigma_{n,max}$ on the plane of maximum shear strain amplitude is zero, so previous eq. reduces to the unmodified shear strain-life relationship. Since the cyclic shear fatigue data were unavailable, the constants were approximated from uniaxial fatigue tests.

Using a Von Mises assumption, the relation between the shear and normal component are

$$\tau_f' = \frac{\sigma_f'}{\sqrt{3}} \tag{2.21}$$

$$\gamma_f' = \sqrt{3}\varepsilon_f' \tag{2.22}$$

where σ_f' is the fatigue strength coefficient, ε_f' the fatigue ductility coefficient, $b_0 = b$, and $c_0 = c$.

The fretting fatigue life perdition analysis was completed using a Somat Lif Est fatigue Life Analysis Software from FEA result for points along the surface of the fatigue specimen at the contact. The damage analysis module in this software resolves the stresses and strains onto various planes and searches for the most damaging combination of loads using the critical plane approach with a choice of damage models [96].

2.3.7 Crossland's multiaxial fatigue criterion

To predict the fretting fatigue crack nucleation risk at the fatigue limit conditions (i.e. 10^6 cycles), the Crossland's multiaxial fatigue [47,101] description is applied. The risk is expressed as a linear combination of the maximum amplitude of the second invariant of the stress deviator $\left(\sqrt{J_2(t)}\right)$ defined by ξ_a, and the maximum value of the hydrostatic pressure $(P_{h\,max})$.

The non cracking condition is expressed by:

$$\xi_a + \alpha_c \cdot P_{h\,max} < \tau_d \tag{2.23}$$

where

$$P_{h\,max} = \max_{t\in T}\left(\frac{1}{3}trace\big(\Sigma(t)\big)\right) \tag{2.24}$$

$$\xi_a = \frac{1}{2}\max_{t_0\in T}\left\{\max_{t\in T}\left[\frac{1}{2}\Big(S(t)-S(t_0)\colon\big(S(t)-S(t_0)\big)\Big)\right]^{1/2}\right\} \tag{2.25}$$

$$\alpha_c = \frac{\tau_d - \sigma_d/\sqrt{3}}{\sigma_d/\sqrt{3}} \tag{2.26}$$

with, S deviatoric part of Σ; σ_d alternating bending fatigue limit; τ_d alternating shear fatigue limit.

The cracking risk can then be quantified through a scalar variable:

$$d_c = \frac{\xi_a}{\tau_d - \alpha_c \cdot P_{h\,max}} \tag{2.27}$$

The cracking condition is then expressed as:

- if d_c is greater that or equal to 1, there is a risk of cracking;
- if d_c is less than 1, there is no risk of cracking.

2.4 The Bauschinger effect

2.4.1 Introduction

If, during a monotonic tensile test, the yield strength was found to increase, the yield strength when the specimen is re-loaded in opposite direction (compressions) decreased (kinematic hardening) or increased (isotropic hardening) by the previous plastic strain in tension [146]. J. Bauschinger (1886) [as cited in Ref. 147] was the first that identified these two values extreme for the yield point. Kinematic hardening of the yield surface is used to describe the Bauschinger (BAU) effect characterized by early re-yielding and subsequent rapid change of work hardening rate [148,149].

Many studies showed that the understanding of BAU effect has several important practical applications.

It has been shown that the BAU effect is an important variable in describing fatigue crack propagation [147,150,151]. Pommier [151] in a study about the BAU effect on the crack growth stated that this effect will modify the plastic strain gradient at the crack tip. It has been stated that the higher is the BAU effect of the material, the largest is the reverse plasticity at the crack tip during unloading. These results in a reduction of the plastic strain gradient at the crack tip and in a spreading of the plastic zone ahead of the crack tip [151]. Consequently, the BAU effect of the material is expected to influence the "kinematic hardening" related to the crack and load history effect in fatigue crack growth.

Chawla and co-authors [152] highlighted the importance of BAU effect on the residual stress relief operations (by stretching). It has been shown that in stretching operation may results a material with a lower flow stress if loading is in direction opposite to the stretching direction.

There are also studies that show that the BAU effect is important for forming processes of materials and for the further mechanical properties of formed components [153-156].

To understand this phenomenon and its possible effect in fatigue initiation we will make some considerations and observations.

The BAU effect is schematically described in Figure 2.17. It can be seen from figure 3.8 that when the materials are loaded uniaxially in one direction (e.g. in tension) into the plastic regime, unloaded to zero stress level, then reloaded in reverse direction

(e.g. compression), they yield during the reloading, at a stress level lower ($\sigma_{yc} < \sigma_{yt}$) than if the reloading were carried out in the original direction.

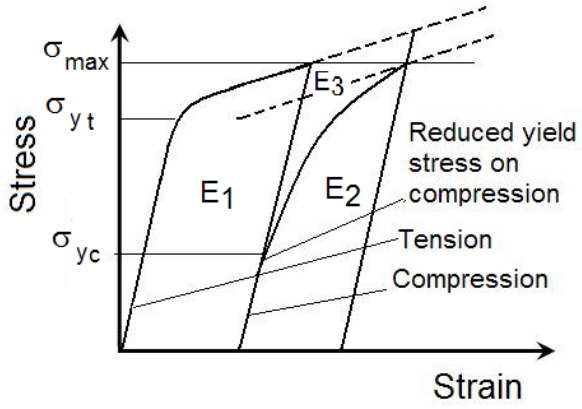

Figure 2.17 Schematic representation of the Bauschinger effect [12]

In the last years it was demonstrated [153,157] that BAU effect is more complex than only a lowering of yield stress, the whole shape of the second loading work-hardening curve is modified. The BAU induces a material anisotropy leading to a shift of the center of the stress-strain hysteresis loop. The BAU effect has been shown to occur in a variety of materials, and it was observed that the effect is more pronounced in fcc materials compared to the bcc materials. BAU effect reflects a material deviation from ideal plastic behaviour.

In view of these complexities it is not surprising that many different features have been used to describe the BAU effect (see 2.4.2). However its possible effects on fatigue are not clear and are rarely used. Regarding fatigue crack propagation only Pommier [151] stated its interest. However, to the author knowledge, it was never used in fatigue initiation life predictions.

2.4.2 Mechanism of the Bauschinger effect

Many studies [153,154,157-159] have been carried out to understand the BAU effect and technical literature presents several explanations for the BAU effect. The physical origins are generally attributed to (i) internal stresses; (ii) dislocation theories; (iii) composite model (Masing´s model or Asaro´s model).

i. Internal stresses

Internal stresses are widely used to study the BAU effect [153,154,158,159].

Indeed, from a microstructural point of view, the BAU effect has been explained in terms of polarization of work-hardening, due to the accumulation of internal stresses during plastic deformation [153,154]. The internal stress corresponds to the stress associated with a local strain process leading to long-range interaction with mobile dislocations.

From a mechanical point of view, the back stress is associated with the translation of the elastic domain, and thus with kinematic work-hardening [153,154].

ii. Dislocation theories

It was suggested that during prestraining a long large stress is build up through the formation of dislocation pile-up at barriers. These barriers are strong enough to block the motion of dislocations.

Yoshida [160] attributed the BAU effect to the short range dislocations with other dislocation interactions (the interactions of dislocations with other dislocations, interstitials, precipitates and other barriers), as well as the long range interaction among individual grains (effect of internal stress field induced by grain constraint and elastic inhomogeneity).

iii. Composite model

Masing´model suggested that there are two phases in a specimen with different mechanical properties (the same elastic constant, but different elastic limits).

When the material undergo the same prestrain in one direction, if this strain is sufficiently high, plastic deformation will occur in the phase which has the lower elastic limit, while the other one will behave elastically. On unloading, when the applied load is zero, one phase will be in tensile stress and other one will be in compressive residual stress. On reloading in the same direction, to the same stress level, both will behave elastically; but on reloading in the opposite direction, the residual stress in the “softer” phase or component will help the applied stress to cause premature yielding. Thus the behaviour is asymmetrical and the system is softer for reverse loading that it was in the virgin stage.

Pommier [157] presented a similar explanation of the BAU effect based on Asaro´s model. It has been stated that responsible for BAU effect can be the difference between the yield stresses of two phases. It has been stated that this difference induces a strain

misfit. In this model the deformation of each grain (elastic and plastic) is equal to the macroscopic deformation of the sample [161].

2.4.3 Evaluation of the magnitude of Bauschinger effect

There are different parameters [153,154,159,161,162] to characterize the BAU effect: Bauschinger stress parameter, Bauschinger strain parameter, Bauschinger energy parameter, the ratio of forward-to-reverse yield, the ratio of Kinematic –to-Isotropic hardening, etc

Chateau et al. [153,154] stated that none of these parameters or group of parameters expresses all the consequences of the BAU effect. In order to characterize more completely the BAU effect these parameters may be used together.

a. Bauschinger stress parameter

The BAU was first defined as lowering effect, the lowering of the elastic limit observed during straining in the particular direction. Figure 2.18 shows a schematic representation of the BAU effect parameters.

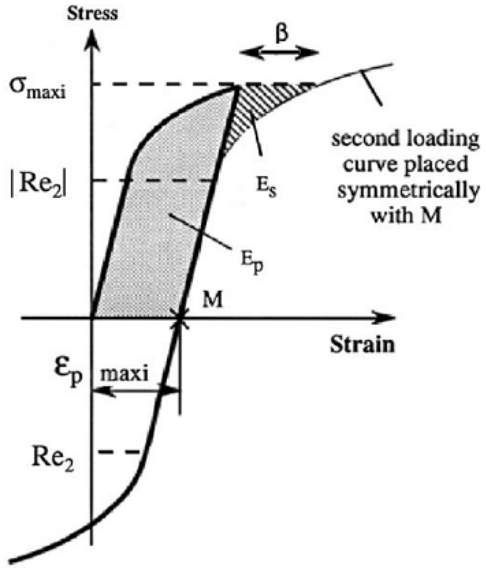

Figure 2.18 Schematic representation of the BAU effect parameters [153]
(σ_{maxi} - the prestress reached during the first loading, Re_2 the reverse loading yield stress, β - the stress shift between the two work hardening curves, E_s – the ratio of the amount of stored and then returned energy, E_p - the plastic prestrain energy, $\varepsilon_{p,maxi}$ - the plastic prestrain)

The BAU stress parameter, β_σ, is a function of the prestress reached during the first loading, σ_{maxi}, and of the reverse loading yield stress, $\sigma_y^{'}$.

$$\beta_\sigma = \frac{\sigma_{max} + \sigma_y^{'}}{\sigma_{max}} \tag{2.28}$$

b. Bauschinger strain parameter

The BAU strain indicator, β_ε, takes into account the strain shift, β, between the two work-hardening curves put in the first quadrant of the stress-strain plane, and it defined as the ratio of the shift to plastic prestrain.

$$\beta_\varepsilon = \frac{\beta}{\varepsilon_{p,max}} \tag{2.29}$$

c. Bauschinger energy parameter

The BAU energy parameter, β_E, is the amount of the stored energy and then returned energy, E_s, to the plastic prestrain energy, E_p.

$$\beta_E = \frac{E_s}{E_p} \tag{2.30}$$

The possible consequence of BAU effect on fatigue and mainly on fatigue initiation will be discussed in chapter 5. In that chapter a new parameter based on BAU effect will be included in both SWT and Morrow equations and it will be shown that it is able to improve the accuracy of the fatigue life predictions.

Chapter 3
Experimental techniques and procedures

In this chapter, the experimental techniques and procedures are presented. The properties of the materials, the geometry of the specimen and pad/pin are presented. Particular consideration is given in this chapter to the new fretting fatigue device. Also in this chapter is presented the new reciprocating wear device. The tests conditions for the fretting fatigue and reciprocating wear tests can be depicted from in this chapter.

3.1 Introduction

In order to accomplish the objectives of the present work two types of tests were carried out:

(i) Fretting fatigue tests.

(ii) Reciprocating wear tests.

The objectives of these tests (the scientific ones) were to understand the mechanisms involved in the fretting fatigue process. In order to quantify qualitative the effect of fretting in fatigue life, some plain fatigue test were carried out. It should be mentioned that the results from the plain fatigue tests are not used here for the life prediction.

3.2 Materials

Throughout this study the specimens were machined from three different alloys as follows: Al-7175 alloy bars; Ck45 steel bars and Ti6Al4V alloy bars.

The pads/pins were machined from 34CrNiMo6 steel bars. These materials are used in components both in the automotive and on the aeronautical industry. The choice of different materials for pads and specimen was based on the fact that there are many applications where contact occurs between dissimilar materials, such as the contact between screw/washer and many other components [30] as for example disk/blade attachments in the higher stages of compressor or turbine part of the aircraft jet engines [45].

Mechanical and chemical properties of the materials

The mechanical properties, the approximate grain size of the materials used are given in Table 3.1. Tables 3.2, 3.3, 3.4 and 3.5 show the chemical composition of the materials used in this study.

Table 3.1 Mechanical properties and the approximate grain size of the materials

Material	Mechanical properties					
	Young modulus [GPa]	0.2% Yield strength [MPa]	Tensile strength[MPa]	Rupture strain [%]	Grain size [μm]	Hardness HV
Al 7175	736	461	535	13.8	4,5	160
Ck45	200	499	793	23.5	35	210
Ti–6Al–4V	115	989	1055	16,1	12	360
34CrNiMo6	235	1100	1204	21.6	15,6	309

Table 3.2 Chemical composition (weight %) of Al 7175 alloy

Elements	**Si**	**Fe**	**Cu**	**Mn**	**Mg**	**Cr**	**Ni**	**Zn**
Weight (%)	0,048	0,18	1,57	0,052	2,54	0,22	0,0029	6,4

Table 3.3 Chemical composition (weight %) of CK45 steel (The value of the carbon is from catalogue)

Elements	**C**	**Mn**	**Si**
Weight (%)	0,45	0,65	0,35

Table 3.4 Chemical composition (weight %) of Ti6Al4V alloy.

Elements	**Al**	**V**	**Fe**	**Sn**	**Ni**
Ti6Al4V	6.1	4.21	0,2	0,003	0,01

Table 3.5 Chemical composition (weight %) of the alloy 34CrNiMo6 (The value of the carbon is from catalogue)

Elements	**C**	**Mn**	**Cr**	**Mo**	**Ni**
Weight (%)	0,34	0,56	1,72	0,23	1,68

The microstructures of these alloys are shown in figure 3.1, and were obtained by Scanning Electron Microscopy (SEM) in the Laboratory of Electronic Microscopy of the the University of Minho. Equipment: Leica Cambridge S360.

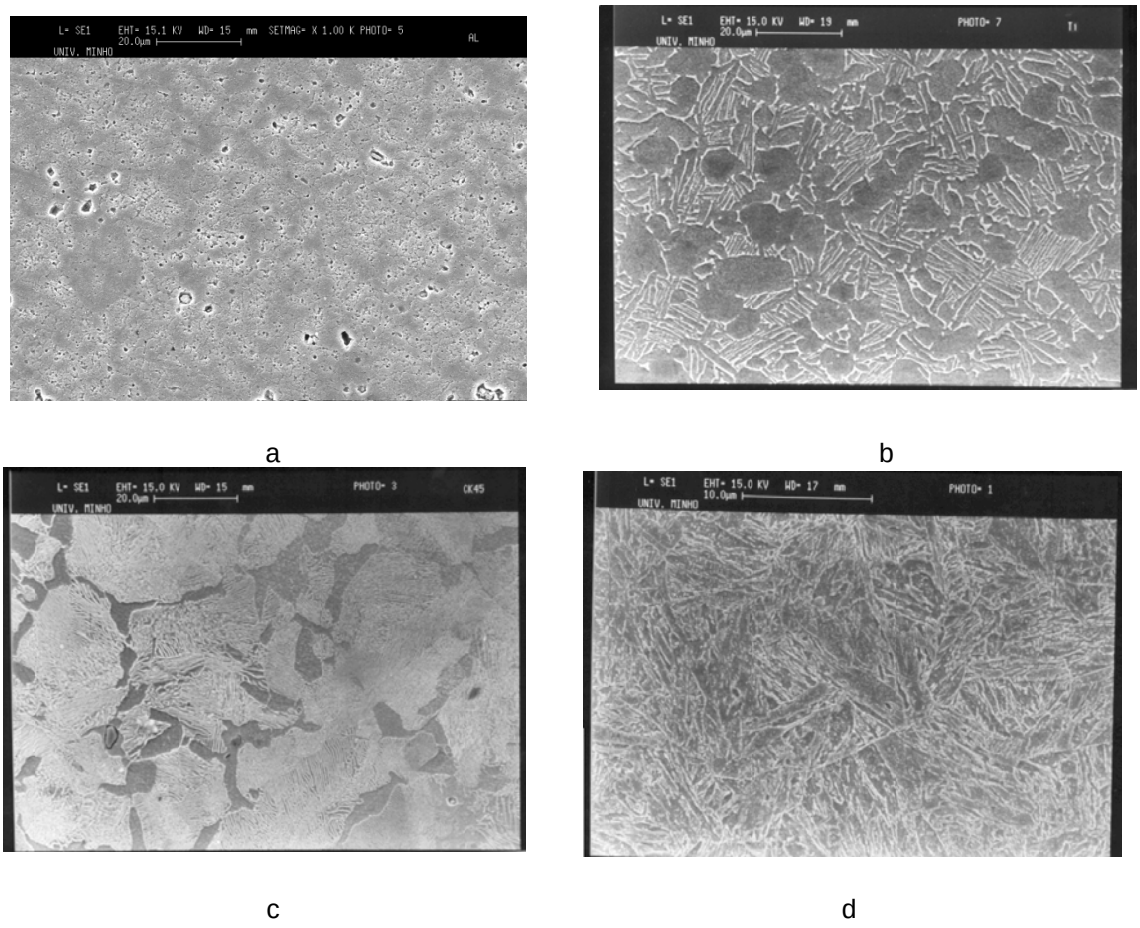

Figure 3.1 The microstructure of the materials used in this study: a. Al 7175; b. Ti6Al4V; c. Ck45; d. 34CrNiMo6 [163]

Fatigue cyclic properties

Fatigue cyclic properties are in Table 3.6.

Table 3.6 Fatigue cyclic properties of the materials

Material / Cyclic properties	Al7175	CK45	Ti6Al4V
	781,74	1319.1	1204.6
	-0.1054	-0.1156	-0.0482
	0.0689	0.6110	1.9154
	-0.5757	-0.5851	-0.8170
	0.1617	0.1965	0.0562
	1116.7	1445.5	1141.6

where: - fatigue strength coefficient [MPa]; - fatigue strength exponent; - fatigue ductility coefficient; - fatigue ductility exponent, - cyclic strain hardening exponent: - cyclic strength coefficient [MPa].

In order to obtain the fatigue properties, for each material six low cycle fatigue tests were performed under strain control, at a frequency of 0,2 Hz, in laboratory environment. The properties that are determined from stabilized hysteresis loops and stabilized life data are the following: fatigue strength coefficient, fatigue strength exponent, fatigue ductility coefficient, fatigue ductility exponent, monotonic hardening exponent, monotonic hardening coefficient; cyclic hardening exponent; cyclic hardening coefficient [163-166]. All the stabilized hysteresis loops with various strain amplitude levels (0.39%, 0.69%, 0.82%, 1.22%, 1.54%, 2.01%) are plotted on the same axes and the cyclic strain curve is defined by the locus of the loop tips. The curves for the elastic strain amplitude-life and for the plastic strain amplitude-life are plotted separate in the same graph. When plotted on log-log scales, both curves become straight lines. If a material is repeatedly cycled under fully reversed strain-controlled loading, the material may respond in one of the following ways: cyclic hardening, cyclic softening, remaining stable, or some combination of these responses. It is important to highlight that, as reported in [163], in relation to Ti6Al4V alloy, the obtained properties may not be very accurate due to the fact that when carrying out the low cycle fatigue tests some heat generated in the specimens and it may have altered the results.

3.3 Equipment and techniques used

I. Geometry of the specimens and pad/pin

The fretting fatigue and plain fatigue experiments were carried out using the specimen and the pad geometries shown in figure 3.2a and 3.2b. The specimen has a special shape with two flat sides (A and B). In this configuration two zones of contact were generated on the flat sides of the specimen. The cross section area of the specimen is 88.32 mm^2. The pad contact surface is spherical, having a radius of 27.5 mm. Figure 3.2c shows the specimen used in the reciprocating wear tests. It has a simple shape with filets in both sides where the axial load is applied. The cross section is a rectangle. Figure 3.2d shows the geometry of the pin used in this investigation.

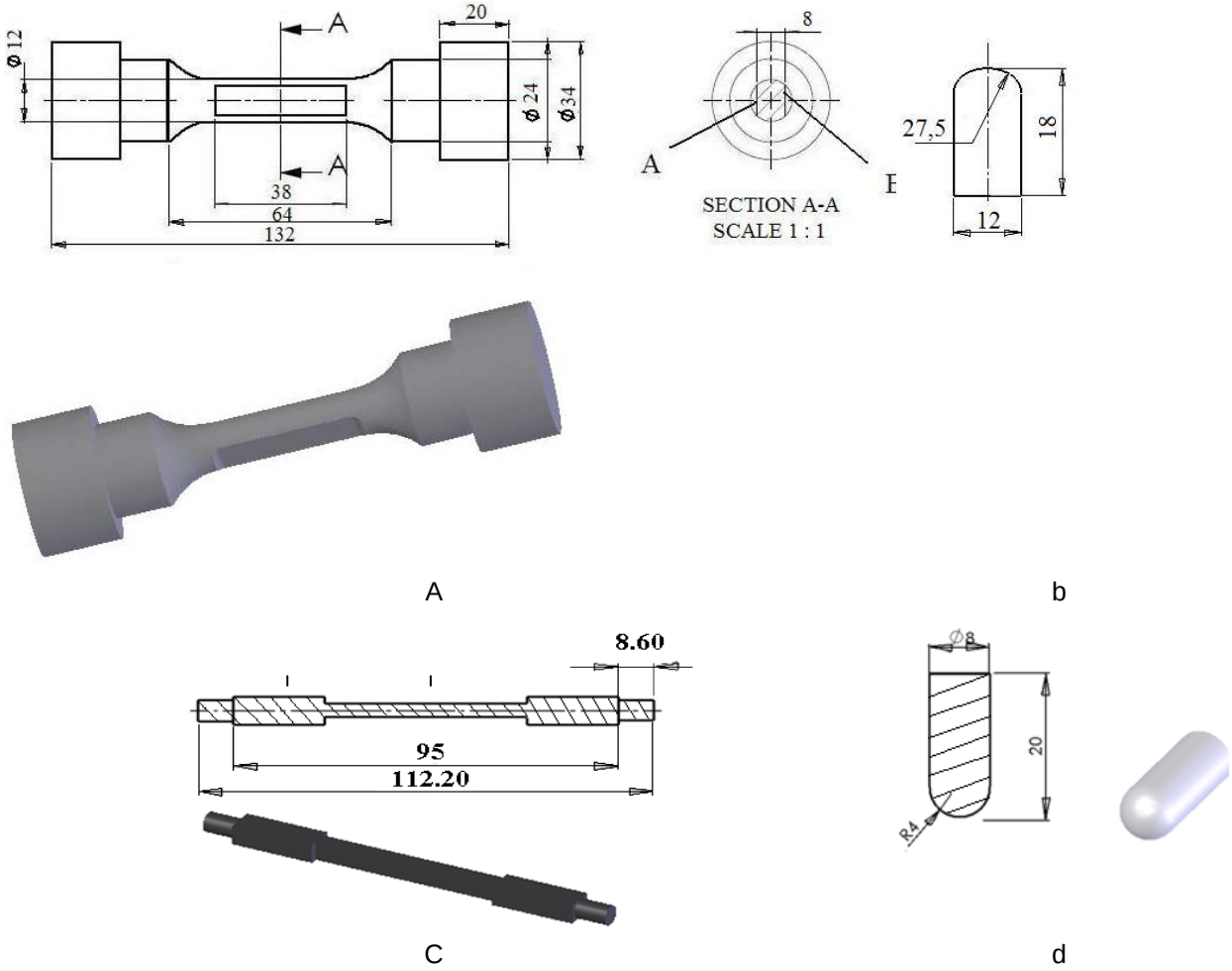

Figure 3.2 Geometry of the specimens and pad/pin: a. specimen used in plain fatigue and fretting fatigue tests; b. pad used in fretting fatigue tests; c. specimen used in reciprocating wear test; d. pin used in reciprocating wear test [124,167-172]

II. Experimental test set-up for fretting fatigue tests

Fretting fatigue testing apparatus has been carefully designed in order to meet the objectives of the test to be performed. The fretting fatigue testing apparatus used in this study has been developed to work in conjunction with a servo hydraulic testing system (DARTEC uniaxial testing machine). The capacity of this machine is 600 000 N under static conditions and 500 000 N for fatigue loading. The maximum cyclic loading frequency of the machine is 50 Hz. A global view of the servo hydraulic testing machine is shown in figure 3.3.

An exploded view of the fretting fatigue apparatus is shown in figure 3.4. This view of the device allows looking at every component separately. Figure 3.5 presents a schematic view of the fretting fatigue apparatus.

In figure 3.6 can be seen a picture of the fretting fatigue apparatus assembled in the servo hydraulic test machine. The fretting fatigue device was conceived to work at ambient temperature, in laboratory environment, but can be adapted to perform at low and high temperature tests.

Figure 3.3 Global view of the servo hydraulic testing system (DARTEC uniaxial testing machine) [167,168]

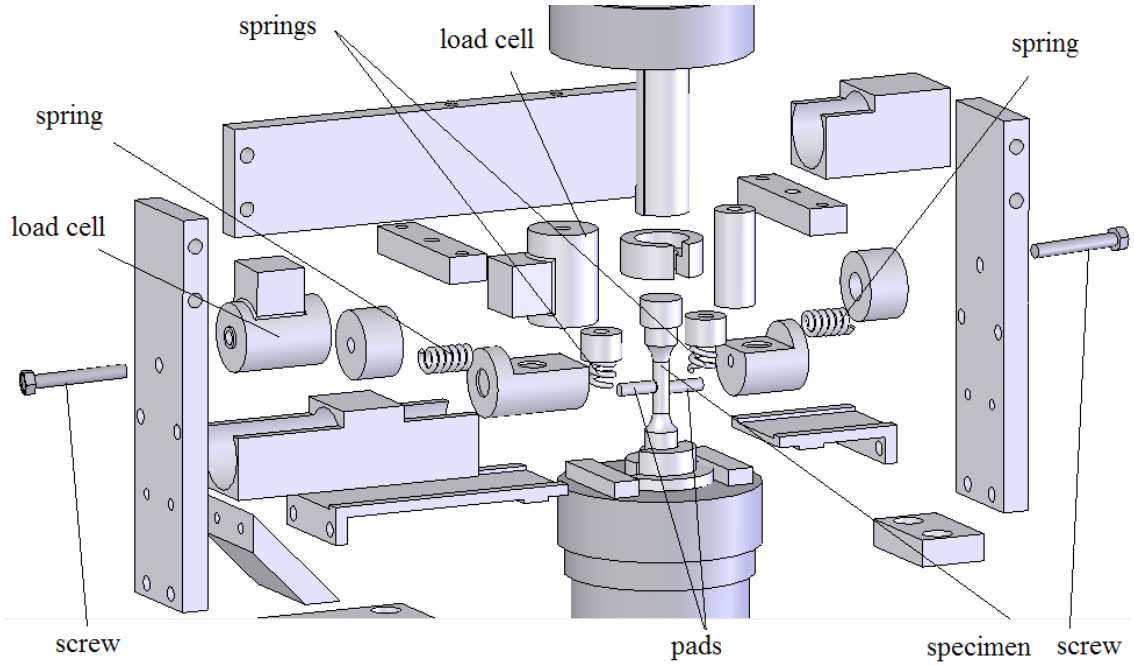

Figure 3.4 Exploded view of the equipment described in this work [167,168]

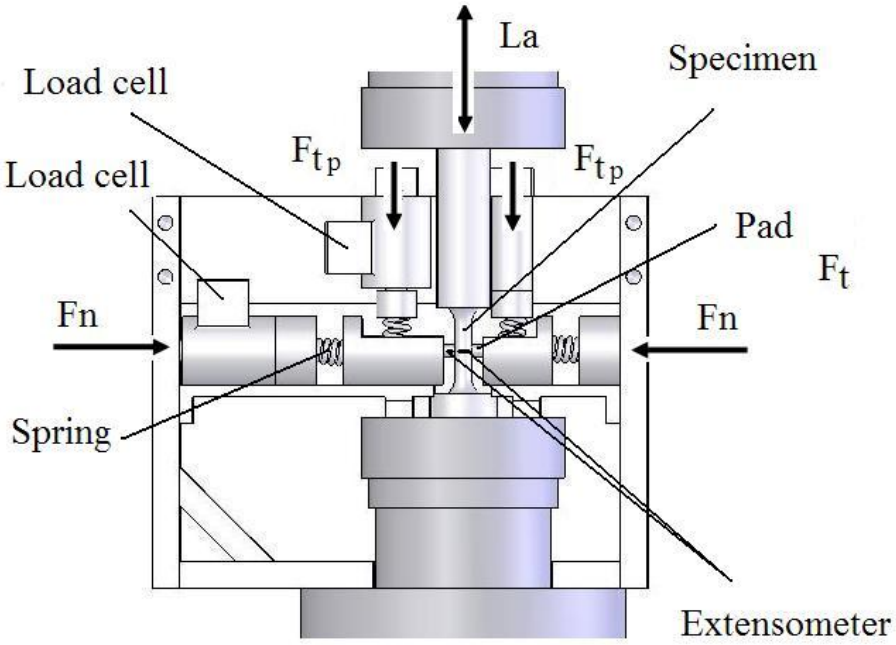

Figure 3.5 Schematic view of the fretting fatigue apparatus F_n- pad normal load; F_{tp}-pad pre-tangential load; L_a – machine axial load [167,168]

Figure 3.7 shows a close-up view of the same apparatus. As can be seen in figure 3.7, the fretting device has two load cells that allow the application (prior to the test) and recording/measurement of the normal and tangential contact loads (during the test). A 1000 N load cell is used to set/measure the pre-tangential/tangential load and a 2500 N

load cell is used to set/measure the normal load. The two pads are pressed normal to the flat faces of the specimen by a pair of compression springs, which are loaded by adjustable screws. Also two vertical compression springs acting on the pad are used to apply the pre- tangential load (to avoid pad movement).

Due to the symmetry of the system the loads are measured only in one side. The loads are applied at the same time in both sides of the specimen. To get the load in the both sides of the specimen a dynamometric key was used.

Particular attention has been given to the measurement of the relative displacement. In order to measure the relative displacement between the contacting bodies (specimen and pad) a MTS extensometer was used. It has been adapted to the shape of both specimen and pads. As can be seen in figure 3.8 a knife edge of the extensometer was attached to the pad where a cut has been made (so that the knife edge does not slip during the test), and the other knife edge was attached to the specimen. The extensometer was clamped to the specimen and to the pad with two metal springs. Besides, special glue was applied along both edges of the extensometer. It should be mentioned that the knife edges of the extensometer were fixed exactly perpendicular to the surfaces of the specimen surface and on the pad, because only in this case the exactly relative displacements between two points (one on the specimen and the other one on the pad) could be read. It should be mentioned that the pads are interchangeable and it can be used any geometry.

Figure 3.9 presents the schematic test configuration. The axial cyclic load applied to the specimen was monitored with the load cell of the machine.

Figure 3.6 Fretting fatigue apparatus assembled in the servo hydraulic test machine [167,168]

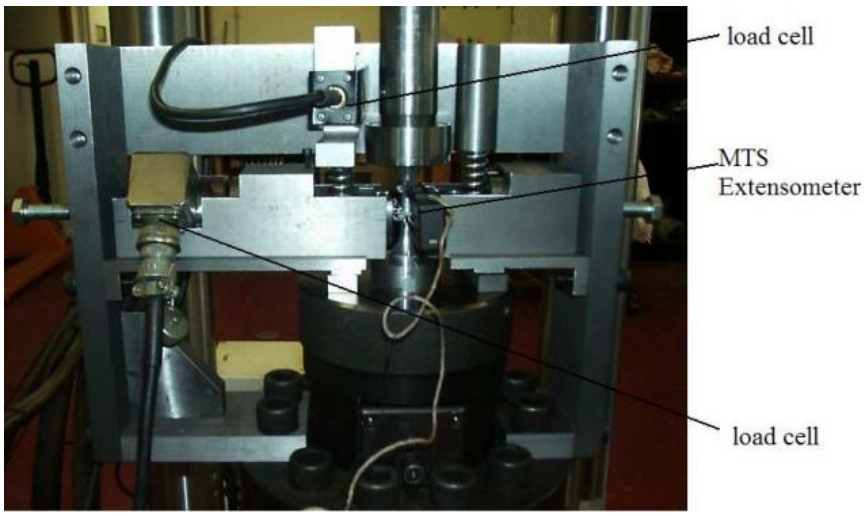

Figure 3.7 Close-up view of the fretting fatigue apparatus [167,168]

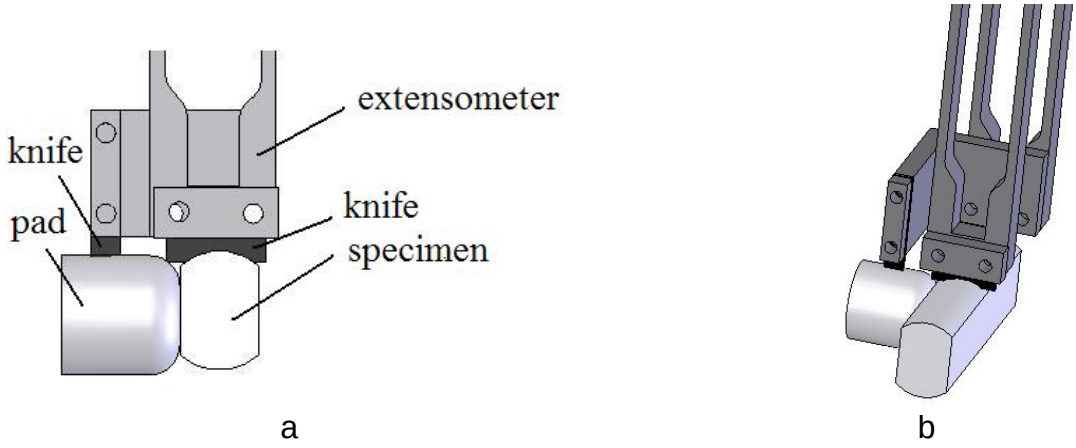

Figure 3.8 Schematic of the position of the extensometer: a. top view, b. isometric view [167,168]

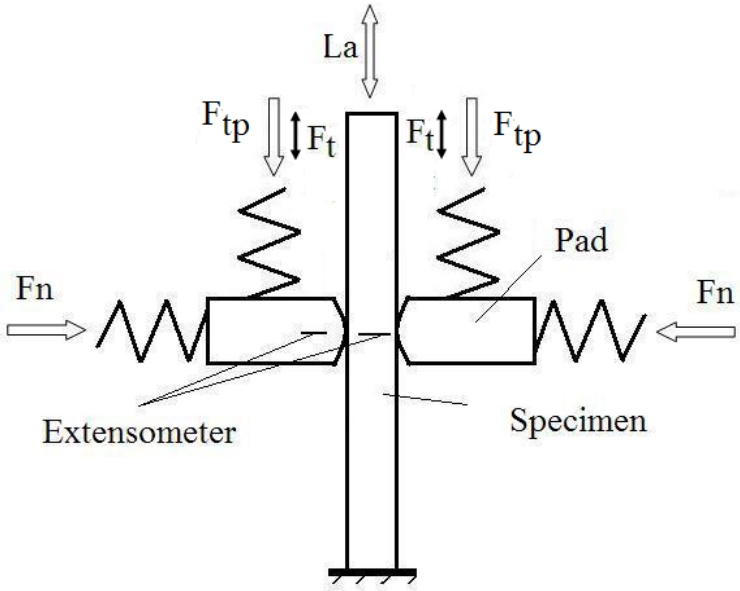

Figure 3.9 Schematic test configuration [124]

III. Experimental test set-up for the reciprocating wear tests

A reciprocating pin-on-plate tribometer PLINT-TE67 was used to evaluate the wear of Al7175/34CrNiMo6, Ck45/34CrNiMo6 and Ti6Al4V/34CrNiMo6 contact pairs. The PLINT-TE67 machine is normally used to study the friction coefficient and wear of the materials. Figure 3.10 shows the experimental setup.

Figure 3.10 Wear experimental test setup and the data acquisition system [170,172]

In order to apply an elastic stress (either in tension or in compression) on the specimen, a new device that used a screw to introduce the load and a load cell to measure its value, was specifically designed and constructed to work in conjunction with a pin-on-plate testing machine. Figure 3.11 shows the exploded view of this device. A picture of this device is presented in figure 3.12. The stress (tension and compression) applied on the specimen was obtained by using screws and nuts placed in both sides of the wear device (see figure 3.12).

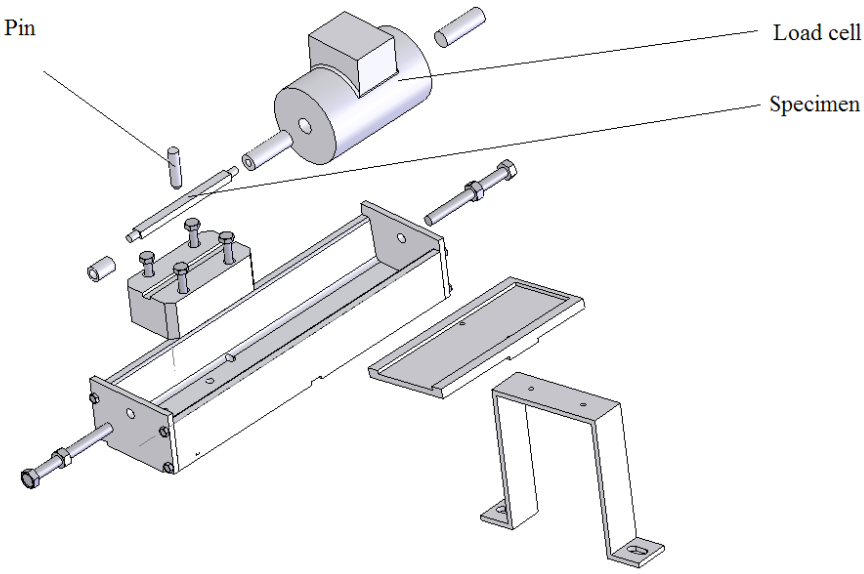

Figure 3.11 Exploded view of the wear device

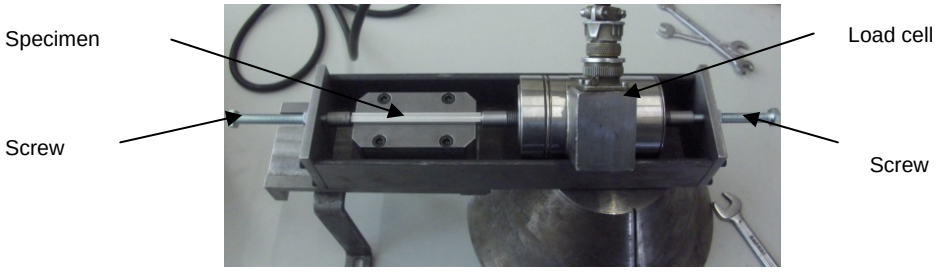

Figure 3.12 Picture of the wear device [169,170,172]

The pin is pressed against the specimen by applying pneumatically the normal load which induces the contact pressure between the pin and the specimen (see figure 3.13). The top of the pin was fixed to the load arm with a chuck (holding device consisting of adjustable jaws).

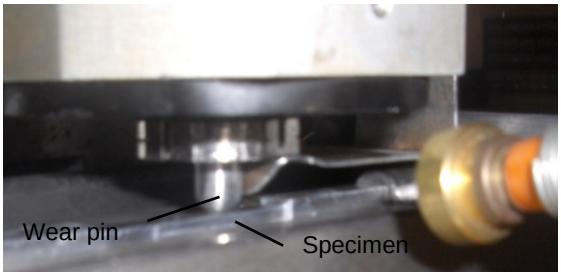

Figure 3.13 A view of the contact pairs: pin-specimen [172,173,174]

IV. Specimen preparation

Prior to the tests the surface of specimens and pads/pins were polished with abrasive paper, finished with diamond spray (1 μm), and then cleaned ultrasonically in alcohol as to provide a standard surface.

It is already known that the level of the residual stress depends on the manufacturing process, the type of material and the component criticality, and it may or may not be significant. In order to be sure that the material would be entirely free from initial residual stresses induced during manufacturing and processing, the specimens were heat-treated prior to the test, according to heat treatments suggested for the material by its supplier.

3.4 Characterisation techniques

I. Data acquisition and control software system for fretting fatigue tests

The parameters that can be recorded (and some of them controlled) during a fretting fatigue test with this new apparatus are the following:

a. The normal contact load that is applied to either side of the specimen by means of the spring and screw;

b. The tangential contact load that is applied to avoid the movement;

c. The relative displacement between contacting surfaces (specimen and pad).

To monitor these three variables two load cells and one extensometer are used. (previously presented)

To record all the variables in real time a data acquisition system (Spider 8) that can be seen in figure 3.14 was used. The data acquisition system show in figure 8 sends the information to the computer. It has been used a program (Catman 3.1) that records the data at the same time from the two load cells and from the extensometer.

The computer that works in conjunction with the servo hydraulic test machine records different testing variables such as the machine axial cyclic load that is applied on the specimen, the time, the number of cycles, the stroke and the strain.

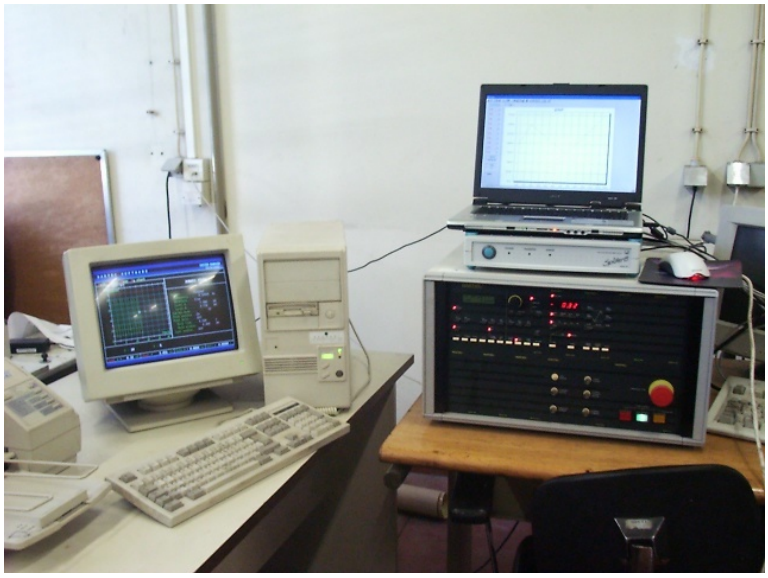

Figure 3.14 Data acquisition system [167,168]

II. Data acquisition system for reciprocating wear tests

The desired value of the axial load applied to the specimen was set up by means of a load cell mounted on the specimen, in association with a data acquisition system (Spider 8) conveying information to a personal computer (program used – Catman 3.1). Another data acquisition system associated to the tribometer recorded different testing variables including sliding distance and friction coefficient. A picture of the data acquisition system along with the wear experimental setup is depicted in figure 3.10.

3.5 Test conditions

i. Fretting fatigue tests

For this study were performed several series of fretting fatigue tests. Eighteen specimens manufactured from Al7175 alloy were subjected to fretting fatigue test. Sixteen specimens manufactured from Ck45 steel were subjected to fretting fatigue test. Eighteen specimens manufactured from Ti6Al4V alloy were subjected to fretting fatigue test. All tests were carried out at ambient temperature, in laboratory environment, and at a cyclic frequency of 4 Hz, at a stress ratio, $R = 0.1$.

The tests conditions for the fretting fatigue tests for all three materials are presented in Tables 3.7. Another four fretting fatigue tests for Al7175 alloy and four for Ck45 steel were carried out to assess how the roughness and the depth of the contact areas change with the number of cycles. The first experiment was interrupted after 5 cycles, the second interrupted after 100 cycles and the third interrupted after 500 cycles. An experiment for each material was run out till fracture of the specimen. The testing conditions for the interrupted fretting fatigue tests are presented in Table 3.8.

Table 3.7 Loading conditions of fretting fatigue tests

Material	Machine axial load, L_a [kN] *R*=0,1	Normal pad load, F_n [N]	Tangential pad pre – load, F_t [N]
Al7175	1.9-19.0 1.8-18.0 1.6-16.0 1.2-12.0	750 950 1200	450 600 800
Ck45	3.7-37.00 3.4-34.00 3.0-30.00		
Ti6Al4V	7.0-70.0 6.2-62.0 5.5-55.0 4.8-48.0 4.2-42.0 3.5-35.0		

Table 3.8 Loading conditions for the interrupted tests

Material	Machine axial load, L_a [kN], *R*=0,1	Normal pad load, F_n [N]	Tangential pad pre – load, F_t [N]
Al7175	1.8-18.0	750	450
Ck45	3.4-34.0	1200	800

In order to qualitatively quantify the influence of fretting on fatigue life, six plain fatigue tests were carried out for each material. Table 3.9 shows the loading conditions for plain fatigue tests for the all materials used in this study.

Table 3.9 Loading conditions for the plain fatigue tests

Material	Machine axial load, L_a [kN], R=0,1
Al7175	2.60-26.00 2.70-27.00 2.70-27.00 2.90-29.00 3.20-32.00 3.50-35.00
Ck45	3.70-37.00 3.75-37.50 3.80-38.00 3.90-39.00 4.00-40.00 4.10-41.00
Ti6Al4V	6.00-60.00 6.05-60.50 6.10-61.00 6.20-62.00 6.50-65.00 7.00-70.00

ii. Reciprocating wear tests

Figure 3.14 shows schematically the types of reciprocating tests performed in this work: i) applied normal load (Fn) on the pin and alternative displacement (d) of the specimen (the specimen is not subjected to an additional stress state); ii) applied normal load on the pin, alternative displacement of the specimen and additional tensile stress on the specimen; iii) applied normal load on the pin, alternative displacement of the specimen and additional compressive stress state on the specimen. Experiments were carried out with a normal contact load of 150 N and a relative displacement of 2 mm. All tests have been stopped at a sliding distance of 43m. The frequency of the tests was kept constant for all tests at 1 Hz. The additional stress state of the specimen under tension was 208 MPa for Al7175, 312.5 MPa for Ck45 and Ti6Al4V, and under compression -208 MPa for Al7175 and -312.5 MPa for Ck45 and Ti6Al4V. The applied peak contact pressure was around 132 MPa for all the tests (obtained by the Hertzian equation). All the tests were performed in laboratory environment.

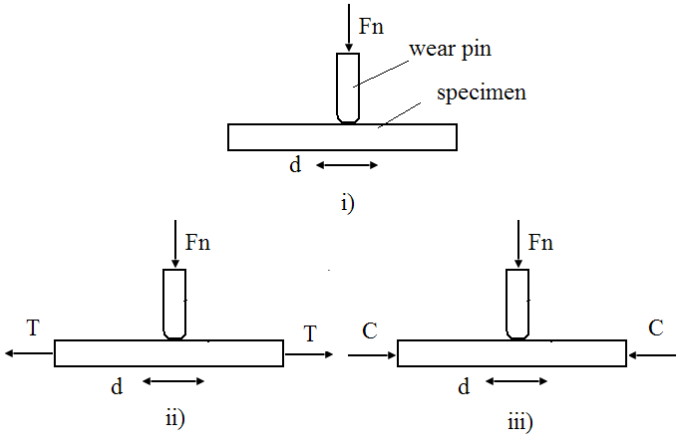

Figure 3.15 Schematic test configurations [124,164,172]

iii. Numerical simulation

Numerical simulations were carried out in order to assess what would be the effect of the additional elastic stress on the average roughness of the surface. For the numerical simulations the COSMOSWorks code has been employed. Several linear analyses were performed applying an additional stress level, as introduced by the external load of ±208 MPa. The model was meshed with linear tetrahedral elements (4 corners node connected by six straight edges). The global size of the element is 0.2 mm. This mesh size proved to be adequate for the linear analysis. The numerical simulations results are presented in chapter 4 (4.2.3 New physical model - reciprocating sliding wear under an additional stress state).

3.6 Errors of measurements

As it is well known the experimental techniques have inherent errors. Knowing the potential source of errors is essential to understanding the quality of the obtained data.

In order to gain confidence in the results presented in this work a brief presentation of the errors of the instruments used is provided.

1. Load cells

a. The load cell to measure the normal load

Sensotec 250kgf, Model: UG/4669-05, SN 656817, Capacity 2500 N, Non-linearity (max) $\pm 0.03\%\ F.S.$, Hysteresis (max) $\pm 0.03\%\ F.S.$

b. The load cell to measure the tangential load

TMN 1000 N, Model TKA-100A, SN 134, Capacity 100kN, Calibration coefficient $\frac{0.02495kgf}{1} \times 10^{-6}$, Nonlinearity $0{,}03\%RO$

c. The load cell to set the additional load in reciprocating wear tests

Sensotec 4903 N, Model UG/4668-02, SN 496773, Capacity: 4903 N, Non-linearity (max) $\pm 0.03\%\ F.S.$, Hysteresis (max) $\pm 0.03\%\ F.S.$

d. The load cell to apply the normal load on the reciprocating wear tests

Model: DF2S, Max Capacity 150N, Sensitivity (Cn) $2 \pm 10\% \frac{mV}{V} (1kg: 1.8 \pm 10\%)$, Hysteresis error $\pm 0.0300\%\ of\ Cn$, Off center load error $\pm 0.0500\%$

2. *Extensometer* – to measure the displacement between the two contacting bodies

Calibrations were carried out to increase the measuring accuracy and enable to measuring the linearity (hysteresis and sensibility error). The extensometer model used is 632.12C-20 SN 258, Gauge length 25 mm, Range +22.5/-2.5 mm, measurement error $\pm 0.3\%$.

3. *Roughness measurements* – The roughness measurement were carried out through a mechanical profilometer (Perthometer S5P Mahr-Perthen)with a resolution of $0{,}001\mu m$.

3.7 Comments on experimental techniques

A novel device capable of reproducing the fretting fatigue phenomenon was specially designed. It is a very versatile apparatus that has as main advantage the ability to control and measure a number of different variables during the test. It is able to set and record the normal and tangential loads and the relative displacement specimen/pads. Every small detail (load or displacement) can be detected and recorded by the equipment. This made possible to assess the influence of the referred variables and in this way allowed a better understanding of the fretting fatigue phenomena. The most significant feature of this apparatus is the new and more reliable way to measure the relative displacement (without needing to include the system compliance).

Chapter 4
Experimental results and discussion

In this chapter are presented the experimental results and the discussion of the fretting fatigue and reciprocating wear tests. Also the morphological characterisation of the contact surface by different techniques is treated in this chapter.

4.1 Fretting fatigue tests

4.1.1 Output of the fretting fatigue tests

The fretting fatigue specimens were tested up to rupture. A summary of the fretting fatigue tests: specimen number, loading conditions and number of cycles to failure are presented in Tables 4.1 - 4.3.

Table 4.1 Experimental fretting fatigue life results for Al7175 alloy

No.	Machine axial load, L_a [kN]	Normal pad load, F_n [N]	Tangential pad pre – load, F_t [N]	Nr of cycles to failure
AlB1	1.9-19.0	1200	600	50342
AlB2		950		60897
AlA5		750		82,231
AlD1				77,618
AlD2				124,442
AlA3			800	50,106
AlA4				50,707
AlB5			450	116,335
AlA1				60,930
AlA2				97,933
Al_9				76,456
AlB4	1.8-18.0	1200	600	133086
AlB3		950		70907
AlA6		750	800	66,199
AlA7			600	97,437
AlA8			450	113,927
AlB6	1.6-16.0	1200	600	211,115
Al_9	1.2-12.0			408,423

Table 4.2 Experimental fretting fatigue life results for Ck45 steel

No.	Machine axial load, L_a [kN]	Normal pad load, F_n [N]	Tangential pad pre – load, F_t [N]	Nr of cycles to failure
A6	3.7-37.00	1200	800	234,988
Doubt4			600	318,124
A7		950	800	325,728
A10		750	800	121,436
A3			600	391,983
A2			600	280,899
A4			450	543,444
A5			450	569,399
A9	3.4-34.00	1200	800	230,343
A11			600	630,440
Doubt 5			450	1,245,675
A12				785,129
A13		950	800	467,803
A14		750		948,433
A15	3.0-30.00	1200	600	3,338,833
A1		750		617,101

Table 4.3 Experimental fretting fatigue life results for Ti6Al4V alloy

No.	Machine axial load, L_a [kN]	Normal pad load, F_n [N]	Tangential pad pre – load, F_t [N]	Nr of cycles to failure
Ti_FF1	7.0-70.0	1200	800	26,466
Ti_FF2	6.2-62.0			28,491
Ti_FF3	5.5-55.0			43,330
Ti_FF4		950		50,117
Ti_FF5		750		55,322
Ti_FF6	4.8-48.0	1200		79,862
Ti_FF12				54,081
Ti_FF9			600	71,886
Ti_FF10			450	103,336
Ti_FF13				85,897
Ti_FF17				51,,968
Ti_FF18			600	57,772
Ti_FF7		950	800	52,169
Ti_FF11				49,050
Ti_FF8		750		52,156
Ti_FF14	4.2-42.0	1200	600	107,499
Ti_FF15			800	86,168
Ti_FF16	3.5-35.0			490,323

4.1.2 Morphological characterisation of fretting fatigue damage

The damage mechanisms were examined using three techniques: scanning electron microscopy (SEM), surface profilometry and optical microscopy.

(i) Scanning electron microscopy

High resolution images (with SEM) of the fretting fatigue surfaces for the specimen are presented on Figure 4.1i for Al 7175 alloy, on Figure 4.1ii for Ck 45 steel and on Figure 4.1iii for Ti6Al4V alloy. The three experiments presented here were carried out till fracture of the specimen (Al 7175 – 66.199 cycles, Ck45 – 785.129 cycles and Ti6Al4V – 52.156 cycles).

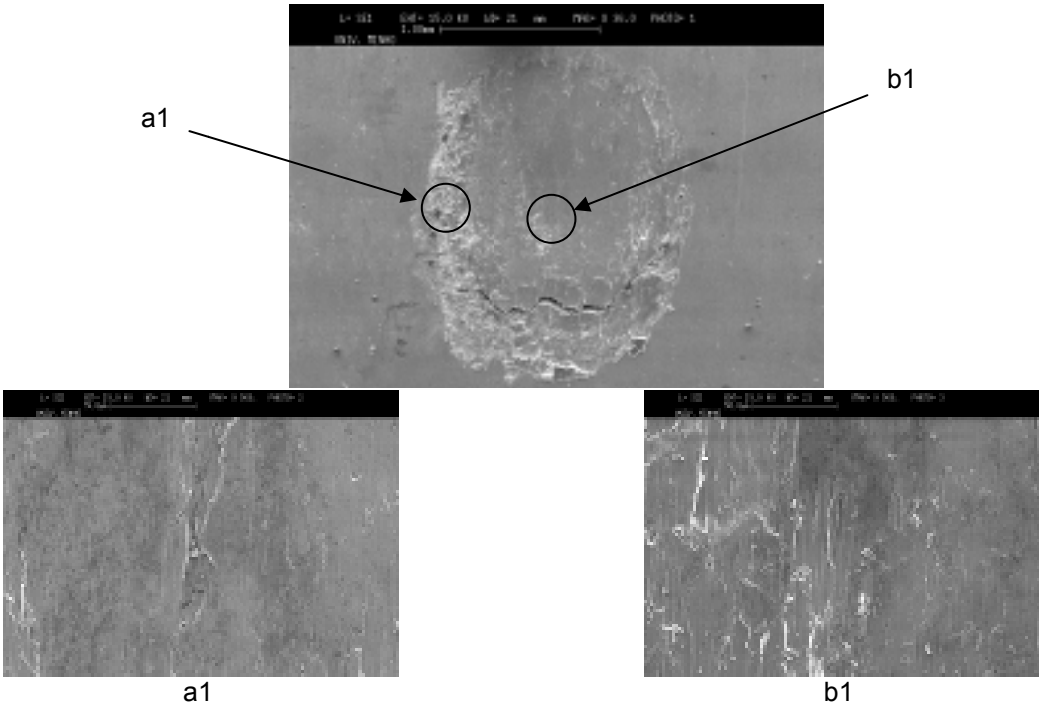

i. Al7175 - 66.199 cycles

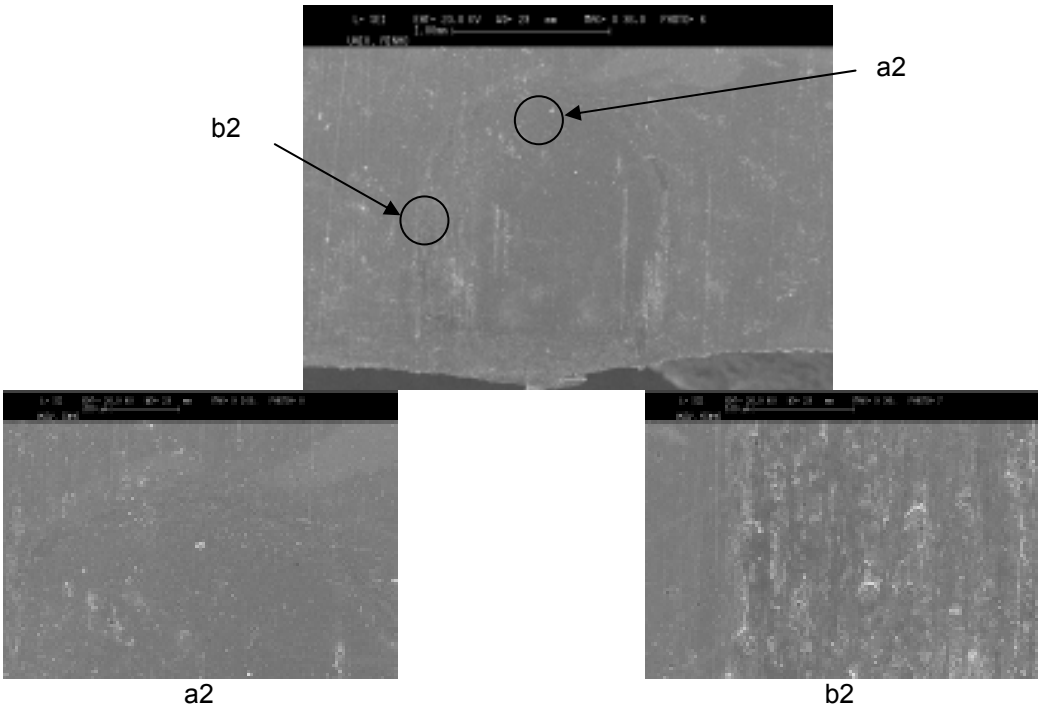

ii. Ck45 - 785.129 cycles

Figure 4.1 High resolution images of three samples surface obtained with the scanning electron microscope (SEM) (cont.)

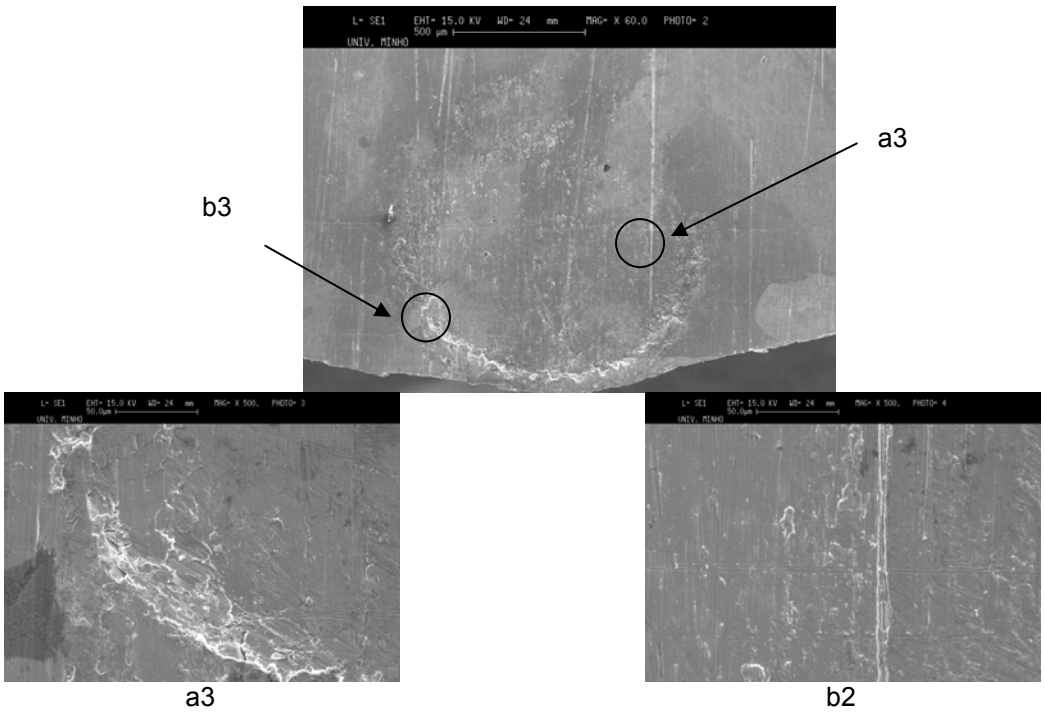

iii. - Ti6Al4V (52.156 cycles)

Figure 4.1 High resolution images of three samples surface obtained with the scanning electron microscope (SEM)

(ii) Surface profilometry and optical microscopy

A Mahr Perthen profilometer was used to characterize the contact area after the fretting fatigue tests. Five measurements of the profile and of roughness perpendicular to the sliding direction were performed.

Table 4.4 presents the results of the roughness (R_a) and the depth of the damage area for the specimens subjected to interrupted fretting fatigue tests (0, 5, 100, 500 cycles) for two materials, Al7175 and Ck45.

The roughness presented in Table 4.4 is the averaged value of these measurements. As it is well known R_a is the average deviation of the profile from the centre line over a length (L) of assessment [175], being given by

$$R_a = \frac{1}{L} \int_{x=0}^{x=L} |y| \, dx \tag{4.1}$$

The measurements of the average roughness, R_a, are done according to DIN 4768 standard. The form and the waviness are suppressed with a waviness filter. Waviness will place a mean line into the measured profile. Evaluations based on this line do not take into account the waviness contained therein and accept, as planned, only the remaining roughness.

Table 4.4 Results of the roughness, , the depth of the damage area and the elastic stress concentration factor on fretting fatigue tests

Nr cycles	[μm]		Depth [μm]			
	Al	Ck	Al	Ck	Al	Ck
0	0.07	0.04	0	0	-	-
5	0.13	0.20	0.75	5	-	-
100	0.14	0.45	2.75	6	-	-
500	0.20	0.58	3.5	10	-	-
End	1.2	1.2	53.75	14	1.27	1.09

Table 4.5 shows the scar region of the fretted surfaces and the corresponding profiles for the specimens (Al7175 alloy) subjected to interrupted fretting fatigue tests (0, 5, 100, 500 cycles). Figure 4.2 shows the high resolution image of a sample surface obtained by SEM, the schematic changes of profile during the test and the real profile at the end of the test.

Table 4.5 Scar region of the fretted surfaces with number of cycles and the roughness (Al7175)

Cycles	0	5	100	500	66199 (rupture)
Scar region	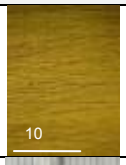	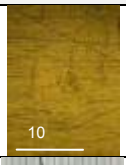			
Profiles					

Figure 4.2 High resolution image of a sample surface obtained with the scanning electron microscope (SEM): a. Al7175 (66.199 cycles), b. Schematic evolution of profiles (from left to right) during the test and the real profile at rupture [124,128,171]

When the fretting fatigue tests were concluded, a concavity was formed at the fretted surface of the specimen due to contact of the fretting pads. It can be seen from Table 4.4 that by increasing the number of cycles the roughness increased. The depth of the damaged surfaces shows that the concavity increases with the number of cycles.

After final rupture the depth of the damage surface of the Al7175 specimen is much higher (53.75 μm) that the depth of the Ck45 alloy (14 μm). The Ck45 depth is about 0.25% of the Al7175 alloy. This result means that most probably the depth of the damaged area may be the cause of the fretting fatigue life reduction as will be seen later in this chapter. As a fact higher depth means a higher stress concentration factor (figure 5.4).

In the scar region (Table 4.5) two regimes are identified: gross slip and partial slip. The test starts in gross slip (5 and 100 cycles pictures), when no stick region has been formed yet in the contact. Then, after a few hundred cycles, the regime changes to partial slip (500 cycles). The contact consists then on two zones, stick and slip. This regime will remain till the end of the test (Table 4.5 and figure 4.2).

In figure 4.1 can be better seen the two zones of the contact region. In the centre of the contact it is localized a smooth zone, named stick zone and around this a rough zone, named slip zone. The presence of the stick and the slip zones in the contact region shows clearly the partial slip regime [32]. In figure 4.1i can be clearly seen a crack that is located at the interface between the two zones present in the contact. Such location of the fretting fatigue crack has been described in several research papers [90,173].

The location and dimension of the stick and slip zones change during the test. This evolution confirms in part the variation of the tangential load (Figure 4.4, subsequently presented) and of the relative displacement amplitudes (Figure 4.7, subsequently presented) which were based on the occurrence a partial slip regime.

4.1.3 Evolution of the most significant parameters during a fretting fatigue test (Asymmetrical fretting scar formation)

During a fretting fatigue test, due to changes within the contact zones (stick and slip), the parameters (for example: normal load, tangential load, relative displacement etc.) that influence fretting fatigue phenomenon change. Those changes are also influenced by the fretting fatigue device. The results presented in this section show the evolution of the most significant parameters: normal load, tangential load, relative displacement amplitude and dynamic coefficient of friction, in fretting fatigue. It should be mentioned that normal and tangential loads are the parameters that were set deliberately in the beginning of the test. The relative displacement between the specimen and pad is not imposed.

Four representative tests have been selected: two tests for Al7175 alloy (AlA3 and AlA5), a test for Ck45 steel (A3) and a test for Ti6Al4V alloy (FF14). The initial conditions of the tests are previously presented (see Tables 4.1 – 4.3). The material of the pad is a conventional 34CrNiMo6 steel.

Figure 4.3 shows the evolution of the minimum and maximum normal load, F_n. and figure 4.4 shows the evolution of the minimum and maximum tangential load F_t, during the tests.

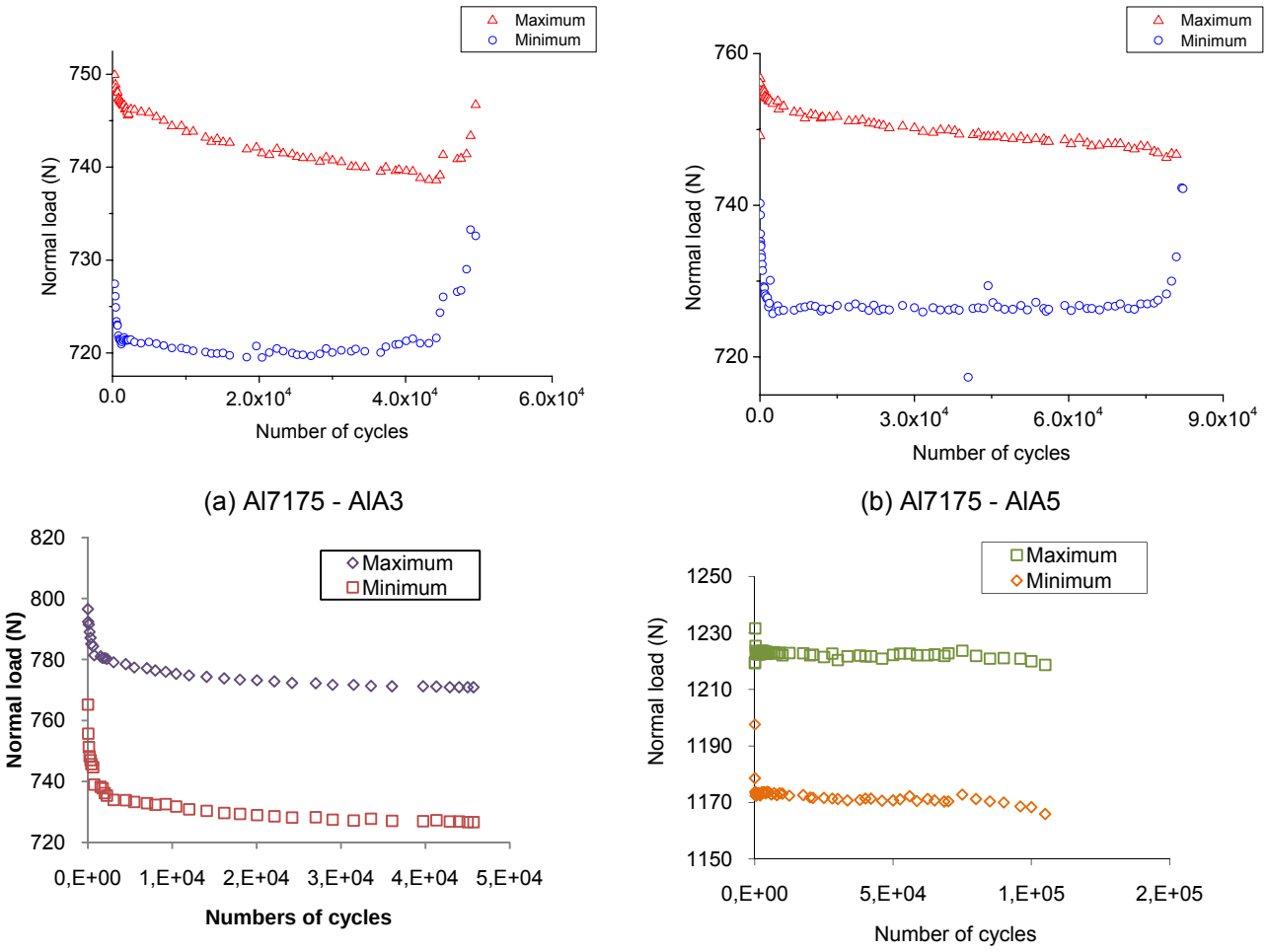

(a) Al7175 - AlA3

(b) Al7175 - AlA5

(c) Ck45- A3

(d) Ti6Al4V - FF14

Figure 4.3 Evolution of minimum and maximum normal load [128]

It can be seen that the maximum and minimum normal load (Figure 4.3) slightly decreases during the tests only at the end of the test, it stated to increase. The results regarding the evolution of the minimum and maximum normal loads during fatigue life showed three stages (Figure 4.3). Initially, they sharply decrease. This may be explained by the breakage of initial roughness material peaks and an initial accommodation of the roughness peaks of the steel pad in the softer specimen (Table 4.5 and Figure 4.2). After a few hundred cycles, on stage 2, it is observed a constant

decrease of both maximum and minimum loads (Figure 4.3). This stage 2 corresponds to the gradual development of the fretting scar on the specimen contact surface allowing the pad to 'penetrate' the specimen, thus decreasing the normal load. Near the end of the test there is stage 3 where the normal load increases (sharply in the case of Al7175 alloy). The reason lies on the bending deformation of the specimen due to an existing and propagating crack.

Perhaps the most important in terms of normal load is the maximum normal load because it is the one that is responsible for the maximum stress occurring in the specimen. Regarding the global variation along the test, e.g. in aluminium case (test AlA3) the maximum normal load changes from 750 N to 738 N. This is a very small change (about 1.6%) and it is expected that it does not have a substantial influence on fatigue life. The variation in the case of Ck45 alloy was about 2.65% and in the case of Ti6Al4V was 1.05%. The reason for this small variation of the normal load relies on the use of the two compression springs (see Figures 3.5 and 3.9). Contrarily to Jin and Mall [31] that observed a substantial drop on normal load during the test, several other researchers [46,49-53,174] used a system similar to the one used in the present work, with springs to keep the normal load roughly constant. Relating to normal load it is corroborated that it is possible to keep the normal load approximately constant during a fretting fatigue test.

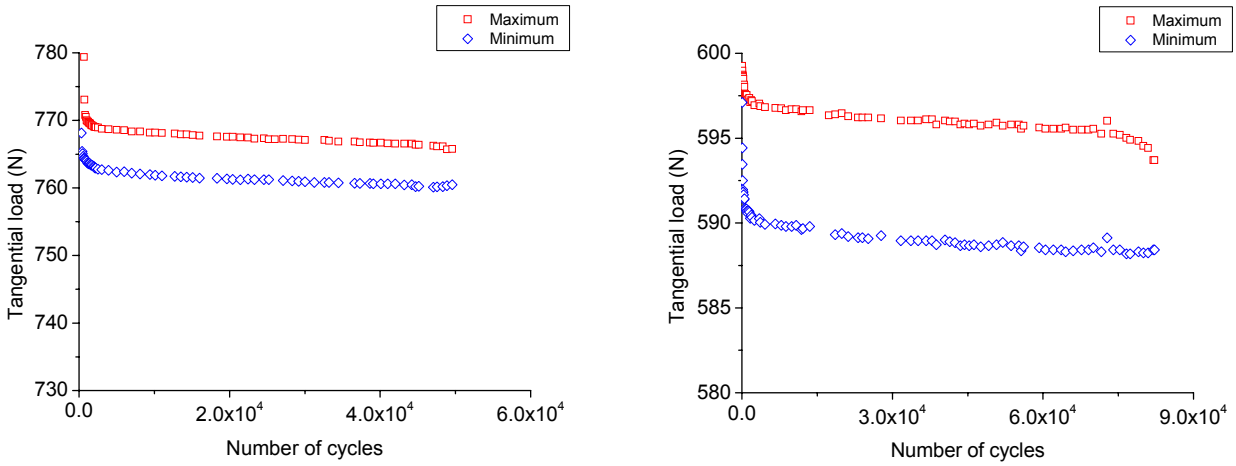

(a) Al7175 - AlA3 (b) Al7175 - AlA5

Figure 4.4 Evolution of minimum and maximum tangential load [128] (cont.)

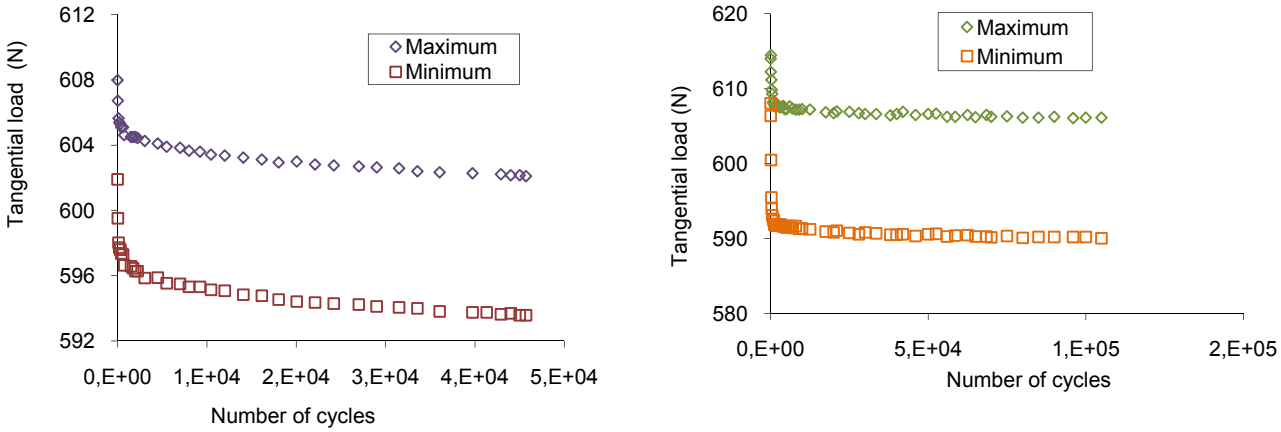

(c) Ck45- A3 (d) Ti6Al4V - FF14

Figure 4.4 Evolution of minimum and maximum tangential load [128]

The minimum and the maximum tangential load (Figure 4.4) suffered a drop in the beginning of the test, and then slightly decreased during the test. The tangential load is a consequence of the contact friction between pads and specimen. The minimum and the maximum values of the tangential load also have three stages (figures 4.4). In stage 1 it suffers a drop due to the initial accommodation of the roughness peaks on both surfaces (running-in period). This is also the reason why the amplitude increases in this period. In stage 2, after a few hundred cycles, the fretting scar starts to develop and the pad starts to have the relative movement (pad-specimen) constrained by the fretting scar. What is interesting to observe is that the constraint should increase the tangential load. As a fact the scar should not allow the pad to remain in its initial position (sliding in relation to the specimen) but on the contrary it should cause the pad to move along with the specimen. The effect would result in an increased dislocation of the pad and a consequent increase of the tangential load (higher compression of the vertical springs (see Figures 3.5 and 3.9). The reason for the observed behaviour may lie on the fretting scar geometry evolution during the test (Table 4.5 and Figure 4.2). It is observed that the scar profile changed with the damage evolution (or fatigue life). It can be observed an asymmetrical fretting scar formation. This asymetrical scar will push the pads downwards (the pads are constrained by the fretting scar) thus decreasing both the maximum and the minimum tangential loads. Thus, instead of an increase in tangential load during the test due to the fretting scar formation, as the scar deepest side moved downwards is causing a decrease in tangential load.

Prior to a comparison of tangential load evolution with other studies, it is important to go through the explanation for the asymmetrical scar evolution. During a wear cycle, the specimen stress state changes from a minimum to a maximum value due to the fatigue cycle (minimum machine load to maximum machine load). It is expected that the

wear sensitivity changes with the stress state of the material (specimen). Mitchell and Shrotriya [121] stated by that the bulk material responds differently to wear depending on its stress state. This study revealed that for a constant contact pressure the wear rate is accelerated by compressive stresses while the tensile stresses tended to suppress it. They based this behavior in a surface damage and repassivation process. Other studies report that compressive additional stresses, based on plastic residual stresses, are beneficial to wear [119,176].

Thus, although the previous results provide contradictory and not fully explained results it is clear that the stress state of the specimen influences the wear rate. The wear sensitivity to the stress state of the specimen may be the reason for the asymmetrical shape of the fretting scar. A study [169] on the Al7175 behaviour under reciprocating wear, at different stress states, provides deeper evidence of the previous mentioned asymmetrical scar formation [169].

Based on this scar asymmetrical formation it is interesting to observe other literature results on tangential load evolution (stage 2). Jin and Mall [22], working with a Ti6Al4V alloy, observed an increase of tangential load while Yongqing Fu and co-authors [27], working with a TiN coating, observed a decrease of tangential load during the test. Thus, there are contradictory results seeming to be the relevant variable the specimen material. Some materials may be more wear sensitive than others to the specimen stress state developing a more asymmetrical fretting scar, in which case the tangential load would decrease. Other materials, less specimen stress state wear sensitive, may develop a more symmetrical scar and in this case the tangential load would increase during the test.

It is also important to observe the variation of the tangential load amplitude (Figure 4.5) along the test since it is linked to the relative displacement amplitude, and this last parameter strongly influences fatigue life (Figure 2.4). The evolution of the relative displacement amplitude, δ, is shown in Figure 4.6. The ratio of the tangential load to the normal load (F_t/F_n -dynamic coefficient of friction) is presented in Figure 4.7. It should be mentioned that for the Ck45 steel in the graphs are presented only the initiation period due to the large number of cycles.

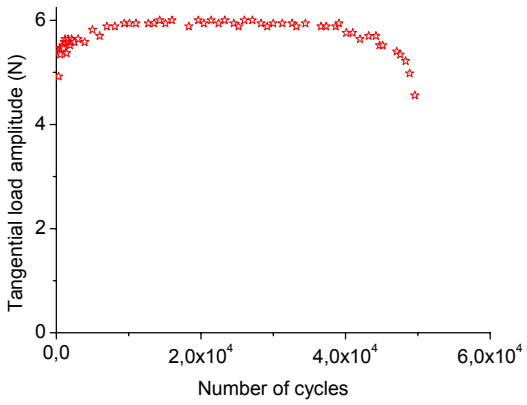

(a) Al7175 - AlA3

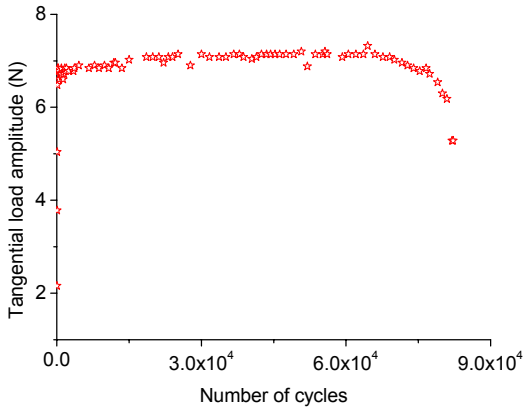

(b) Al7175 - A lA5

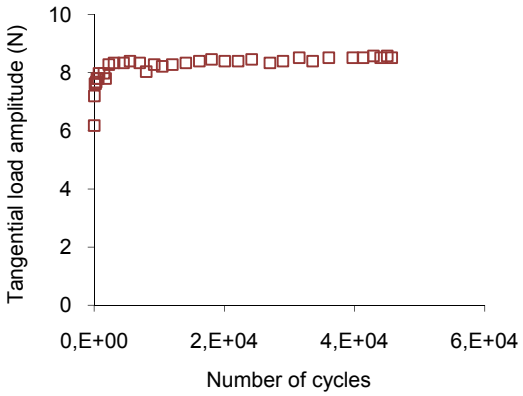

(c) Ck45- A3

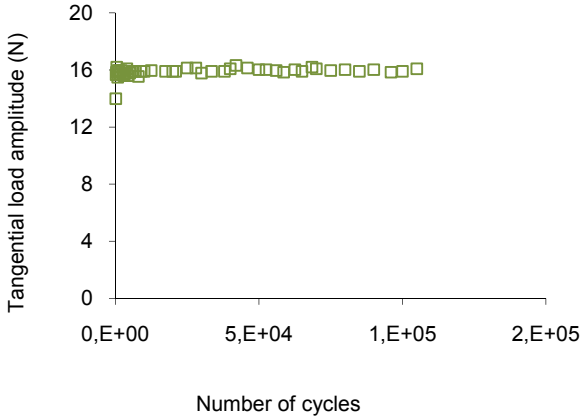

(d) Ti6Al4V - FF14

Figure 4.5 Evolution of tangential load amplitude [128]

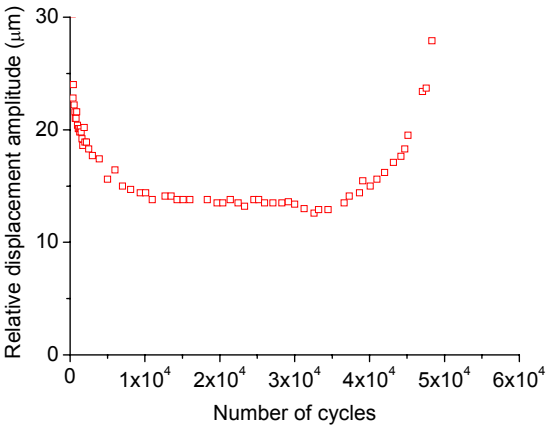

(a) Al7175 - AlA3

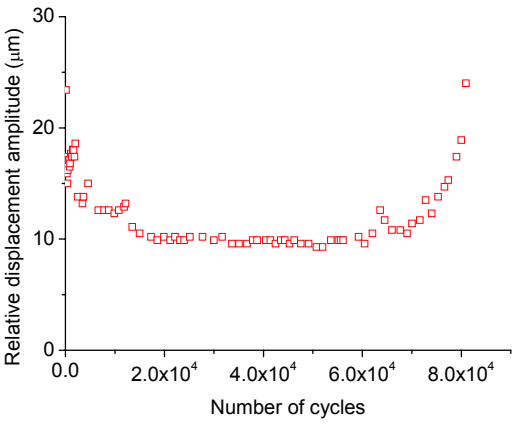

(b) Al7175 - AlA5

Figure 4.6 Evolution of the relative displacement amplitude [128] (cont.)

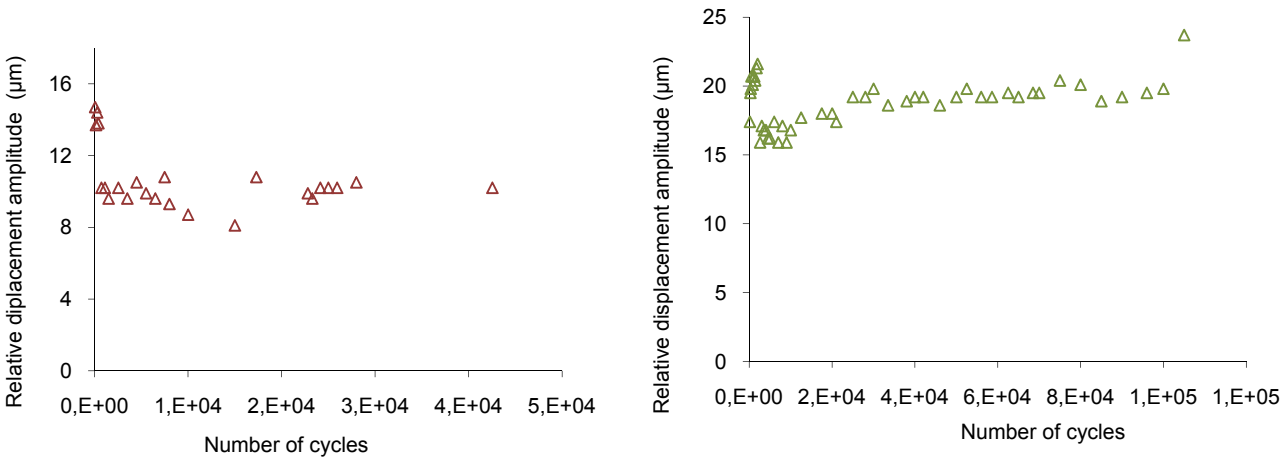

(c) Ck45- A3 (d) Ti6Al4V - FF14

Figure 4.6 Evolution of the relative displacement amplitude [128]

The tangential load amplitude increases during stage 1, remains nearly constant on stage 2, and starts to decrease till final rupture in stage 3 (figure 4.5). This variation of the tangential load amplitude is a typical variation of the partial slip regime when the contact region has a stick and a slip zone [26,61,65] as observed in this work. At the beginning of the test there is mainly a slip region, but from a certain point on a stick region starts to develop. This increasing stick region keeps the pad rigidly connected with the specimen, increasing the tangential load by restraining the relative displacement. The relative displacement amplitude starts to decrease when there is an existing propagating crack. What is interesting to observe is that although the variation in tangential load amplitude is not substantial even the small variations may originate substantial, relative displacement amplitude changes (Figure 4.6), which is very detrimental in terms of fatigue life, as will be seen later in this work.

Thus, regarding the evolution of the tangential load both the scar formation and the slip-stick zone evolution are involved in its explanation.

The relative displacement amplitude is strongly linked to the tangential load amplitude. It follows exactly the mirror shape of the tangential load amplitude but with a bigger extent. This means that small changes in tangential load amplitude may cause substantial changes in relative displacement.

The relative displacement amplitude decreases because the stick zone increases with fatigue life (see Table 4.5). As the stick zone increases the pad movement becomes more difficult. Furthermore, as the scar develops and becomes deeper, the pads keep confined inside the scar and slipping between pads and specimen becomes more difficult. The increase in relative displacement amplitude at the end of the test is due to the propagation of the crack.

Regarding the global variation along a test the relative displacement amplitude changes from example in the case of Al7175 alloy (test AlA3) from 25μm to about 12μm, a variation of about 52% (about 56% for Ck45 and about 75% for Ti6Al4V).

Furthermore, the flat region where the relative displacement amplitude remains constant is only about 50% of the total life of the specimen (see Figure 4.6). The other 50% are spent under bigger relative displacement amplitudes. As is known these changes in relative displacement amplitude may substantially change the fatigue life. Figure 2.4 shows a general curve where it is clear the strong dependence of fatigue life on small changes of relative displacement amplitude [165]. Thus, special attention should be paid to a changing value of amplitude during the fretting fatigue tests [8]. Possibly, this parameter should not be regarded as constant in fatigue life predictions, but as a changing one depending on fretting fatigue life stage.

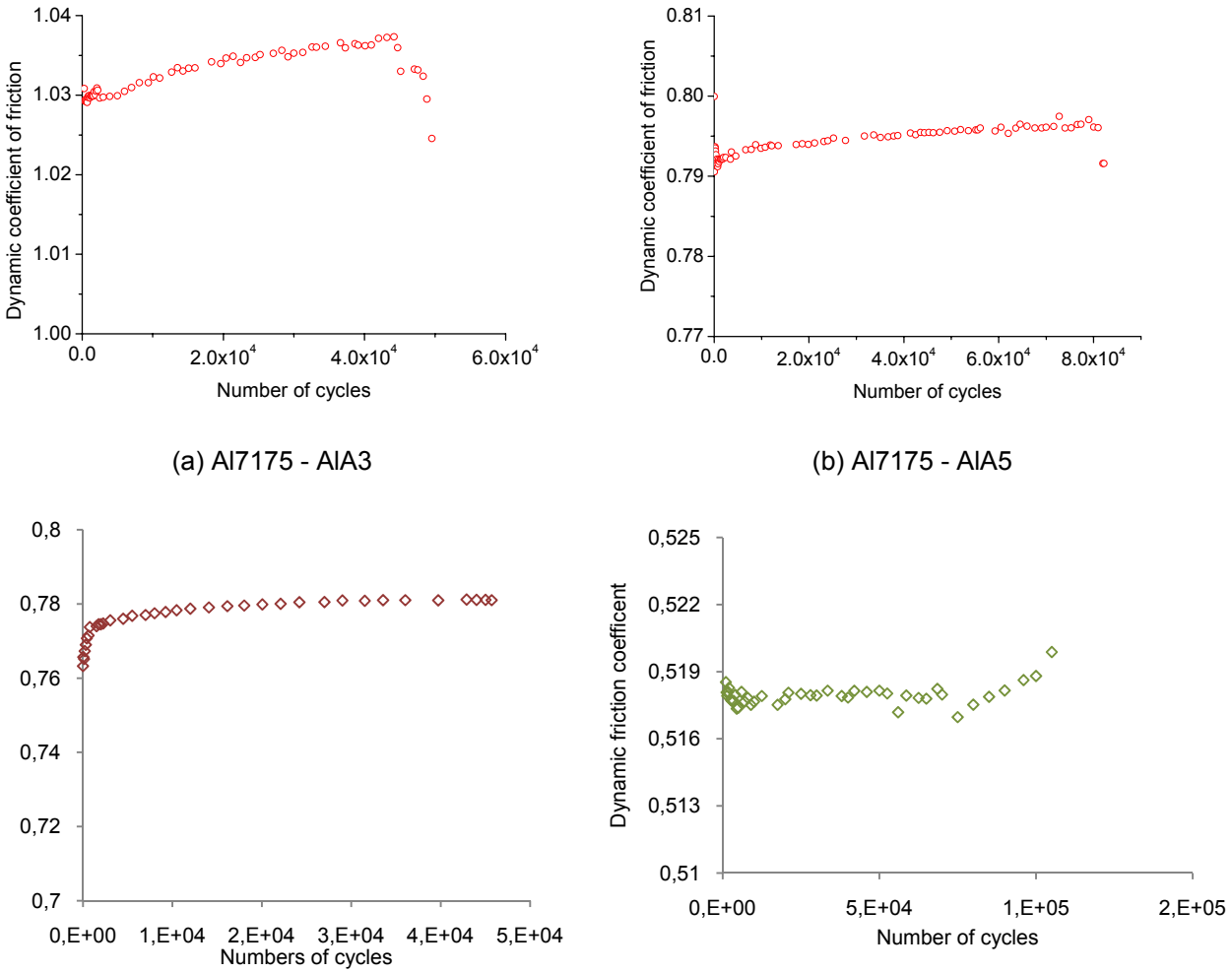

Figure 4.7 Evolution of the dynamic coefficient of friction [128]

The dynamic coefficient of friction (COF) was calculated as the ratio of the tangential to the normal load. It is well known that COF depends on the contact slip regime [25]. Regarding the evolution of the COF there is an increase during the whole test and a sharp decline at the end due to crack propagation. The increase has been explained by the partial slip regime [25] or by increase in the real area of contact [58]. However, as observed in this work, the scar evolution also constrains the tangential load. The pads have the relative movement (pad-specimen) constrained by the scar. Thus, the COF increases almost linearly with the scar depth evolution, and an "apparent" COF, exists as shown in Figure 4.7. Therefore, it is not only due to the contact slip regime but also (and eventually mainly) due to the scar evolution, that the value of the COF evolved as shown on Figure 4.7. This confirms the observations of reference [58].

4.1.4 Some considerations on the modification of the fretting contact via varying normal load and tangential load

Based on the results of previous works it is clear that, despite the coverage of the variables that affect the fretting phenomena, there are still ambiguities and contradictions regarding the degradation process, mainly in the partial slip regime where the contact zone is more complex compared with gross slip. It is already known that the difficulty in partial slip regime is that there is a competition between wear and cracking (between the slip and stick zones).

The results presented in this section show the modification of the fretting contact (size of the slip and stick zones, roughness, depth, dynamic COF) via varying normal and tangential load. The results are presented only for Ti6Al4V and Al7175 alloys. In the case of Ck45 steel the contact zone was not clear and no conclusion could be drown. Only the results from the roughness measurements are presented in the case of Ck45. These results will help to determine the stress concentration factor (5.1.3 Stress concentration factor due to "wear damage area" – fundamentally new approach) based on the depth of the damaged area, and the surface finishing factor (5.1.4 Surface finishing factor due to the surface roughness) based on the average surface contact roughness.

I. The modification of fretting contact via varying normal load

In order to see the influence of normal load on the modification of the fretting contact zone it should be mentioned that the tangential load (F_t) and the axial load (L_a) are kept constant. The only variable is the normal contact load (F_n).

Figure 4.8 shows the variation of the stick zone with normal contact load. Figure 4.9 shows the variation of the depth of the contact zone with normal contact load. Figure 4.10 shows the variation of the dynamic (kinetic) coefficient of friction (COF) with normal contact load.

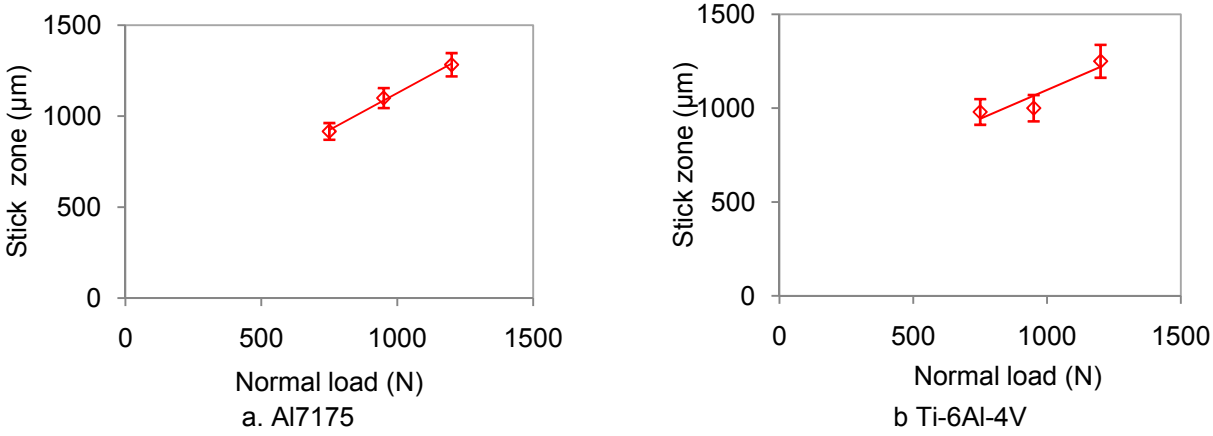

Figure 4.8 Variation of the stick zone with normal load

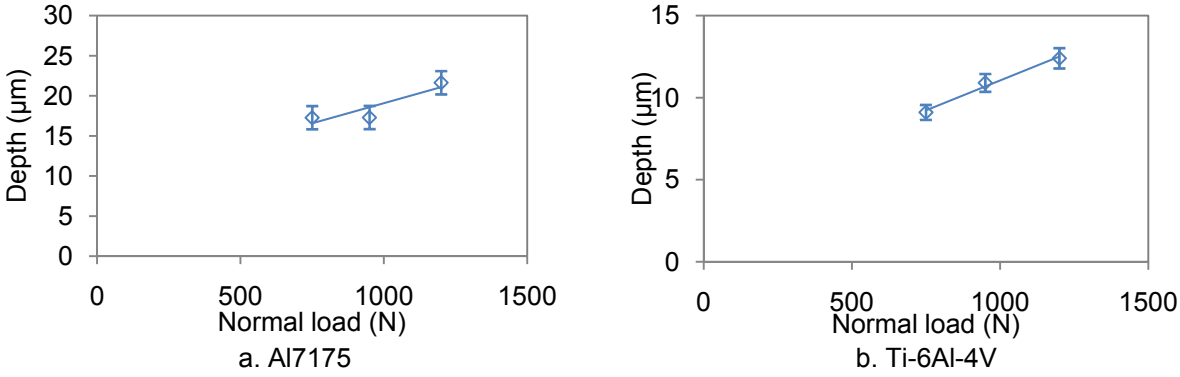

Figure 4.9 Variation of the depth with normal load

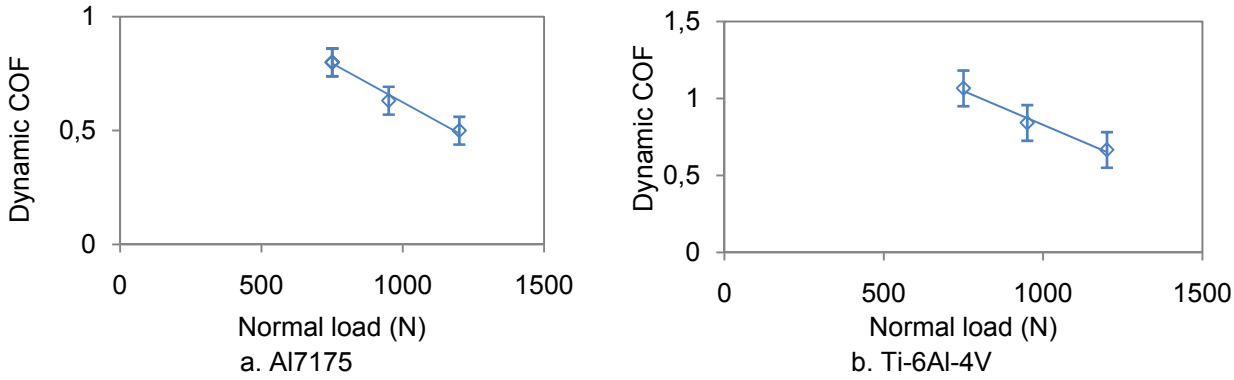

Figure 4.10 Variation of the dynamic coefficient of friction with normal contact load

It is observed in figure 4.8 that stick zone increases with increasing the normal load. From figure 4.11 can be depicted that the overall size of the contact area increases with increasing the normal load. These are expected results because according to Bowder and Tabor theory [118], the real area of contact between two surfaces is directly proportional to the applied normal load. So, it is expected an increase on the area of contact with increasing the normal load. However in the fretting fatigue case the increase in the contact area cannot be attributed only to normal load, because there is an inter-relation between several parameters (normal load, tangential load, relative displacement amplitude, material combination, environment etc.). As it is known solid materials subjected to loads deform in either elastic or plastic manner. In most contact situation we find a mixture of both elastic and plastic deformation. Even if the surfaces of the pad and specimen are very well polished there will always be some discontinuities and when the two contacting bodies are loaded against each other they make contact only at the tips of asperities. Thus the load applied to the solids in contact may induce a general elastic behaviour in the bulk of the solid bodies, but since the actual contact must occur at the tips of the surface asperities these may be subjected to localized plastic deformation at their tips. The amount of plastic/elastic deformation must obviously depend on the value of the applied load and the degree of plastic deformation increases with increasing the load. This plastic flow causes an increase in the area of contact until the real area of the contact is gust sufficient to support the load. Under this conditions, for an ideal elastic-plastic material

$$A \cdot p_0 = F_n \tag{4.3}$$

where A – the real area of the contact; p_0 is the yield pressure of the material, F_n is the normal load.

Thus, this deformable nature of the material in contact allows the coexistence of a zone of sticking and zones of microslip. As a primary effect tangential load and as a

secondary effect the relation between the normal and tangential loads (COF) play an important role in the coexistence of the stick and slip zone. It is already known that only by increasing the tangential load, the area of slip increases until, when $F_t = \mu F_n$, they met at the centre of the contact and macroslip take place throughout the contact zone. So in the stick region $F_t < \mu F_n$ and within the slip regions $F_t = \mu F_n$.

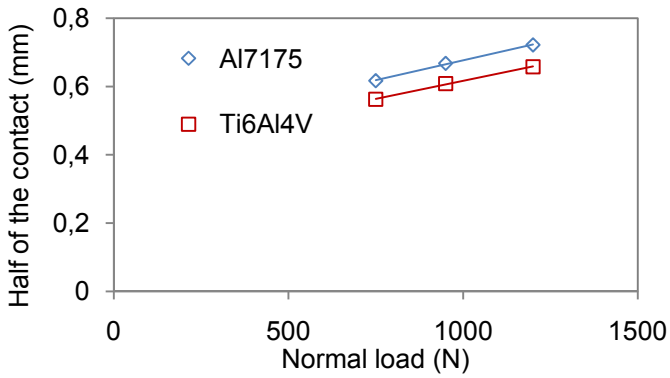

Figure 4.11 Variation of the half of contact with normal load

The results shown in figure 4.9 indicate that there is a linear increase of the depth with increasing normal load within the whole range of the normal load investigated.

The increase of the depth can be explained by the synergetic effects between the stress state and wear in the contact region. It can be seen from figure 4.12 that the peak Hertzian contact pressure and also the half of the contact zone increase with increasing normal load. It can be seen from figure 4.13 that the maximum pressure for the sphere on plane configuration is in the middle of the contact. With increasing normal load (contact pressure – figure 4.12) the wear depth development will become faster and the elimination of the surface layers will be accelerated. As the contact pressure increases the depth of the concavity becomes larger. In partial slip regime the formation of the concavity can be related with the plastic deformation of the specimen.

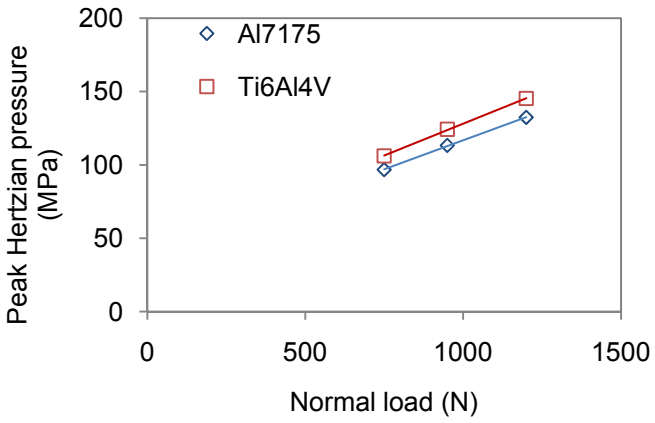

Figure 4.12 Variation of the peak Hertzian pressure with normal load

The concavity that is formed plays an important role since there it is induced a stress concentration. Based on the depth measurements from the final geometries of the damaged areas (fretting scar) the stress concentration factor was determined. As can be seen from figure 5.4 [124] the stress concentration factor increases with the concavity depth (5.1.3 Stress concentration factor due to “wear damage area” – fundamentally new approach).

If the normal load on the contact increases then the plastic zone also grows. The plastic strains can become very much larger with significant changes in the surface profile. For example, if only the normal load will be applied on the specimen through pad it will be induced equal compression strain in both sides of the contact zone (figure 4.14a). But when the tangential load is applied (F_t) there will compression strain in one side and tensile strain in the other side of the contact zone. And for each fatigue cycle the strain in each side will change from tensile strain and compression strain.

As it is well known the maximum normal load it is the one that is responsible for the maximum stress occurring in the specimen. It can be seen from figure 4.15 that the maximum stress (which takes into consideration all the stresses involved into the fretting contact) increases with increasing the normal load.

The microscopic photographs (Table 4.5) [128,170] show that the contact zone increases with the number of cycles. The increase of the slip zone is strongly dependent on the wear behaviour of the material.

Figure 4.16 shows that the fretting fatigue life decreases with increasing depth. This is due to the concavity that is formed which gives rise to a stress concentration. This has a great influence on fretting fatigue life. As a fact most of the fatigue cracks initiate on the sites of stress concentration where the stress has a maximum value.

Figure 4.17 shows that fretting fatigue life decreases with increasing maximum fretting fatigue stress $\sigma_{max,FF}$ (it includes all loads involved into the fretting contact). Figure 4.18 shows that the relative displacement amplitude increases with increasing the maximum fretting fatigue stress.

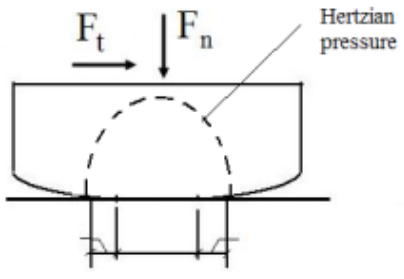

Figure 4.13 Contact between specimen-pad and the Hertzian pressure distribution

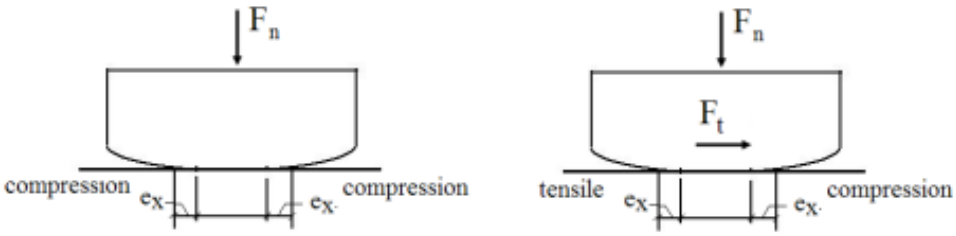

a b

Figure 4.14 Contact zone: a. normal load; b. normal plus tangential load

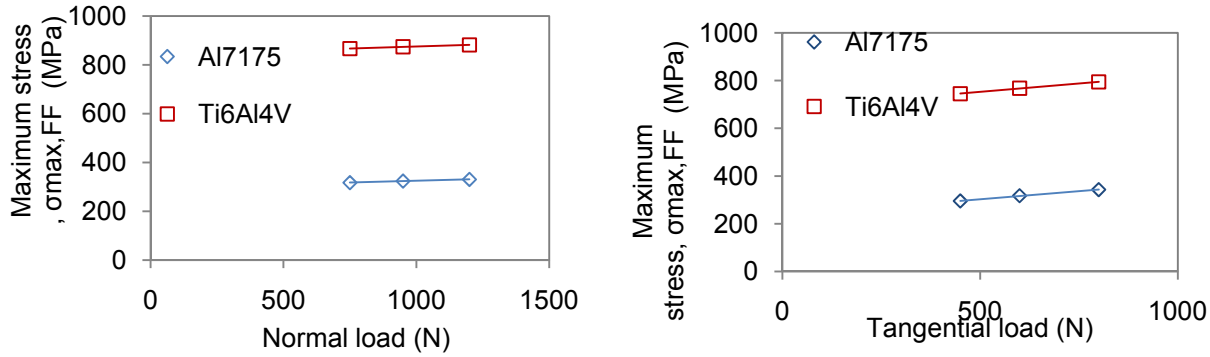

a b

Figure 4.15 Variation of the maximum fretting fatigue stress with: a normal load and b. tangential load

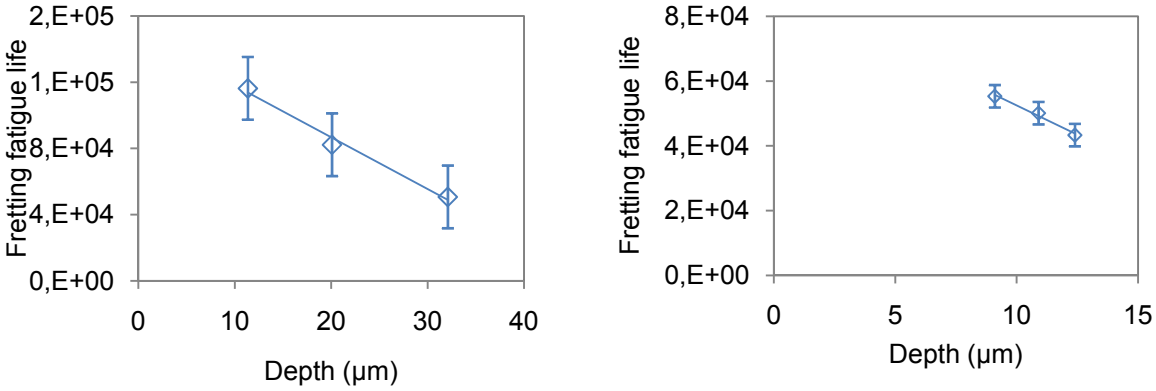

a. Al7175 b. Ti6Al4V

Figure 4.16 Fretting fatigue life vs. depth

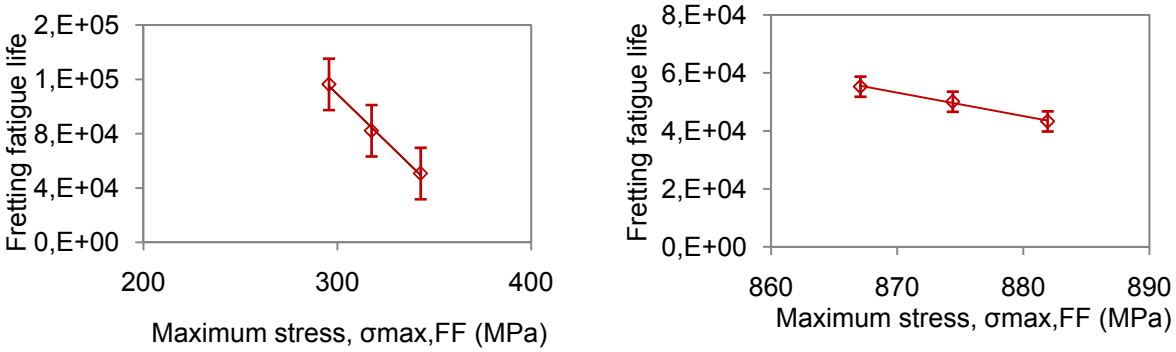

a. Al7175 b. Ti6Al4V

Figure 4.17 Fretting fatigue life vs. maximum fretting fatigue stress

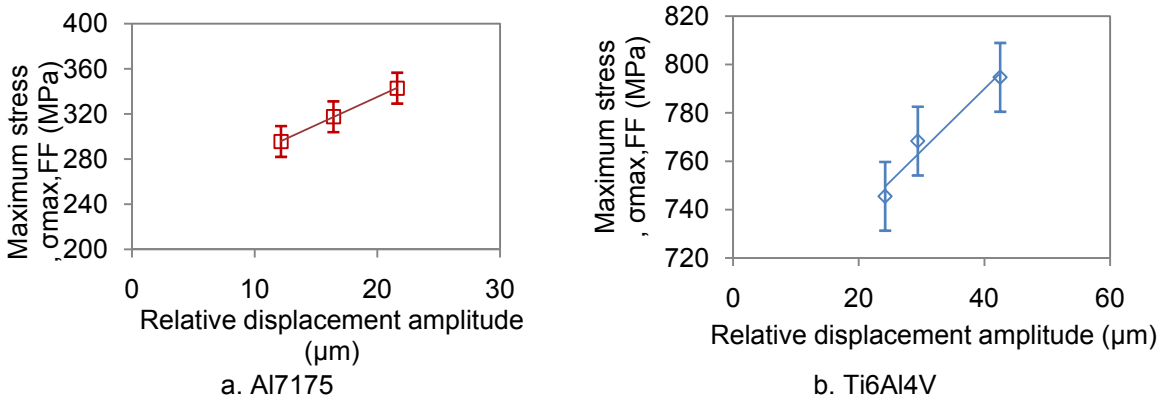

Figure 4.18 Maximum fretting fatigue stress vs. relative displacement amplitude

Figure 4.10 shows that the dynamic COF decreases with increasing normal contact load. When the two bodies are in contact and sliding past one another, a dynamic frictional force opposes the direction of slip. The two surfaces stop sliding when the external forces that cause the surfaces to slip no longer exceed the dynamic frictional forces.

An increase in COF will modify the stress level and changes the location of the maximum loading. Less COF should lead to less slip region, and consequently low damaged area. So, the relation between the normal and tangential loads is very important and has a great influence on distribution of the fretting fatigue contact zones.

Regarding the connection between normal and tangential loads it can be seen from figure 4.19 that the normal load has an influence on the imposed tangential load. The tendency showed that the tangential load decreases with the normal load. The measured tangential load is slightly smaller than the initial imposed one, due to the energy release at the fretting contact, local deformations, friction etc. A smaller tangential load leads to a smaller slip zone.

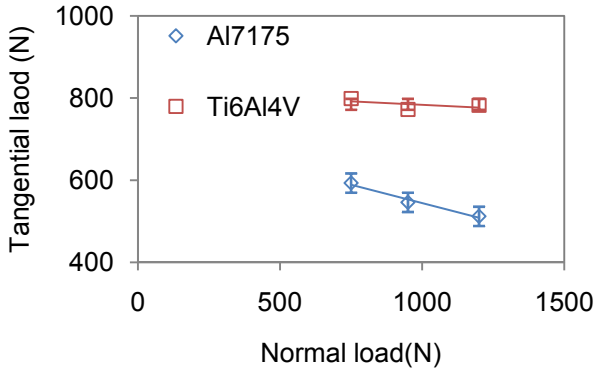

Figure 4.19 Normal load vs. tangential load

The increase of the slip zone can also be explained by the decrease of the dynamic COF with normal load (figure 4.10). The decrease of COF induces an increase in the relative displacement. This increase in the slip zone can be explained also based on the local plastic deformation which gives rise to ratcheting and shakedown processes.

It should be mentioned that the peak Hertzian pressure (figure 4.12), the half of contact (figure 4.11) and the maximum fretting fatigue stress, $\sigma_{max,FF}$, (figure 4.18) are determined using an analytical procedure, while the other results are experimentally determined. The analytical relations used are presented elsewhere (2.3.3 Smith-Watson-Topper model).

II. The modification of fretting contact via varying tangential load

To investigate the influence of tangential load on the modifications of the fretting contact zone, several tests with the same normal and axial loads were selected. The only parameter that is varied is the tangential load.

Figure 4.20 shows the variation of the slip zone with the tangential load. Figure 4.21 shows the variation of the depth and relative displacement amplitude with tangential load. Figure 4.22 shows the variation of the dynamic coefficient of friction with tangential load.

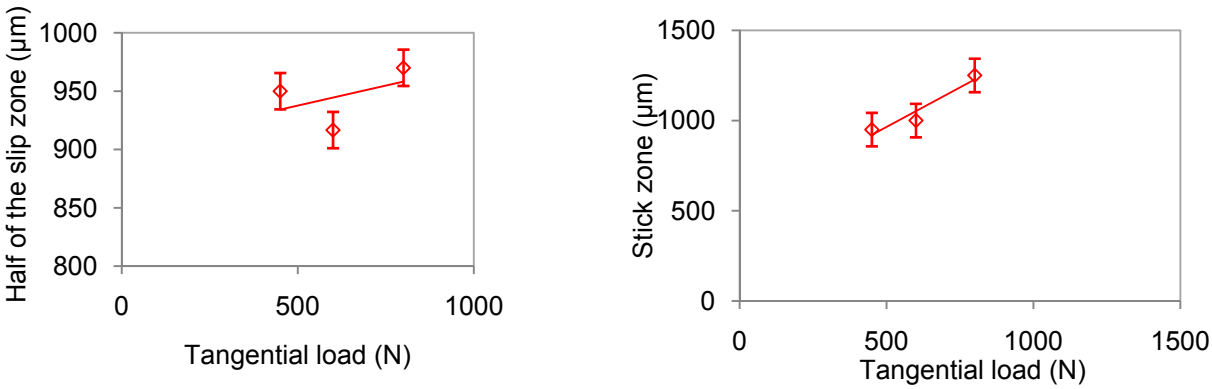

a. Al7175 b. Ti-6Al-4V

Figure 4.20 Variation of the slip (half of the slip zone) and stick zones with tangential load

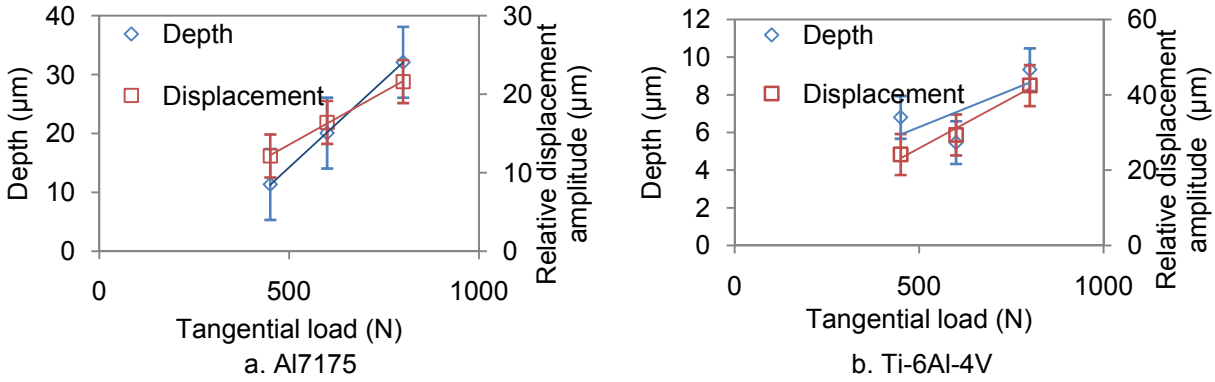

Figure 4.21 Variation of the depth and relative displacement amplitude with tangential load

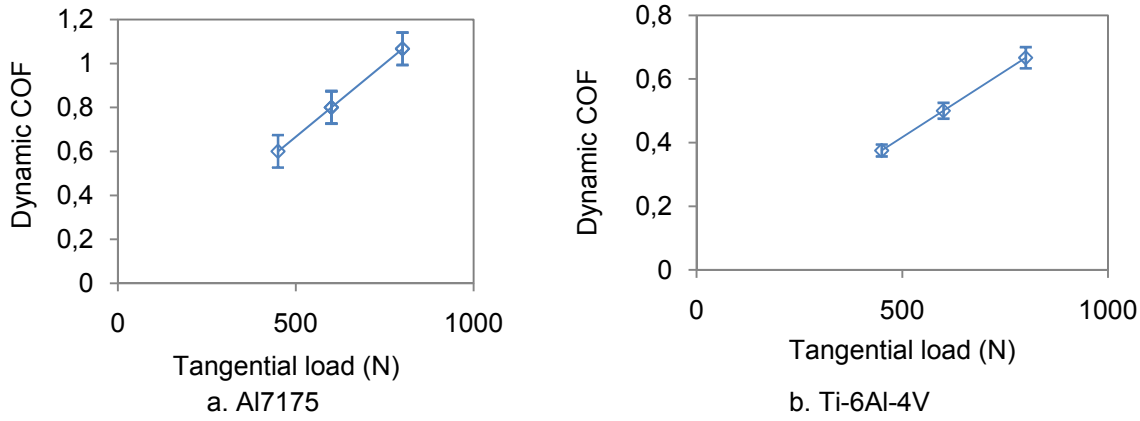

Figure 4.22 Variation of the dynamic coefficient of friction with tangential load

The results presented in figure 4.20 show that the slip zone increases with increasing tangential load. This behaviour is due to the pad that is more 'fixed' with a higher tangential load which allows a bigger relative movement between specimen and pad. The tangential load is the parameter that has the bigger influence in the relative displacement values. As the tangential load increases, the area of the slip zone increases. When the tangential load reaches μF_n the regime will change from partial slip to gross slip. Regarding the materials response it can be seen that the intensity of the fretting fatigue process (the modification on the stick and slip zones) is much more prominent for Ti6Al4V alloy compared with Al7175.

From figure 4.21 can be seen that the depth and also the relative displacement amplitude increase with increasing tangential load.

Regarding the increase of depth with increasing tangential load, the explanation is based on the stress state of the specimen. As has been already stated previously in the fretting fatigue case the specimen stress state changes with the machine load cycle, and it is reasonable to expect that the wear behaviour of materials might be affected by the specimen stress state. Regarding the behavior of the relative displacement with increasing tangential load, it is strongly linked with the changes on slip zone. Relative

displacement should follow exactly the mirror tendency of the slip zone. By increasing the slip zone the relative displacement should increase. From figure 4.23, subsequently presented (and also figure 2.4) can be observed that any small change in relative displacement amplitude may substantially change the fatigue life. Thus, special attention should be paid to a changing value of relative displacement amplitude during the fretting fatigue tests because fretting fatigue life is very susceptible to the relative displacement [8]. The relative displacement amplitude is strongly linked to the tangential load amplitude. This means that small changes in tangential load amplitude may cause substantial changes in relative displacement. Many studies showed that relative displacement amplitude is a key variable in fretting fatigue life, because it seems to be the principal cause of the damage [8, 22, 26, 65]. Much attention has been given in previous studies to the average or maximum value of the relative displacement amplitude and respective fatigue life.

It can be seen from figure 4.22 that the dynamic COF increases with increasing tangential load. The dynamic COF increased linearly with increasing depth of the hole being more difficult for the pad to move relative to the specimen, and it can be the reason of the increase. What it is interesting to highlight is that the highest COF corresponds to the deeper hole (figures 4.21, 4.22).

III. The modification of roughness via varying normal and tangential loads

Figure 4.23 shows the variation of the roughness values with increasing normal and tangential load. Figure 4.23 also shows the variation of the normalized roughness by stick/slip dimensions ratio with increasing normal and tangential load. The reason for this last figure lies on the fact that roughness is different in the stick and in the slip zones and measurements are an average of both zones (roughness is bigger in slip zone). Further to this, R_a values were measured at the end of the test (after final rupture). It was shown before that roughness changes with the number of cycles (fatigue life) (see Table 4.2).

For comparative purposes, the average roughness for the initial virgin surface is 0.07 μm for Al7175 alloy, 0,04 μm for Ck 45 steel, and 0.08 μm for Ti6Al4V alloy. The roughness presented in Figure 4.23 is the average value of five measurements for each fretting fatigue damaged area.

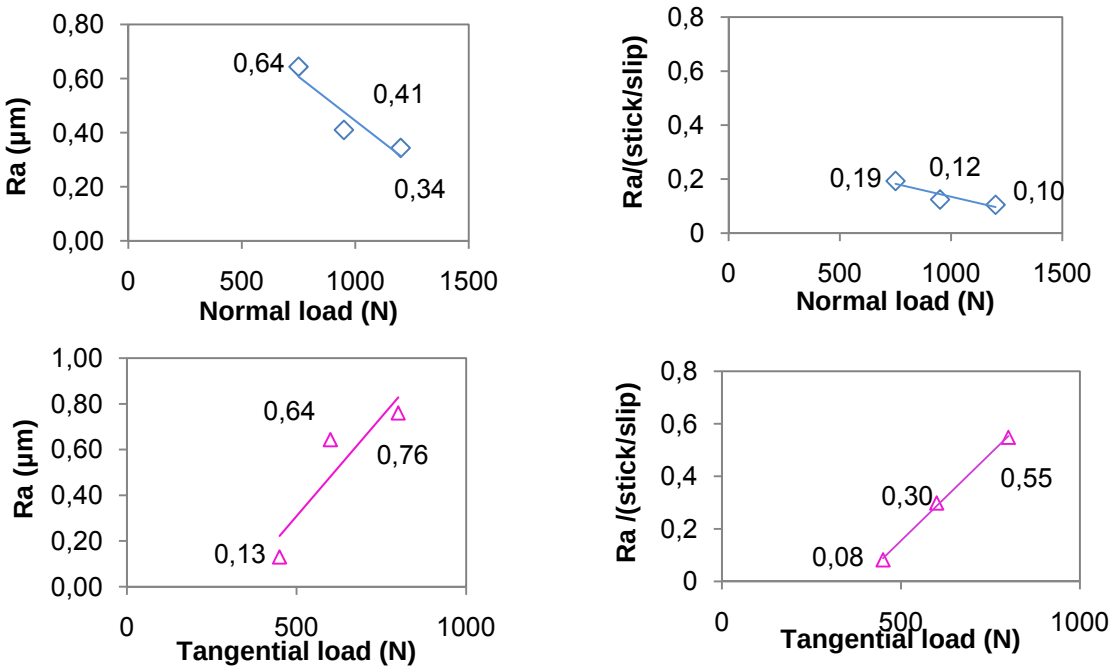

Al7175

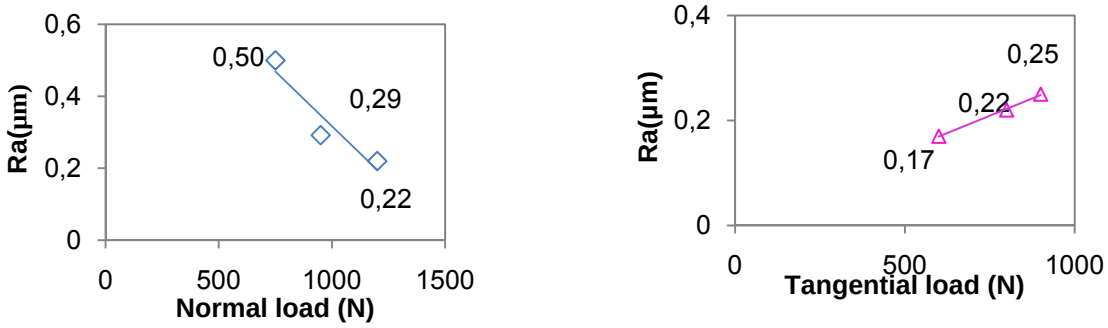

Ck45

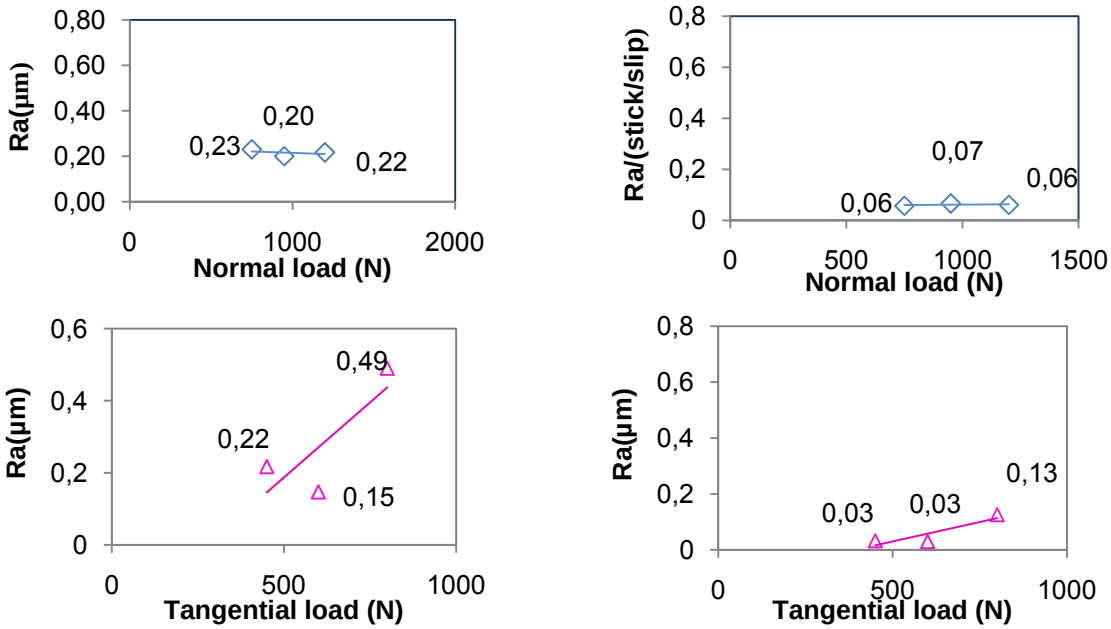

Ti6Al4V

Figure 4.23 Variation of the roughness (R_a) and of the normalized roughness $\left(R_a/(\frac{stick}{slip})\right)$, with the normal and tangential load

The results presented in figure 4.23 show that roughness decreases with increasing normal load. It can also be seen that roughness increases with increasing the tangential load. It has been demonstrated [27, 61, 86] that the increase on the roughness value is due to the increase in the slip zone size. This is due to the fact that the pad is more 'fixed' with increasing tangential load and it causes a bigger relative movement between the specimen and pad (the size of the slip zone increases).

Regarding the decrease of roughness with the normal load, the explanation is based on the fact that the stick zone increases with increasing normal load, and this leads to a smaller slip zone (less damage).

As fretting fatigue cracks initiate predominantly at the interface between the two contact zones (slip and stick), the surface roughness values seem to be sufficiently important (substantially high roughness values) in order to be considered relevant in fatigue life predictions (issue developed in chapter 5). Based on the roughness of the damaged area measurements it will be proposed a factor that takes it into consideration in life predictions.

4.1.5 The effect of relative displacement on fretting fatigue life

Figure 4.24 presents the effect of relative displacement on fretting fatigue life for Al7175 alloy, Ck45 steel and Ti6Al4V alloy. For Al7175 alloy and Ck45 two series of fretting fatigue tests (two different machine loads) are presented, and for Ti6Al4V alloy only one series (one machine load). In all three graphs the results were compared with the work of Ambrico [173].

This part of the present study shows the importance of the magnitude of the relative displacement amplitude on fretting fatigue life. Vingsbo and Soderberg [8, 86] found that the fretting fatigue life initially decreases with the increasing relative displacement till a minimum fretting fatigue life is observed at a certain point. By increasing relative displacement range after this critical point the fretting fatigue life increases (figure 2.4).

The same strong dependence was found in the present study, as shown on Figure 4.24. In this figure, after the work of Ambrico [173] it is also depicted the typical variation of fretting fatigue life with relative displacement for a wide range of variation of the latter parameter. The critical point, for Ambrico, is about 40 μm. There are studies that show for the same material different values for this critical point. For example, Jin and Mall in

their study found that the critical relative displacement amplitude for Ti6Al4V alloy was between 50 and 60 μm [22].

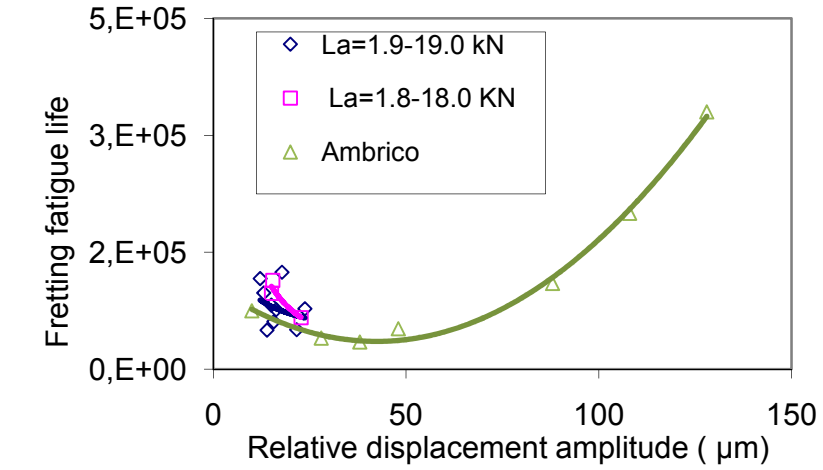

a. Al7175

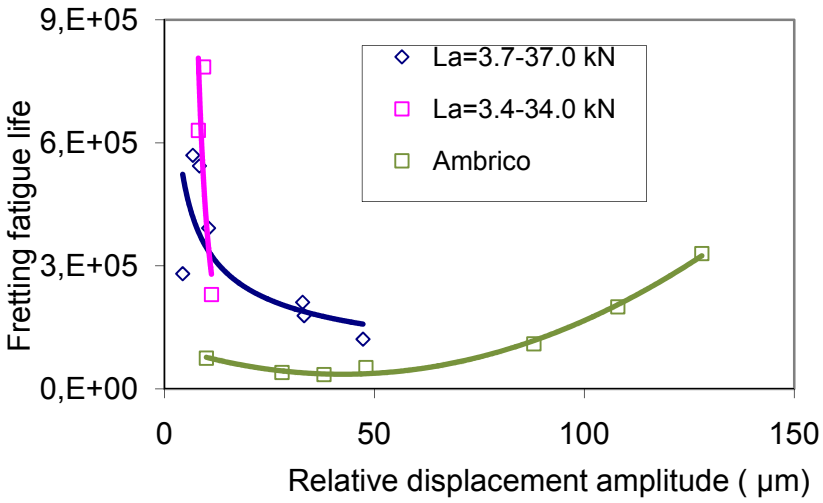

b. Ck45

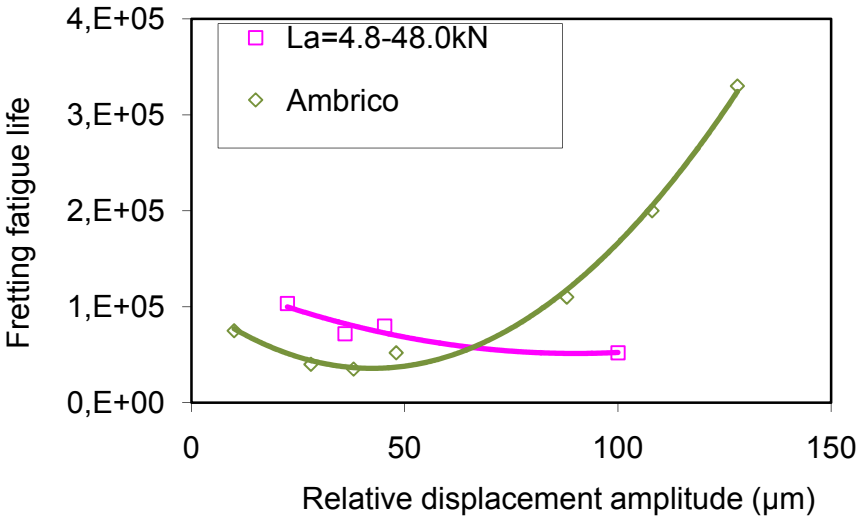

c. Ti6Al4V

Figure 4.24 Fretting fatigue life vs. relative displacement amplitude: L_a - machine axial load [170]

What is interesting in the present study is that for identical relative displacements the resistance to fretting fatigue was different for all the materials used in this study. The resistance to fretting fatigue is much lower for Al7175 and Ti6Al4V alloys than for the CK45 steel. It can be seen form figure 4.24 that for a relative displacement of around 22 μm the fretting fatigue life was 66199 cycles for Al7175 alloy, around 200 000 cycles for Ck45 steel and 103334 for Ti6Al4V alloy.

Thus the relative displacement effect on fretting fatigue life is strongly material dependent. The Al7175 and T6Al4V alloys seem to be much more sensitive to relative displacement than the CK45 steel. Further the critical point seems to be also strongly dependent on the material.

4.1.6 Evolution of the fretting fatigue loops

Figure 4.25 shows the evolution of the fretting fatigue hysteresis loops for Al7175 alloy, Ck45 steel and Ti6Al4V alloy. The fretting fatigue loops are based on the tangential load and on the relative displacement amplitude. The tangential load was normalized by its maximum value.

As it is known the fretting regimes (slip or stick or even stick-slip) can be also identified by plotting the tangential load vs. relative displacement [13]. In Figure 4.25a it can be seen that in Al7175 alloy case, two fretting condition regimes are present. At the beginning of the test the fretting fatigue hysteresis loop has a quadratic shape which is consistent with the gross slip regime. Then, after a few hundred cycles, the shape of the fretting loops changes. They are close to an elliptical shape which is consistent with a partial slip regime, or a mixed contact of a slipping and sticking zone. In figures 4.25 b (Ck45 steel) and c (Ti6Al4V alloy), it can be seen that the regime was partial slip throughout the entire fretting fatigue life.

Once more this evolution confirms in part the variation of the tangential load amplitude (Figure 4.5) and the relative displacement amplitude (Figure 4.6).

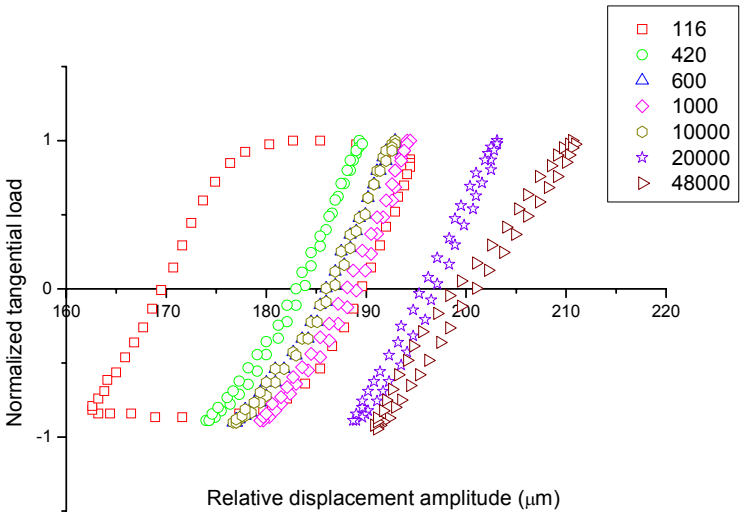

a. Al7175

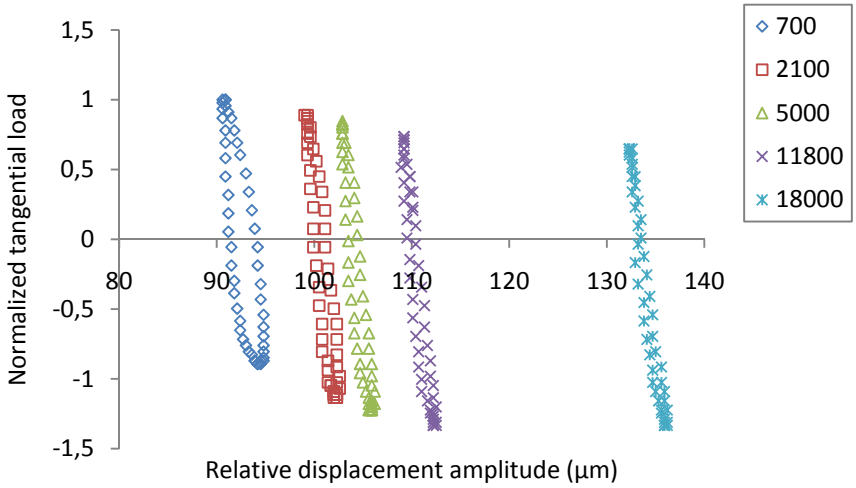

b. Ck45

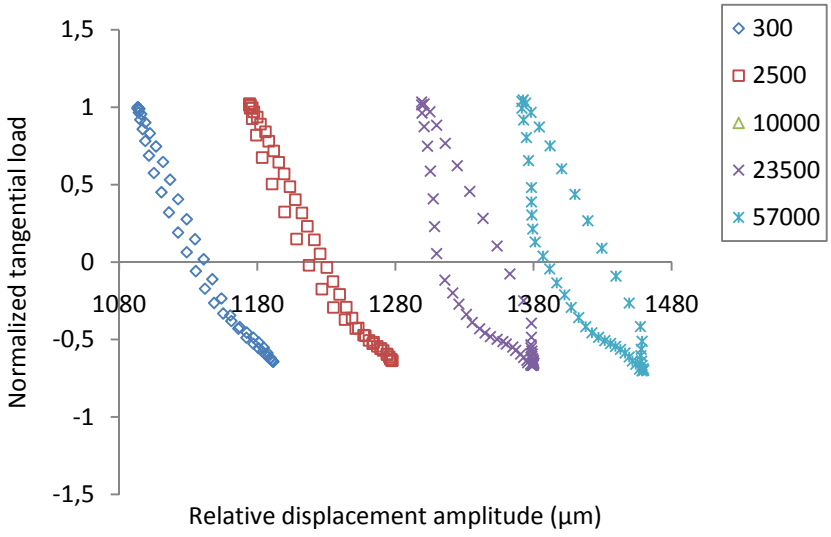

c. Ti6Al4V

Figure 4.25 Evolution of the fretting fatigue loops with the number of cycles

4.1.7 Plain fatigue tests

a. Output of the plain fatigue tests

A few number of plain fatigue tests, carried out at the same *R* ratio as fretting fatigue tests, have been performed with the only purpose of seeing the influence of the fretting effect on fatigue life.

A summary of the plain fatigue tests: specimen number, loading condition and number of cycles to failure are presented in Table 4.6.

Table 4.6 Loading conditions and number of cycles to failure (plain fatigue tests)

Test		Machine axial load, L_a [kN]	Nr of cycles to failure
Al7175 alloy	AF1	2.60-26.0	5,000,000
	AF2	2.70-27.0	1,636,199
	AF3	2.70-27.0	1,347,973
	AF4	2.90-29.0	192,639
	AF5	3.20-32.0	67,374
	AF6	3.50-35.0	29,495
Ck45 steel	CF1	3.70-37.00	5,000,000
	CF2	3.75-37.50	5,000,000
	CF3	3.80-38.00	298,912
	CF4	3.90-39.00	235,680
	CF5	4.00-40.00	136,140
	CF6	4.10-41.00	48,660
Ti6Al4V alloy	TF1	6.00-60.00	2,470,301
	TF2	6.05-60.50	179,449
	TF3	6.10-61.00	162,516
	TF4	6.20-62.00	165,832
	TF5	6.50-65.00	133,402
	TF6	7.00-70.00	123,342

b. Fretting fatigue vs. Plain fatigue – The synergetic effect

Figures 4.26 presents the relation between the normalized maximum stresses used in fretting fatigue and plain fatigue tests, and the number of cycles to failure for Al7175 alloy, Ck45 steel and Ti6Al4V alloy. The stress was normalized with respect to the tensile strength of the material. The same pad loading conditions (normal and tangential load) were used for all the fretting fatigue tests (for each material).

On Figure 4.26 it is clear the difference between the plain fatigue life and fretting fatigue life of the alloys used in this work. It can be depicted that there is a bigger difference between fretting fatigue life and plain fatigue life on Al7175 and Ti6Al4V alloys as compared to Ck45 steel. Lee and Mall [177] in their study concluded that the reduction of fatigue strength by fretting is generally attributed to the increase of tensile

and shear stresses within the contact region and to surface or subsurface damage by the oscillatory relative movement.

In the present study the normal loads applied to the pads (Hertzian contact stress) were the same for all the materials (Al7175, Ck45 and Ti6Al4V). Thus the bigger difference between fretting fatigue life and plain fatigue life on Al7175 and Ti6Al4V as compared to Ck45 cannot be attributed only to the stress levels due to the contact stresses. The higher fretting effect should then be attributed mainly to the wear damage effect. Lindley [178] also reported that the damage evolution, namely through its wear performance, may be the responsible for the reduced fretting fatigue performance. An understanding of the wear damage evolution on fretting fatigue tests is therefore fundamental.

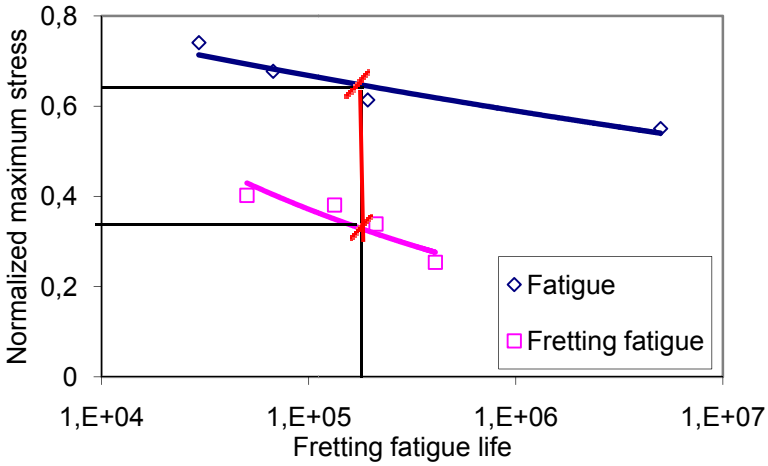

a. Al7175

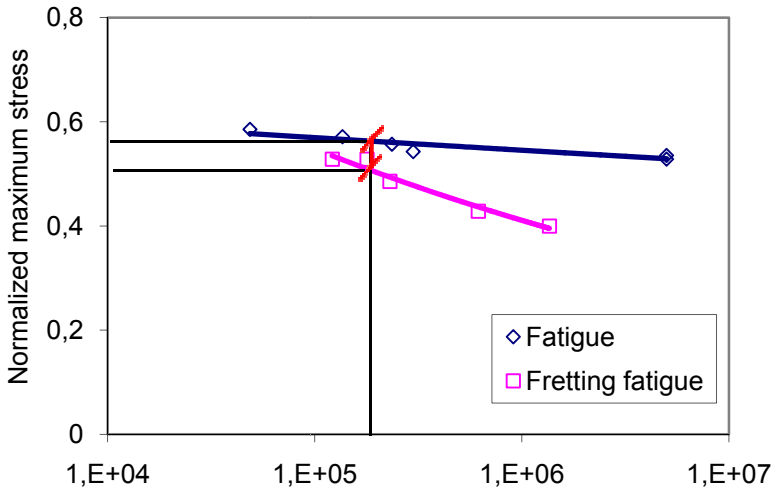

b. Ck45

Figure 4.26 The normalized maximum stress vs. fretting fatigue and plain fatigue life (cont.)

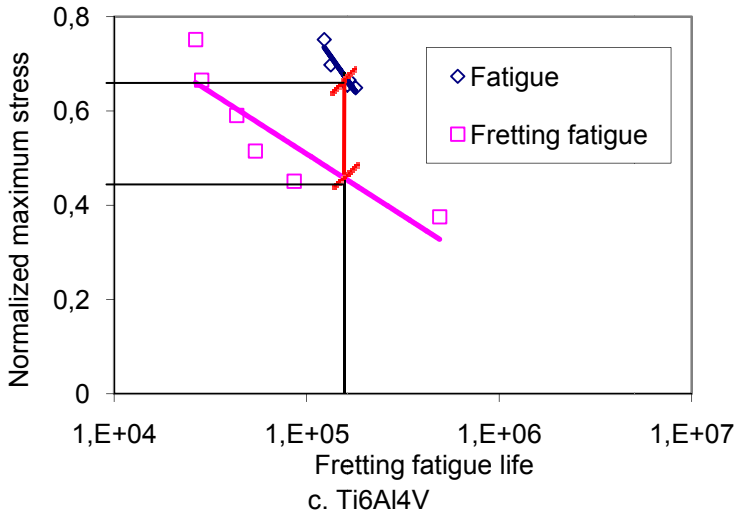

Figure 4.26 The normalized maximum stress vs. fretting fatigue and plain fatigue life

Thus, a first preliminary conclusion is that during a fretting fatigue test as the scar depth increases faster for the Al7175 alloy, the stress concentration factor is higher for that alloy specimen as compared to the Ck45 alloy where the scar depth is much smaller (see Table 4.5).

4.2 Reciprocating wear tests

In fretting fatigue case the specimen stress state changes with the machine load cycle, and it is reasonable to expect that the wear behaviour of materials might be affected by the specimen stress state. The different wear behaviour (different stress state) during a fatigue cycle is proposed to be the cause for the asymmetrical fretting fatigue scar (see 4.1.3 Evolution of the most significant parameters during a fretting fatigue test (Asymmetrical fretting scar formation)). In order to validate this assumption several reciprocating wear tests under an additional elastic stress state were carried out. The results from the reciprocating wear tests were then extrapolated to the fretting fatigue case. It was observed that the additional elastic bulk stress has a substantial influence on the wear behaviour of the materials used in the study. It was concluded, therefore, that it is pertinent to take it into consideration in wear assessment, and consequently in fretting fatigue predictions. In order to take into account the elastic bulk stresses imposed by external loading, a physical model that is a modification of the Archard´s model for the prediction of wear volume was proposed.

4.2.1 Wear behaviour under additional elastic stress states

The materials used in this study (Al7175, Ck45, Ti6Al4V) experienced a substantial difference on the wear behaviour when the specimen was under compression or under tension.

The results of the reciprocating wear tests are presented in figures 4.27, 4.28. The data points in all the graphs represent the mean values of five tests. For each wear track were performed five measurements. The error bars represent the interval of variation of the measured values.

(i). Depth of the wear scar

Figure 4.27 shows the depth of the wear scar for all three additional bulk stress conditions (zero stress, tension, and compression).

It can be seen from figure 4.27a (Al7175 alloy) and 4.27b (Ck45 steel) that depth decreases under tensile stresses and increases under compressive stresses. The titanium alloy has a different behaviour. From figure 4.27c it can be seen that the depth

increased under both tensile compressive stresses. The increase of the depth in much more pronounced under tensile stresses.

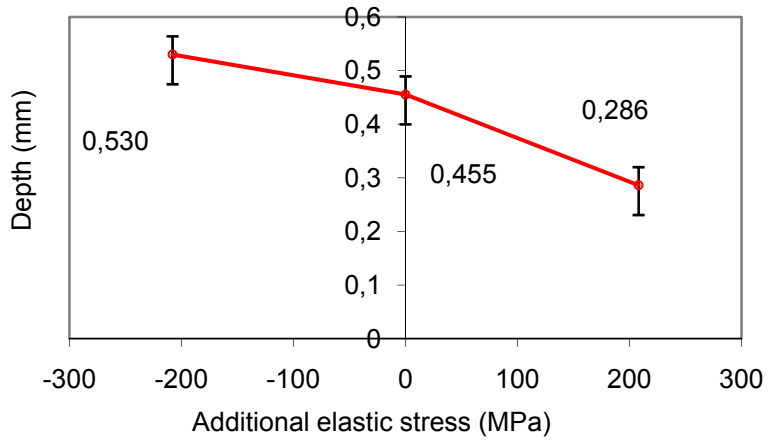

a. Al7175

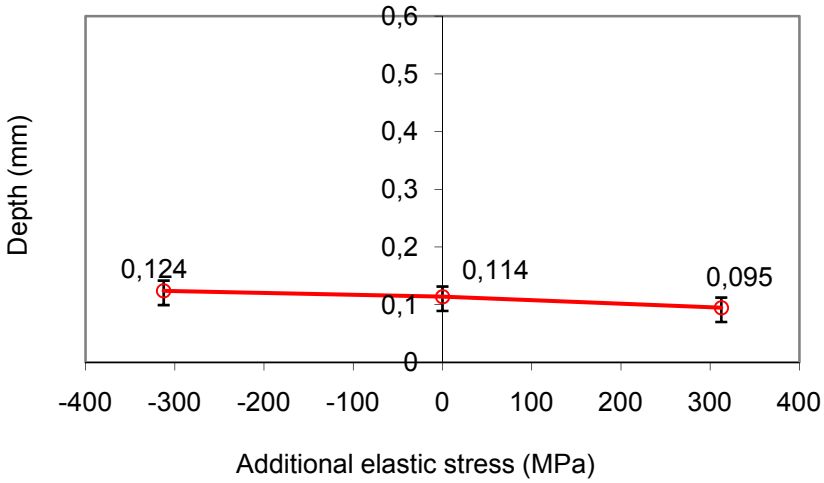

b. Ck45

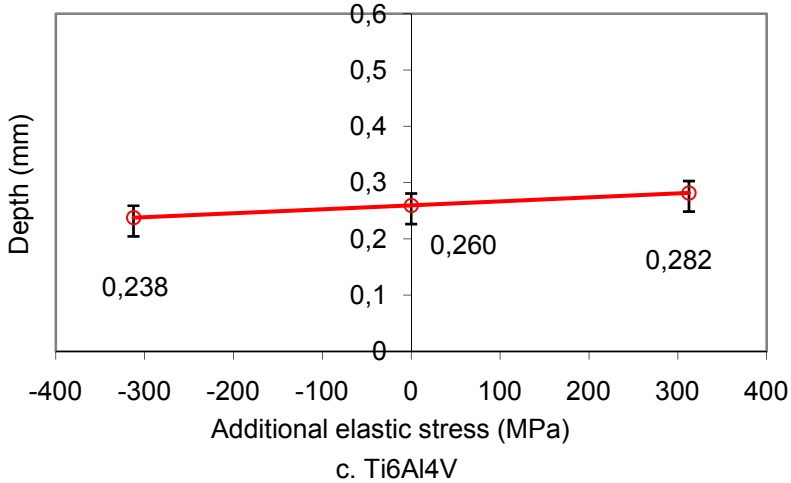

c. Ti6Al4V

Figure 4.27 Evolution of the scar depth as a function of the additional bulk stresses [167]

(ii). Wear volume

Figure 4.28 presents the experimental and predicted wear volume as a function of the additional elastic stresses.

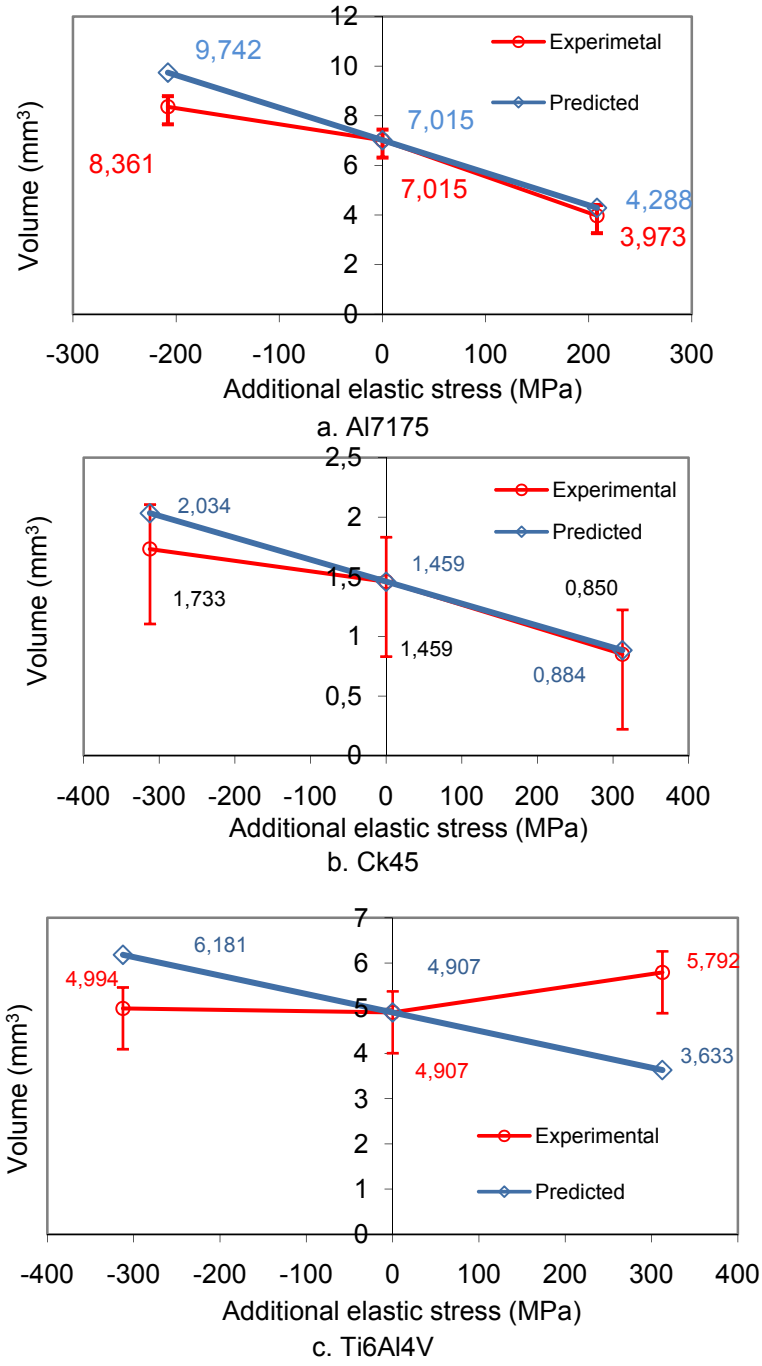

Figure 4.28 Evolution of the experimental and predicted wear volume as a function of the additional elastic stresses: a. Al7175 alloy, b. Ck 45 steel, c. Ti6Al4V alloy [169,171]

For Al7175 alloy (figure 4.28a) the wear volume decreased about 43% when the specimen was under tensile stresses and increased about 19% when the specimen was under compressive stresses, as compared to no additional elastic stress state. In the

case of Ck45 steel (figure 4.28b) the wear volume decreased about 41% when the specimen was under tensile stresses and increased about 18% when the specimen was under compressive stresses, as compared with no additional stress value. In the case of Ti6Al4V alloy (figure 4.28c) the wear volume increased about 2% under compressive stresses and 25% under tensile stresses.

From the results presented on figure 4.28 it can be seen that the additional stress states, both in tension and in compression, have a substantial influence on wear, being therefore appropriate to consider it in the wear predictions. It is worth nothing that the additional stress level as introduced by the external load is ±208 MPa for Al7175 alloy, and ±312.5 MPa for Ck45 steel and Ti6Al4V alloy. In order to compare the response between the material it should be mentioned that the additional elastic stress state in the case of Al7175 alloy and Ck45 steel is around 38% of the rupture strength and only 29% in the case of Ti6Al4V alloy.

From Figure 4.28 it is clear that the Al and ck alloys show the same clear evolution of wear with additional elastic stress. The Ti alloy has smaller variations and the variation of wear volume with the additional stress is smaller than the measurement error.

(iii). Proposed modified Archard's model

In order to quantify the wear volume, the Archard's model (equation 2.3) was modified in order to take into account the effect of an additional elastic stress, either in tension or in compression, imposed by an external load. The modified Archard's model [169] can be expressed in the following mathematical form:

$$V = K\frac{F_n}{H}S\left(1 - \frac{\sigma_{add}}{\sigma_r}\right) \tag{4.2}$$

where: σ_{add} is the additional elastic stress and σ_r is the tensile strength.

The wear coefficient, K, was defined in this work as the wear volume, V, divided by the normal load, F_n, and also divided by the sliding distance, S. The wear coefficient was determined in this way for the zero load case. In compression or tension case, the wear coefficient may change but in this case was used the same wear coefficient for all the cases as no difference on hardness has been obtained.

The predicted results are also presented in figure 4.28 and it can be seen that there is a good correlation between experimental and predicted values for Al7175 alloy and Ck45 steel. The prediction is not adequate for Ti6Al4V alloy, maybe due to the

lower additional stress level (in relation to Yield stress) compared with the Al7175 alloy and Ck45 steel.

(iv). Evolution of the coefficient of friction with sliding distance

Figure 4.29 shows the evolution of the coefficient of friction with sliding distance.

The red line presented in figure 4.29 highlights the behaviour of the average friction coefficient in a typical wear test. After a first period it remains constant during the all test. In the present study the friction coefficient sharply increases at the beginning of the test and increases linearly with the sliding distance. This could be due to the increase of the scar depth along the test. As the scar depth increases the pin has a higher resistance to slide along the inclined plans of the scar surfaces.

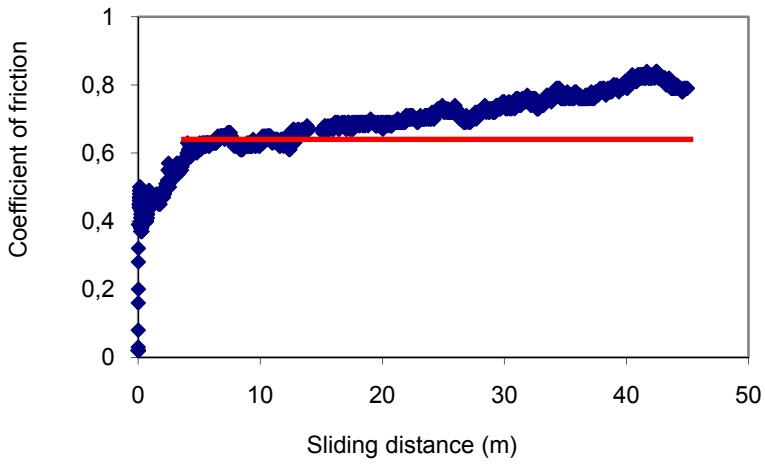

a. Al7175

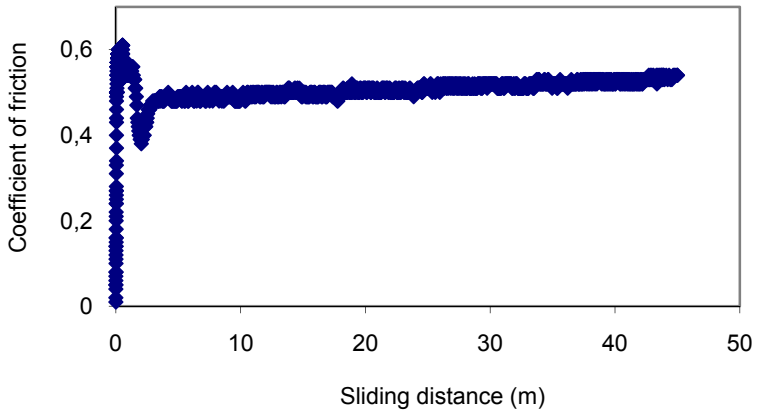

b. Ck45

Figure 4.29 Evolution of the friction coefficient with sliding distance [169,171] (cont.)

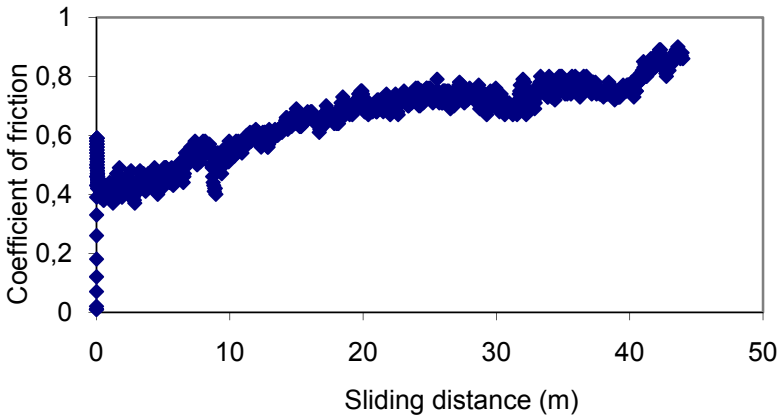

c. Ti6Al4V

Figure 4.29 Evolution of the friction coefficient with sliding distance [169,171]

In order to physically explain the wear behaviour when the material is under an additional stress state, in the elastic domain, the following aspects will be discussed subsequently: wear mechanism; hardness, roughness; additional stress state (tensile or compressive) with plastic and elastic deformation; micro-roughness as a function of grain size and orientation and macro roughness as a function of the material finishing process.

4.2.2 Morphological characterisation of the contact surface

In order to have a good characterization of the contact surface, after each test the specimens were ultrasonically cleaned to eliminate as much debris as possible.

The following independent techniques were used:

i) scanning electron microscopy (SEM).

ii) surface profilometry;

iii) hardness measurements.

i) Scanning electron microscopy (SEM)

Figure 4.30 shows the high resolution images (obtained by SEM) of the wear surfaces for specimens under three additional stress states: compression, zero stress and tension. Scanning electron microscopy (SEM) studies showed a similar wear mechanism for all three test cases (Figure 4.30). The worn area is of an oval shape, being possible to observe that the material is plastically deformed in the sides in all cases.

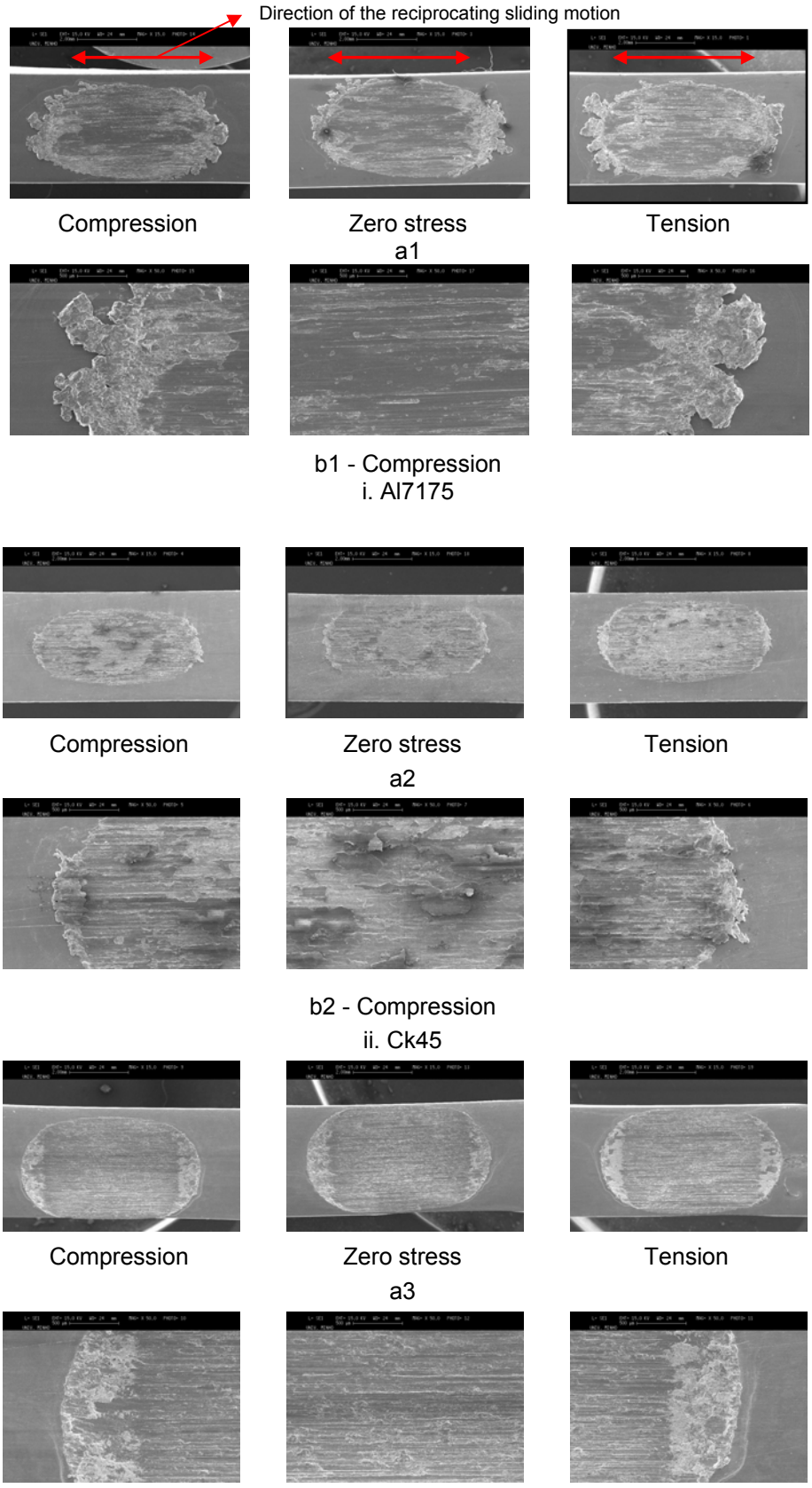

Figure 4.30 High resolution images of the wear surfaces: a1, a2, a3 - global view of the wear tracks; b1, b2, b3 - amplified views of the wear tracks for the compression case

SEM was also used to determine if there was material transfer from one surface to the other. No transfer was found between matting materials in none of the three tests. So observed differences in wear volume cannot be attributed to the material transfer effect.

ii) Surface profilometry

A Mahr Perthen profilometer was used to characterize the wear scar on all specimens. Five measurements of profile in the longitudinal and transversal directions of each specimen have been carried out. The depth, length, area and volume are the average values of these measurements. All measurements were performed in AutoCAD, as shown in figure 4.31. Figure 4.32 shows the surface profiles for the specimen (manufactured from Al7175 alloy) for all three loading conditions.

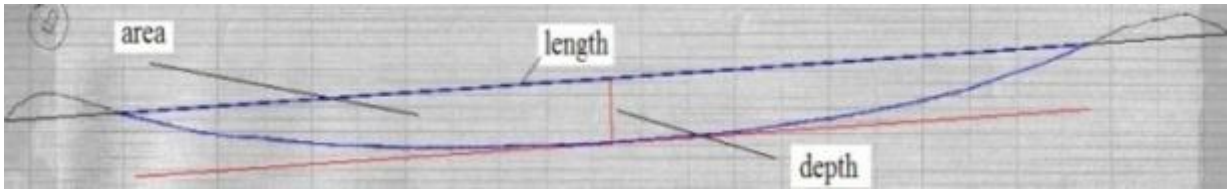

Figure 4.31 The measurement technique of the depth, length, area of the central profile of the wear scar [169,171]

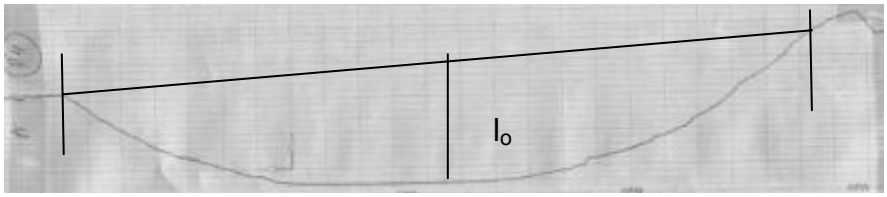

a. compression

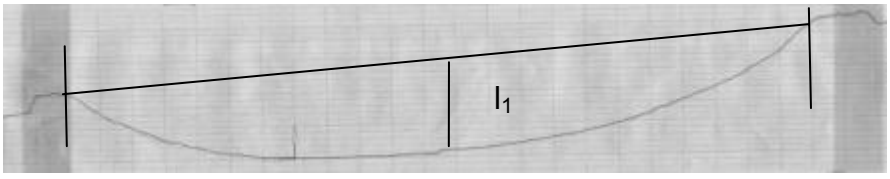

b. zero load

c. tension

Figure 4.32 Surface profile for the specimen tested a. compression ($l_0 > l_1 > l_2$)

Five measurements of the average roughness R_a in the longitudinal and transversal directions on each wear track were performed. In order to see if in real tests

this effect is observed, measurements of roughness on tests performed with the different additional elastic bulk stresses (positive and negative) were performed. Figure 4.33 shows the roughness in the wear track as a function of the additional bulk stresses after the test reached 43m of sliding distance.

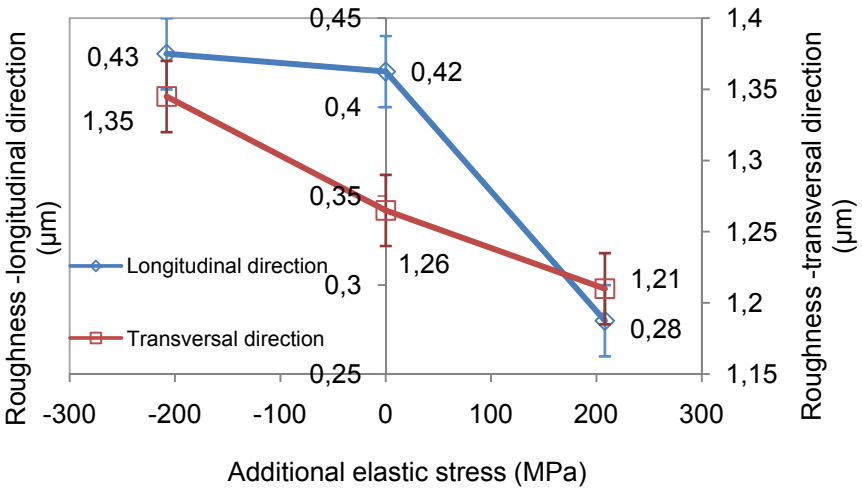

a. Al7175 alloy (in the longitudinal and transversal directions)

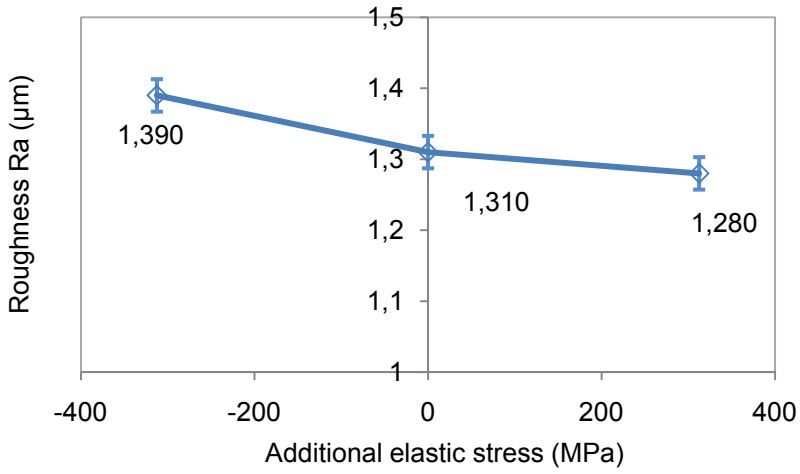

b. Ck45 steel (longitudinal direction)

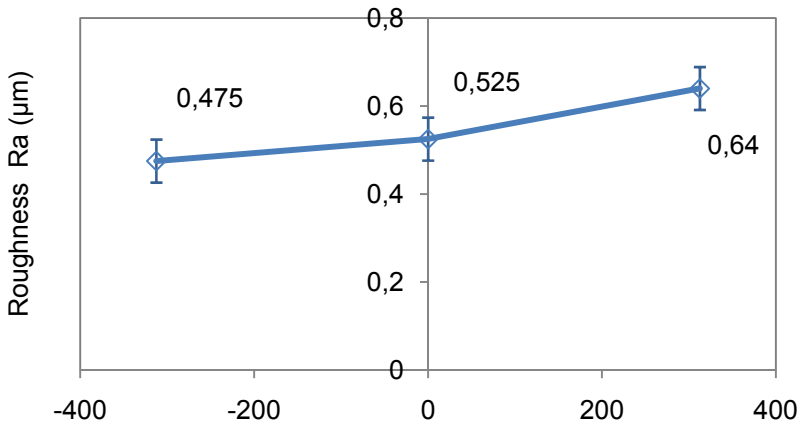

(c) Ti6Al4V alloy (longitudinal direction)

Figure 4.33 Evolution of the roughness as a function of the additional elastic stresses [169,171]

It can be seen that (with the exception of Ti alloy where changes are small) the roughness values are higher in tests performed with bulk additional compressive stresses then in tests performed with bulk additional tensile stresses. These results show that during the wear tests the roughness value on the contact region, not only is higher due to the initial compressive additional stresses in the specimen, as shown on figure 4.33, but remains higher during the whole process, thus facilitating material removal, and therefore decreasing the wear resistance. Under additional tensile stresses the specimen´s roughness decreases, remaining lower during the whole test thus increasing the wear resistance.

Thus, the macro-roughness effect is in accordance with the wear results in this study where wear increases due to the additional elastic compressive stresses and diminishes with additional elastic tensile stresses.

iii) Hardness tests

The Vickers hardness tests were conducted in accordance with standards using a macrohardness tester with a Vickers pyramid indenter. The Vickers hardness was measured for all three elastic stress conditions, from tension to compression.

Five hardness readings were taken for each condition from which the average value was calculated. Two series of hardness tests were carried out with different normal loads, 15 N and 30 N. Figure 4.34 shows the surface hardness as a function of the additional bulk stresses.

The main point to highlight is that hardness did not change significantly with the additional stress state. It can be seen a small raise of the hardness value when the material is subjected to compression. Under tension no substantial change in hardness was observed. Moreover, the changes are very small when compared to the standard deviation. It should be mentioned that the measurements of hardness were not taken on the wear track but on the fresh surface specimen, only as a function of the additional elastic stress state.

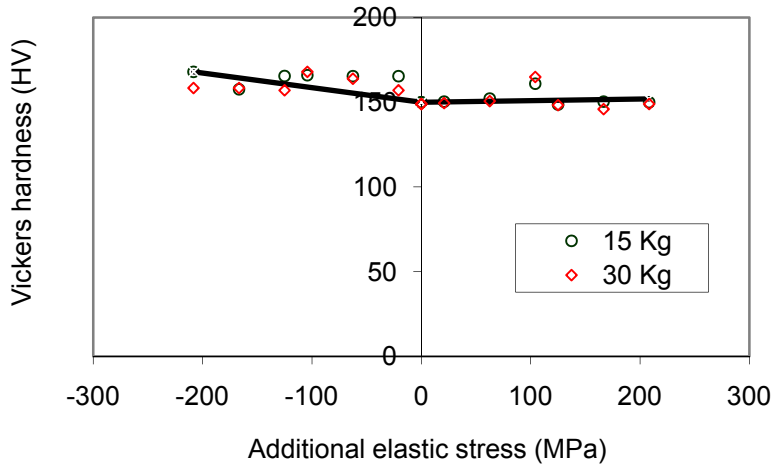

a. Al7175 aloy

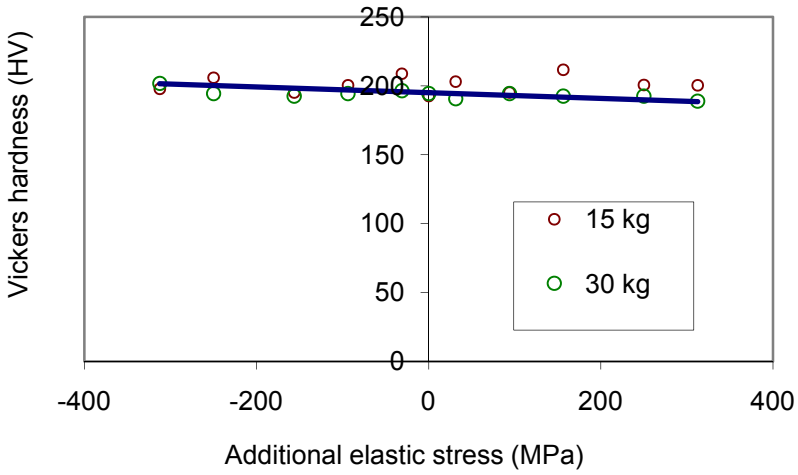

b. Ck 45 steel

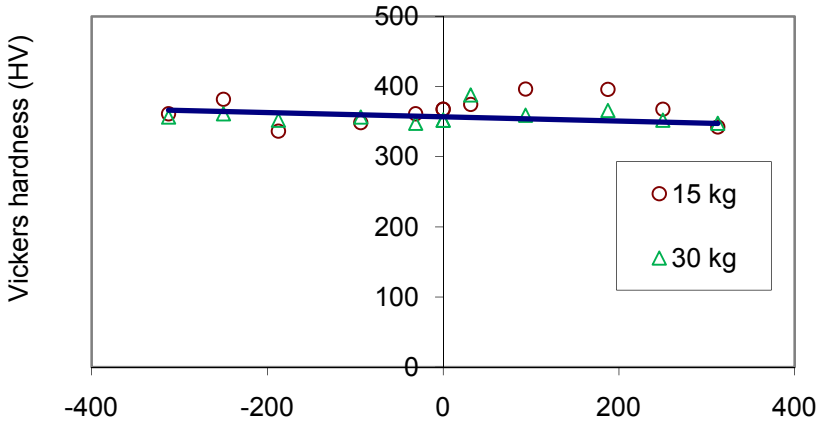

c. Ti6Al4V alloy

Figure 4.34 Evolution of the hardness as a function of the additional elastic stresses [169,171]

Thus, it is considered that no correlation can be drawn between additional stress and hardness. This effect has also been observed by Kokubo and by Sines and Carlson [as reported in 127]. A possible reason for this is the low stress levels on the material

(elastic domain). Although it is expected that there exist changes in hardness due to additional elastic stress states, it seems that the sensitivity of the hardness measurement process is not able to detect those changes. It is also worth nothing that the published studies where changes in hardness with stress state were observed, are those where the material suffered large plastic deformation [119,120]. This is the case of processes such as cold and hot rolling, shot peening, and, more recently, laser shock processing and ultrasonic peening. Due to the plastic deformation the previous processes introduce compressive stresses, resulting in an increase in hardness.

Thus, a first aspect to take into consideration is that when elastic additional stress states exist in the material they may substantially interfere in its wear behaviour, as obtained in this study and in ref. [120] but they do not substantially change its hardness values. This effect has not been taken into account in existing wear models since these models are essentially based on hardness. Thus, in the particular case of elastic deformations, it seems that hardness is not the main parameter governing the wear behaviour of the material.

4.2.3 New physical model - reciprocating sliding wear under an additional stress state

a. Initial explanation

Additional stress state with plastic deformation. Additional stress states can be introduced with severe surface plastic deformations, introducing surface residual stresses, and with elastic deformations due to external loads or due to thermal deformations.

Results with residual plastic compressive stresses show that they are in general beneficial to wear behaviour [119,120]. On the other hand residual plastic tensile stresses are supposed to have a detrimental effect on wear. It is also stated that the value of the contact pressure on the wear tests, has also a fundamental influence on the wear behaviour. It is reported that if the contact pressure is high the beneficial effect of the compressive residual stresses may disappear. The critical contact pressure level reported in ref. [120] was about 100 MPa. It was also observed that hardness increases with compressive stresses [120].

Thus, the presence of residual stress states as obtained with severe plastic deformations of the material, generally gives rise to a beneficial effect of compressive stresses on wear.

Additional stress state with elastic deformation. Only one very recent study [119] tries to establish a relation between wear and additional stress states on the elastic domain. This study was performed under very specific conditions. Although the additional elastic stress state reached only 40% of the yield strength of a CrCoMo alloy, the contact stress, due to the size of the pin was very high, varying from 0,9 to 3,7 GPa. In this reference [121] the compressive elastic additional stresses were detrimental and tensile elastic additional stresses were beneficial. Results were explained based on a repasssivation of an oxide film formed at the surface and on the ability of the additional elastic compressive field to retard the amount of energy dissipated into the substrate, making it more likely for the film to be damaged.

Results of the present research (figures 4.27, 4.28 Al7175 and Ck45) show the same tendency of those of ref [121], e.g. beneficial effect of additional elastic tensile stresses and detrimental effect of additional elastic compressive stresses. However the stresses involved in the contact are very different between the present study (contact stress in the elastic domain was ±132 MPa) and those on the research on ref. [123] (contact stresses in the plastic domain = 0,9 to 3,7 GPa). The contact size scales are also very different since in ref. [121] tests are on a nano-scale and in the present study on a milimeter scale. Thus, a different approach will be used for the explanation of the wear behaviour in the present study. Although the aluminium is also expected to form an oxide layer after each pin sliding movement, it does not seem that the oxide layer is resistant enough in order to avoid the contact between pin and specimen. Otherwise the film would avoid the specimen surface to be damaged. And it was verified that the aluminium scar has a substantial depth. Therefore it is assumed that the oxide film layer on the specimen surface is removed by the first edge on the pin that contacts the oxide at each movement, the pin thus remaining in contact with the aluminum bulk material.

A first point to highlight at this moment is that the results are completely different if the additional stresses are elastic or plastic. Under compressive plastic additional stresses, as observed with residual stresses, the wear behaviour is improved [119,120], while with additional compressive elastic stresses the wear resistance has decreased in both studies, namely ref. [121] and the present work. Thus it appears that wear may be governed by different mechanisms in the two previous situations.

A physical model that may be able to explain the wear behaviour under additional elastic stress states, as obtained in the present work, will be subsequently presented. The physical model is based on both grain shape and orientation, and on micro and macro-roughness.

b. Changes on micro-roughness due to grain shape and orientation

Several metallic materials, under an additional stress state (either tensile or compressive) will experience deformation changes in grain shape. This may provide an explanation for its different wear behaviour under different additional stress states, as will be subsequently explained.

Results show that there is higher wear resistance under tensile stresses (lower wear volume – figure 4.28 a and b) and a lower wear resistance under compressive stresses (higher wear volume). When the material is either under tensile or compressive stress, there occurs deformation of the crystalline network (based on Hooke's law). Under tensile stresses the grains will elongate in the loading direction and will be aligned with the direction of the wear track. In the perpendicular direction grains will decrease in size (Poisson´s coefficient) [179-183]. Titanium is usually leading to a refinement of the structural fragments to sizes of less then 1 μm, enhancement of the strength, and the appearance of strong anisotropy of mechanical properties. The deformations in the titanium when this is under compressive stresses and zero load lead to a refinement of their structure and improve the mechanical characteristics. When the material is under tensile stresses seems that is leading to a strong anisotropy of properties, which is frequently undesirable. This can explain the different behavior of titanium alloy.

A physical model of wear based on grain orientation when the material is subjected to an additional elastic stress state is shown schematically on table 4.7. Under tensile stresses the grains structure will behave like fibers, resulting in a very strong structure. Belomte et al [180], stated that if the grains are elongated and, furthermore, they are conveniently aligned, the materials will exhibit superior wear properties as well as other mechanical properties. The reason for this behaviour may rely on the fact that, for a certain sliding length, there is a smaller number of interfaces. As the interface originates a small depression, less interfaces means a smoother surface, less roughness and less wear volume. In this work the roughness at the grain dimension is called micro-roughness.

Table 4.7 Changes in grain shape during the wear tests. P – external load; sl – reciprocating sliding motion

Cases	Initial grain shape	Shape after external load	Shape after external load and reciprocation sliding motion
Zero load			
Tensile stress			
Compressive stress			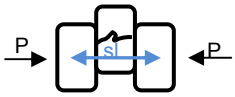

Under compressive stresses, as schematically shown in table 4.7, there are more interfaces or bonds, due to the compressive stresses some grains are also pulled-out being then easily removed by the sliding pin, this resulting in a poor wear resistance. Thus, this process increases simultaneously the number and the height of the micro-asperities making it easier for the pin to remove more material, thus creating a bigger depth along the wear track and increasing the wear volume in comparison with the other stress levels – no additional stress and tensile stress cases. Therefore, the number of micro-asperities as well as their height change with an additional stress state, being smaller under tensile additional stresses and higher under compressive additional stresses, as compared with the zero load case. Thus the effect of micro-roughness would be in accordance with the wear results in this study where wear increases for elastic compressive stresses and diminishes for elastic tensile stresses.

This effect of grain size deformation on roughness due to additional elastic stress states may be considered a micro-roughness effect because the asperities are at the grain size level. Roughness due to machining or other finishing process originates a macro-roughness effect. Both the macro-roughness effect (figure 4.33), along with the micro-roughness effect may be able to explain the difference in wear due to the additional elastic stress state, as will be subsequently shown.

c. Changes on macro - roughness

A physical model of classical sliding wear has been presented in ref [184] and is shown in figure 4.35. The asperities are flattened in the direction of motion and plastic flow occurs below the original surface. Roughness decreases during the first part of the

test (called running process) and its importance is negligible from that point on. Its effect is traditionally neglected on the wear analysis in sliding wear tests.

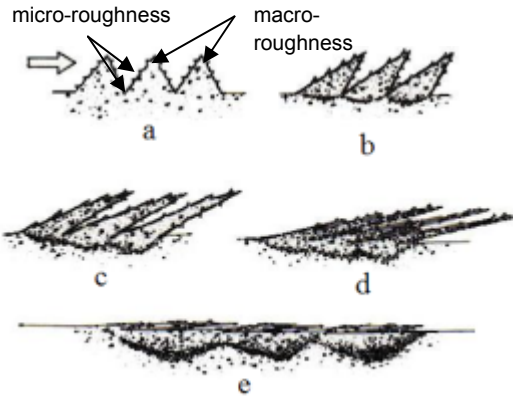

Figure 4.35 Physical model – sliding wear – roughness [184]

However, in reciprocating wear tests the phenomena may be different. Figure 4.36 shows a physical model of reciprocating wear. In this case the effect of the first motion or cycle of the pin on the surface is to bend the asperities in the sliding direction. The return movement causes a shift in the inclination of the asperities. Thus, in each cycle the asperities turn forwards and backwards in the sliding direction. With the increase on number of cycles peaks will break down and new asperities will be formed. A new rough surface is created, this happening for each stroke of the pin on the surface of the specimen. Contrarily to the flattening effect on the classical sliding wear, where roughness is important only at the beginning of the test, in the reciprocating tests roughness may be renewed during the test. In the latter case the roughness effect may last during the whole test being then pertinent to assess what could be the effect of the additional elastic stress state in roughness and eventually in wear.

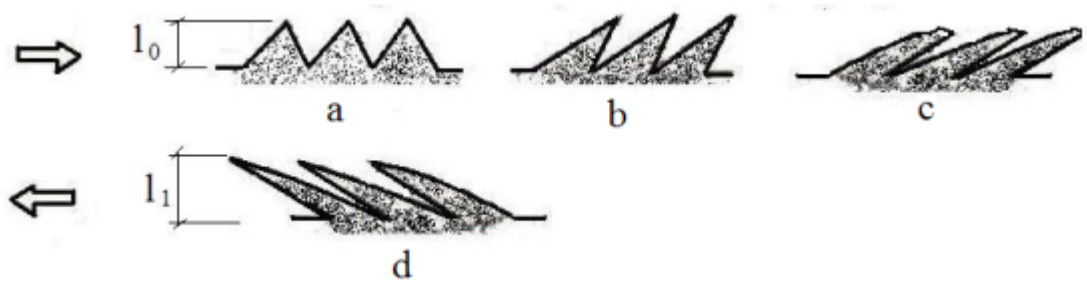

Figure 4.36 Physical model – Reciprocating wear – roughness ($l_0 < l_1$) [169]

Accepting that roughness is an important variable during the whole wear test, it is shown on figure 4.37 what would be the effect of additional stresses on the changes in shape of the asperities. Under tensile stresses (figure 4.37b) the asperities will be elongated in the loading direction (based on elastic deformation theories – Hooke's

law). Roughness will then decrease and this will lead to an improved wear resistance. Under compressive stresses (figure 4.37c) the asperities will be sharper giving rise to deeper peaks and valleys this resulting in an increase in wear volume.

In order to validate the physical model presented in figure 4.37, a numerical simulation on a surface with asperity peaks similar to the roughness peaks on figure 4.37 was carried out (recall 3.5 Test conditions). The deformation scale is amplified 1665 times in order to highlight the evolution of roughness. Figure 4.37d presents the results of the numerical simulation (the deformed shape). It can be clearly seen that under compressive stresses the peaks height increases while when the material is under tensile stresses the height of the peaks decreases.

It is interesting to observe that either based on micro-roughness effects, macro-roughness effects or both at the same time, the evolution of wear with additional elastic stress states can be explained based on the previous physical model. Whether the micro-roughness or the macro-roughness is the predominant variable on wear behaviour will depend on the surface finishing state of each testing case.

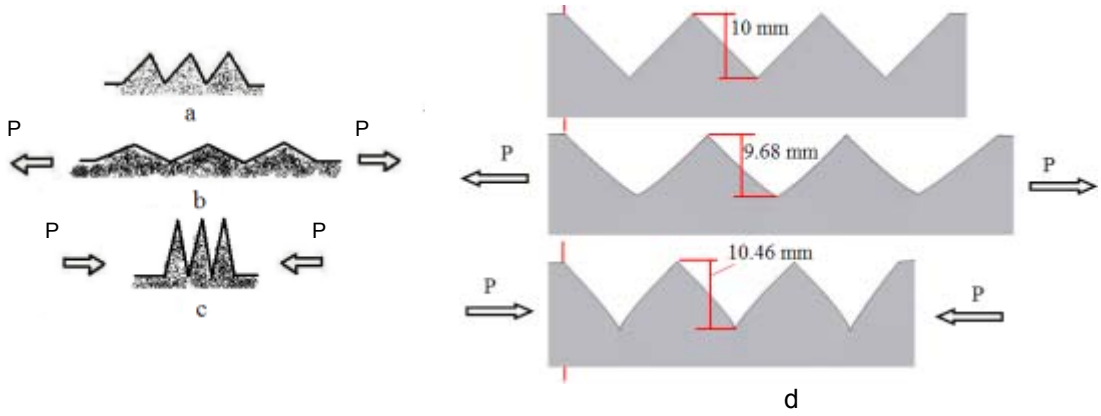

Figure 4.37 Physical model (left), and simulation (right) of effect for the additional stresses: a. zero load; b. tension; c. compression; d. numerical simulation (deformed shape); P – external load [169]

4.4 Conclusion of the experimental results

The conclusions drawn from the experimental results are as follows:

Fretting fatigue tests

- The present study confirmed the presence of the asymmetrical fretting scar formation in fretting fatigue situations (rarely highlighted in technical literature). The explanation is based on the stress state of the specimen and also on the evolution/modification of the most significant parameters during fretting fatigue tests, namely normal load, tangential load and relative displacement. This approach allows a better understanding of the interdependence of the referred variables, as well as the behavior of dependent variables such as dynamic friction coefficient, fretting loops and contact area evolution.
- It has been concluded that depth that forms on the contact area is giving rise to a stress concentration that should be included in fretting fatigue life predictions (stress concentration factor).
- It was concluded that surface roughness is a relevant parameter and this should be considered in fretting fatigue life predictions (surface finishing factor).
- It was confirmed the typical variation of the relative displacement amplitude with the fretting fatigue life. It was concluded that the relative displacement amplitude is strongly material dependent. It was observed that aluminium and titanium alloys are much more sensitive to relative displacement then Ck45 steel.
- The evolution and the shape of the fretting fatigue loops confirmed the partial slip regime (mixed contact of slipping and sticking zones).
- The difference between the plain fatigue life and fretting fatigue life is much higher on Al7175 and Ti6Al4V alloys as compared with Ck45 steel.

Reciprocating wear tests

- Additional stress states in the elastic domain have a substantial influence on the wear behaviour of the materials. Wear increases for elastic compressive stresses and diminishes for elastic tensile stresses, for Al7175 alloy and Ck45 steel (the different behavior of Ti6Al4V alloy is due to the low stress level). This effect is not taken into account in existing models. It was concluded, therefore, that it is pertinent to take it into consideration in wear assessment, and consequently in fretting fatigue predictions.

- Wear behaviour under different additional elastic stress states (either tensile or compressive), on materials, may be explained by micro-roughness (grain shape changes) and /or by macro-roughness states. Application of compressive stresses increased the roughness, while the tensile stresses decreased the roughness of the wear scar.
- A modification to the Archard´s model, in order to incorporate the effect of an additional elastic stress (either tensile or compressive), gives a good correlation between predicted and experimental wear volumes in the case of Al7175 alloy and Ck45 steel.

Chapter 5
Prediction models of fretting fatigue life and discussion

Chapter 5 is dedicated to the development of models for the prediction of fretting fatigue life. In this chapter is presented the theoretical base of the present approach, considering the modifications with the stress concentration factor effect and the surface finish factor (roughness) effect. Also, a new parameter is proposed which affects the plastic term component of the models, so-known "Bauschinger effect".

5.1 Present approach

5.1.1 Initial remarks

The flow chart presented in figure 5.1 shows how the current approach converts load and material properties (mechanical and fatigue) into a fretting fatigue life prediction. To predict the fretting fatigue initiation life two models were selected: the SWT (see 2.3.3 Smith – Watson – Topper (SWT) model) and Morrow models (subsequently presented). These models were chosen because they are the most robust models in terms of intrinsic material properties. In order to obtain good predictions of the fretting fatigue life two modifications to the previous models, concerning the damage zone, were proposed in this work. Both modifications (highlighted in red in Figure 5.1) are related to the effect of the contact damaged area in fatigue life. The first modification, herein called the "fretting scar effect", takes the of a stress concentration factor, K_t, and is related to the global shape of the scar geometry. The second modification is a surface finishing factor, K_s and is related with the nature of the surface (roughness). This modification is based on the fact that fretting fatigue cracks initiate predominantly at the surface between the two contact zones (slip and stick). In this region, the surface roughness condition seems to be sufficiently important (substantially high roughness values) in order to be considered relevant in fretting fatigue life predictions.

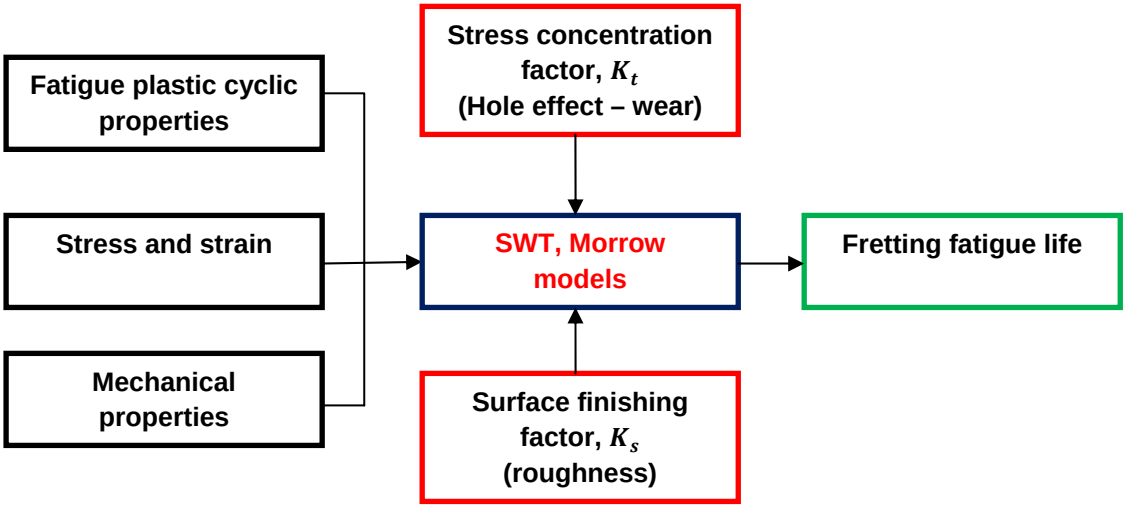

Figure 5.1 Flow chart for predicting analytically fretting fatigue life [124]

5.1.2 New approach - Morrow parameter

5.1.2.1 Morrow´s model in the plain fatigue situation

Morrow [12] used the original strain-life relation (eq. 2.5) and introduced the mean stress effects. In the technical literature [180-184] there are two approaches to include the effects of the machine load mean stress (σ_m) on Morrow´s equation.

The first approach [181,182] consists in applying the machine load mean stress only to the elastic term of the strain-life relation (eq. 2.5) as follows:

$$\varepsilon_a = \left(\frac{\sigma_f' - \sigma_m}{E}\right)\left(2N_f\right)^b + \varepsilon_f'\left(2N_f\right)^c \tag{5.1}$$

This approach considers that the machine load mean stress affects mainly the elastic term and may be neglected in the plastic term. In figure 5.2 can be seen the effect of the machine load mean stress in the elastic term of the strain –life (dashed red line).

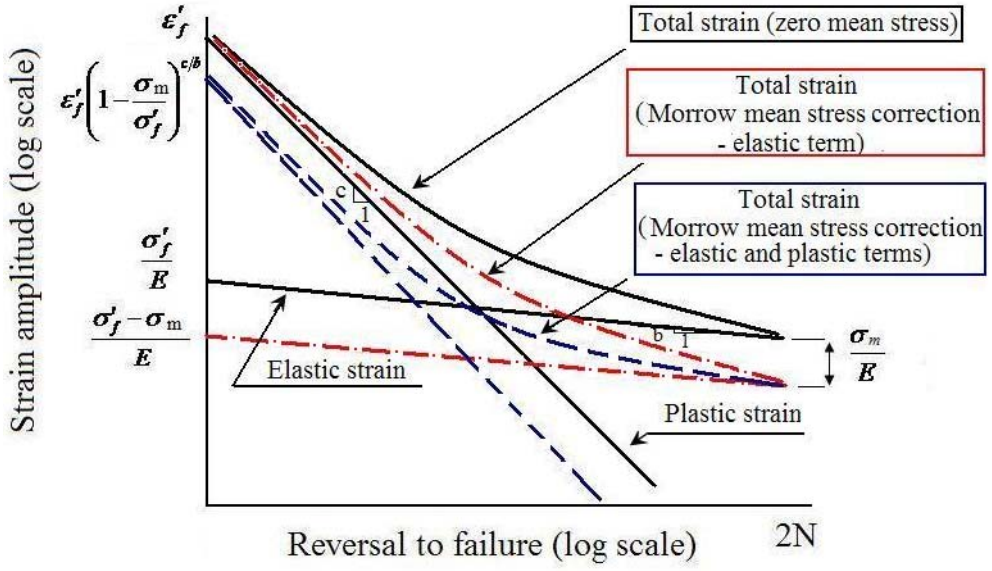

Figure 5.2 Effect of machine load mean stress on strain-life curves [124]

The second approach [185,186] considers the influence of the machine load mean stress in both the elastic and the plastic terms as follows:

$$\varepsilon_a = \frac{\sigma_f'}{E}\left(1 - \frac{\sigma_m}{\sigma_f'}\right)\left(2N_f\right)^b + \varepsilon_f'\left(1 - \frac{\sigma_m}{\sigma_f'}\right)^{c/b}\left(2N_f\right)^c \tag{5.2}$$

Figure 5.2 shows the effect of the machine load mean stress on both the elastic and the plastic terms (dashed grey line).

5.1.2.2 Morrow´s parameter to be applied to a fretting fatigue situation

This work suggests a modification to the Morrow´s parameter, in order to use it in a fretting fatigue situation. The modification consist in the substitution of the machine load mean stress, σ_m, (eq. 5.1 - for elastic term and eq. 5.2 – for the elastic and plastic term), by a global mean stress, $\sigma_{m,global}$, that takes into consideration the mean stress effect caused by the machine loading cycle, as well as the effect of the normal and tangential stresses caused by the contact pad-specimen.

The global mean stress is given by

$$\sigma_{m,global} = \sigma_m + 2p_0\sqrt{\mu F_{t,m}/F_{n,m}} \tag{5.3}$$

where $F_{t,m}$ is the mean value of the tangential load; $F_{n,m}$ is the mean value of the normal load.

In this case the Morrow equation, when the global mean stress is applied only to the elastic term, takes the following form:

$$\varepsilon_{a,FF} = \left(\frac{\sigma_f' - \left(\sigma_m + 2p_0\sqrt{\mu F_{t,m}/F_{n,m}}\right)}{E}\right)\left(2N_f\right)^b + \varepsilon_f'\left(2N_f\right)^c \tag{5.4}$$

and when the global mean stress is applied on the elastic and plastic terms, the Morrow equation takes the following form:

$$\varepsilon_{a,FF} = \frac{\sigma_f'}{E}\left(1 - \frac{\sigma_m + 2p_0\sqrt{\mu F_{t,m}/F_{n,m}}}{\sigma_f'}\right)\left(2N_f\right)^b + \varepsilon_f'\left(1 - \frac{\sigma_m + 2p_0\sqrt{\mu F_{t,m}/F_{n,m}}}{\sigma_f'}\right)^{c/b}\left(2N_f\right)^c \tag{5.5}$$

5.1.3 Stress concentration factor due to “wear damage area” – fundamentally new approach

When the fretting fatigue tests were concluded a concavity was formed at the fretted surface of the specimen due to contact of the fretting pads. Also, it was observed the variation of the depth of the fretting scar with normal or tangential load (see 4.1.4 Some considerations on the modification of the fretting contact via varying normal load and tangential load). The depth increased linearly with increasing normal load (figure 4.9) and with tangential load (figure 4.21). Based on these experimental observations and on the remark that any small change on the discontinuity geometry has a significant

effect on the stress distribution around it, a stress concentration factor is determined as a function of the fretting scar depth.

The concentration factor, K_t was obtained from the final geometries of the damaged areas (figure 4.2), and determined by numerical simulation. The geometry of the damaged area used in the numerical simulation was simplified to a spherical cap. The stress concentration factor, K_t, in this particular situation depends on the depth of the fretting scar, p_t, the length of the fretting scar, l, the length of the specimen L ,the width of the specimen, W, and the height of the specimen, d.The depth, p_t, and length, l, of the fretting scar were obtained from the real profiles. The dimensions of the specimen are the ones presented in figure 3.2). Although the stress concentration factor, K_t, evolves during the life of the specimen, with the evolution of the damaged area, in this work the value of K_t is associated to the final maximum scar depth (at the end of the test). Furthermore, this value is an average of the obtained profiles for the different tests, under same loading conditions.

It is depicted on figure 5.3 the evolution of the stress concentration factor as a function of the wear scar depth.

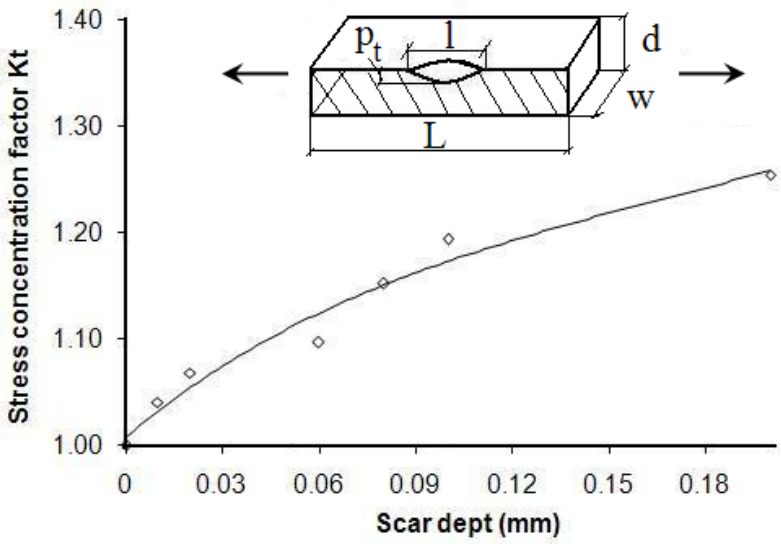

Figure 5.3 Stress concentration factor as a function of fretting scar depth: p_t depth of the fretting scar; l length of the fretting scar; L length of the specimen; Wwidth of the specimen; d height of the specimen [124]

This approach works very well for situations in which only the elastic stresses and strains are presented. However, most components may appear to have nominally cyclic elastic stresses, but some stress concentrations present in component result in local cyclic plastic deformation. Under these conditions, another approach, so-called Neuber's rule is often invoked to determine the local stresses and strains. This method

assumes that the product of the stress and strain concentration factors is constant and therefore can account for the non-linear material response at the fretting scar (damaged area).

Neuber [1,17,186-190] hypothesized that the elastic stress concentration factor (K_t) is the geometric means of the true stress and strain concentration factors:

$$K_t = \sqrt{K_\sigma K_\varepsilon} \tag{5.6}$$

Then Neuber's rule (eq. 5.6) can be expressed as

$$K_t = \sqrt{\frac{\sigma_{max}}{S} \cdot \frac{\varepsilon}{e}} \tag{5.7}$$

where σ_{max} - maximum stress; S - the nominal stress; ε - maximum strain; e - the nominal strain.

By substituting the nominal strain, e, eq. (5.7) can be written as

$$K_t = \sqrt{\frac{\sigma_{max}}{S} \cdot \frac{\varepsilon \cdot E}{S}} \tag{5.8}$$

Equation 5.8 can be rewritten as follows:

$$K_t = \sqrt{\frac{\sigma_{max} \cdot \varepsilon \cdot E}{S^2}} \tag{5.9}$$

5.1.4 Surface finishing factor due to the surface roughness

Because in fretting fatigue cracks initiate predominantly at the interface between the two contact zones (slip and stick), the surface condition becomes significant for a fatigue test. The surface condition can be characterized by considering two factors: surface irregularities or roughness and residual stress in the surface layer [191].

It has been shown that roughness change with the normal and tangential load (see 4.1.4 Some considerations on the modification of the fretting contact via varying normal load and tangential load). The roughness decreases with increasing normal load and it increases with increasing tangential load.

Based on the experimental results and on the remark that the surface irregularities act like stress concentration it is proposed a factor that takes it into consideration, named here "surface finishing factor".

Figure 5.4 shows an empirical chart [191] used to select the surface finishing modification factor for steels when the measurement of the surface roughness is known.

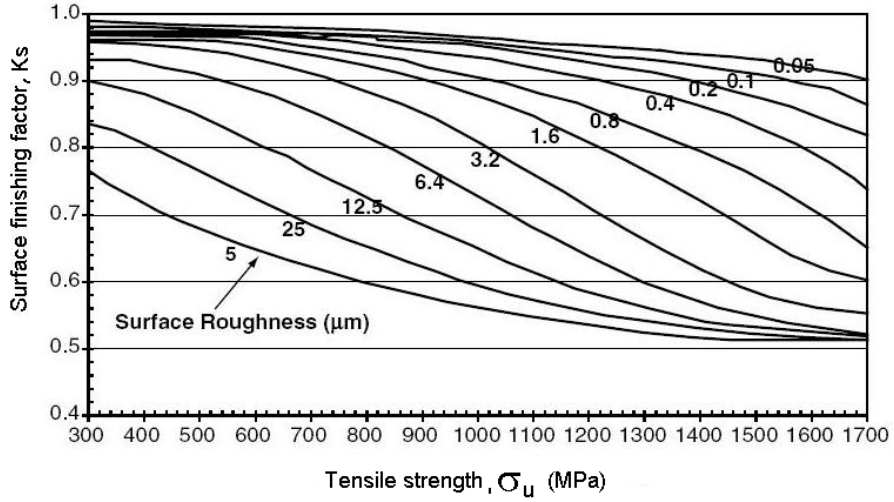

Figure 5.4 Surface finishing factor as a function of the surface roughness and the tensile strength of the material [191]

To the author knowledge the surface finish charts presented in the technical literature are available only for steel. As a result the values for the surface finishing factor used in this work for the three materials are all based on the chart drew for steel.

Further and similarly to what happened in the case of the stress concentration factor, the surface finishing factor used in this work corresponds to the roughness values as measured at the end of the test.

Residual stresses

A brief note should be introduced here regarding residual stresses. One may assume that residual stresses may develop on the specimen-pad contact zone and that it may substantially influence the fretting fatigue life. However, the residual stresses (or its evolution with the number of cycles, when residual stresses are introduced at the beginning of the test) relax due to the contact and wear [192-194]. Although it is stated that initial compressive residual stresses as introduced before the fretting fatigue test, may increase the fretting fatigue life it is also stated that its effect is low because the relaxation effect is very pronounced. No study is concerned with residual stresses that may develop during a fretting fatigue test on the contact zone. Thus, assuming that eventual residual stresses that may develop on the contact zone during the fretting fatigue test will immediately relax, residual stresses are not taken in consideration in this work.

5.1.5 Primary approaches

i. Stress concentration factor effect on predicting fretting fatigue life by SWT and Morrow parameters

The first modification proposed in this work consists in incorporating a stress concentration factor, K_t (figure 5.3) in both (SWT and Morrow) models which takes into consideration the fretting scar that is formed in the contact region. This parameter affects only the elastic term of the models.

The incorporation of the stress concentration factor in the SWT and Morrow´s parameters consists in multiplying by the stress concentration factor, K_t, the maximum stress for the SWT parameter and the global mean stress for the Morrow parameter. The maximum/global mean stress already incorporates the nominal axial (machine) stress, and the normal and tangential contact stresses.

SWT parameter

Eq. 2.15 becomes

$$\left(\sigma_{max} + 2p_0\sqrt{\mu F_{t,max}/F_{n,max}}\right)\cdot K_t\left(\frac{1-2v^2-v^3}{E}\right)\left(\sigma_a + \sigma_{a,F_t}\right) = \frac{\left(\sigma_f'\right)^2}{E}\left(2N_f\right)^{2b} + \sigma_f'\varepsilon_f'\left(2N_f\right)^{b+c} \tag{5.10}$$

Morrow´s parameter

Eqs. 5.4 and 5.5 become

$$\varepsilon_{a,FF} = \left(\frac{\sigma_f' - \left(\sigma_m + 2p_0\sqrt{\mu F_{t,m}/F_{n,m}}\right)\cdot K_t}{E}\right)\left(2N_f\right)^b + \varepsilon_f'\left(2N_f\right)^c \tag{5.11}$$

$$\varepsilon_{a,FF} = \frac{\sigma_f'}{E}\left(1 - \frac{\left(\sigma_m + 2p_0\sqrt{\mu F_{t,m}/F_{n,m}}\right)\cdot K_t}{\sigma_f'}\right)\left(2N_f\right)^b + \varepsilon_f'\left(1 - \frac{\left(\sigma_m + 2p_0\sqrt{\mu F_{t,m}/F_{n,m}}\right)\cdot K_t}{\sigma_f'}\right)^{c/b}\left(2N_f\right)^c \tag{5.12}$$

ii. Surface finishing factor effect on predicting fretting fatigue life by SWT and Morrow parameters

Besides the incorporation a stress concentration factor, K_t in both models, this work proposes another modification, which consists in incorporating a surface finishing

factor, K_s (figure 5.4). It takes into consideration the surface roughness. This parameter also affects only the elastic term of both models.

SWT parameter

Eq. 5.10 becomes

$$\left(\sigma_{max} + 2p_0\sqrt{\mu F_{t,max}/F_{n,max}}\right) \cdot \frac{K_t}{K_s}\left(\frac{1-2\upsilon^2-\upsilon^3}{E}\right)\left(\sigma_a + \sigma_{a,F_t}\right) = \frac{\left(\sigma_f'\right)^2}{E}\left(2N_f\right)^{2b} + \sigma_f'\varepsilon_f'\left(2N_f\right)^{b+c} \tag{5.13}$$

Morrow´s parameter

Eqs. 5.11 and 5.12 become

$$\varepsilon_{a,FF} = \left(\frac{\sigma_f' - \left(\sigma_m + 2p_0\sqrt{\mu F_{t,m}/F_{n,m}}\right)\cdot\left(K_t/K_s\right)}{E}\right)\left(2N_f\right)^b + \varepsilon_f'\left(2N_f\right)^c \tag{5.14}$$

$$\varepsilon_{a,FF} = \frac{\sigma_f'}{E}\left(1 - \frac{\left(\sigma_m + 2p_0\sqrt{\mu F_{t,m}/F_{n,m}}\right)\cdot\left(K_t/K_s\right)}{\sigma_f'}\right)\left(2N_f\right)^b + \varepsilon_f'\left(1 - \frac{\left(\sigma_m + 2p_0\sqrt{\mu F_{t,m}/F_{n,m}}\right)\cdot\left(K_t/K_s\right)}{\sigma_f'}\right)^{c/b}\left(2N_f\right)^c \tag{5.15}$$

5.2 Application of SWT parameter to the fretting fatigue situation

Figure 5.5 shows the analytical fretting fatigue life prediction based on the SWT parameter which takes into consideration only the maximum stress effects (eq. 2.15 - dashed red line). It also shows the estimated life obtained using the SWT parameter affected by the stress concentration factor, K_t (Neuber), proposed in this work (eq. 5.10 – solid green line). It also shows the estimated life obtained using the SWT parameter affected by both modifications proposed in this work, the stress concentration factor, K_t , and the surface finishing factor, K_s (eq. 5.13 – dashed blue line).

The maximum stress involved in the fretting contact is given by eq. 2.11. Eq. 2.15 (see 2.3.3 Smith-Watson-Topper (SWT) model) has been used in fretting fatigue predictions [195] and already incorporates the local contact stresses and the mean stress.

The main aspects to highlight are that the stress concentration factor and the surface finish factor incorporated in SWT parameter are not sufficient in the case of Ti6Al4V alloy and worsen the prediction in the case of Ck45 steel. Good predictions are obtained, with the SWT parameter, in the case of Al7175 alloy.

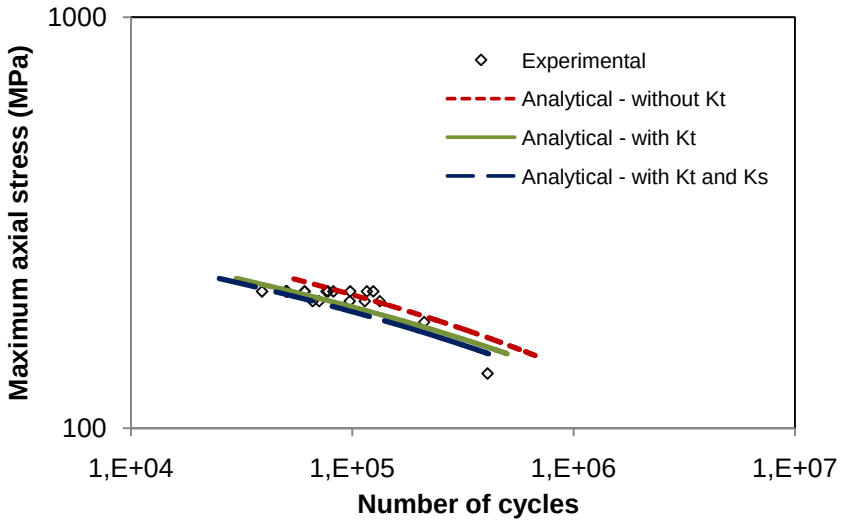

a. Al7175

Figure 5.5 Maximum axial stress (σ_{max}) vs. number of cycles (SWT – K_t and K_s) (cont.)

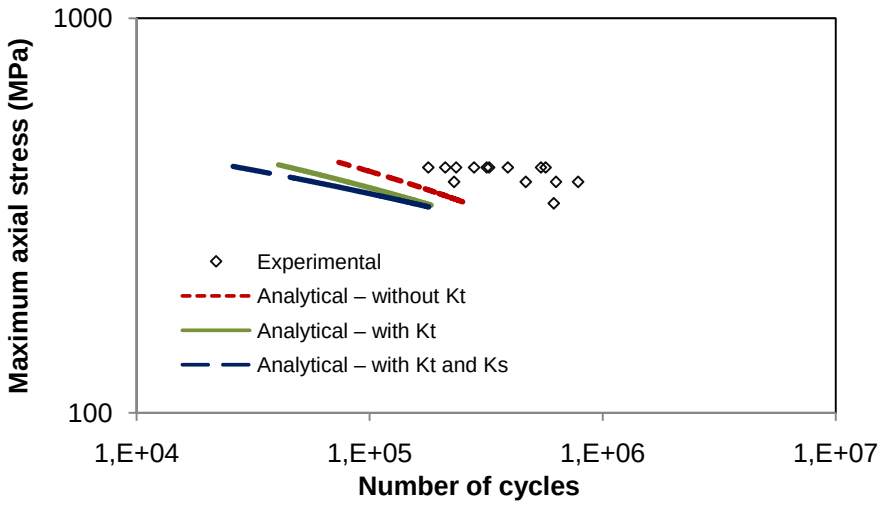

b. Ck45

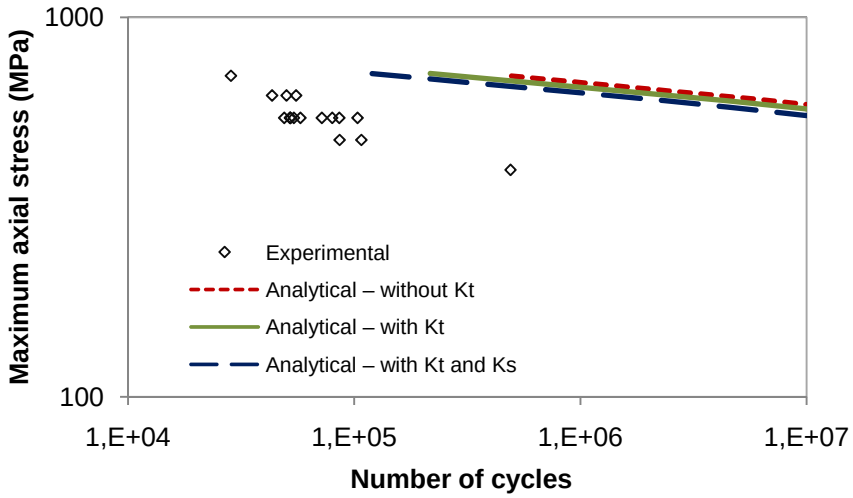

c. Ti6Al4V

Figure 5.5 Maximum axial stress (σ_{max}) vs. number of cycles (SWT – K_t and K_s)

5. 3 Application of Morrow parameter to the fretting fatigue situation

The Morrow´s parameter is a new approach regarding the fretting fatigue situation. First it was introduced the global mean stress effects $\sigma_{m,global}$ (eq. 5.3) which takes into consideration both the mean stress effect caused by the machine loading cicle and the effects of the normal and tangential stresses. Then two modifications were applied - the first modification was the introduction of the stress concentration factor, K_t (Neuber) (eqs. 5.11 and 5.12) and the second modification was the introduction of the surface finishing factor, K_s (eqs. 5.14 and 5.15).

I. First modification - Global mean stress only on the elastic term

Figure 5.6 shows the analytical prediction based on Morrow´s parameter taking into consideration the effect of the global mean stress only on the elastic term, with (eq. 5.11 – solid green line) and without (eq. 5.4 – dashed red line) the effect of the stress concentration factor, K_t (Neuber). Also figure 5.7 shows the analytical prediction based on Morrow's parameter taking into consideration the effect of the surface finishing factor, K_s (eq. 5.14 – dashed blue line).

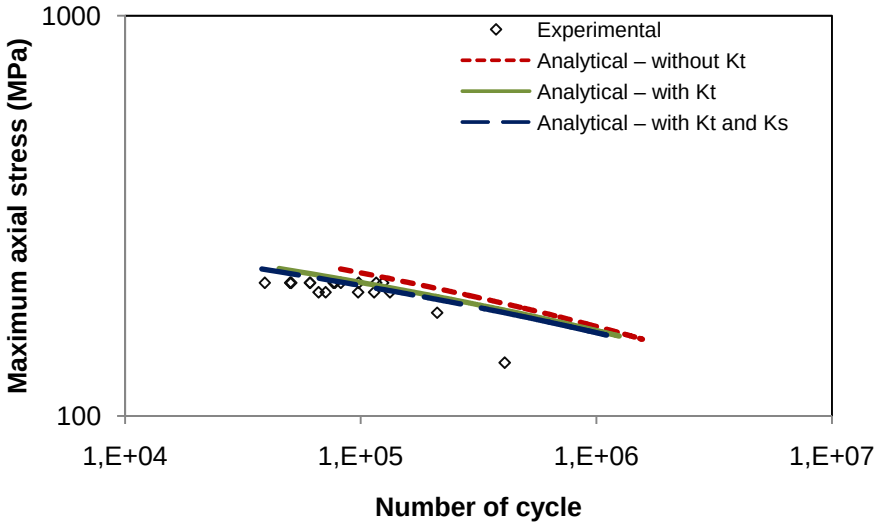

a. Al7175

Figure 5.6 Maximum axial stress (σ_{max}) vs. number of cycles (Morrow (elastic) – K_t and Ks) (cont.)

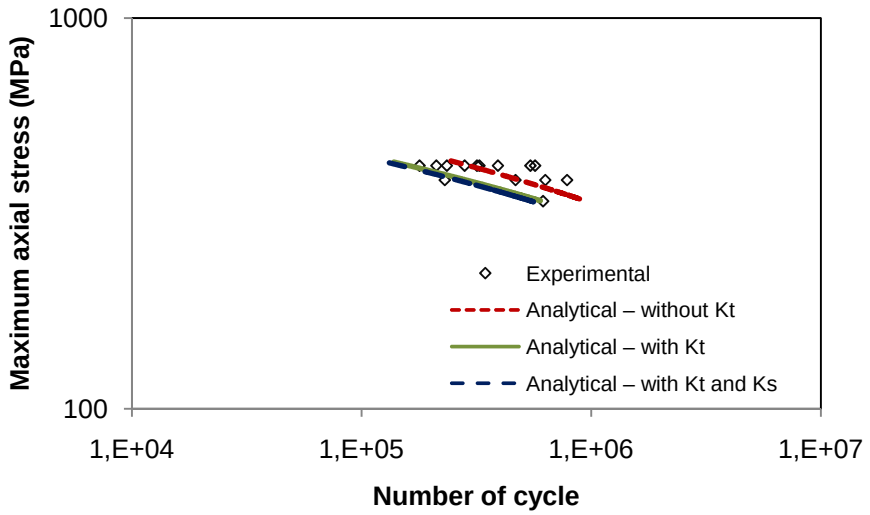

b. Ck45

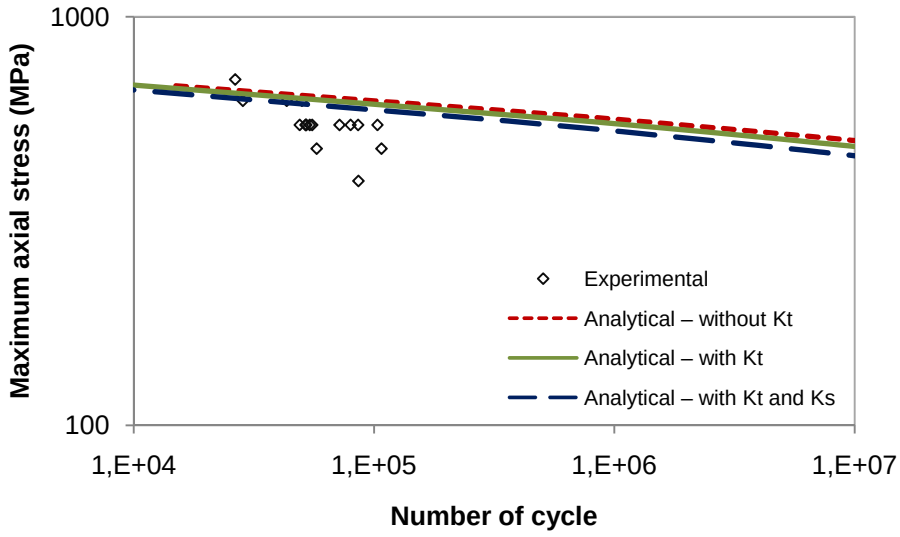

c. Ti6Al4V

Figure 5.6 Maximum axial stress (σ_{max}) vs. number of cycles (Morrow (elastic) – K_t and Ks)

The analytical prediction obtained with eq. 5.4, slightly over-estimates the fretting fatigue life in the case of Al7175 alloy (figure 5.6a - dashed red line). Using the modified Morrow parameter defined by eq. 5.11 alone with the stress concentration factor slightly improves the correlation between analytical and experimental results (figure 5.7a – solid green line). A slight improvement in the prediction of fretting fatigue life was obtained in the case of Al7175 alloy (figure 5.6a – dashed blue line) when the surface finishing factor was added to the Morrow's model.

In the case of Ck45 steel the analytical prediction obtained with Morrow´s parameter gives a better prediction of the fretting fatigue life (figure 5.6b).

In the case of Ti6Al4V alloy it can be seen from figure 5.6c that the prediction was good only for medium life (around 100,000 cycles). For shorter lives the prediction is underestimated while for longer lives the prediction is overestimated.

The aspects to highlight are that the stress concentration factor incorporated in the Morrow´s parameter when the global mean stress affects only the elastic term is sufficient, in the case of Al7175 alloy and Ck45 steel, to obtain a better life prediction. An improvement of life prediction was obtained in the case of Ti6Al4V alloy for lives between 10,000 and 100,000 cycles. For a life bigger than 100,000 cycles, it can be seen from figure 5.6c that the life is overestimated.

A slight improvement in the prediction of fretting fatigue life, in the case of Ti6Al4V alloy, was obtained for life around 100,000 cycles.

II. Second modification - Global mean stress on the elastic and plastic terms

Figure 5.7 shows the experimental results and analytical prediction based on Morrow´s parameter taking into consideration the effect of the global mean stress on both the elastic and plastic terms, with (eq. 5.12- solid green line) and without (eq. 5.5 – dashed red line) the effect of the stress concentration factor, K_t (Neuber). Also figure 5.7 shows the analytical prediction based on Morrow's parameter taking into consideration both modifications: the effect of the stress concentration factor, K_t and the effect of the surface finishing factor, K_s (eq. 5.15 – dashed blue line).

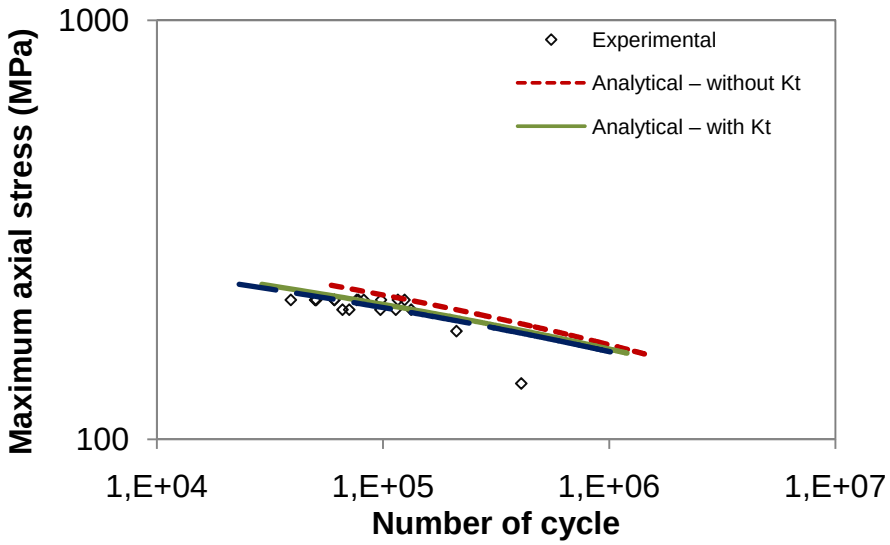

a. Al7175

Figure 5.7 Maximum axial stress (σ_{max}) vs. number of cycles (Morrow (elastic and plastic) – K_t and Ks) (cont.)

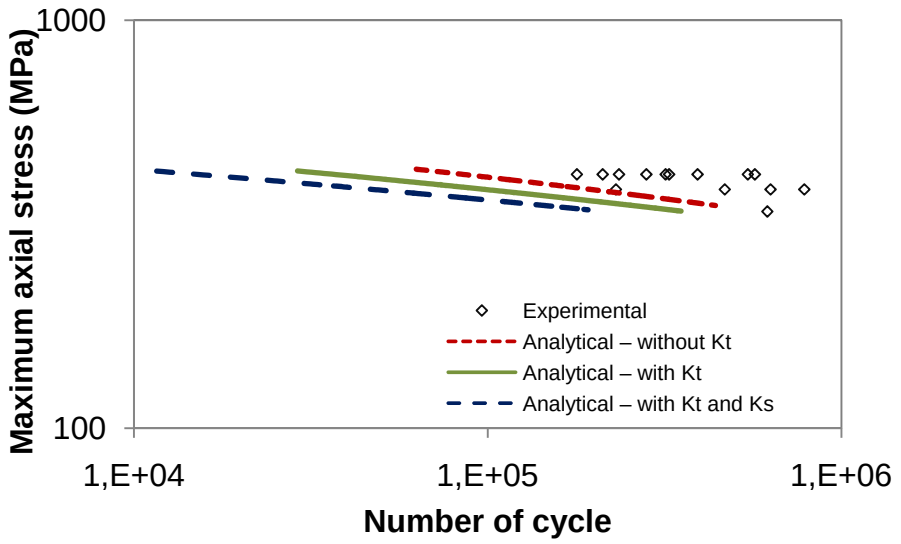

b. Ck45

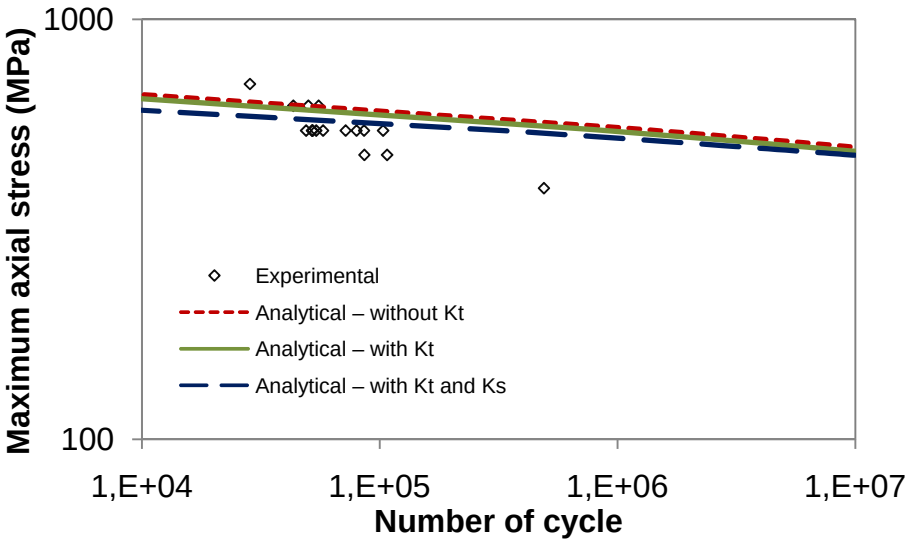

c. Ti6Al4V

Figure 5.7 Maximum axial stress (σ_{max}) vs. number of cycles (Morrow (elastic and plastic) – K_t and Ks)

In the case of Al7175 alloy, when the global mean stress affects only the elastic term, (figure 5.6a - solid red line) the correlation is slightly worse than when both the elastic and plastic terms (figure 5.7a - solid red line) are affected. However, and as expected, the elastic term is dominant on this prediction [186,187].

In the case of Ck45, when the global mean stress affects both the elastic and plastic term the prediction is slightly underestimated (figure 5.7b) compared with the prediction where only the elastic term is affected by the global mean stress (figure 5.6b). The important aspect to highlight is that the plastic term of Morrow's equation for this material has a substantial influence on fretting fatigue life prediction.

In the case of Ti6Al4V alloy, when the global mean stress affects the elastic and plastic terms (figure 5.7c –dashed red line) the prediction is slightly better that when

only the elastic term was affected by the global mean stress (figure 5.6c – dashed red line). This is valid only for a life around 100,000 cycles. It is important to highlight that in relation to Ti6Al4V alloy, the predictions may not be very accurate due to the fact that when obtaining low cycle fatigue properties some heat generated in the specimens [163] and those properties may not be very accurate.

5. 4 Conclusions on SWT and Morrow parameters

It can be observed that the SWT parameter best prediction (eq. 5.10, figure 5.5) is more adequate then Morrow´s parameter best prediction (eq. 5.12 figure 5.6) in the case of Al7175 alloy. Morrow's parameter was more adequate in the case of Ck45 steel.

Regarding the use of the stress concentration factor on the proposed modified Morrow and SWT parameters, it is observed that it may have a substantial effect on fretting fatigue predictions. As a fact, it is well known that the stress concentration factor is very important in the case of fatigue loading. If the specimen is subjected to an axial tensile or compressive load the stress is assumed to be the same across the section. However, in the presence of any sudden change of section (hole, sharp corner, notch, etc.), the local stress will rise significantly [184]. The stress increases because of the fretting scar that is formed (Table 4.5 and figure 4.2) which affects the stress distribution near it. Therefore, the maximum stress alone (eq. 2.11) no longer describes the global state of stress in the part.

Reading the use of the stress finishing factor on the proposed modified Morrow and SWT parameters, it is observed that it may also have a substantial influence on fretting fatigue life predictions. As a fact it is well known that the surface state has a high influence on fatigue life [196]. Surface roughness has negative effect on plain fatigue resistance [197], because surface micro-cracks nucleate more easily on a rough surface. This modification is based on the fact that fretting fatigue cracks initiate predominantly at the surface between the two contact zones (slip and stick). In this region, the surface roughness condition seems to be sufficiently important (substantially high roughness values) in order to be considered relevant in fatigue life predictions.

5. 5 Application of Bauschinger effect

5.5.1. Initial remarks

The Bauschinger effect is related to a deviation from the expected plastic behavior of the materials. To the authors knowledge no one has used this effect in fatigue initiation predictions. Only Pommier [151] stated its interest in fatigue crack propagation. She stated that it would change plastic deformed areas both ahead and behind the crack tip affecting the residual stress field ahead of the crack tip but also the closure level behind the crack tip. However its possible effects on fatigue initiation were not discussed up to this work.

This work proposes that Bauschinger effect should be incorporated in fatigue life initiation predictions. Thus, a new parameter that affects the plastic term component of the models is proposed. It will be seen that this parameter may substantially improve fretting fatigue predictions.

The flow chart presented in figure 5.8 present the final picture of the modifications introduced to the SWT and Morrow models, in this work - along with the two previous effects that were already incorporated, K_t and K_s, it is included now the BAU effect.

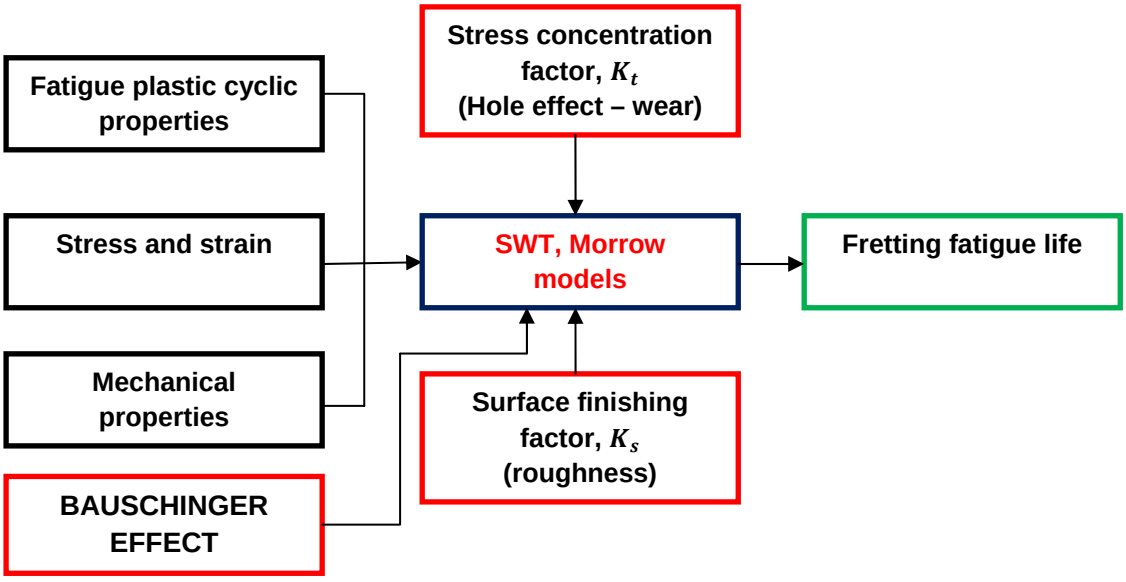

Figure 5.8 Flow chart for predicting analytically fretting fatigue life (BAU effect correction)

The SWT and Morrow models include several intrinsic properties of the material: fatigue strength coefficient, fatigue strength exponent, fatigue ductility coefficient, fatigue ductility exponent. These properties are obtained from stabilized hysteresis

loops (Figure 5.9). Figure 5.9 shows schematically a cyclic hysteresis loop and highlighted in red is the BAU effect. It can be seen that when obtaining the previous properties, they do not incorporate or reflect the BAU effect. Thus, both the SWT and Morrow models do not take the BAU effect into consideration.

Subsequently, a brief discussion on the possible effects of the BAU effect on fatigue life predictions will be made. It will be shown in this section that this effect may strongly affect the fatigue life predictions.

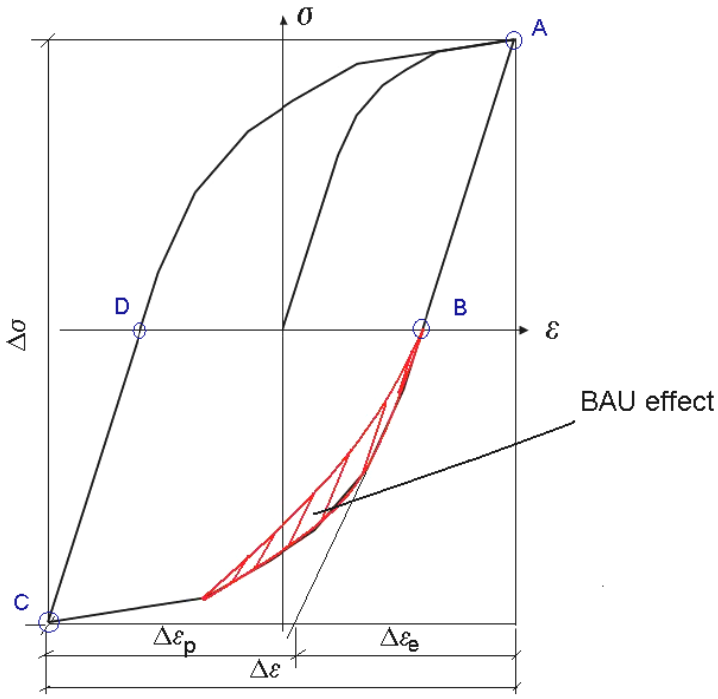

Figure 5.9 Cyclic Hysteresis Behaviour - BAU effect

5.5.2 Possible consequences of the BAU effect

In order to incorporate the BAU effect into the SWT and Morrow models two approaches are presented. The *First approach* is based on energy based models. *The second approach* is based on the theories as internal stresses; dislocation theories; composite model (Masing´s model or Asaro´s model).

First approach – energy based models

The first interpretation is based on the fact that the stored energy in each cycle is reduced, due to the Bauschinger effect (Figure 5.9 and 5.10).

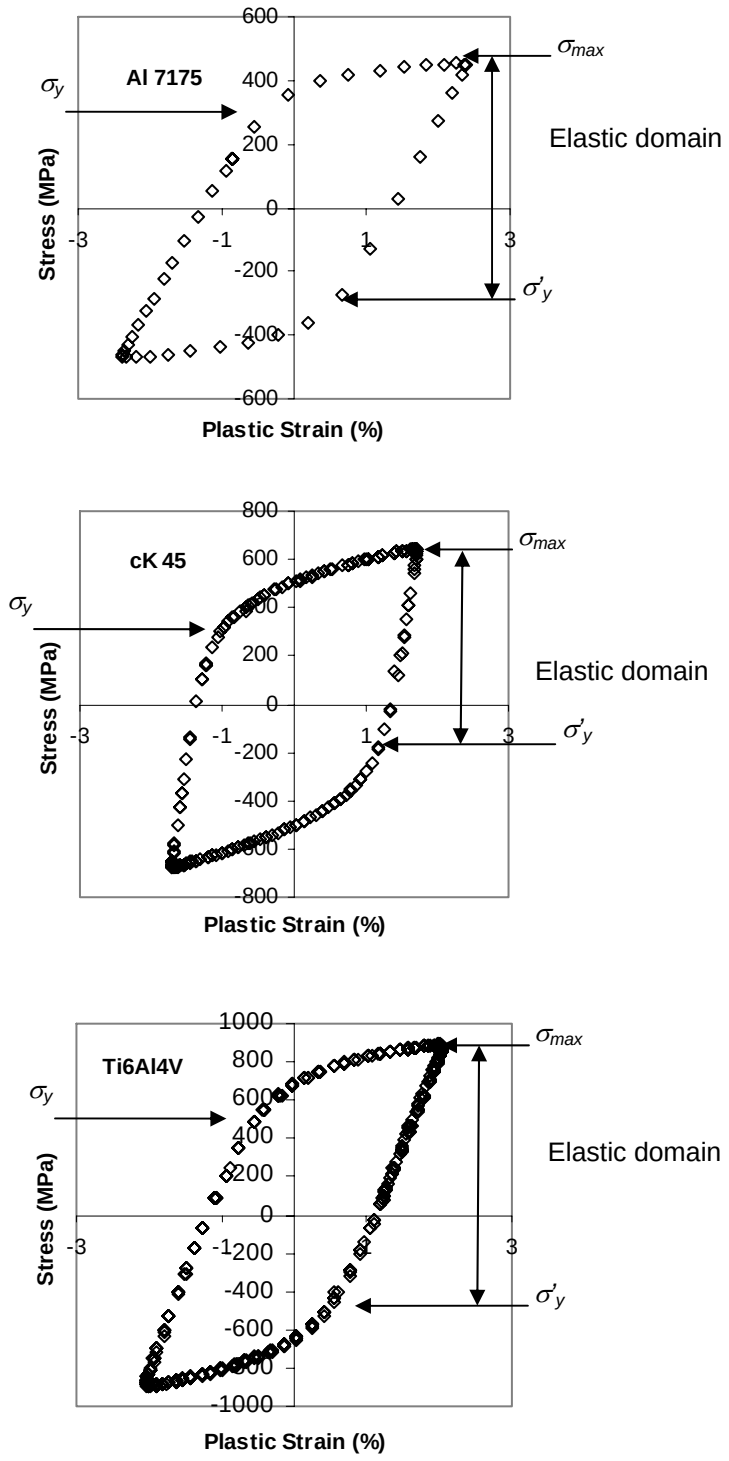

Figure 5.10 Cyclic Hysteresis Behaviour: a) Al7175; b) Ck45; c) Ti6Al4V. σ_{max}-maximum stress; σ_y – yield stress; σ'_y – reverse yield stress [163]

On Figure 5.10 can be seen the different Bauschinger effect of the three different materials. Thus, the fatigue life will be extended. In terms of the BAU effect on the SWT and Morrow models, its interpretation is given in figure 5.11. It can be seen that when

the BAU effect is incorporated in the plastic term of the models (by multiplying it with the fatigue strength coefficient) it will lead to an increase on fretting fatigue life.

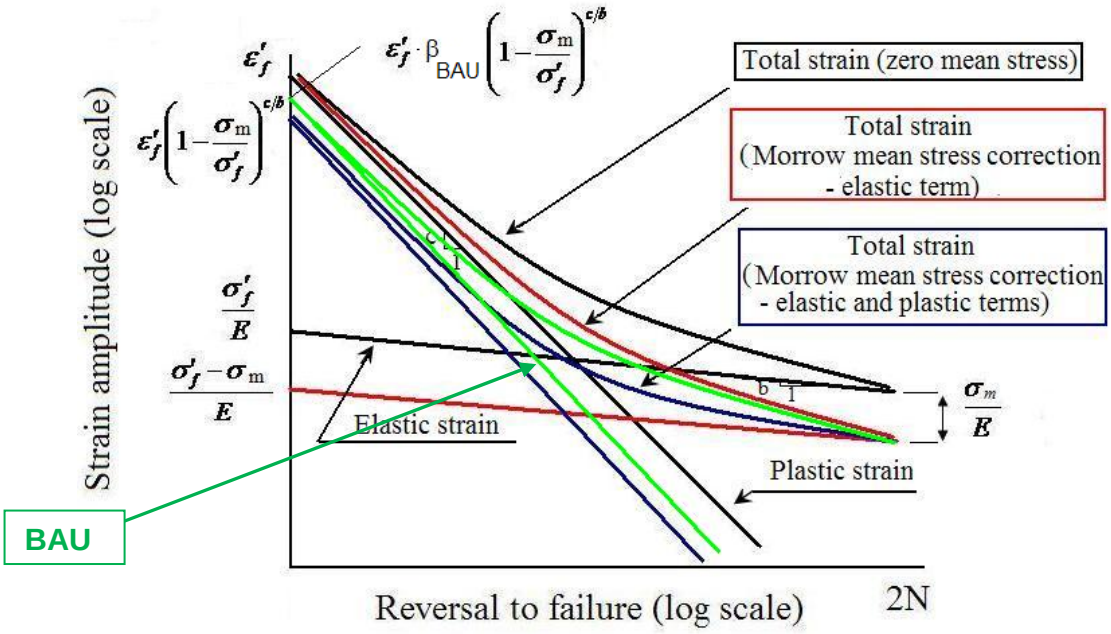

Figure 5.11 Strain life curves showing the BAU effect correction – increasing fatigue life

The proposed Bauschinger stress parameter is determined as follows:

$$\beta_{BAU} = \frac{\sigma_{max}}{\sigma_y^{'}} \tag{5.16}$$

where σ_{max} - maximum stress; $\sigma_y^{'}$– reverse loading yield stress.

This parameter, although not directly obtained based on the energy quantification (on the hysteresis loop), is proposed to represent the decrease in energy accumulation in each cycle. Other parameters with the same consequence (increase in fatigue life) may also be used.

This first approach proposes the modification of the plastic term of both models, by multiplying the fatigue ductility coefficient by BAU stress parameter (eq. 5.16).

When the BAU stress parameter is incorporated in the plastic term of the SWT equation (5.13), it takes the following form:

$$\left(\sigma_{max} + 2p_0\sqrt{\mu F_{t,max}/F_{n,max}}\right)\cdot\frac{K_t}{K_s}\left(\frac{1-2\upsilon^2-\upsilon^3}{E}\right)\left(\sigma_a + \sigma_{a,F_t}\right) = \frac{\left(\sigma_f^{'}\right)^2}{E}\left(2N_f\right)^{2b} + \sigma_f^{'}\varepsilon_f^{'}\cdot\beta_{BAU}\cdot\left(2N_f\right)^{b+c} \tag{5.17}$$

In the case of Morrow equations when the BAU stress parameter is incorporated in the plastic term, equation 5.15 becomes:

$$\varepsilon_{a,FF} = \frac{\sigma_f'}{E}\left(1 - \frac{\left(\sigma_m + 2p_0\sqrt{\mu F_{t,m}/F_{n,m}}\right)\cdot(K_t/K_s)}{\sigma_f'}\right)(2N_f)^b + \varepsilon_f' \cdot \beta_{BAU} \cdot \left(1 - \frac{\left(\sigma_m + 2p_0\sqrt{\mu F_{t,m}/F_{n,m}}\right)\cdot(K_t/K_s)}{\sigma_f'}\right)^{c/b}(2N_f)^c \quad (5.18)$$

The values obtained for the BAU stress parameter are presented in Table 5.1.

Table 5.1 Results of the Bauschinger stress parameter

Parameter/Material	Al7175	Ck45	Ti6Al4V
σ_{max} [MPa]	50.4692	59.89929	96.54383
σ_y [MPa]	20.2564	19.50103	36.00366
β_{BAU}	2.49	3.07	2.68

Second approach – internal stresses, dislocation theories

The BAU effect on the SWT and Morrow models of the second approach is given in figure 5.12. Again, in this case the BAU effect is incorporated only in the plastic term of both models, by modifying the value of the fatigue ductility coefficient. From the value of the fatigue ductility coefficient that was determined for the stabilized hysteresis loops, it is subtracted the BAU parameter. It can be seen that when the new fatigue ductility coefficient is incorporated in the models it will lead to a reduction of fretting fatigue life. This parameter, also used for convenience, tries to introduce the effect of fatigue life reduction, as proposed by Pommier [151, 157] for fatigue crack propagation.

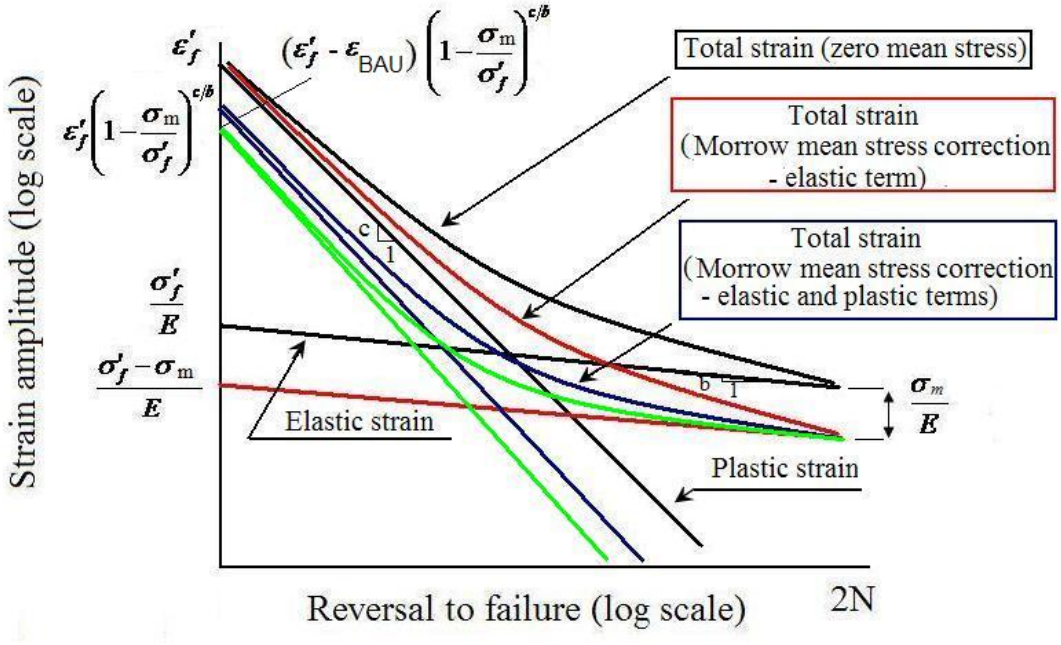

Figure 5.12 Strain life curves showing the BAU effect correction – decreasing fatigue life

The new fatigue ductility coefficient that incorporated the BAU effect is given by:

$$\varepsilon'_{f,BAU} = \varepsilon'_f - \varepsilon_{BAU} \tag{5.19}$$

where: $\varepsilon_f^{'}$ - fatigue ductility coefficient; ε_{BAU} - BAU parameter.

The proposed BAU parameter is given by:

$$\varepsilon_{BAU} = \ln\left(\frac{100}{100 - \beta_{BAU}}\right) \tag{5.20}$$

where: β_{BAU} - BAU stress parameter.

When the new fatigue ductility coefficient (with BAU effect) is incorporated in the plastic term of the SWT eq. 5.13, it takes the following form:

$$\left(\sigma_{max} + 2p_0\sqrt{\mu F_{t,max}/F_{n,max}}\right) \cdot \frac{K_t}{K_s}\left(\frac{1 - 2\upsilon^2 - \upsilon^3}{E}\right)\left(\sigma_a + \sigma_{a,F_t}\right) \tag{5.21}$$

$$= \frac{\left(\sigma'_f\right)^2}{E}\left(2N_f\right)^{2b} + \sigma'_f\varepsilon'_{f,BAU}\left(2N_f\right)^{b+c}$$

In the case of Morrow equations when the new fatigue ductility coefficient is incorporated in the plastic term, equation 5.15 becomes:

$$\varepsilon_{a,FF} = \frac{\sigma'_f}{E}\left(1 - \frac{\left(\sigma_m + 2p_0\sqrt{\mu F_{t,m}/F_{n,m}}\right) \cdot \left(K_t/K_s\right)}{\sigma'_f}\right)\left(2N_f\right)^b \tag{5.22}$$

$$+ \varepsilon'_{f,BAU}\left(1 - \frac{\left(\sigma_m + 2p_0\sqrt{\mu F_{t,m}/F_{n,m}}\right) \cdot \left(K_t/K_s\right)}{\sigma'_f}\right)^{c/b}\left(2N_f\right)^c$$

The values obtained for the new fretting fatigue ductility coefficient are presented in Table 5.2.

Table 5.2 Results of the new fatigue ductility coefficient that incorporates the BAU

Parameter/Material	Al7175	Ck45	Ti6Al4V
ε_{BAU}	0.0252	0.03119	0.02718
ε'_f	0.0689	0.6110	1.9154
$\varepsilon'_{f,BAU}$	0.0437	0.5798	1.8882

5.5.3 First approach- energy based models

The first approach is based on energy based models and leads to an increase of fretting fatigue life. This increase on fretting fatigue life can have a beneficial (a better fretting fatigue life prediction, which agrees well with the experimental results) or a detrimental effect on life prediction.

Several fatigue damage criteria based on energy have been proposed in the technical literature [12,198]. Many researchers [198] consider that the energy dissipation per cycle in hysteresis loops is an excellent parameter to determine the useful life for a component/specimen. Energy based models are mainly related to plastic properties and depend on the hysteresis loop shape. The hysteresis loop shape is strongly dependent on cyclic plasticity and on the Bauschinger effect of the materials.

On the microscopic level, the cyclic plastic strain is related to the movement of dislocations, and the cyclic stress is related to the resistance to their motion. Thus, the plastic strain energy per cycle may be regarded as a composite measure of the amount of fatigue damage per cycle, and the fatigue resistance of a metal may be characterized in terms of its capacity to absorb and dissipate plastic strain energy [12].

The strain energy method [189] are based on the assumption that the damage due to the cyclic loading is a function of the absorbed plastic strain energy density, ΔW_p, and that part of the elastic strain energy, which facilitates crack growth, ΔW_e (see figure 5.13).

As the hysteresis loop is decreasing due to the BAU effect there will be less energy dissipated for each cycles, so this will lead to an increase on fatigue life.

It can be seen from Table 5.1 that the magnitude of BAU effect on Ck45 steel is much higher (3.7) then on Al7175 (2.49) and Ti6Al4V (2.68) alloys. It is expected also that the effect on fretting fatigue life will be different.

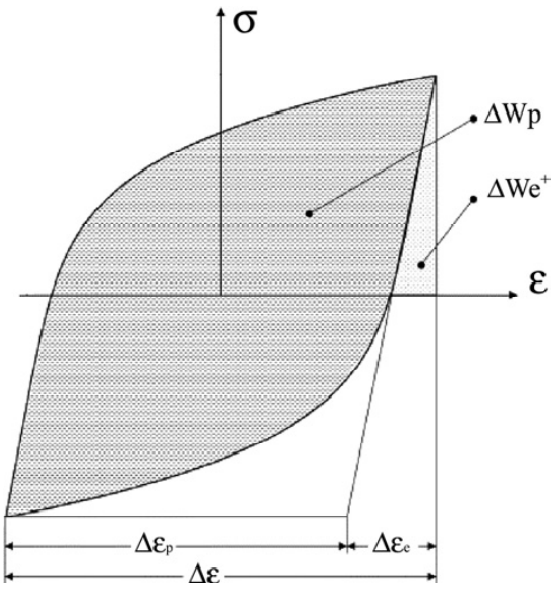

Figure 5.13 Schematic showing how the total strain energy density consists of the plastic strain energy density plus the tensile elastic strain energy density [189]

SWT parameter – energy based models

Figure 5.14 shows the analytical fretting fatigue life prediction based on the SWT parameter which takes into consideration the stress concentration factor, K_t and the surface finishing factor, K_s (eq. 5.13 – dashed blue line). It is also shown the estimated life obtained using the SWT parameter (with K_t and K_s incorporated) affected by the BAU effect (eq. 5.17 – solid green line).

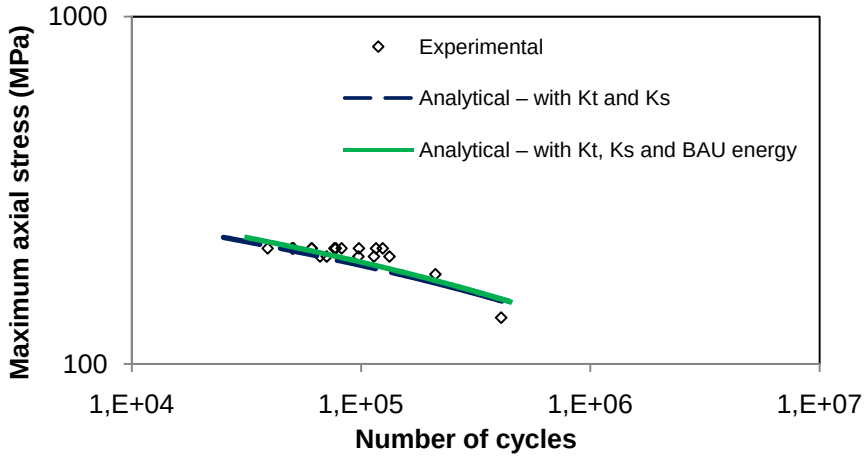

a. Al7175

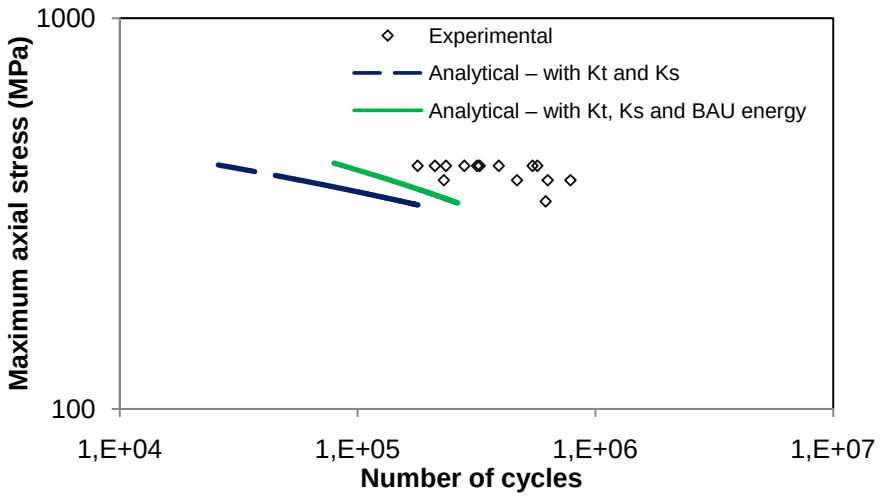

b. Ck45

Figure 5.14 Maximum axial stress (σ_{max}) vs. number of cycles (SWT – Kt, Ks and BAU energy) (cont.)

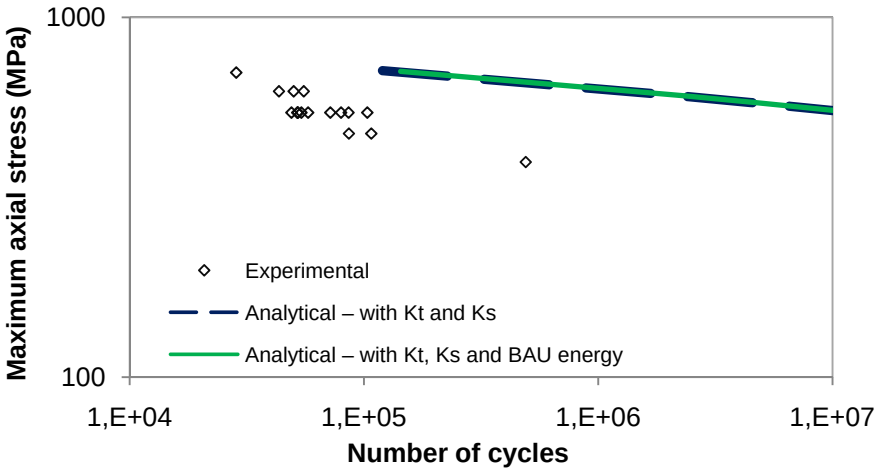

c. Ti6Al4V

Figure 5.14 Maximum axial stress (σ_{max}) vs. number of cycles (SWT – Kt, Ks and BAU energy)

The main aspect to highlight is that the BAU effect introduced in the SWT parameter has a very small effect on fretting fatigue life in the case of Al7175 and Ti6Al4V alloys (figure 5.14a,c), that is neither beneficial nor detrimental.

From figure 5.14b it can be seen that the BAU effect in the case of Ck45 steel has a significant effect on fretting fatigue life. The predicted results in the case of Ck45 steel are much closer to the experimental results when the BAU effect was introduced into the model.

Morrow parameter - Global mean stress on the elastic and plastic terms

Figure 5.15 shows the analytical prediction based on Morrow´s parameter taking into consideration the effect of the stress concentration factor, K_t (Neuber) and the surface finishing factor, K_s (eq. 5.15 – dashed blue line). Also the estimated life obtained using the Morrow´s parameter affected by the BAU effect when it leads to an increase on fretting fatigue life (eq. 5.18 – solid green line) is presented in figure 5.15.

It can be seen that also in Morrow´s case the BAU effect did not have any influence on fretting fatigue life when it was applied to the Al7175 and Ti6Al4V alloys (figure 5.15a,c).

In the case of Ck45 steel (figure 5.15b) can be seen that BAU effect improved the prediction of fretting fatigue life.

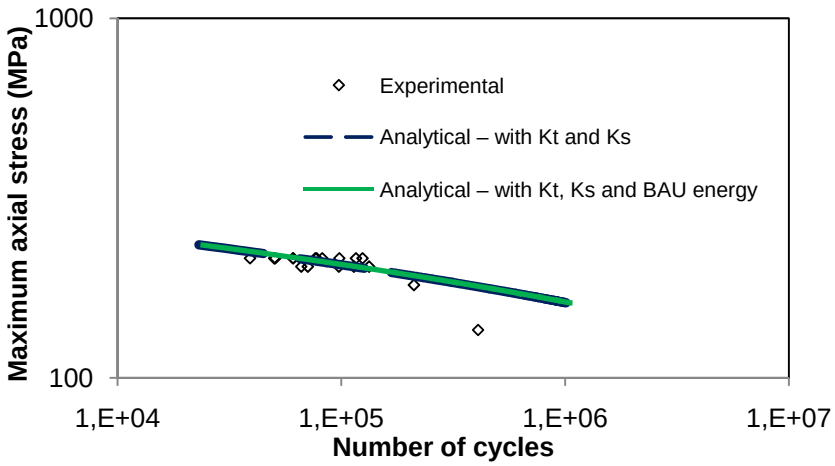

a. Al7175

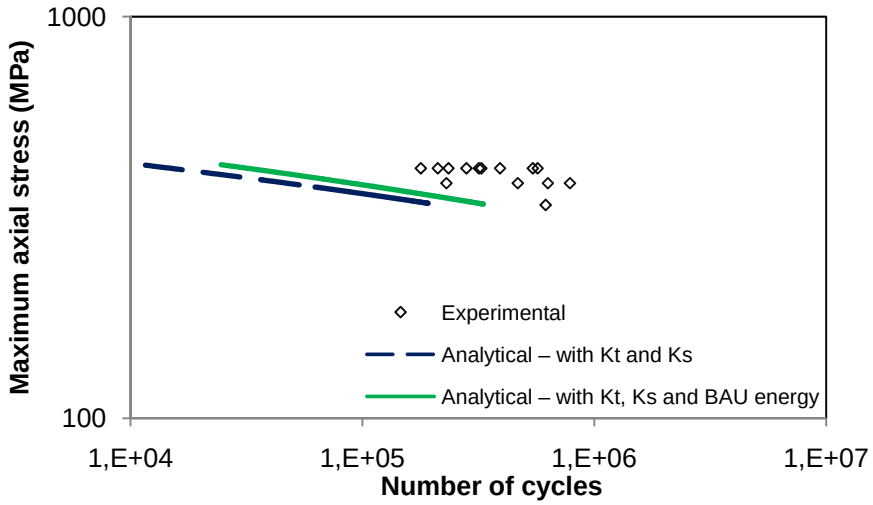

b. Ck45

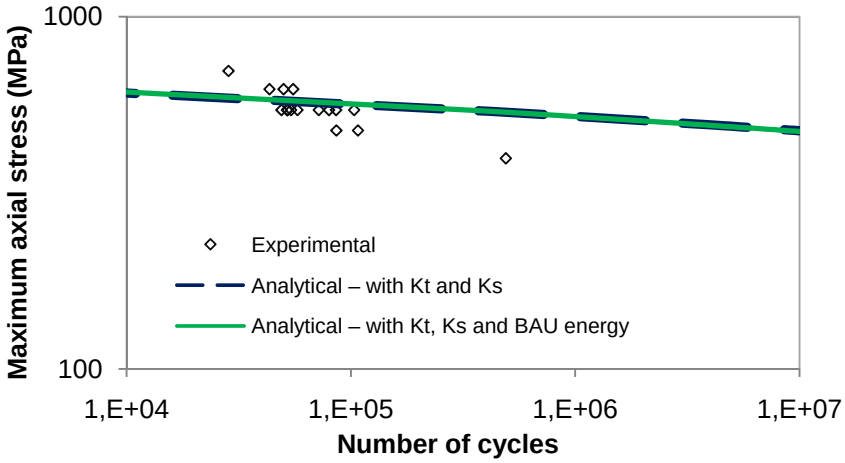

c. Ti6Al4V

Figure 5.15 Maximum axial stress (σ_{max}) vs. number of cycles (Morrow elastic and plastic– K_t and BAU effect)

5.5.4 Second approach – internal stresses, dislocation theories

Contrarily to the first approach are the theories that consider that the BAU effect (internal stresses; dislocation theories; composite model (Masing´s model or Asaro´s model) is characterized by an early re-yielding and smooth elastic–plastic transition with a rapid change of work-hardening rate, is followed by the plastic deformation with an apparent permanent softening, leading to a decrease on fatigue life (see section Mechanism of the Bauschinger effect).

The decrease on fretting fatigue life when the BAU effect is incorporated into the models can lead to a better or worst prediction, depending on the material.

SWT parameter

Figure 5.16 shows the analytical fretting fatigue life prediction based on the SWT parameter which takes into consideration the stress concentration factor, K_t (Neuber) and surface finishing factor, K_s (eq. 5.13 – dashed blue line). Also the estimated life obtained using the SWT parameter affected by the BAU effect when it leads to a decrease on fretting fatigue life (eq. 5.21) is presented in figure 5.16 (eq. 5.21 – solid green line).

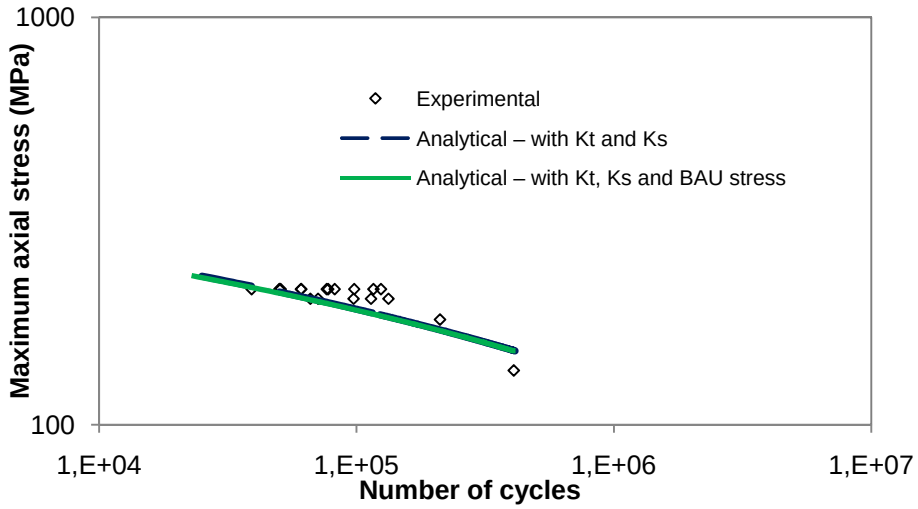

a. Al7175

Figure 5.16 Maximum axial stress (σ_{max}) vs. number of cycles (SWT – K_t and BAU effect- stress) (cont.)

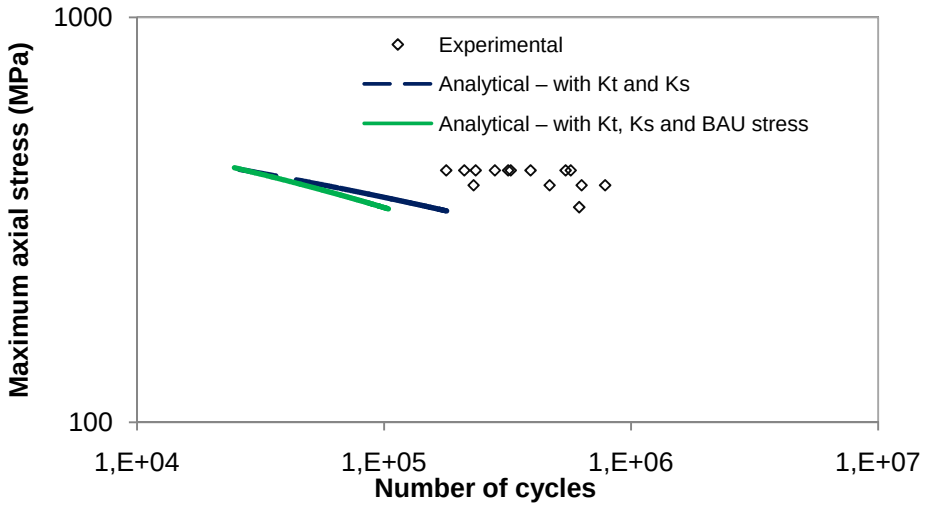

b. Ck45

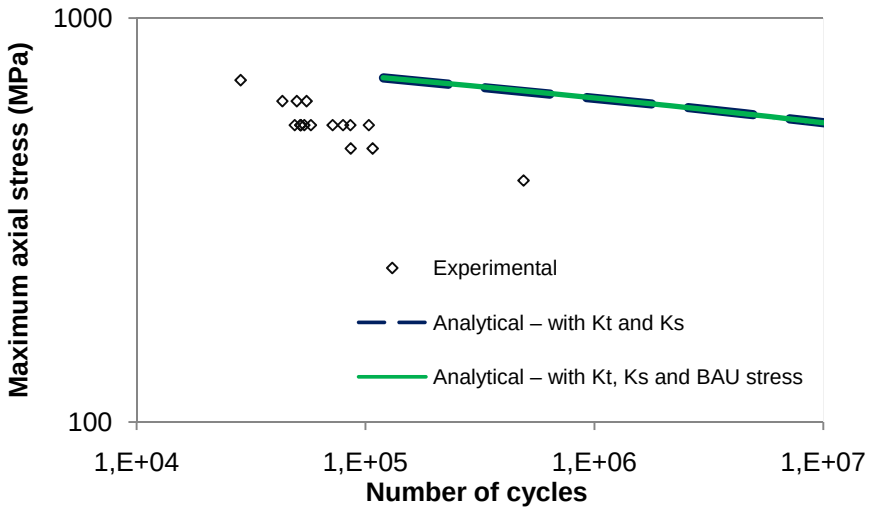

c. Ti6Al4V

Figure 5.16 Maximum axial stress (σ_{max}) vs. number of cycles (SWT – K_t and BAU effect- stress)

From figure 5.16 a and c, it can be seen that in the case of Al7175 and Ti4Al4V alloys the BAU effect did not have any influence on fretting fatigue life. In the case of Ck45 steel (figure 5.16b) when the BAU effect was incorporated in the SWT parameter it had a significant influence on fretting fatigue life. This correction is leading to a worse prediction in the case of Ck45 steel.

Morrow parameter - Global mean stress on the elastic and plastic terms

Figure 5.17 shows the analytical prediction based on Morrow´s parameter taking into consideration the effect of the stress concentration factor, K_t (Neurber), surface finishing factor, K_s (eq. 5.15 – dashed blue line), and also the estimated life obtained

using the Morrow´s parameter affected by the BAU effect when it leads to a decrease on fretting fatigue life (eq. 5.22 – solid green line).

The first aspect to highlight, regarding the internal stresses approach, is that when the BAU effect was incorporated the influence is very small in both approaches. Only a small change occurs in SWT approach for ck45 alloy.

In relation to the energy based approaches it is verified that the BAU effect improves the accuracy of the predictions. This is observed mainly for the alloy with higher BAU effect, ck45, but also for the Al7175 alloy. The Ti6Al4V alloy is not affected by the BAU effect.

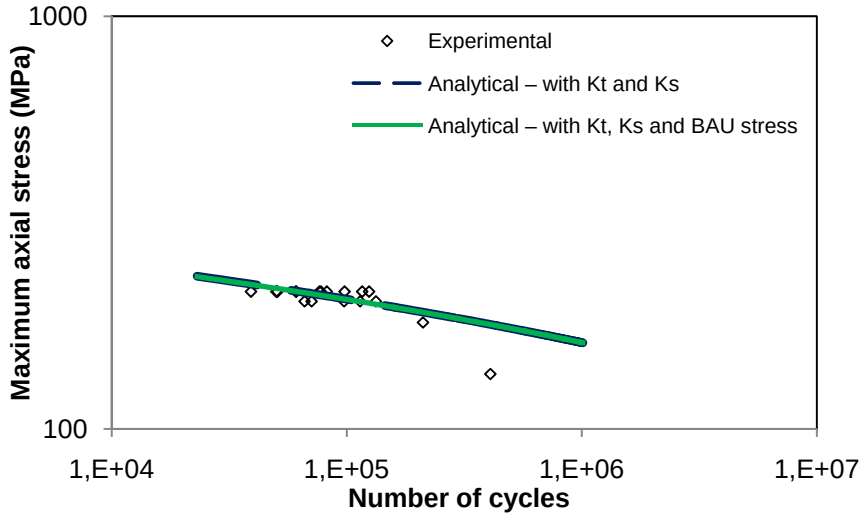

a. Al7175

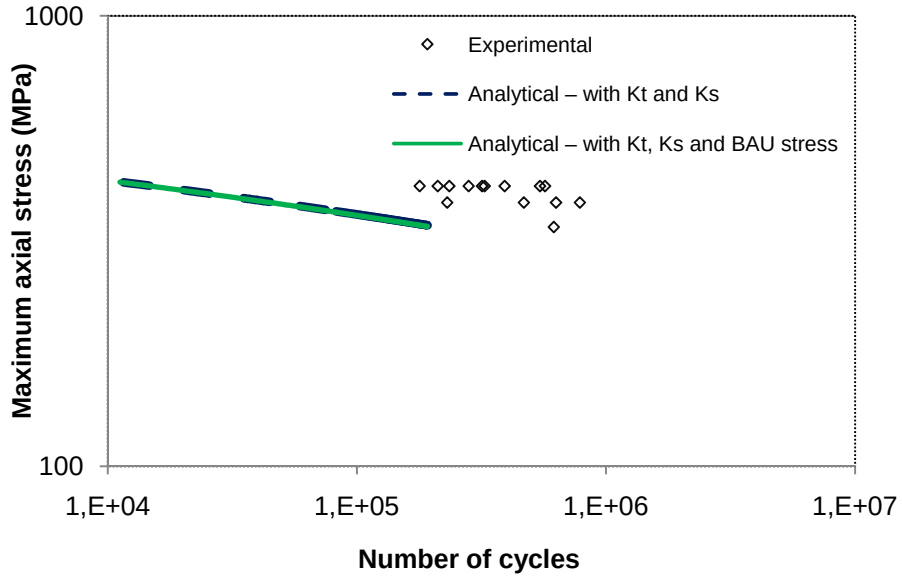

b. Ck45

Figure 5.17 Maximum axial stress (σ_{max}) vs. number of cycles (Morrow - elastic and plastic – K_t and

BAU effect) (cont.)

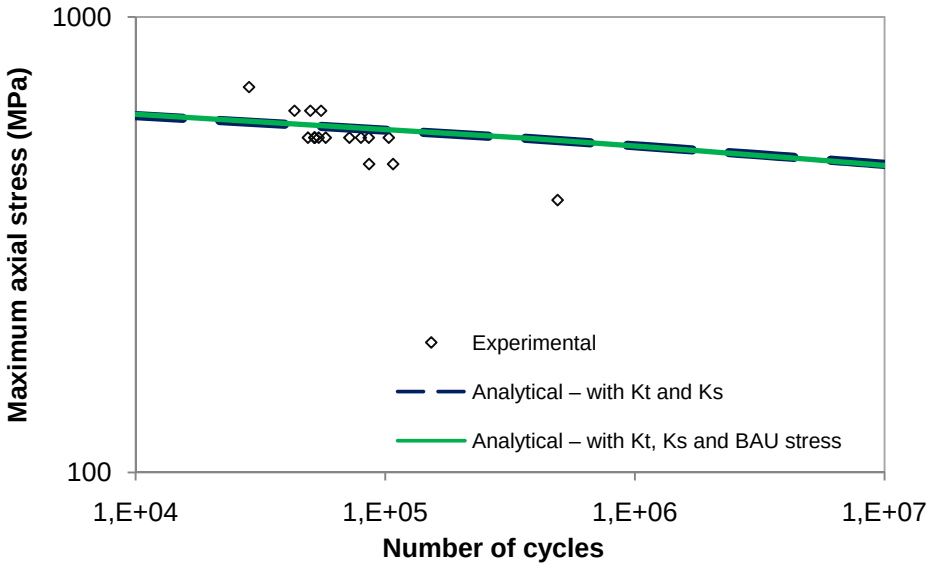

c. Ti6Al4V

Figure 5.17 Maximum axial stress (σ_{max}) vs. number of cycles (Morrow - elastic and plastic – K_t and BAU effect)

It should be mentioned that by incorporating the BAU effect into the both models it can be seen that it does not have any influence on the materials that have a very small BAU effect but improved the life of the materials that have a significant BAU effect. It can be concluded that now both models used in this study are more universal (general) equations.

Regarding the two BAU approaches presented in this work, energy based and internal stresses/dislocation theories, is the opinion of the author of this work that the one that should prevail is the energy based approach. The reason lies on the fact that makes more sense, physically speaking, that the reduction in the energy consumption per cycle would increase the fatigue life. Furthermore the explanation, as presented by Pommier [146, 151, 157], which caused an increase in damage due to the BAU effect is based on physical aspects (residual stresses and crack closure) either ahead and behind the crack tip. It was not defined which (ahead or behind) was the most relevant. Pommier demonstrated that it is relevant on crack propagation (because there exists a crack) but not on crack initiation (no existing crack – no crack closure).

Regarding the BAU effect, and mainly due to the fact that it was never used in fatigue initiation models, the author of this work decided that it should be verified in circumstances where not so many variables are present. As a fact, in fretting fatigue different variables are introduced on the contact region (additional contact stresses, wear, etc). Thus, it was decided to see what would be the BAU effect in plain fatigue

tests, in order to validate the assumption that the BAU effect is relevant of fatigue predictions. In annex B some S-N curves are presented. In that study it will be demonstrated the relevance of the BAU effect in fatigue life predictions. The main conclusion is that if the BAU effect is relevant in plain fatigue conditions it is also appropriate to include it in fretting fatigue situations.

5.6 Conclusions on the prediction models results

In order to develop a method that could be useful for practicing engineers to estimate the fretting fatigue life, two strain based fatigue models have been chosen. The first approach is the Smith-Watson-Topper´s model and the second approach is the Morrow´s model. These models were chosen because they are the models that include more intrinsic material properties being then more appropriate to understand either the influence of the material properties as well as to establish a comparison among different materials. The former model was already used in fretting fatigue while the latter was tested for the first time in this work.

The main aspects to highlight regarding the approach of this chapter are:

- Morrow´s model is used for the first time to predict the fretting fatigue life. Morrow´s model was modified in order to introduce the local stresses involved in the fretting fatigue process (normal, tangential and axial loads);

- A fundamentally new parameter that is proposed is the calculation on the stress concentration factor, K_t, (the effect of the damaged area herein called the “fretting scar effect”) that was determined by numerical simulation. This alteration was applied to the Morrow´s model and to the SWT model;

- Another parameter that was proposed in this work is the introduction of the effect of roughness of contact area in the form of a surface finish factor, K_s. This alteration was applied to the Morrow´s model and to the SWT model;

- Finally it was also proposed a new parameter that affects the plastic strain component of the models - the Bauschinger effect, which reflects a material deviation from the ideal plastic behaviour. The energy-based approach is the approach that seems to make more sense to use.

The main aspects to highlight regarding the predictions, by using the two previous modified models, and the three proposed modifications, are:

- Ck45 alloy predictions are sensitive to all three parameters. Al7175 and Ti6Al4V alloys predictions are sensitive mainly to stress concentration and roughness effects;

- Al7175 is predicted with accuracy by using both models and by taking into consideration all the three effects (stress concentration, roughness, and BAU**)**;

- Ck45 alloy is not predicted with accuracy. The stress concentration factor and the roughness parameters worsen the prediction. The BAU effect improves the prediction. If predicted with BAU effect but without K_t and K_s excellent predictions could be obtained. As a fact in annexe B it is proved the relevance of the BAU effect, and in chapter 3 it was shown that ck45 is the less sensitive of the three materials to the fretting fatigue conditions (normal and tangential loads and wear);

- Ti6Al4V alloy was never properly predicted by the two models. This could be related with the fact that on obtaining low cycle fatigue properties some heat generated in the specimens [163] and those properties may not be very accurate.

As a general conclusion on this chapter it can be said that it seems relevant to incorporate the three variables in both models, for fretting fatigue life quantifications. Better correlations between predicted life and experimental results were obtained by introducing the effects of the stress concentration factor, surface finishing factor and BAU effect. The grade of improvement depends on the model and material tested. Thus it seems that the previous equations may become more robust, in terms of materials properties incorporation, and more universal, if the variables proposed in this work are incorporated.

Chapter 6
Conclusions and recommendations for future work

Chapter 6 gives the major concluding remarks and findings for this research program together with possible future lines of work related with the present research.

6.1 Conclusions

The research describes the fretting fatigue phenomena in a comparative way for three different materials (Al7175, Ck45 and Ti6Al4V). It consists in both experimental and analytical work.

The main conclusions of this work can be drawn as follows:

Experimental work

- A newly fretting fatigue apparatus has been designed and build. It is a very versatile apparatus that has as main advantage the ability to measure a number of different variables during the test. It is able to set and record the normal and tangential loads and the relative displacement specimen/pads. The measurement of the relative displacement is direct and does not need to take into account the compliance of the system. This allowed a better understanding of the influence of this very important variable while keeping constant all the other parameters. Every small detail (load or displacement) can be detected and recorded by the equipment. This made possible to assess the influence of the referred variables and in this way allowed a better understanding of the fretting fatigue phenomena. The most significant feature of this apparatus is the way to measure the relative displacement.

- By observing the variation of the referred variables (normal and tangential loads and the relative displacement amplitude) it was confirmed the presence of the asymmetrical fretting scar formation in fretting fatigue situations (rarely highlighted in the technical literature). It was also confirmed the typical variation of fretting fatigue life with relative displacement. It was confirmed that fretting fatigue life is very sensitive to the relative displacement amplitude. It was possible to, in a robust way, understand and correlate the different variables playing a role on the fretting fatigue process, namely normal and tangential loads, axial machine load, relative displacement, scar depth and shape, and roughness evolution. These parameters allowed a consistent understanding of the fretting fatigue phenomena.

- The results of the experimental work highlight the synergic effect between fatigue and fretting/wear. The damage induced by fretting increased the fatigue damage, resulting in a shorter life of the component (specimen). It was observed that Al7175 and Ti6Al4V alloys are more sensitive to fretting fatigue than Ck45 steel, this being justified by the well known poor tribological characteristics of the aluminium and titanium alloys (as confirmed by the reciprocating wear tests). The CK45 alloy developed a smaller wear scar which resulted in lower values of the stress concentration factor and, consequently, higher relative fretting fatigue life.

- As the fretting fatigue phenomena is strongly influenced by the connection between the stress state (fatigue – axial load and fretting – normal and tangential load) and the wear in the contact region, it was expected that the wear and consequently the fretting fatigue behaviour/performance of the materials might be differently affected when the material (specimen) is in tension or compression. The design and the utilities of the new developed reciprocating wear device have been described. It permits to see the influence of an additional elastic stress state on wear behaviour of materials. From the investigation of the wear behaviour of the materials when subjected to additional elastic stress states, it was concluded that it has a substantial influence on wear behaviour. It was proposed a physical and analytical model to describe the wear behavior of the materials under different additional elastic stress states (either tensile or compressive). It was explained by micro-roughness (grain shape changes) and /or by macro-roughness states. A modification in the Archard model has been proposed in order to incorporate the effect of an additional stress (either tensile or compressive), giving a good correlation between predicted and experimental wear volumes. From this analysis was understood the asymmetrical scar formation in fretting fatigue tests.

- The scar damage was also quantified in terms of its shape and surface finishing. It allowed define two new variables, to incorporate in the fretting fatigue process, namely the stress concentration factor and the surface finishing factor.

Analytical work

- The models chosen for consideration were two strain based fatigue models. The first approach was the Smith-Watson-Topper´s model and the second approach was Morrow´s model. The former model is already used in fretting fatigue while the latter is an original developed in the present work. Mean stress effects are included in both models. Morrow´s model was modified in order to introduce the local stresses involved in the fretting fatigue process (normal, tangential and axial).

- One of the main advances of this analytical approach was the introduction of the effect of the damaged area in the form of a stress concentration factor, K_t. It was shown that it may have a substantial influence in some materials.

- The second advance was the introduction of the surface finishing factor, K_s. It was shown that it may have a strong influence on fretting fatigue life predictions. This parameter was observed to be also very material dependent.

- The third main advance of this work is concerned with the incorporation of a material intrinsic property of the materials, namely the Bauschinger effect, *BAU*. It was shown that it has a substantial influence on fatigue life and consequently on fretting fatigue life. This parameter is also highly material dependent.

- By the introduction of the previous three parameters improved correlations could be obtained mainly in the case of the Al7175 and the ck45 alloys.

- It is also the opinion of the author of this work that the previous two models become more robust and more universal equations if the three parameters are incorporated. Thus, both the SWT and Morrow´s parameters can be used as an engineering tool for estimation of fretting fatigue life.

6.2 Recommendations for future work

- In order to have a complete picture of wear behaviour, when the specimen is under an additional stress state, another wear tests should be performed: tests under more values of an additional stress state; more tests with different relative displacements. It will also help to validate the physical wear model that was proposed in this work for a wide range of conditions.

- In order to generalize the BAU effect when it is incorporated into the SWT and Morrow´s models, this should be extended to a range of different materials, mainly for the plain fatigue case.

- BAU effect should be comprehensively understood and a more robust parameter, physically based should be developed.

- The experimental work should continue to determine the effect of a controlled environment (temperature, corrodibility etc) as most investigations reported cases of fretting in normal atmospheres, but there are also cases when fretting occurs in different conditions. These effects should be incorporated in fretting fatigue equations.

References

[1] N.E. Dowling, Mechanical Behavior of Materials: Engineering Methods for Deformation, Fracture, and Fatigue, 2nd edition, Pretince Hall, 1998.

[2] J.A. Araújo, D. Nowell, The effect of rapidly varying contact stresses fields on fretting fatigue, International Journal of Fatigue 24 (2002) 763-775.

[3] G.W. Powell, ASM Handbook, Volume 11: Failure Analysis and Prevention, ASM International, Materials Park, OH, 1986.

[4] S.E. Kinyon, D.W. Hoeppner, Spectrum load effects on the fretting behavior of Ti-6Al-4V, "Fretting Fatigue: Current Technology and Practices," ASTM STP 1367, D.W. Hoeppner, V. Chandrasekaran, and C.B. Elliot, Ed., ASTM, West Conshohocken, PA, 2000, pp. 282-92.

[5] A. Vadiraj, M. Kamaraj, Characterization of fretting fatigue damage of PVD TiN coated biomedical titanium alloys, Surface&Coatings Technology 200 (2006) 4538-4542.

[6] N.R. Lovrich, Fretting fatigue of Ti-6Al-4V, Experimental characterisation and simple design parameter, Thesis.

[7] D.A. Hills**,** D**.** Nowell**,** Mechanics of Fretting Fatigue**,** Kluwer Academic Publishers, Dordrecht, 1994.

[8] O. Vingsbo, S. Soderberg, On fretting maps, Wear 126 (1988) 131–147.

[9] D.A. Hills, D. Nowell, J. J. O´Connor, On the mechanics of fretting fatigue, Wear 125 (1988) 129-156.

[10] M. Massinghan, P.E. Irving, The effect of variable amplitude loading on stress distribution within a cylindrical contact subjected to fretting fatigue, Tribology International 39 (2006) 1084–1091.

[11] M.P. Szolwinsky, T.N. Farris, Observation, analysis and prediction of fretting fatigue in 2024-T351 aluminum alloy, Wear 221 (1998) 24–36.

[12] D.F. Socie, G.B. Marquis, Multiaxial fatigue, SAE International 2000.

[13] H. Proudhon, S. Fouvry, J.Y. Buffiére, A fretting crack initiation prediction taking into account the surface roughness and the crack nucleation process volume, International Journal of Fatigue 27 (2005) 569–579.

[14] S.A. Namjoshi, A. Shantanu, S. Mall, V.K. Jain, O. Jin, Fretting fatigue crack initiation mechanism in Ti-6Al-4V, Fatigue Fract Engng Mater Struct 25 (2002) 955-964.

[15] D.W. Hoeppner, Fretting fatigue case studies of engineering components, Tribology International 39 (2006) 1271-1276.

[16] F.S. Silva, Fatigue degradation of materials as a tool for damage assessment**,** The annals of "Dunarea de Jos" University of Galati. Fascicle IX. Metallurgy and materials science N0. 1 – 2008, ISSN 1453 – 083x.

[17] American Society of Metals, ASM Metals Handbook Volume 19 – Fatigue and Fracture.

[18] N.K. Ramakrishna Naidu, S.G.S. Raman, Effect of contact pressure on fretting fatigue behaviour of Al-Mg-Si alloy AA6061, International journal of Fatigue 27 (2005) 283-291.

[19] A.B. Hamid, R.K. Yahya, Influence of fretting on the fatigue strength at the vise clamp-specimen interface, Bull. mater. Sci. 26, (2003), 749-754.

[20] A.L. Hutson, L. Chambon, Observations of fretting fatigue micro-damage of Ti-6Al-4V, Wear 255 (2003) 259–268.

[21] M.H. Attis, R B. Waterhouse, editors. Standardization of fretting fatigue test methods and equipment, ASTM STP 1159, American Society Testing Materials, Philadelphia, 1992.

[22] O. Jin, S. Mall, Effects of independent pad displacement on fretting fatigue behavior of Ti–6Al–4V, Wear 253 (2002) 585–596.

[23] G.W. Stachowiak, A.W. Batchelor, Engineering Tribology, 2rd ed., Butterworth-Heinemann, 2001.

[24] J.M. Dobromirski, Variables of fretting process: are there 50 of them? In: M. Helmi Attia and R.B. Waterhouse, Editors, *Standardization of fretting fatigue tests and equipment, ASTM STP 1159*, American Society for Testing and Materials, Philadelphia (1992) 60–66.

[25] J.J. Madge, S.B. Leen, P.H. Shipway, The critical role of fretting wear in the analysis of fretting fatigue, Wear 263 (2007) 542-551.

[26] O. Jin a, S. Mall, J. H. Sanders, S.K. Sharma, Durability of Cu–Al coating on Ti–6Al–4V substrate under fretting fatigue, Surface & Coatings Technology 201 (2006) 1704–1710.

[27] Y. Fu, J. Wei, A.W. Batchelor, Some considerations on the mitigation of fretting damage by the application of surface-modification technologies, Journal of Materials Processing Technology 99 (2000) 231-245.

[28] M.H. Zhu, Z.R. Zhou, Ph. Kapsa, L. Vincent, Radial fretting fatigue damage of surface coatings, Wear 250 (2001) 650–657.

[29] C.H. Hager, J. Sanders, S. Sharma, A. Voevodin, A. Segall, The effect of temperature on gross slip fretting wear of cold-sprayed nickel coatings onTi6Al4Vinterfaces, Tribology International 42 (2009) 491–502.

[30] M. Buciumeanu, A.S. Miranda, A.C.M. Pinho, F.S. Silva, Design improvement of an automotive-formed suspension component subjected to fretting fatigue, Engineering Failure Analysis 14 (2007) 810-821.

[31] O. Jin, S. Mall, Effects of slip on fretting behavior: experiments and analyses, Wear 256 (2004) 671-684.

[32] R. Magaziner, O. Jin, S. Mall, Slip regime explanation of observed size effects in fretting, Wear 257 (2004) 190-197.

[33] C. Santus, Fretting fatigue of aluminium alloy in contact with steel in oil drill pipe connections, modeling to interpret test results, International Journal of Fatigue 30 (2008) 677-688.

[34] K. Iyer, Peak contact pressure, cyclic stress amplitudes, contact semi-width and slip amplitude: relative effects on fretting fatigue life, International Journal of Fatigue 23 (2001) 193-206.

[35] W. Ren, S. Mall, J.H. Sanders, S.K. Sharma, Evaluation of coatings on Ti–6Al–4V substrate under fretting fatigue, Surface & Coatings Technology 192 (2005) 177– 188.

[36] C. Navarro, M. Garcia, J. Dominguez, A procedure for estimating the total life in fretting fatigue, Fatigue Fract Engng Mater Struct 26 (2003) 459-468.

[37] C. Li, S. Panier, S. Hariri, Application of a simplified method to evaluate the inelastic state due to fretting fatigue, Tribology International 39 (2006) 1092–1099.

[38] O.P. Datsyshyn, V.M. Kadyra, A fracture mechanics approach to prediction of pitting under fretting fatigue conditions, International

Journal of Fatigue 28 (2006) 375–385.

[39] C.L. Neslen, S. Mall, S. Sathish, Nondestructive Characterization of Fretting Fatigue Damage, Journal of Nondestructive Evaluation 23 (2004) 153-16.

[40] B. Alfredsson, A. Cadario, A study on fretting friction evolution and fretting fatigue crack initiation for a spherical contact, International Journal of Fatigue 26 (2004) 1037–1052.

[41] www.ntsb.gov.

[42] H.A. Fadag, S. Mall, V.K. Jain, A finite element analysis of fretting fatigue crack growth behavior in Ti–6Al–4V, Engineering Fracture Mechanics 75 (2008) 1384–1399.

[43] M. Buciumeanu, A.S. Miranda, F.S. Silva, Effect of relative displacement and normal contact load on fretting fatigue behaviour of Ti6Al4V alloy, Ciência e Tecnologia dos Materiais 20 (2008) 92-98.

[44] K. Nakazawa, N. Maruyama, T. Hanawa, Effect of contact pressure on fretting fatigue of austenitic stainless steel, Tribology Internatinal 36 (2003) 79-85.

[45] H. Lee, Effect of dissimilar mating materials and contact force on fretting fatigue behavior of Ti-6Al-4V, Tribology International 37 (2004) 35-44.

[46] A. Ramalho, I.M. Correia, J.D. Costa, Fretting fatigue of zinc coated low carbon steel EN H320, Tribology International 33 (2000) 761-768.

[47] S. Fouvry, P. Duó, Ph. Perruchaut, A quantitative approach of Ti-6Al-4V fretting damage: friction, wear and crack nucleation, Wear 257 (2004) 916-929.

[48] H. Proudhon, S. Fouvry, G.R. Yantio, Determination and prediction of the fretting crack initiation: introduction of the (P, Q, N) representation and definition of a variable process volume, International Journal of Fatigue 28 (2006) 707-713.

[49] B. U Wittkowsky, P. R., Birch, J. Dominguez, S. Surech, “An apparatus for quantitative fretting fatigue testing”, Blackwell Science Ltd. Fatigue Fract Engng Struct *22* (1999) 307-320.

[50] S. Mall, S.A. Namjoshi, W.J. Porter, Effects of microstructure on fretting fatigue crack initiation behaviour of Ti-6Al-4V, Materials Science and Engineering A383 (2004) 334—340.

[51] C.D. Lykins, S. Mall, V. Jain, A shear stress-based parameter for fretting fatigue crack initiation, Fatigue Fract Engng Mater Struct24 (2001), 461–473.

[52] C.D. Lykins, S. Mall, V.K. Jain, Combined experimental–numerical investigation of fretting fatigue crack initiation, International Journal of Fatigue 23 (2001) 703–711.

[53] H. Lee, S. Mall, J.H. Sanders, S.K. Sharma, R.S. Magaziner, Characterization of fretting wear behavior of Cu–Al coating on Ti–6Al–4V substrate, Tribology International 40 (2007) 1301–1310.

[54] M.P. Szolwinski, T.N. Farris, Observation, analysis and prediction of fretting fatigue in 2024-T351 aluminum alloy, Wear 221 (1998) 24–36.

[55] J.F. Matlik, T.N. Farris, F.K. Haake, G.R. Swanson, G.C. Duke, High-frequency, high-temperature fretting-fatigue experiments, Wear 261 (2006) 1367–1382.

[56] T. Juuma, Torsional fretting fatigue strength of a shrink-fitted shaft with a grooved hub, Tribology International 33 (2000) 537-543.

[57] K. Iyer, S. Mall, Effects of cyclic frequency and contact pressure on fretting fatigue under two-level block loading, Fatigue Fract. Eng. Mater. Struct. 23 (2000) 335–346.

[58] R.S. Magaziner, V.K. Jain, S. Mall, Wear characterization of Ti–6Al–4V under fretting–reciprocating sliding conditions, Wear 264 (2008) 1002–1014.

[59] D. Sarkar, B.V.M. Kumar, B. Basu, Understanding the fretting wear of Ti3SiC2, Journal of the European Ceramic Society 26 (2006) 2441–2452.

[60] U. Bryggman, S. Soderberg, Contact conditions and surface degradation mechanisms in low amplitude fretting, Wear 125 (1988), 39–52.

[61] O. Jin, S. Mall, Influence of contact configuration of fretting fatigue behavior of Ti6Al4V under independent pad displacement condition, International Journal of Fatigue 24 (2002) 1243-1253.

[62] C.H. Hager, J.H. Sander, S. Sharma, Characterization of mixed and gross slip fretting wear regimes in Ti6Al4V interfaces at room temperature, Wear 257 (2004) 167-180.

[63] H. Lee, S. Mall, Fretting behaviour of shot peened Ti-6Al-4V under

slip controlled mode, Wear 260 (2006) 642-651.

[64] X. Huang, R.W. Neu, High-load fretting of Ti–6Al–4V interfaces in point contact, Wear 260 (2006) 642–651.

[65] O. Jin, S. Mall, O. Sahan, Fretting fatigue behaviour of Ti-6Al-4V at elevated temperature, International Journal of Fatigue 27 (2005) 395-401.

[66] Z.R. Zhou, K. Nakazawa, M.H. Zhua, N. Maruyama, Ph. Kapsa, L. Vincent, Progress in fretting maps, Tribology International 39 (2006) 1068–1073.

[67] S. Fouvry, P. Kapsa, L. Vincent, Quantification of fretting damage, Wear 200 (1996) 186-205,

[68] E. Matikas, P.D. Nicolaou, Development of a Model for the Prediction of the Fretting Fatigue Regimes**,** J. Mater. Res. 16 9 (2001), 2716–2723.

[69] W. Huang, B. Hou, Y. Pang, Z. Zhou, Fretting wear behaviour of AZ91D and AM60B magnesium alloys, Wear 260 (2006) 1173–1178.

[70] J.J. Madge, S.B. Leen, P.H. Shipway, A combined wear and crack nucleation–propagation methodology for fretting fatigue prediction, International Journal of Fatigue 30 (2008) 1509–1528.

[71] J.A. Pape, R.W. Neu, A comparative study of the fretting fatigue behaviour of 4340 steel and PH 13-8 Mo stainless steel, International Journal of Fatigue 29 (2007) 2219–2229.

[72] R. Magaziner, O. Jin, S. Mall, Slip regime explanation of observed size effects in fretting, Wear 257 (2004) 190-197.

[73] A.L. Hutson, C. Neslen, T. Nicholas, Characterization of fretting fatigue crack initiation processes in CR Ti-6Al-4V, Tribology International 36 (2003) 133-143.

[74] H. Lee, S. Sathish, S. Mall, Evolution of residual stress under fretting fatigue, Journal of materials science 39 (2004) 7089-7092.

[75] H. Lee, S. Mall, Stress relaxation behaviour of shot-peened Ti-6Al-4v under fretting fatigue at elevated temperature, Materials Science and Engineering A366 (2004) 412-420.

[76] K. Elleuch, H. Proudon, C. Meunier, S. Fouvry, Development of a contact compliance method to detect the crack propagation under fretting, Tribology International 39 (2006) 1262-1270.

[77] J.A. Araujo, D. Nowell, The fretting fatigue limit based on local stress at the contact edge, Fatigue Fract Engng Mater Struct 24 (2001), 791–801.

[78] C. Navarro, J. Domínguez, Initiation criteria in fretting fatigue with spherical contact, International Journal of Fatigue 26 (2004) 1253–1262.

[79] J.A. Araujo, D. Nowel, R.C. Vivacqua, The use of multiaxial fatigue models to predict fretting fatigue life od components subjected to different contact stress fields, Fatigue Fract Engng Mater Struct 27 (2004) 967-978.

[80] J.R. Mayeur, D.L. McDowell, R.W. Neu, Crystal plasticity simulations of fretting of Ti6Al4V in partial slip regime considering effects of texture, Computational Materials Science 41 (2008) 356-365.

[81] H. Lee, S. Mall, Effect of dissimilar mating materials and contact force on fretting fatigue behavior of Ti–6Al–4V, Tribology International 37 (2004) 35–44.

[82] P.J. Golden, A.F. Grandt Jr., Fracture mechanics based fretting fatigue life predictions in Ti–6Al–4V, Engineering Fracture Mechanics 71 (2004) 2229–2243

[83] K. Kubiak, S. Fouvry, A.M. Marechal, A practical methodology to select fretting palliatives: Application to shot peening, hard chromium and WC-Co coatings, Wear 259 (2005) 367–376.

[84] M.C. Gaspar, A. Ramalho, A. Cavaleiro, Effects of the counterface material on the fretting behavior of sputted W-Si-N coatings, Wear 255 (2003) 276-286.

[85] A. Iwabuchi, J.W. Lee, M. Uchidate, Synergetic effect of fretting wear and sliding wear of Co-alloy and Ti-alloy in Hanks´solution, Wear 263 (2007) 492-500.

[86] D. Nowell, D. Dini, Stress gradient effects in fretting fatigue, Tribology International 36 (2003) 71–78.

[87] R.B. Waterhouse, A. J. Trowsdale, Residual stress and surface roughness in fretting fatigue, J. Phys. D: Appl. Phys. 25 (1992) A236-A239.

[88] A. Cadario, B. Alfredsson, Fretting fatigue experiments and analyses with a spherical contact in combination with constant bulk stress,

Tribology International 39 (2006) 1248-1254.

[89] A.E. Giannakopoulos, T.C. Lindley, S. Suresh, Aspects of Equivalence between Contact Mechanics and Fracture Mechanics: Theoretical Connections and a Life-Prediction Methodology for Fretting-Fatigue, Acta mater 46 (1998) 2955±2968.

[90] A. Volchok, G. Halperin, I. Etsion, The effect of surface regular microtopography on fretting fatigue life, Wear 253 (2002) 509-515.

[91] D. Dini, D. Nowell, Prediction of the slip zone friction coefficient in flat and rounded contact, Wear 254 (2003) 364-369.

[92] S. Fouvry, Ph. Kapsa, L. Vincent, Analysis of sliding behaviour for fretting loadings: determination of transition criteria, Wear 185 (1995) 3546.

[93] P.R. Arora, M.S.D. Jacob, M.S. Salit, E.M. Ahmed, M. Saleem , P. Edi, Experimental evaluation of fretting fatigue test apparatus, International Journal of Fatigue 29 (2007) 941–952.

[94] I.G. Goryacheva**,** P.T. Rajeev**,** T.N. Farris**,** Wear in partial slip contact**,** Journal of Tribology 123 (2001) 848–856.

[95] H. Lee, S. Mall, Some observations on frictional force during fretting fatigue, Tribology Letters17, (2004) 491-499.

[96] D. R. Swalla, R. W. Neu, Influence of coefficient of friction on fretting fatigue crack nucleation prediction, Tribology International 34 (2001) 493–503.

[97] J.A. Araújo, D. Nowell, Analysis of pad size effects in fretting fatigue using short crack arrest methodology, International Journal of Fatigue 21 (1999) 947-956.

[98] C. Navarro, S. Muñoz, J. Domínguez, On the use of multiaxial fatigue criteria for fretting fatigue life assessment, International Journal of Fatigue 30 (2008) 32–44.

[99] C.B.Elliot, D.W. Hoeppner, The importance of wear and corrosion on the fretting fatigue behavior of two aluminium alloys, Wear 236 (1999) 128-133.

[100] M. H. Attia, N. S D'Silva, Effect of Mode of Motion and Process Parameters on the Prediction of Temperature Rise in Fretting Wear, Wear 106 (1985) 203–211.

[101] B. Podgornink, M. Kalin, J. Vizintin, F. Vodopivec, Microstructural

changes and contact temperatures during fretting in steel-steel contact, ASME 123 (2001) 670-675.

[102] S. Onder, Fretting fatigue behavior of a titanium alloy Ti-6Al-4V at elevated temperature, Thesis.

[103] S. Fouvry, Ph. Kapsa, L. Vincent, K. Dang Van, Theoretical analysis of fatigue cracking under dry friction for fretting loading conditions, Wear 195 (1996) 21-34.

[104] S. Fouvry, Ph. Kapsa, L. Vincent, An elastic–plastic shakedown analysis of fretting wear, Wear 247 (2001) 41–54.

[105] J. Xu, Z.R. Zhou, C.H. Zhang, M.H. Zhua, J.B. Luo, An investigation of fretting wear behaviors of bonded solid lubricant coatings, Journal of Materials Processing Technology 182 (2007) 146–151.

[106] K. Elleuch, S. Fouvry, Ph. Kapsa, Fretting maps for anodised aluminium alloys, Thin Solid Films 426 (2003) 271–280.

[107] A. T. Kasarekar, F. Sadeghi, S. Tseregounis, Fretting fatigue of rough surfaces, Wear 264 (2008) 719–730.

[108] B. Martin, L. Vincent, C.S. Wright, A.M. Eagles, A.S. Wronski, Fretting wear and cracking in sintered metal matrix composites, Wear 248 (2001) 65–74.

[109] M.C. Dubourg, A. Chateauminois, B. Villechaise, In situ analysis and modeling of crack initiation and propagation within model fretting contacts using polymer materials Tribology International 36 (2003) 109–119.

[110] S.R. Shinde, C.B. Elliott, D.W. Hoeppner, Quantitative analysis of fretting fatigue degradation in 7075-T6 aluminum alloy, Tribology International 40 (2007) 542–547.

[111] C.H. Goh, D.L. McDowell, R.W. Neu, Plasticity in polycrystalline fretting fatigue contacts, Journal of the Mechanics and Physics of Solids 54 (2006) 340–367.

[112] S. Fouvry, Ph. Kapsa, L. Vincent, An elastic–plastic shakedown analysis of fretting wear, Wear 247 (2001) 41–54, A14 - K. Elleuch, S. Fouvry, Ph. Kapsa, Fretting maps for anodised aluminium alloys, Thin Solid Films 426 (2003) 271–280.

[113] Z.R. Zhou, K. Nakazawa, M.H. Zhu, N. Maruyama, Ph. Kapsa, L. Vincent, Progress in fretting maps, Tribology International 39 (2006)

1068–1073.

[114] S. Fouvry, V. Fridrici, C. Langlade, Ph. Kapsa, L. Vincent, Palliatives in fretting: A dynamical approach, Tribology International 39 (2006) 1005–1015.

[115] Y. Kondo, M. Bodai, The fretting fatigue limit based on local stress at the contact edge, Fatigue Fract Enfng Mater Struct 24 (2001) 791-801.

[116] D.R. Swalla, R.W. Neu, D.L. McDowell, Microstructural Characterisation of Ti-Al6-4V Subjected to Fretting, Journal of Tribology 126 (2004) 809-816.

[117] G.X. Chen, Z.R. Zhou Study on transition between fretting and reciprocating sliding wear, Wear 250 (2001) 665–672.

[118] J. Halling, Principles of Tribology, MacMillan Education Ltd, Hampshire-London, 1987.

[119] U. Sanchez-Santana, C. Rubio—Gonzalez, G. Gomez-Rosas. J.L. Ocana, C. Molpeceres, J. Porro, M. Morales, Wear and friction of 6061-T6 aluminium alloy treated by laser shock processing, Wear 260 (2006) 847-854.

[120] I. Yakimets, C. Richard, G. Béranger, P. Peyre, Laser peening processing effect on mechanical and tribological properties of rolling steel 100Cr6, Wear 256 (2004) 311–320.

[121] A. Mitchell, P. Shrotriya, Onset of nanoscale wear of metallic implant materials: Influence of surface residual stresses and contact loads, Wear 263 (2007) 1117–1123.

[122] K. Holmberg, A. Laukkanen, H. Ronkainen, K. Wallin, Tribological contact analysis of a rigid ball sliding on a hard coated surface. Part I: Modelling stresses and strains, Surface & Coatings Technology 200 (2006) 3793 – 3809.

[123] L. Xu, J. Xing, S. Wei, Y. Zhang, R. Long, Study on relative wear resistance and wear stability of high-speed steel with high vanadium content. Wear 262 (2007) 253–261.

[124] M. Buciumeanu**,** I. Crudu, L. Palaghian, A.S. Miranda, F.S. Silva, Influence of wear damage on the fretting fatigue life prediction of an Al7175 alloy, International Journal of Fatigue 31 (2009) 1278–1285.

[125] I.V. Kragelsky, M.N. Dobychin, V.S. Kombalov. Friction&wear.

Calculation methods, Pergamon Press, New York, 1982.

[126] I.M. Hutchings, "Tribology, Friction and Wear of Engineering Materials", Butterworth-Heinemann, 1992.

[127] S. Carlsson, P.L. Larsson, On the determination of residual stresses and the strain fields by sharp indetation testing. Part I: Theoretical and numerical analysis. Acta mater. 49 (2001) 2179-2191.

[128] M. Buciumeanu, A.S. Miranda, F.S. Silva, Evolution of relevant parameters on fretting fatigue tests, Key Engineering Materials 385-387 (2008) 565-568.

[129] N.E. Dowling, Mechanical Behavior of Materials (2nd Ed.), Prentice Hall, New Jersey, USA, 1999.

[130] T. Hattori, M. Nakamura, T. Watanabe, Simulation of fretting fatigue life by using stress- singularity parameters and fracture mechanics, Tribology International 36 (2003) 87-97.

[131] M.P. Szolwinsky, T.N. Farris, Mechanics of fretting fatigue crack formation, Wear 198 (1996) 93-107.

[132] J. Ding, W. S. Sum, R. Sabesan, S.B. Leen, I.R. McColl, E.J. Williams, Fretting fatigue predictions in a complex coupling, International Journal of Fatigue 29 (2007) 1229–1244.

[133] V. Fidrici, S. Fouvry, P. Kapsa, P. Perruchaut, Prediction of cracking in Ti-6Al-4V alloy under fretting-wear: use of the SWT criterion, Wear 259 (2005) 300-308.

[134] A.E. Giannakopoulos, T.C. Lindley, S. Suresh, C. Chenut, Similarities of stress concentrations in contact at round punches and fatigue at notches: implications to fretting fatigue crack initiation, Fatigue Fract Engng Mater Struct 23 (2000) 561–571.

[135] Y.W. Park, T.S. N. S. Narayanan, K.Y. Lee, Effect of fretting amplitude and frequency on the fretting corrosion behaviour of tin plated contacts, Surface & Coatings Technology 201 (2006) 2181–2192.

[136] T. Hattori, T. Watanabe, Fretting fatigue strength estimation considering the fretting wear process, Tribology International 39 (2006) 1100–1105.

[137] T. Hattori, M. Yamashita, N. Nishimura, Fretting fatigue strength and life estimation in ultra high cycle region considering the fretting wear

process, JSME International Journal 48 (2005) 246-250.

[138] ASM Metal Handbook Volume 18 – Friction, Lubrication and Wear technology.

[139] R.S. Magaziner, Examination of contact width of fretting fatigue, Thesis.

[140] H.O. Fuchs, R. I. Stephens, Metal fatigue in engineering, Wiley & Son, New York 1980.

[141] J. Dominguez, Cyclic variations in friction forces and contact stresses during fretting fatigue, Wear 218 (1998) 43-53.

[142] C. Vallellano, J. Domínguez, A. Navarro, Influence of R ratio and stick zone eccentricity on the prediction of the fretting fatigue limit with spherical contact, International Journal of Fatigue 29 (2007) 1208–1219.

[143] H. Lee, S. Mall, Investigation into tangential force and axial stress effects on fretting fatigue behavior, ASME 128 (2006) 202-209.

[144] S. Naboulsi, S. Mall, Fretting fatigue crack initiation behaviour using process volume approach and finite element analysis, Tribology International 36 (2003) 121-131.

[145] H. Lee, O. Jin, S. Mall, Fretting fatigue behavior of Ti–6Al–4V with dissimilar mating materials, International Journal of Fatigue 26 (2004) 393–402.

[146] S. Pommier, A study of the relationship between variable level fatigue crack growth and the cyclic constitutive behaviour of steel, International Journal of Fatigue 23 (2001) S111–S118.

[147] R.P. Skelton, H.J. Maier, H.J. Christ, The Bauschinger effect, Masing model and the Ramberg–Osgood relation for cyclic deformation in metals, Materials Science and Engineering A238 (1997) 377–390.

[148] V. Maurel, L. Rémy, F. Dahmen, N. Haddar, An engineering model for low cycle fatigue life based on a partition of energy and micro-crack growth, International Journal of Fatigue 31 (2009) 952–961.

[149] F. Yoshida, T. Uemori, A model of large-strain cyclic plasticity describing the Bauschinger effect and workhardening stagnation, International Journal of Plasticity 18 (2002) 661–686.

[150] A.H. Noroozi, G. Glinka, S. Lambert, A two parameter driving force for fatigue crack growth analysis, International Journal of Fatigue 27

(2005) 1277–1296.

[151] S. Pommier, Cyclic plasticity and variable amplitude fatigue, International Journal of Fatigue 25 (2003) 983–997.

[152] N. Chawla, B. Jester, D. T. Vonk, Bauschinger effect in porous sintered steels, Materials Science and Engineering A346 (2003) 266-272.

[153] M. Choteau, P. Quaegebeur, S. Degallaix, Modelling of Bauschinger effect by various constitutive relations derived from thermodynamical formulation, Mechanics of Materials 37 (2005) 1143–1152.

[154] M. Choteau, P. Quaegebeur, S. Degallaix, Prise en compte de l'effet Bauschinger dans l'acier X2CrNiMo17-12-2 par deux lois de comportement, C. R. Acad. Sci. Paris 328 (2000) 451–456.

[155] A.R. Setoodeh, H. Attariani, Nanoscale simulations of Bauschinger effects on a nickel nanowire, Materials Letters 62 (2008) 4266–4268.

[156] B.K. Chun, J.T. Jinna, J.K. Lee, Modeling the Bauschinger effect for sheet metals, part I: theory, International Journal of Plasticity 18 (2002) 571–595.

[157] S. Pommier, P. Bompard, Bauschinger effect of alloys and plasticity induced crack closure: a finite element analysis. Fatigue Fract. Eng. Mater. Struct. 23 (2000) 129-139.

[158] A. Plumtree, H.A. Abdel-Rauf, Cyclic stress–strain response and substructure, International Journal of Fatigue 23 (2001) 799–805.

[159] C. Guillemer-Neel, V. Bobet, M. Clavel, Cyclic deformation behaviour and Bauschinger effect in ductile cast iron, Materials Science and Engineering A272 (1999) 431–442.

[160] F. Yoshida, A constitutive model of cyclic plasticity, International Journal of Plasticity 16 (2000) 359±380.

[161] L.S. Tóth, A. Molinari, N. Zouhal, Cyclic plasticity phenomena as predicted by polycrysal plasticity, Mechanics of Materials 32 (2000) 99-113.

[162] J.B. Jordon, M .F. Horstemeyer, K. Solanki, Y. Xue, Damage and stress state influence on Bauschinger effect in aluminum alloys, Mechanics of Materials 39 (2007) 920-931.

[163] F.S. Silva, Estudo da influnênsa da torção está tistica sobre os mecanismos de cresimento de fendas de fadiga a diferentes

temperaturas, Phd thesis.

[164] F.S. Silva, Fatigue crack propagation after overloading and underloading at negative stress ratios, International Journal of Fatigue 29 (2007) 1757–1771.

[165] F.S. Silva, Crack closure inadequacy at negative stress ratios, International Journal of Fatigue 26 (2004) 241–252.

[166] F.S. Silva, The importance of compressive stresses on fatigue crack propagation rate, International Journal of Fatigue 27 (2005) 1441–1452.

[167] M. Buciumeanu**,** A.S. Miranda, F.S. Silva, Some Considerations on the Development of an Apparatus for Fretting Fatigue Testing", 10th Portuguese Conference on Fracture, 22-24 February, Guimaraes, Portugal, 2006.

[168] M. Buciumeanu, A. S. Miranda, Silva, F.S.,: "Development of a Fretting Fatigue Apparatus", Anales de Mecánica de la Fractura I (2006) 323-328.

[169] M. Buciumeanu**,** I. Crudu, L. Palaghian, A.S. Miranda, F.S. Silva, Influence of an additional elastic stress on dry wear behaviour in reciprocating tests, Tribology International 42 (2009) 1101-1107.

[170] M. Buciumeanu, A.S. Miranda, F.S. Silva, Influence of Wear Properties on Fretting Fatigue Life of a CK45 Alloy and the Al7175 Alloy, Materials Science Forum 587-588 (2008) 971-975.

[171] M. Buciumeanu**,** A.S. Miranda, F.S. Silva, Damage evolution of Al7175 and Ck45 alloys under fretting fatigue, The Annals of University "Dunarea de Jos" of Galati, Fascicole VIII, 2007 (XIII), ISSN 1221-4590, Tribology.

[172] M. Buciumeanu**,** A. S. Miranda, F. S. Silva, Wear behaviour of the Al7175 alloy under different bulk stress states, The Annals of University "Dunarea de Jos" of Galati, Fascicole VIII, 2008 (XIV), ISSN 1221-4590, Tribology.

[173] J.M. Ambrico, M.R. Ambrico, Plasticity in fretting contact, Journal of the Mechanics and Physics of Solids 48 (2000) 2391-2417.

[174] C.D. Lykins, S. Mall, V. Jain, An evaluation of parameters for predicting fretting fatigue crack initiation, International Journal of Fatigue 22 (2000) 703-716.

[175] J.A. Williams, Engineering tribology, Oxford University Press**,** 1994.

[176] Yakimets I, Richard C, Béranger G, Peyre P, Laser peening processing effect on mechanical and tribological properties of rolling steel 100Cr6. Wear 256 (2004) 311–320.

[177] H. Lee, S. Mall, S. Sathish, Investigation into effects of re-shot-peening on fretting fatigue behavior of Ti–6Al–4V, Materials Science and Engineering A 390 (2005) 227–232.

[178] T.C. Lindley, Fretting fatigue in engineering alloys, International Journal of Fatigue 19 (1997) 39–49.

[179] J.H. Han, J.Y. Suh, K. K. Jee, J.C. Lee, Evaluation of formability and planar anisotropy based on textures in aluminum alloys processed by a shear deforming process. Materials Science and Engineering A 477 (2008) 107–120.

[180] M. Belmonte, P. Miranzo, M. I. Osendi, J. R. Gomes, Wear of aligned silicon nitride under dry sliding conditions. Wear 266 (2009) 6–12.

[181] K.H.Z. Gahr, M. Mathieu, B. Brylka, Friction control by surface engineering of ceramic sliding pairs in water. Wear 263 (2007) 920–929.

[182] Z.H. Xie, M. Hoffman, R.J. Moon, P.R. Munroe, Y.B. Cheng, Sliding wear behaviour of Ca α-sialon ceramics at 600 ˚C in air, Wear 260 (2006) 1356–1360.

[183] Z.H. Xie, M. Hoffman, R.J. Moon, P.R. Munroe, Y.B. Cheng, Sliding wear of calcium α -sialon ceramics. Wear 260 (2006) 387–400.

[184] A.D. Sarkar**,** Wear of metals, Pergman Press, England, 1976.

[185] Salerno G, Magnabosco R, C. de Moura Neto, Mean strain influence in low cycle fatigue behaviour of AA7175-T1 aluminum alloy, International Journal of Fatigue 29 (2007) 829-835.

[186] T.L. Teng, P.H. Chang, Effect of residual stresses on fatigue crack initiation life for butt- welded joints, Journal of Materials Processing Technology 145 (2004) 325-335.

[187] A.M.J. Pinho da Cruz, J.D.M. Costa, L.F.P. Borrego, J.A.M. Ferreira, Fatigue life prediction in AlMgSi1 lap joints weldments, Int Jnl of Fatigue 22 (2000) 601-610.

[188] T. Kang, Y.L. Lee, A thermo-mechanical fatigue damage model for variable temperature and loading amplitude conditions, International

Journal of Fatigue 29 (2007) 1797-180.

[189] P.J. Hurley, M.T. Whittaker, S.J. Williams, W.J. Evans, Prediction of fatigue initiation lives in notched Ti 6246 specimens, International Journal of Fatigue 30 (2008) 623–634.

[190] V. Farahani, T. Kodric, A. Ghahramani, A method of fatigue life prediction in notched and un-notched components, Journal of Materials Processing Technology 169 (2005) 94–102.

[191] Y.L. Lee, J. Pan, R. Hathaway, M. Barkey, Fatigue testing and analysis: Theory and practice, Elsevier Butterworth-Heinemann, Burlington, Massachusetts, 2005.

[192] H. Lee, S. Sathish, S. Mall, Evolution of residual stress under fretting fatigue, Journal of materials science 39 (2004) 7089 – 7092.

[193] D.J. Smith, G.H. Farrahi, W.X. Zhu, C.A. McMahon, Experimental measurement and finite element simulation of the interaction between residual stresses and mechanical loading, International Journal of Fatigue 23 (2001) 293–302.

[194] A. King, A. Steuwer, C. Woodward, P.J. Withers, Effects of fatigue and fretting on residual stresses introduced by laser shock peening, Materials Science and Engineering A 435–436 (2006) 12–18.

[195] W.S. Sum, E.J. Williams, S.B. Leen, Finite element, critical-plane, fatigue life prediction of simple and complex contact configurations, International Journal of Fatigue 27 (2005) 403-416.

[196] S.K. Ås, B. Skallerud, B.W. Tveiten Surface roughness characterization for fatigue life predictions using finite element analysis, International Journal of Fatigue 30 (2008) 2200-2209,

[197] S. Curtis, E. R. de los Rios, C. A. Rodopoulos, A. Levers, Analysis of the effects of controlled shot peening on fatigue damage of high strength aluminium alloys, International Journal of Fatigue 25 (2003) 59–66.

[198] R.P. Skelton, Hysteresis, yield, and energy dissipation during thermo-mechanical fatigue of a ferritic steel, International Journal of Fatigue 26 (2004) 253–264.

Annex A
Sensitivity analysis

In annex A are provided the results of a sensitivity analysis in order to verify the sensitivity of models and of the materials used in this work at the elastic or the plastic domain.

A.1 Initial remarks

Fatigue properties are an integral part of materials comparison activities and offer information for structural life estimation in many engineering applications. The models chosen to estimate the fretting fatigue life are two strain fatigue models: SWT and Morrow models. These models were chosen because they are the models that include more intrinsic material properties being then more appropriate to understand either the influence of the material properties as well as to establish a comparison among different materials. It was observed from the predictions that a model is more adequate for a material and is not giving good prediction for another material. For example, the SWT model is working very well for Al7175 alloy (see figure 5.6a), while for Ti4Al6V alloy (see figure 5.6c) the predicted life is overestimated compared with the experimental life.

As these models (SWT and Morrow models) are quite complex due to the many parameters involved, it may be interesting to understand the responsiveness of the models to eventual modifications on both the elastic and plastic terms. Thus, a sensitivity analysis was carried out. Sensitivity analysis helps to build confidence into model by studying the uncertainties that are often associated with parameters in models.

Figure A-1 shows the “black box” of the sensitivity analysis. The input parameters of this system are the loading conditions and the geometry of the contacting bodies (in this particular case: specimen and pad). The output is the predicted fretting fatigue life. The commanding variables are the fatigue properties of the materials: fatigue strength coefficient, fatigue strength exponent, fatigue ductility coefficient, fatigue ductility exponent.

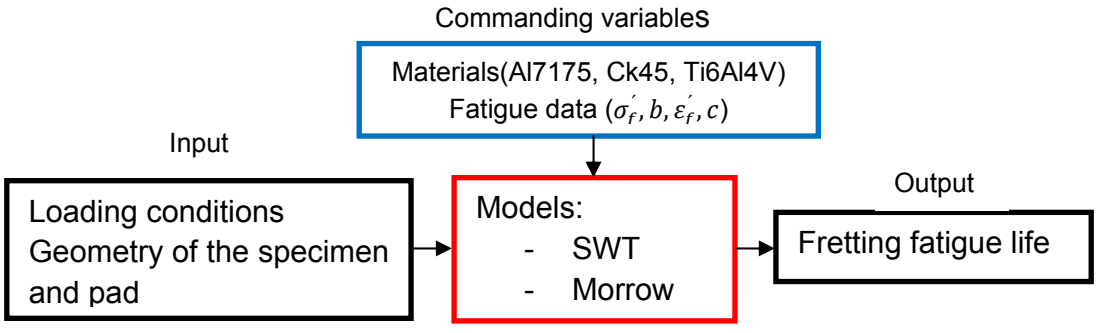

Figure A-1 The “black box” of the sensitivity analysis

A.2 Sensitivity analysis procedure

First the fatigue cyclic properties of the materials were determined (see 3.3 Materials) and life was predicted using both models (recall 5.2 Application of SWT parameter to the fretting fatigue situation and 5.3 Application of Morrow parameter to the fretting fatigue situation). The relations used for this sensitivity analysis are: i) in the case of the SWT mode, equation 2.15 (2.3.3 Smith-Watson-Topper model), and ii) in the case of the Morrow model, equation 5.5 (5.1.2.2 Morrow´s parameter to be applied to a fretting fatigue situation). The predicted life obtained with the previously mentioned relations will be considered in this analysis as the initial fretting fatigue life (the optimum solution, like a reference). Afterwards for each material (Al7175, Ck45 and Ti6Al4V) and model (SWT and Morrow), an input parameter will be changed independently (increased by 10%), while keeping the other parameters unchanged. It will be determined the predictions for each case and the results discussed in order to see the influence of each parameter in fretting fatigue life.

As can be seen from equations 2.15 (SWT model) and 5.5 (Morrow's model) they both use the same parameters only there are incorporated differently. As a result, it should be expected that the models will give a different response.

Both models from the mathematical point of view are represented by a power law function. The fatigue strength and ductility coefficients are the intercepts of the elastic line and plastic line, respectively, with the coordinate system (figure 2.15 – 2.3.2 The basic strain – life equation). The fatigue strength and ductility exponents are the slopes of the elastic and plastic lines, respectively (figure 2.15).

A.3 Sensitivity of materials

As it is already known usually the fatigue life behaviour is displayed in plot of log strain versus log cycles to failure (figure 2.15 – 2.3.2 The basic strain – life equation).

For all three materials used in this research these graphs have been built in order to determine the fatigue cyclic properties of the materials. In order to better understand the response between the materials (the sensitivity of the materials to the elastic and plastic domain), the fatigue life diagrams has been drawn when a fatigue cyclic parameter was increased by 10%.

Figure A-2 shows the fatigue life behaviour in the Al7175 alloy case. Figure A-3 shows the fatigue life behaviour in the Ck45 steel case. The fatigue life behaviour in the Ti6Al4V alloy case is presented in figure A-4. Tables A-1, A-2 and A-3 present a summary of the sensitivity analysis results.

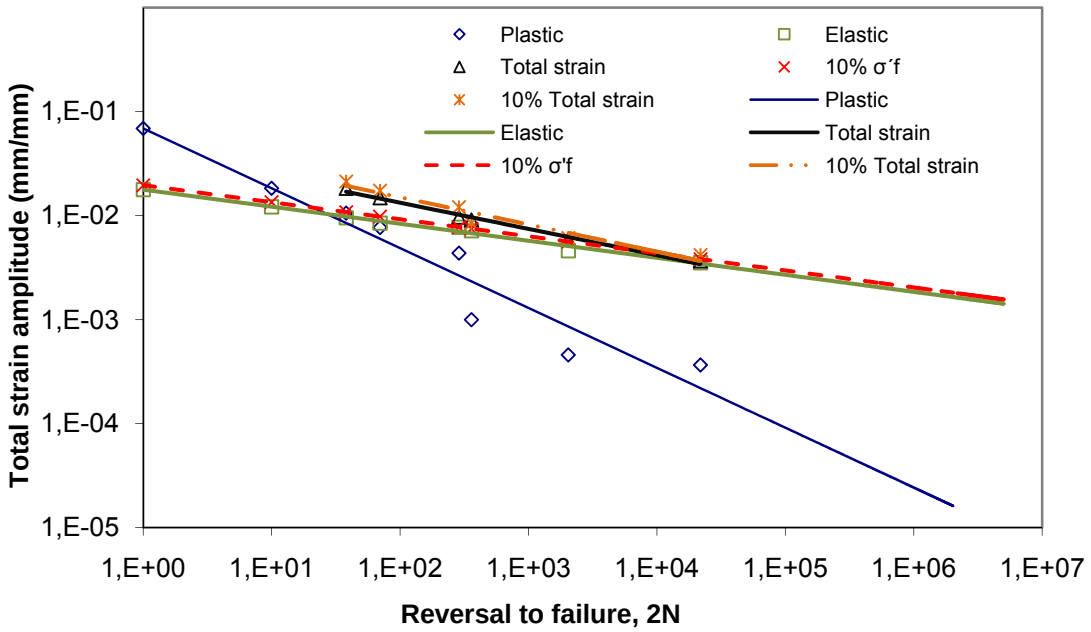

a. 10% increase of the fatigue strength coefficient

Figure A-2 Total strain life curves for Al7175 alloy (cont.)

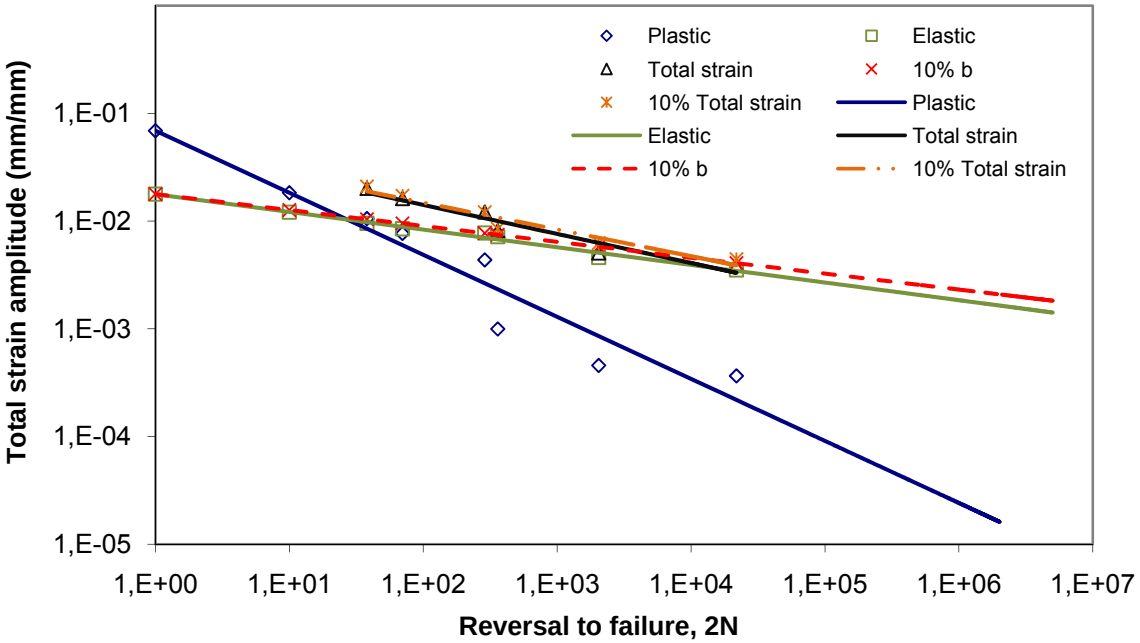

b. 10% increase of the fatigue strength exponent

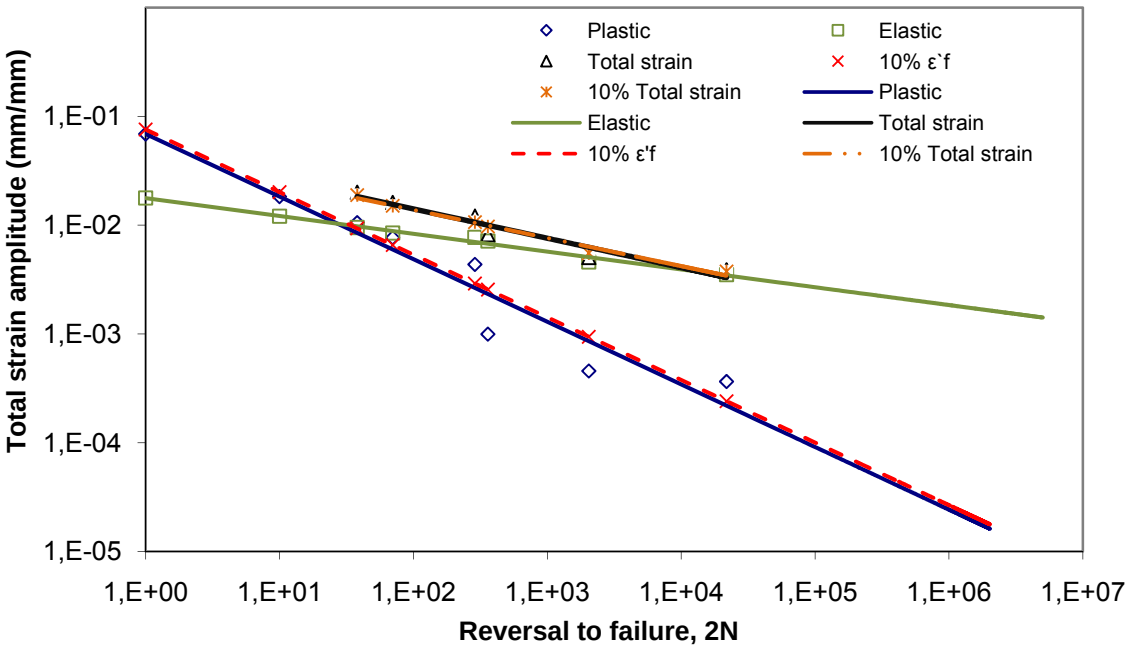

c. 10% increase of the fatigue ductility coefficient

Figure A-2 Total strain life curves for Al7175 alloy (cont.)

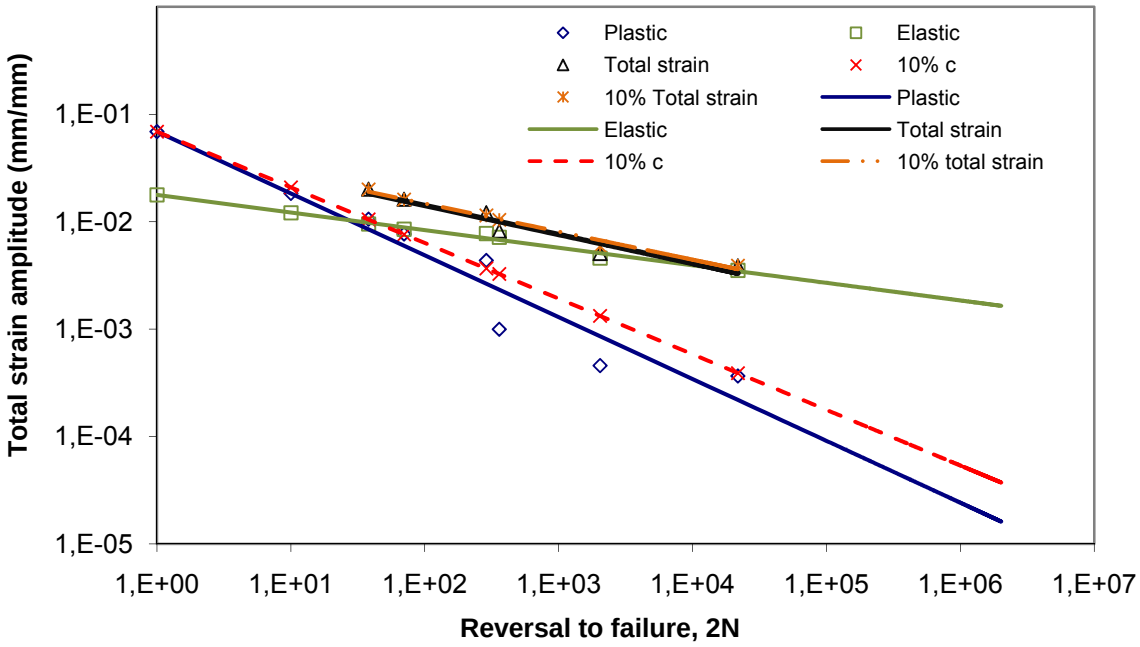

d. 10% increase on the fatigue ductility exponent

Figure A-2 Total strain life curves for Al7175 alloy

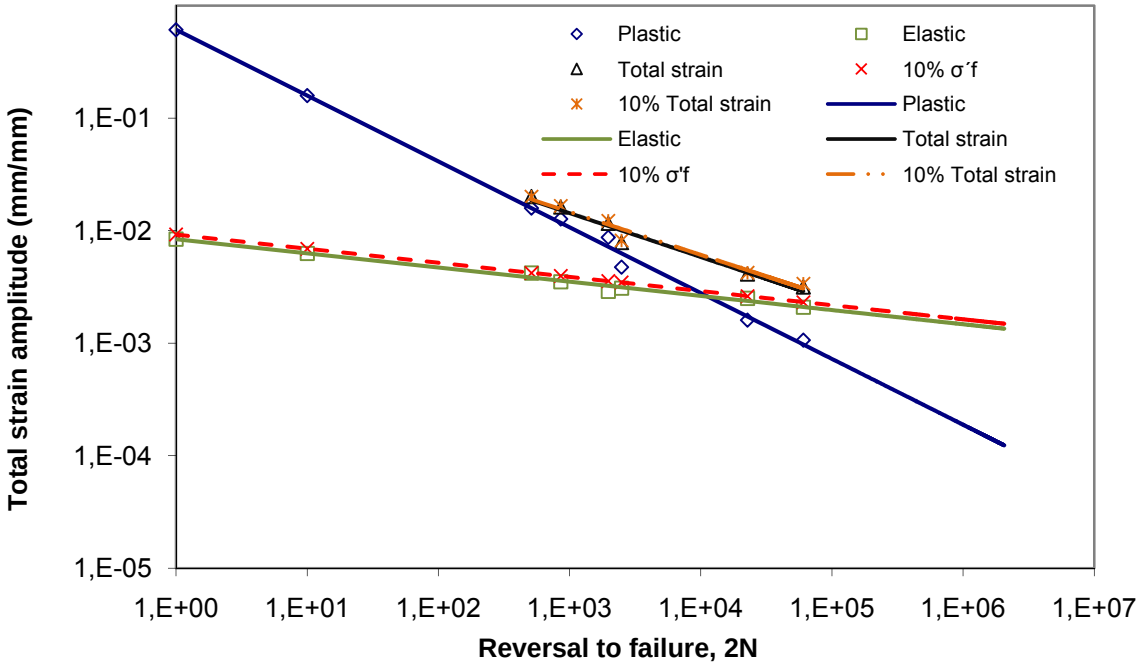

a. 10% increase of the fatigue strength coefficient

Figure A-3 Total strain - life curves for Ck45 steel (cont.)

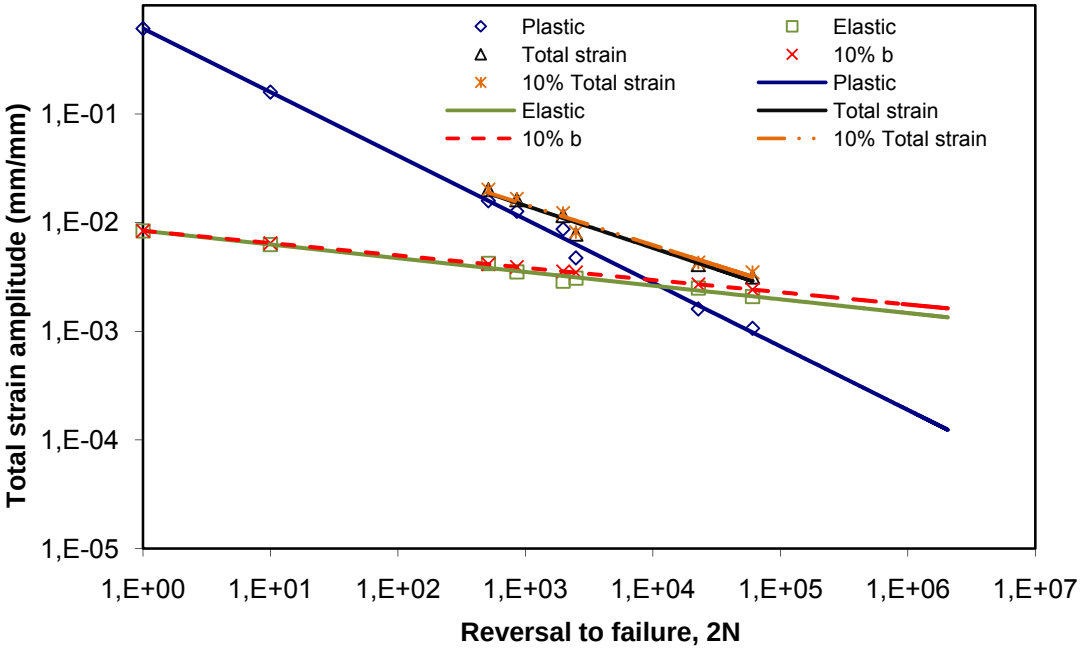

b. 10% increase of the fatigue strength exponent

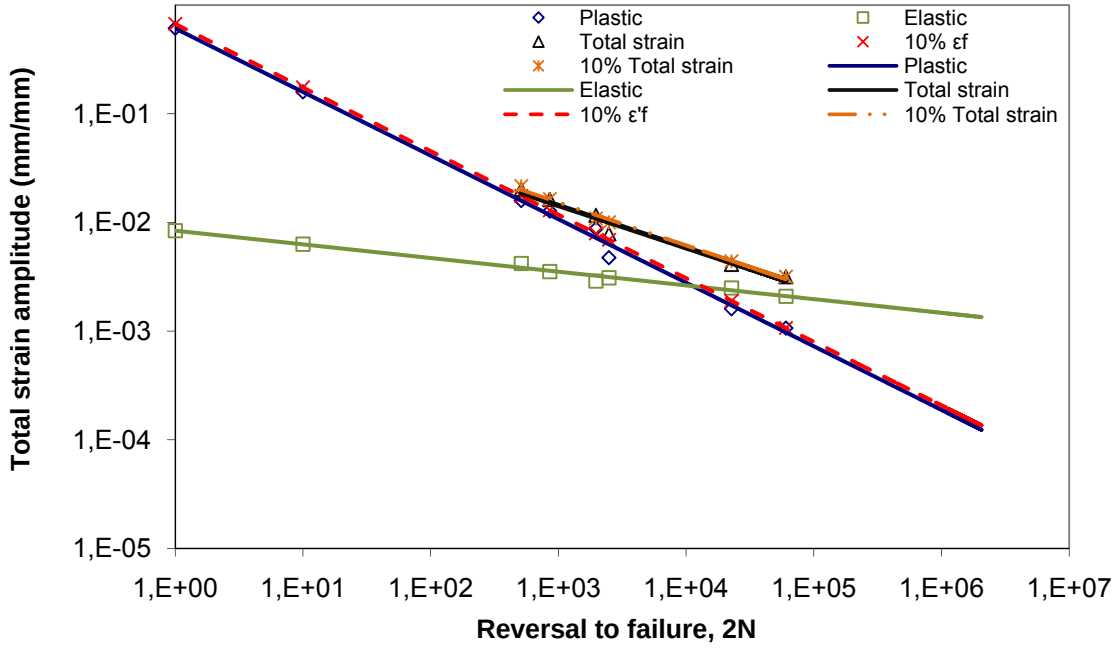

c. 10% increase of the fatigue ductility coefficient

Figure A-3 Total strain - life curves for Ck45 steel (cont.)

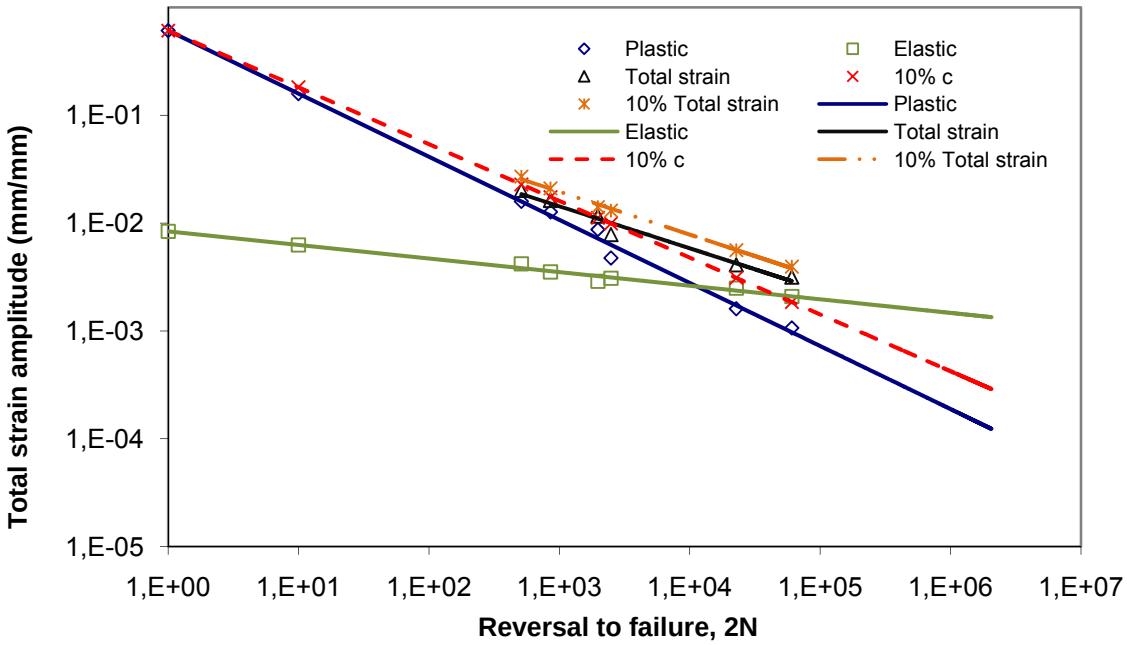

d. 10% increase on the fatigue ductility exponent

Figure A-3 Total strain - life curves for Ck45 steel

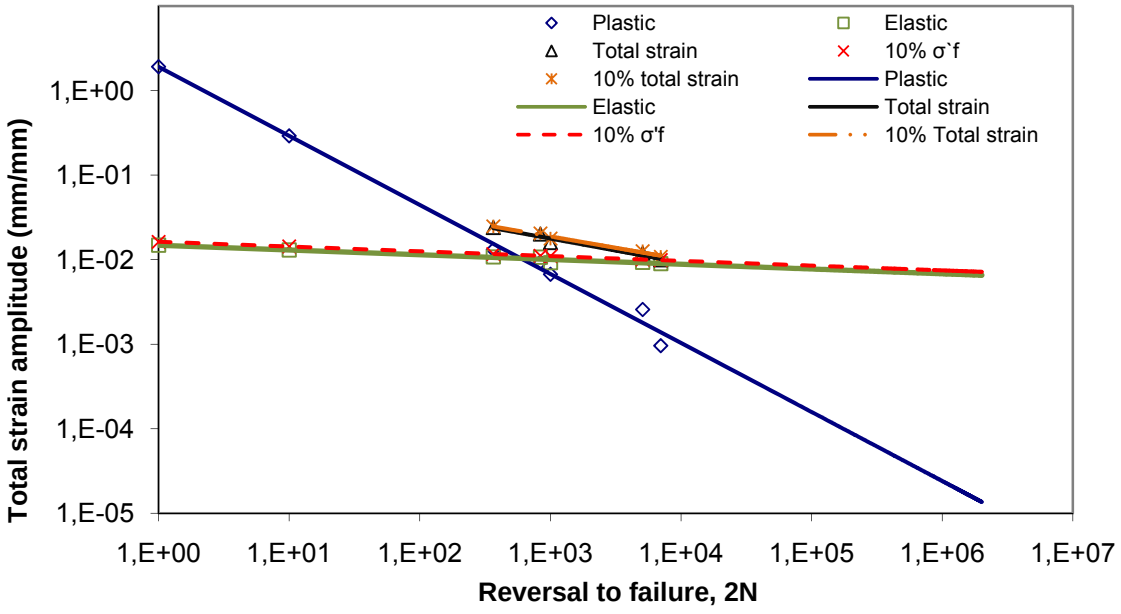

a. 10% increase of the fatigue strength coefficient

Figure A-4 Total strain - life curves for Ti6Al4V alloy (cont.)

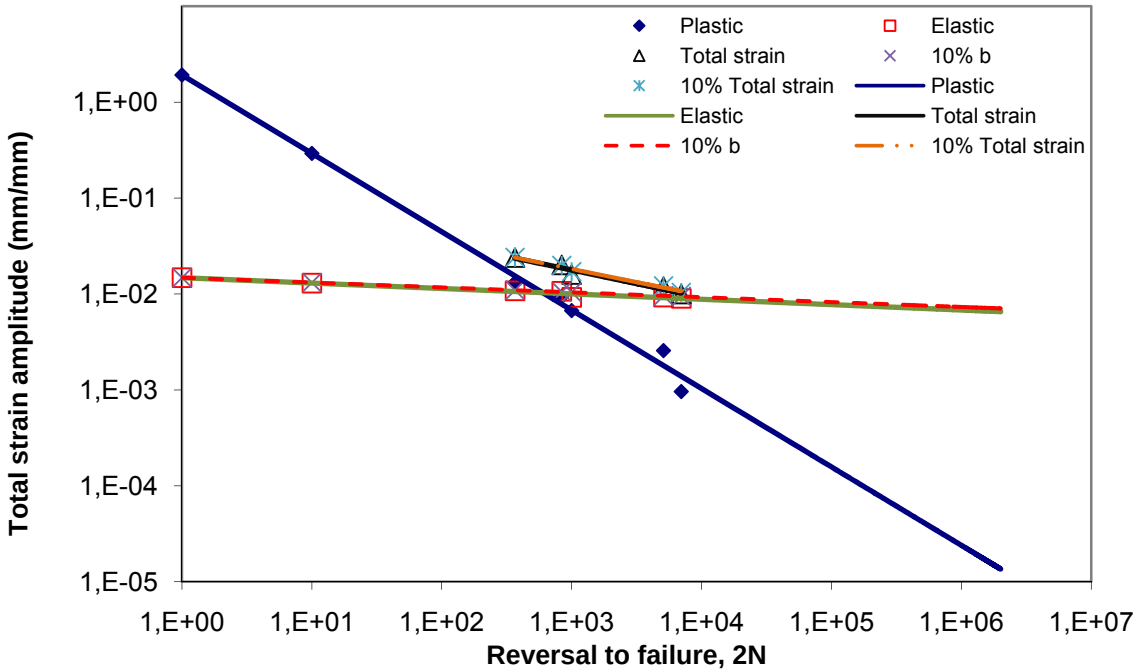

b. 10% increase of the fatigue strength exponent

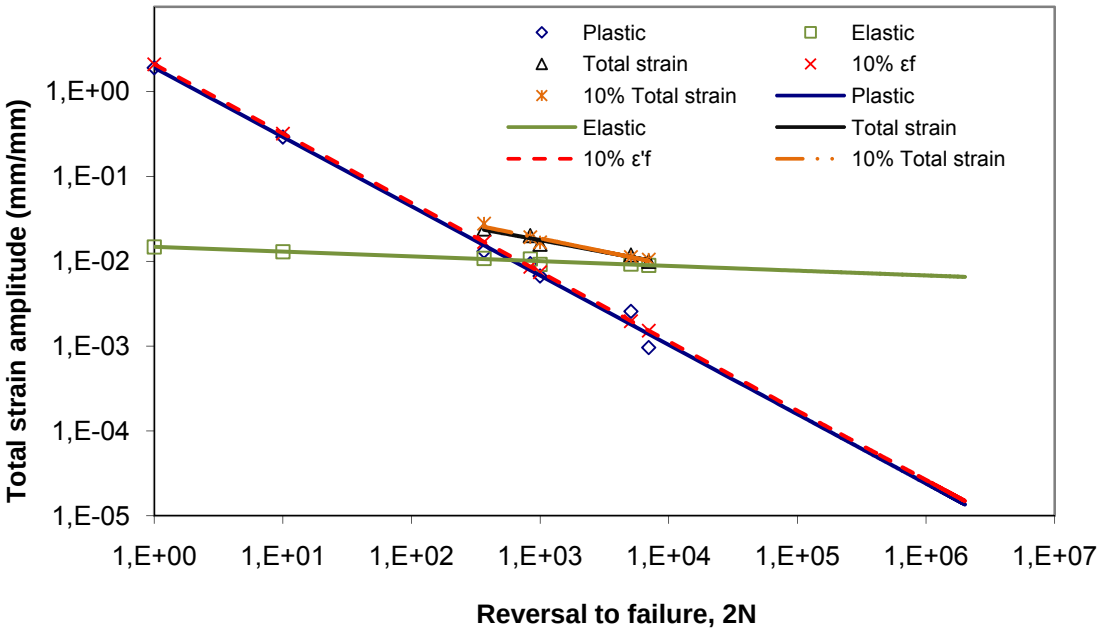

c. 10% increase of the fatigue ductility coefficient

Figure A-4 Total strain - life curves for Ti6Al4V alloy (cont.)

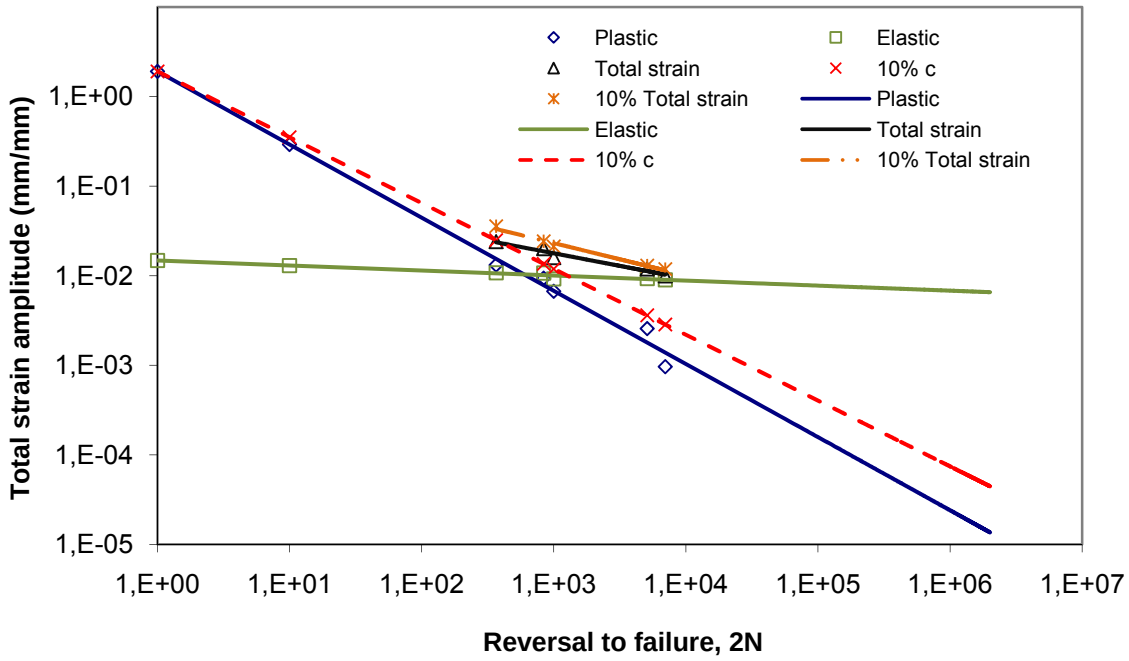

d. 10% increase on the fatigue ductility exponent

Figure A-4 Total strain - life curves for Ti6Al4V alloy

For all three materials it was observed an increase of fatigue life when the fatigue strength coefficient was increased by 10%. It can be seen that also the transition fatigue point (this point corresponds to the fatigue life when the magnitude of the plastic strain amplitude is equal with the elastic strain amplitude) was modified when the fatigue strength coefficient was increased by 10%. It results in an increase of the elastic plastic region.

Also, when the fatigue strength exponent was increased with 10% an increase of life was obtained. As the fatigue strength exponent is the slop of the elastic line, it is clear that an increase by 10% will be valid only for a domain of fatigue life.

Regarding the fatigue properties that represent the plastic behaviour (fatigue ductility coefficient and fatigue ductility exponent) a very small change in life was obtained, mainly for Ck45 steel.

The plastic domain in the case of Al7715 and Ti6Al4V alloys is important only till around $3 \cdot 10^6$ cycles while in the case of Ck 45 steel the plastic domain will be important for longer lives, till around 10^8cycles. For the lives obtained in this study around 10^5 cycles the elastic domain is predominant for Al7175 and Ti6Al4V. It can be observed that in the case of Ck45 steel for the lives studied also the plastic component is important.

A.4 Sensitivity of models

For easy comparison of the models the tests chosen have an experimental life around 100,000 cycles.

Fatigue strength coefficient, $\sigma_f^{'}$

Figure A-5 shows the analytical fretting fatigue life prediction based on SWT parameter (equation 2.15) and on Morrow parameter (equation 5.5). Also in this graph are presented the analytical life prediction when based on SWT and Morrow models when the fatigue strength coefficient was increased by 10%.

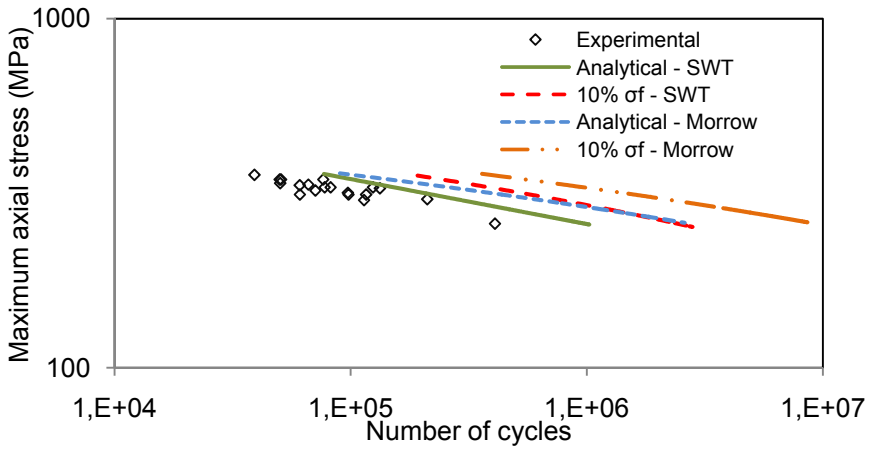

a. Al7175

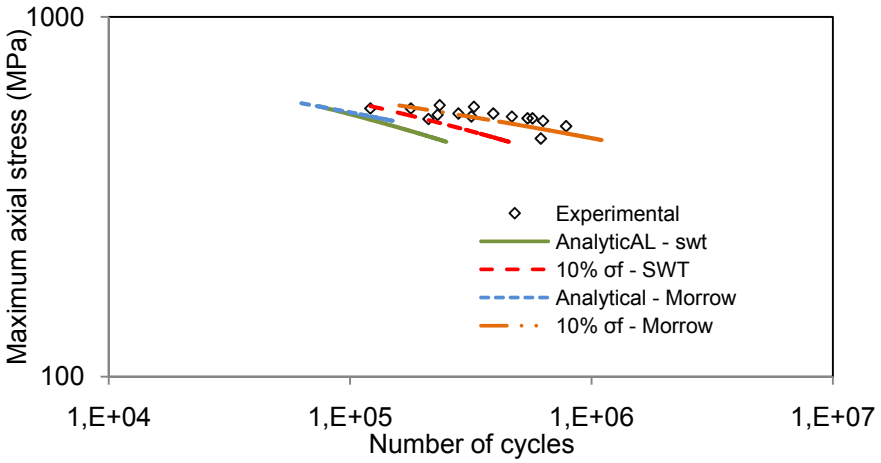

b. Ck45

Figure A-5 Fretting fatigue life behaviour with an increase of the fatigue strength coefficient (cont.)

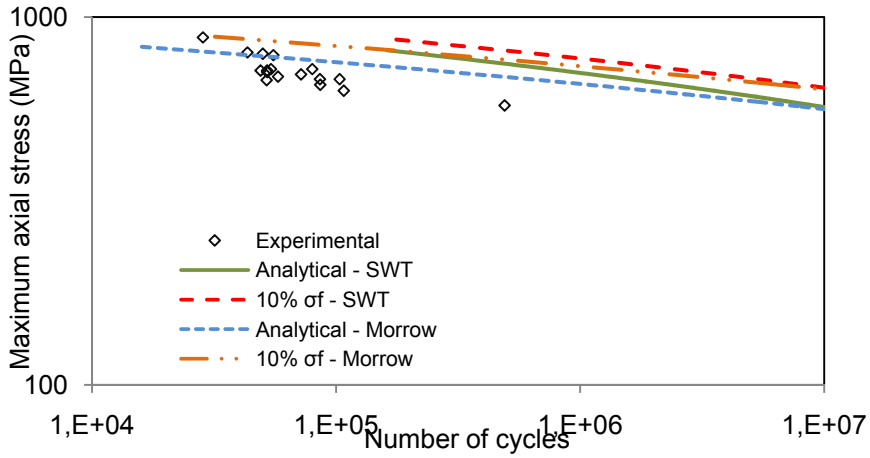

c. Ti6Al4V

Figure A-5 Fretting fatigue life behaviour with an increase of the fatigue strength coefficient

Fatigue strength exponent, b

Figure A-6 shows the analytical fretting fatigue life prediction based on SWT parameter (equation 2.15) and on Morrow parameter (equation 5.5). Also in this graph are presented the analytical life prediction when based on SWT and Morrow models when the fatigue strength exponent was increased by 10%.

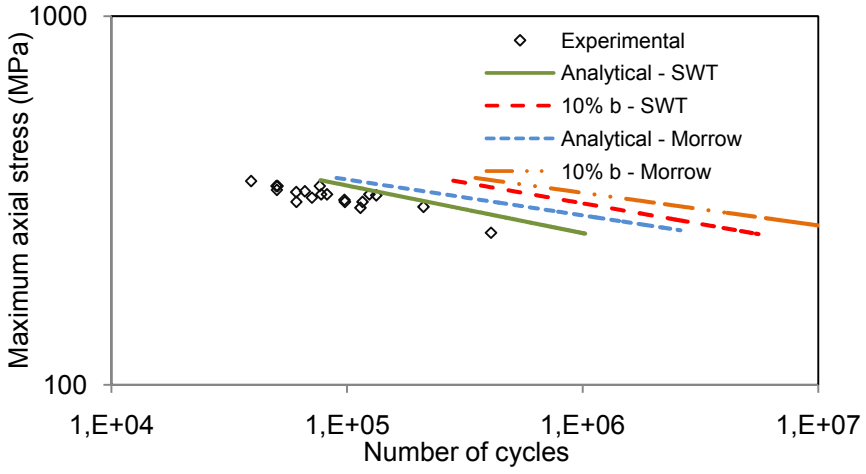

a. Al7175

Figure A-6 Fretting fatigue life behaviour with an increase of the fatigue strength exponent (cont.)

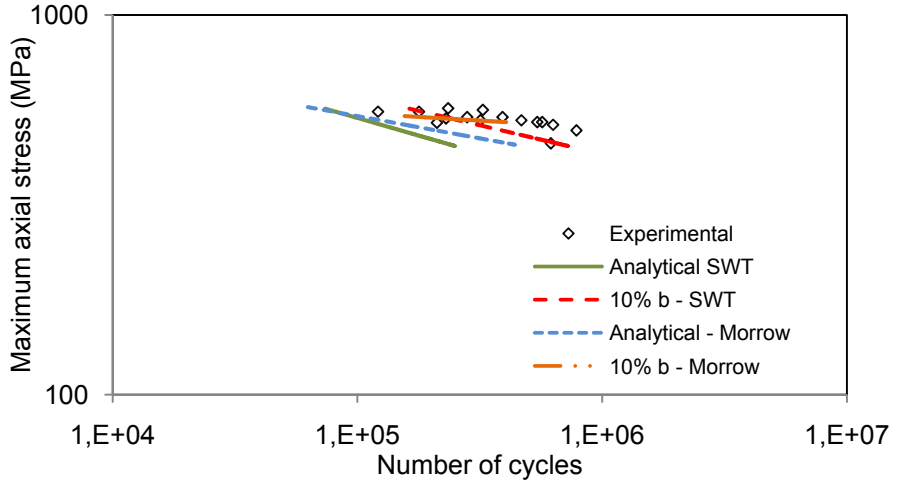

b. Ck45

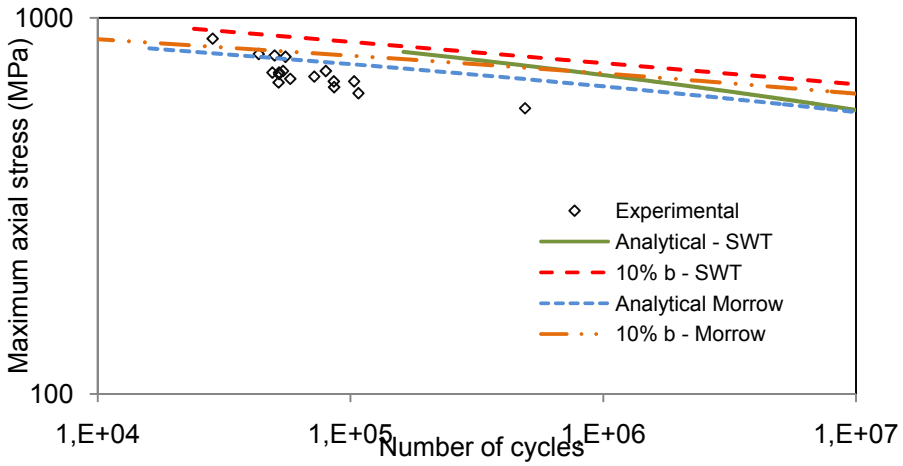

c. Ti6Al4V

Figure A-6 Fretting fatigue life behaviour with an increase of the fatigue strength exponent

Fatigue ductility coefficient, $\varepsilon_f^{'}$

Figure A-7 shows (for Al7175 alloy, Ck45 steel and Ti6Al4V alloy) the analytical fretting fatigue life prediction based on SWT parameter (equation 2.15) and on Morrow parameter (equation 5.5). Also in this graph are presented the analytical life prediction when based on SWT and Morrow models when the fatigue ductility coefficient was increased by 10%.

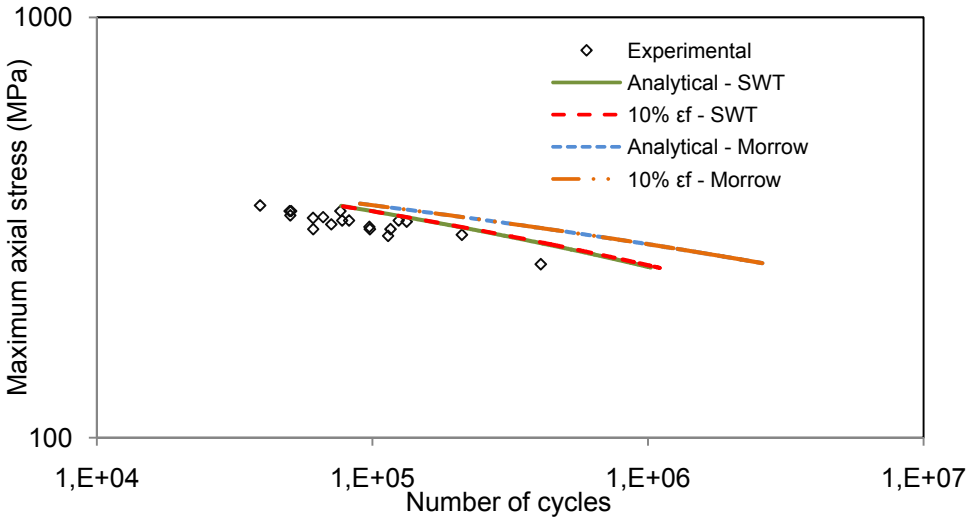

a. Al7175

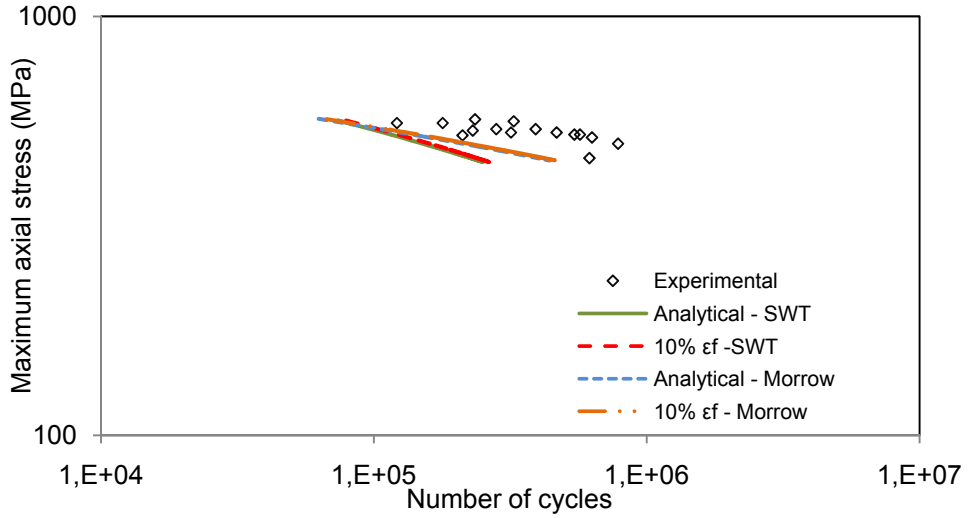

b. Ck45

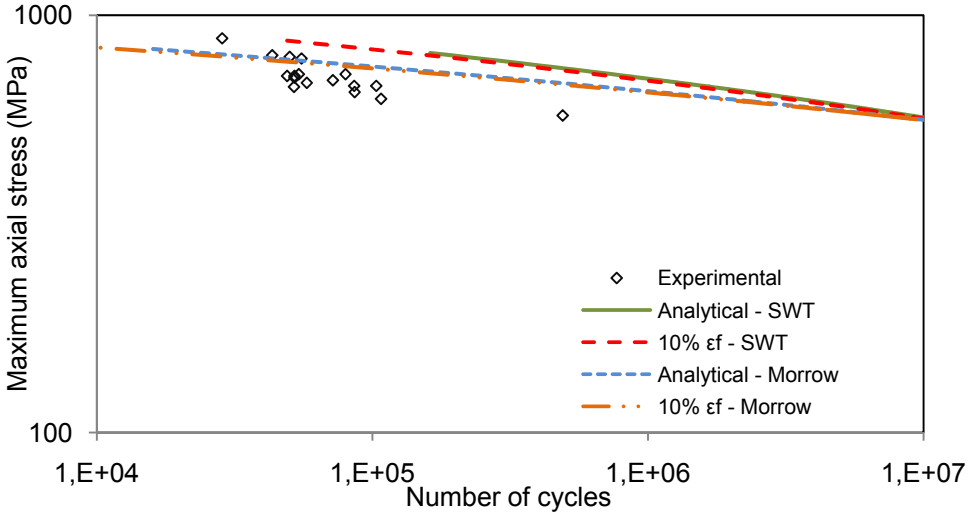

c. Ti6Al4V

Figure A-7 Fretting fatigue life behaviour with an increase of the fatigue ductility coefficient

Fatigue ductility exponent, c

Figure A-8 shows the analytical fretting fatigue life prediction based on SWT parameter (equation 2.15) and on Morrow parameter (equation 5.5). Also in this graph are presented the analytical life prediction when based on SWT and Morrow models when the fatigue ductility exponent was increased by10%.

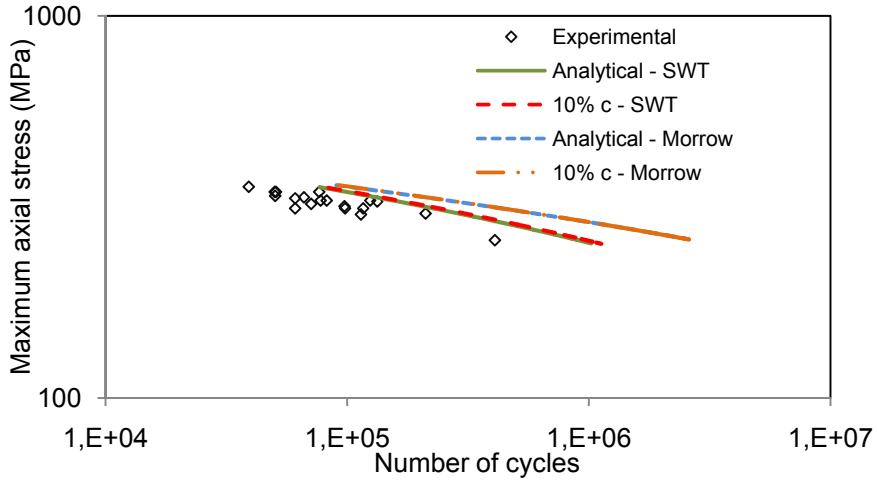

a. Al7175

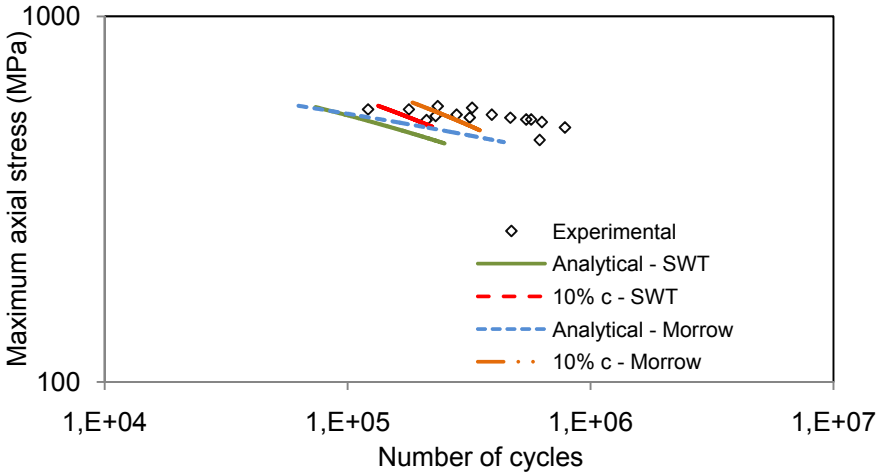

b. Ck45

Figure A-8 Fretting fatigue life behaviour with an increase of the fatigue ductility exponent (cont.)

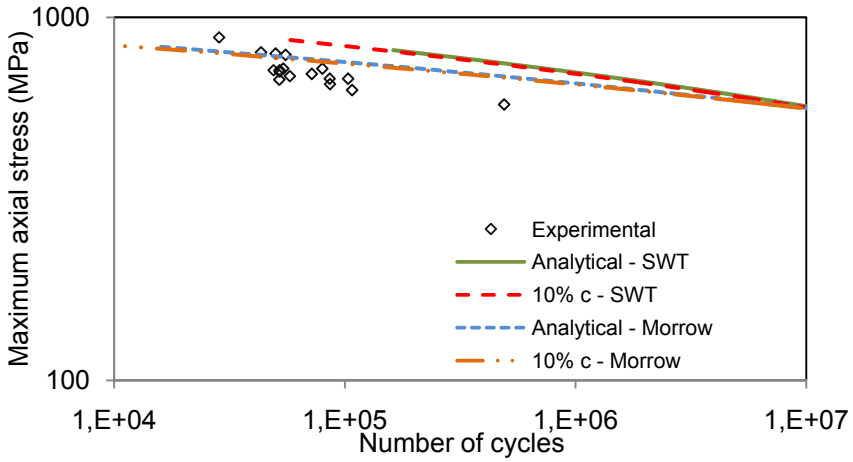

c. Ti6Al4V

Figure A-8 Fretting fatigue life behaviour with an increase of the fatigue ductility exponent

Table A-1 Summary of the sensitivity analysis result for Al7175 alloy

Fatigue cyclic properties / Models	Experimental life	Predicted life	Elastic component		Plastic component	
			10%σ_r	10%b	10%ε_r	10%c
SWT	133086	140,000	144% 342,100	280% 532,000	-	-
Morrow		200,000	260% 720,000	315% 831,019	-	-

Table A-2 Summary of the sensitivity analysis result for Ck45 steel

Fatigue cyclic properties / Models	Experimental life	Predicted life	Elastic component		Plastic component	
			10%σ_r	10%b	10%ε_r	10%c
SWT	121,436	91,000	68% 153,000	131% 211,000	7% 97,400	78% 162,500
Morrow		98,829	157% 254,029	169% 266,129	5% 104,029	148% 245,129

Table A-3 Summary of the sensitivity analysis result for Ti6Al4V

Fatigue cyclic properties / Models	Experimental life	Predicted life	Elastic component		Plastic component	
			10%σ_r	10%b	10%ε_r	10%c
SWT	103,336	997,100	288% 3,870,650	397% 4,960,000	-	-
Morrow		360,000	577% 2,400,000	344% 1,600,000	-	-

The first aspect to highlight is that in Al71575 alloy case a better prediction was obtained with the SWT (figure 5.14a) that with Morrow´s parameter (figure 5.15a).

For easy comparison, for each material will be chosen a test with a experimental life around 10^5 cycles

Fatigue strength coefficient, $\sigma_f^{'}$

In the case of Al7175 alloy, for an experimental life of 133086 cycles, the predicted life using SWT parameter was 140,000 cycles, while using Morrow´s parameter the predicted life was 200,000 cycles (see Table A-1 and Figure A-5a). The discussion is valid for a stress level around 300 MPa in the case of Al 7175 alloy. It can be seen that for SWT model (Al7175 alloy) the predicted life increased by 144% (342,100 cycles) with increasing the fatigue strength coefficient by 10%. Also, in the case of Morrow model the predicted life increased by 260% (720,000 cycles) with increasing the fatigue strength coefficient. It can be concluded that in this range of fretting fatigue life Morrow parameter is much more sensitive to a change in fatigue strength coefficient than SWT parameter.

In the case of Ck 45 steel both models predicted a similar result. For an experimental life of 121,436 cycles, the predicted life when SWT parameter was used it was 91,000 cycles and in the case of Morrow´s parameter was 98,829 cycles (Table A-2 and Figure A-5b). The discussion is valid for a stress level around 500 MPa. In the case of SWT model (Ck45 steel) the predicted life increased by 68% (153,000 cycles) with increasing the fatigue strength coefficient by 10%. By using the Morrow's parameter the predicted life increased by with 157% (254,029 cycles) with increasing the fatigue strength coefficient. Also in the case of Ck45 steel the increase on life is higher in the case of Morrow's model comparing with SWT model.

In the case of Ti6Al4V alloy it was chosen a test with an experimental life of 103,336 cycles (Table A-3 and Figure A-5c). The analytical prediction that was considered here like a reference is very far from the experimental results. The predicted life obtained with SWT was 997,100 cycles, while with Morrow´s parameter was 360,000 cycles. When the fatigue strength coefficient was increased by 10% the life predicted with SWT was higher than the initial life with 288% (3,870,650 cycles). The life predicted with Morrow´s parameter when the fatigue strength coefficient was increased by 10% was 2,400,000 cycles (577% higher than the initial analytical predicted life). The discussion in the case of Ti6Al4V alloy is valid only for the level of stress around 680 MPa.

Fatigue strength exponent, b

From figure A-6a and Table A-1 (Al7175 alloy) can be seen that the predicted life with SWT model increased by 280% (532,000 cycles - red line) and with Morrow's model was increased by 315% (831,019 cycles – orange line)

From figure A-6b and Table A-2 (Ck45 steel) can be observed that the predicted life with SWT model increased by 131% (211,000 cycles – red line) and with Morrow's model it increased by 169% (266,129 cycles – orange line) by increasing the fatigue strength exponent was increased by 10%.

Figure A-6c and Table A-3 show the change on predicted fretting fatigue life of Ti6Al4V alloy when the fatigue strength exponent was increased by 10%. It can be seen that the predicted life increased by 397% (4,960,000 cycles – red line) in SWT model case and with 344% (1,600,000 cycles – orange line) for Morrow model case.

Fatigue ductility coefficient, $\varepsilon_f^{'}$

Figure A-7 shows the changes on the initial fretting fatigue life prediction when the fatigue ductility coefficient was increased by 10% (SWT model – red line and Morrow´s model – orange line).

No change on predicted life (with both models) was observed in the case of Al7175 and Ti6Al4V (Figure A-7a and c) by increasing the fatigue ductility coefficient. A slight increase in life was obtained in case of Ck45 steel (Figure A-7b). For SWT parameter the predicted life increased by 7% (97,400 cycles – red line) and for Morrow´s parameter by 5% (104,029 cycles – orange line).

Fatigue ductility exponent, c

Figure A-8 shows the changes on the predicted fretting fatigue life (SWT model – green line and Morrow´s model – blue line) when the fatigue ductility exponent was increased by 10% (SWT model – red line and Morrow´s model – orange line).

When the fatigue ductility exponent was increased by 10%, no changes in life were obtained for Al7175 (Figure A-8a) and Ti6Al4V (Figure A-8c) alloys. In the case Ck45 steel (Figure A-8b), it was obtained an increase by 78% (162,500 cycles – red line) for SWT parameter and by 148% (245,129 cycles – orange line) for Morrow parameter.

A.5 Conclusions of sensitivity analysis

Some final remarks can be drawn from the sensitivity analysis:

- It has been concluded that, for a life of about 10^5 cycles, although both models are sensitive to the elastic component, Morrow's model is more sensitive.
- Regarding responses between the materials, it is clear that Ck45 is the material that keeps the plastic importance for longer lives. Thus, for Ck45 the plastic component is very relevant for 10^5 cycles although the elastic term is dominant.
- For the same life Al7175 and Ti6Al4V alloys are basically dependent on the elastic term.

Annex B
Bauschinger effect on SWT and Morrow's models (plain fatigue situation)

In annex B are provided the results of rotating bending fatigue tests and the analytical life prediction using the SWT and Morrow models. Bauschinger effect was incorporated in both models in order to obtain a better prediction.

B.1 Initial remarks

In order to verify the influence of BAU effect on life predictions when it is incorporated into the SWT and Morrow models several rotating bending fatigue tests were carried out.

Fifteen specimens manufactured from Al7175 alloy and fourteen specimens manufactured from Ck45 steel were tested. All tests were carried out at ambient temperature, in laboratory environment, and at a stress ratio, $R = -1$. Specimens were polished with abrasive paper, finished with diamond spray (1 μm). Only two materials (Al7175 and Ck45) were tested in this study.

The rotating bending fatigue experiments were carried out using the specimen shown in figure B-1. Figure B-2 presents the schematic test configuration. Table B-1 shows the loading conditions for fatigue tests.

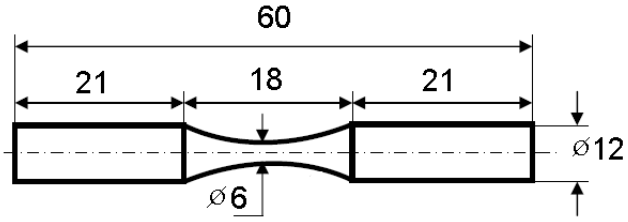

Figure B-1 Geometry of the specimen used in the rotating bending fatigue tests

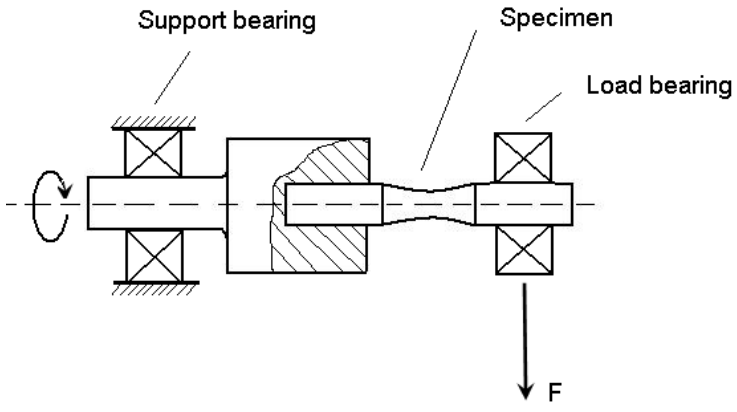

Figure B-2 Schematic test configuration

Table B-1 Loading conditions for the plain fatigue tests

Material (Al7175 alloy)	Stress [MPa]	Material (Ck45 steel)	Stress [MPa]
Al_PF1	325	Ck_PF1	449
Al_PF2	267	Ck_PF2	395
Al_PF3	206	Ck_PF3	340
Al_PF4	159	Ck_PF4	284
Al_PF4i	182	Ck_PF4i	305
Al_PF5	182	Ck_PF4ii	320
Al_PF6	174	Ck_PF4iii	350
Al_PF7	180	Ck_PF5	380
Al_PF8	174	Ck_PF6	340
Al_PF9	169	Ck_PF7	330
Al_PF10	292	Ck_PF8	320
Al_PF11	163	Ck_PF8i	373
Al_PF11i	226	Ck_PF9	329
Al_PF12	235	Ck_PF9i	355
Al_PF13	184	Ck_PF10	359

B.2 Prediction models and BAU effect

To predict the fatigue life in plain conditions the same models used in fretting fatigue were selected: SWT and Morrow's models.

SWT and Morrow's models

The SWT model used to estimate the fatigue life can be written as follows:

$$\sigma_{max} \cdot \varepsilon_a = \frac{\left(\sigma_f'\right)^2}{E}\left(2N_f\right)^{2b} + \sigma_f'\varepsilon_f'\left(2N_f\right)^{b+c} \tag{B-1}$$

The Morrow's model used to estimate the fatigue life is given by the following relation:

$$\varepsilon_a = \left(\frac{\sigma_f'}{E}\right)\left(2N_f\right)^{b} + \varepsilon_f'\left(2N_f\right)^{c} \tag{B-2}$$

BAU effect on SWT and Morrow's models

In order to incorporate the BAU effect into the SWT and Morrow models in the plain fatigue situation the same approaches have been adopted as in the fretting fatigue situation (see 5.4 Application of Bauchinger effect). The first approach is based on energy models and the second approach is based on the theories of internal stresses. It should be mentioned that the values of the BAU for both approaches are exactly the same as in the fretting fatigue situation (see Table 5.1 Results of the Bauschinger stress parameter and Table 5.2 Results of the new fatigue ductility coefficient that incorporates the BAU).

First approach – energy based models

This first approach proposes the modification of the plastic term of both models, by multiplying the fatigue ductility coefficient by BAU parameter.

When the BAU parameter is incorporated in the plastic term of the SWT equation (B-1), it takes the following form:

$$\sigma_{max} \cdot \varepsilon_a = \frac{\left(\sigma_f'\right)^2}{E}\left(2N_f\right)^{2b} + \sigma_f'\varepsilon_f' \cdot \beta_{BAU} \cdot \left(2N_f\right)^{b+c} \tag{B-3}$$

In the case of Morrow equations when the BAU parameter is incorporated in the plastic term, equation (B-2) becomes:

$$\varepsilon_a = \left(\frac{\sigma_f'}{E}\right)\left(2N_f\right)^b + \varepsilon_f' \cdot \beta_{BAU} \cdot \left(2N_f\right)^c \tag{B-4}$$

Second approach – internal stresses, dislocation theories

Also in this situation the BAU effect is incorporated in the plastic term of both models. In fact, it is modified the value of the fatigue ductility coefficient.

When the BAU parameter is incorporated into the plastic term of the SWT equation (B-1) it takes the following form:

$$\sigma_{max} \cdot \varepsilon_a = \frac{\left(\sigma_f'\right)^2}{E}\left(2N_f\right)^{2b} + \sigma_f'\varepsilon_{f,BAU}'\left(2N_f\right)^{b+c} \tag{B-5}$$

In the case of Morrow equations when the BAU parameter is incorporated in the plastic term, equation B-2 becomes:

$$\varepsilon_a = \left(\frac{\sigma_f'}{E}\right)\left(2N_f\right)^b + \varepsilon_{f,BAU}'\left(2N_f\right)^c \tag{B-6}$$

B.3 Results

i. Initial predictions

SWT model – initial prediction

Figure B-3 shows the analytical fatigue life prediction based on the SWT parameter (eq. B-1 - solid red line).

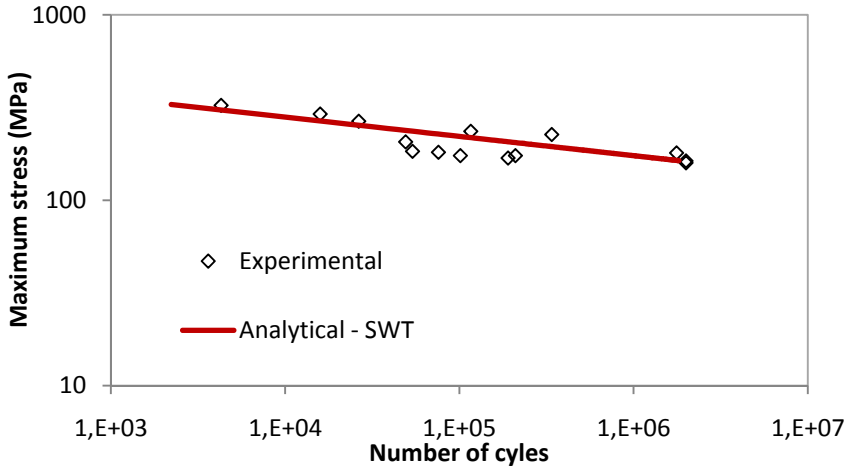

a. Al7175 alloy

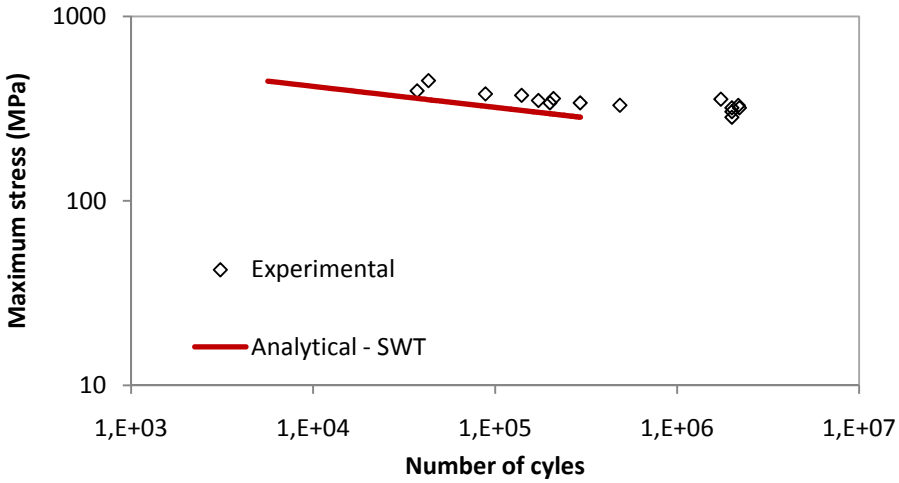

b. Ck45 steel

Figure B-3 Maximum stress (σ_{max}) vs. number of cycles (SWT – without BAU)

In figure B-3 can be seen that the use of the SWT parameter gives very good fatigue life predictions in the case of the Al7175 alloy (Figure B-3a) and underestimates the fatigue life in the case of the Ck45 steel (Figure B-3b).

Morrow's model – initial prediction

Figure B-4 shows the analytical fatigue life prediction based on the Morrow's parameter (eq. B-2 - solid red line).

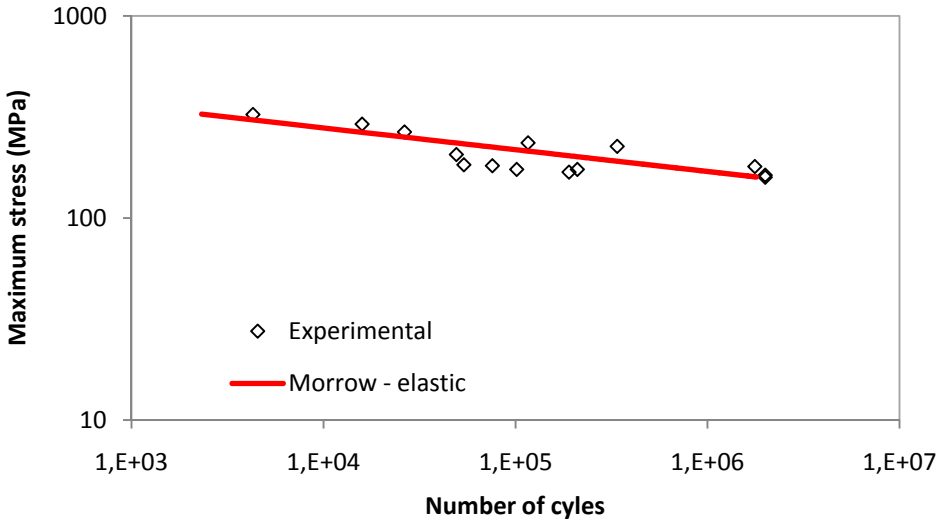

a. Al7175 alloy

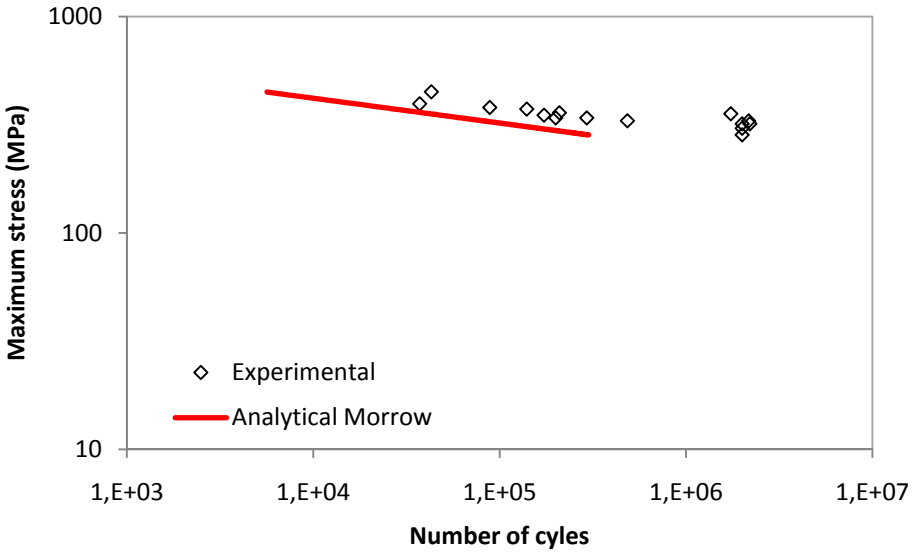

b. Ck45 steel

Figure B-4 Maximum stress (σ_{max}) vs. number of cycles (Morrow – without BAU)

In figure B-4 can be seen that the use of the Morrow's parameter gives also very good fatigue life predictions in the case of the Al7175 alloy (Figure B-4a) and also underestimates the fatigue life in the case of the Ck45 steel (Figure B-4b).

ii. First approach- energy based models

SWT parameter – energy based models

Figure B-5 shows the analytical fatigue life prediction based on the SWT model (eq. B-1 – solid red line). It is also shown the estimated life obtained using the SWT model affected by the BAU parameter from the point of view of energy based models (eq. B-3 – dashed green line).

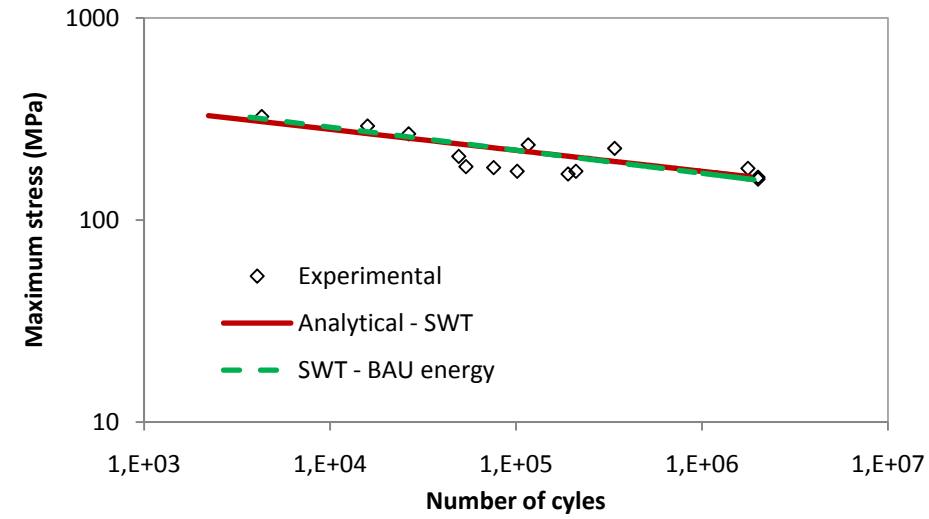

a. Al7175 alloy

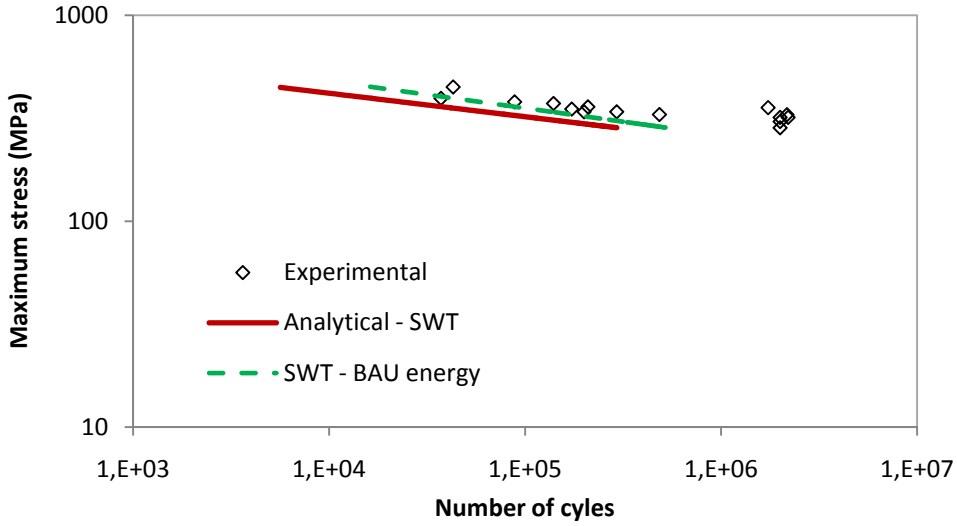

b. Ck45 steel

Figure B-5 Maximum stress (σ_{max}) vs. number of cycles (SWT – with BAU energy)

It can be seen form figure B-5 that BAU parameter introduced in the SWT model has an insignificant effect on fatigue life in the case of Al7175 alloy (Figure B-5a). When

the BAU parameter is taken into consideration in the case Ck45 steel a significant change on fatigue live is obtained (Figure B-5b). The predicted results in the case of Ck45 steel are much closer to the experimental results.

Morrow's model – energy based models

Figure B-6 shows the analytical fatigue life prediction based on the Morrow's model (eq. B-2 – solid red line). It is also shown the estimated life obtained using the Morrow's model affected by the BAU parameter from the point of view of energy based models (eq. B-4 – dashed green line).

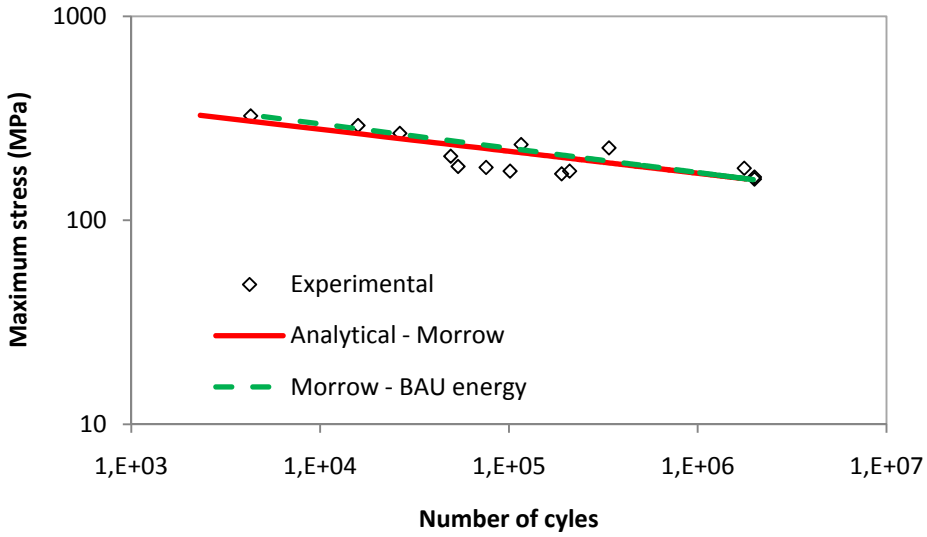

a. Al7175 alloy

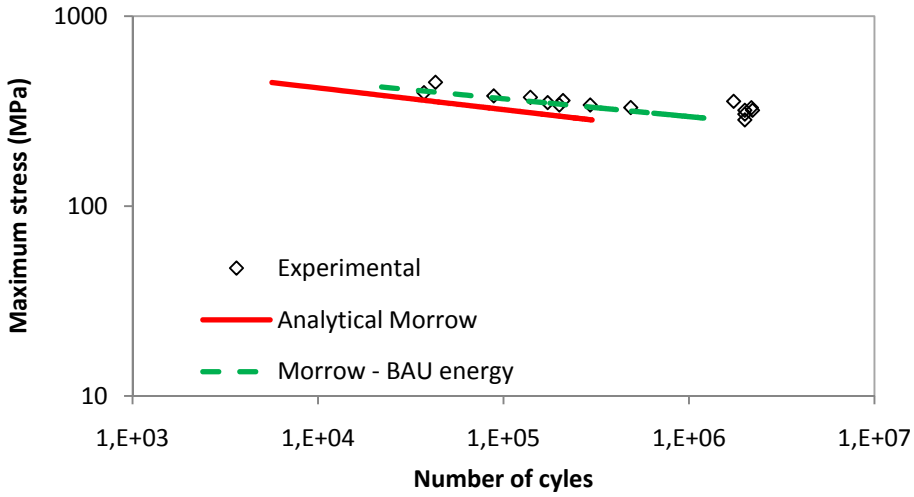

b. Ck45 alloy

Figure B-6 Maximum stress (σ_{max}) vs. number of cycles (Morrow – with BAU energy)

It can be seen that also in Morrow´s case the BAU effect did not have any influence on fatigue life when it is applied to the Al7175 alloy (figure B-6a).

In the case of Ck45 steel (figure B-6b) can be seen that the BAU effect has a substantial effect on fatigue life and the predicted results agree well with the experimental results.

iii. Second approach – internal stresses, dislocation theories

SWT parameter – internal stresses

Figure B-7 shows the analytical fatigue life prediction based on the SWT parameter (eq. B-1 – solid red line). It is also shown the estimated life obtained using the SWT parameter affected by the BAU effect from the point of view of internal stresses (eq. B-5 – dashed green line).

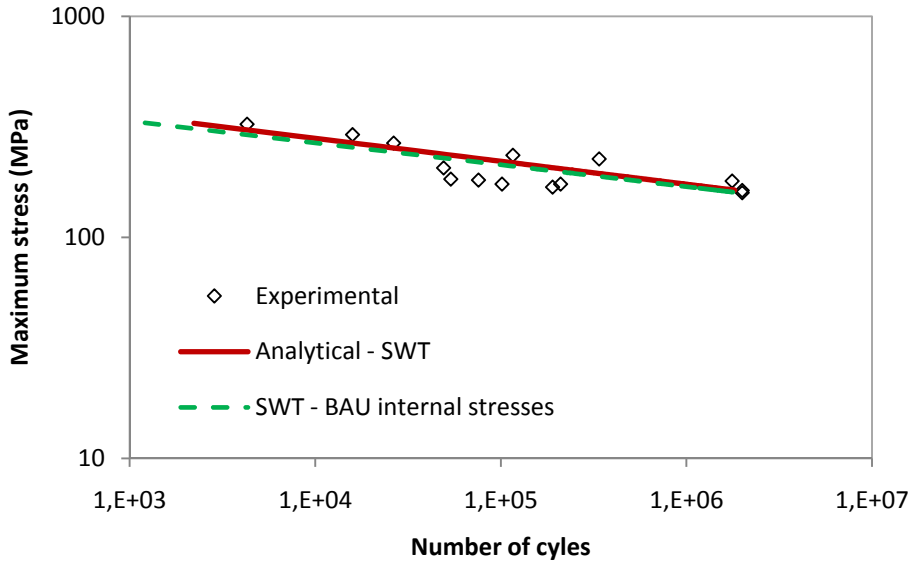

a. Al7175 alloy

Figure B-7 Maximum stress (σ_{max}) vs. number of cycles (SWT – with BAU internal stresses) (cont.)

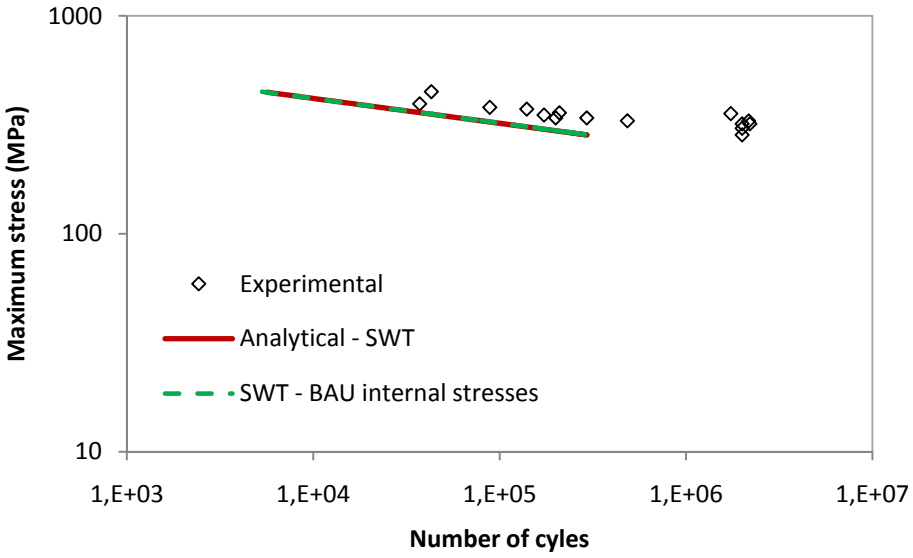

b. Ck45 steel

Figure B-7 Maximum stress (σ_{max}) vs. number of cycles (SWT – with BAU internal stresses)

From figure B-7, it can be seen that in the case of Al7175 alloy and Ck45 steel the BAU effect did not have any influence on fatigue life.

Morrow's model– internal stresses

Figure B-8 shows the analytical fatigue life prediction based on the Morrow's model (eq. B-2-solid red line). It is also shown the estimated life obtained using the Morrow's model affected by BAU parameter from the point of view of internal stresses (eq. B-6 – dashed green line).

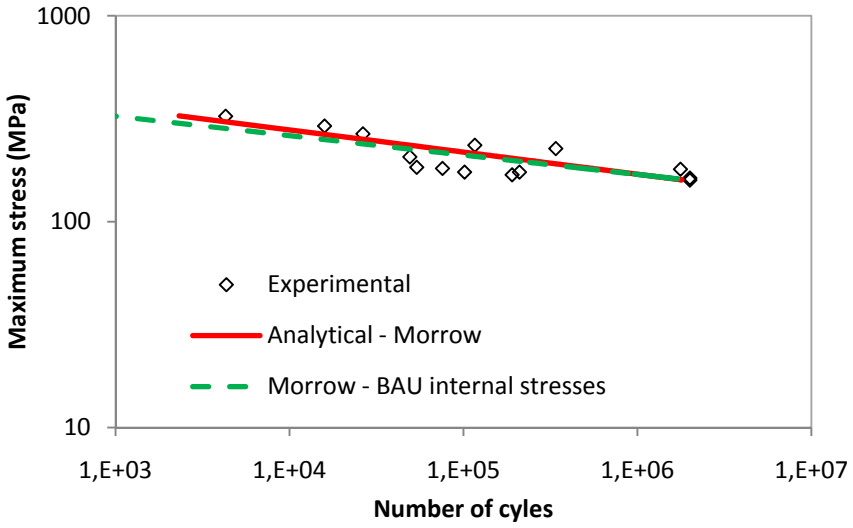

Al7175

Figure B-8 Maximum stress (σ_{max}) vs. number of cycles (Morrow– with BAU internal stresses) (cont.)

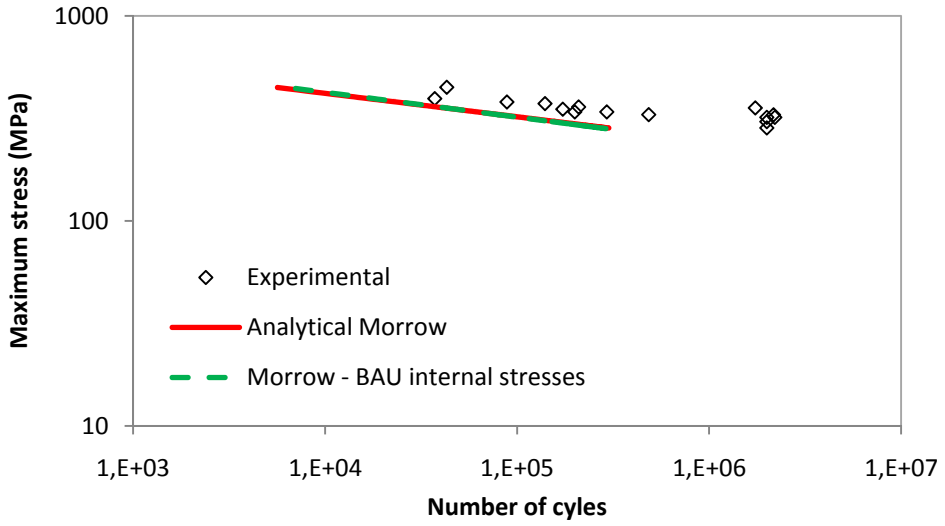

Ck45

Figure B-8 Maximum stress (σ_{max}) vs. number of cycles (Morrow– with BAU internal stresses)

From figure B-8 it can be seen that in the case of Al7175 alloy and Ck45 steel the BAU effect did not have any substantial influence on fatigue life.

B.4 Conclusions

Some final remarks can be drawn from the tests in this annex:

- The first remark is that both models used in the present study give similar fatigue life predictions. Comparing the two materials, the models estimate well the fatigue life in the case of Al7175 alloy, while in the case of Ck45 steel they underestimate the lives;

- The BAU effect, as proposed in this work, has a substantial influence on life predictions, when an energy based approach is used. A significant BAU effect takes place in Ck45 steel while the BAU effect has a very small influence in Al7175 alloy;

- Fatigue life predictions are much better with the incorporation of the energy based BAU effect (the Ck45 steel improves the prediction while the Al7175 does not improve but it is not detrimental). This effect agrees well with the material properties because it is observed that by incorporating the BAU effect into the both models it does not have any influence on the materials with a very small BAU effect but improves the life predictions of the materials that have a significant BAU effect;

- It is validated the use of the BAU effect in fretting fatigue situations because it is valid in simpler situations as in the plain fatigue case;

- Finally it can be concluded that both models used in this study (SWT and Morrow) become more universal (general) equations if the BAU effect is incorporated.